



**HAL**  
open science

# A groundwater basin multidisciplinary approach to conceptualize subsurface flow and trace nitrate contamination sources. Lake Titicaca, Bolivia

Gabriela Patricia Flores Aviles

## ► To cite this version:

Gabriela Patricia Flores Aviles. A groundwater basin multidisciplinary approach to conceptualize subsurface flow and trace nitrate contamination sources. Lake Titicaca, Bolivia. Hydrology. Université Grenoble Alpes, 2019. English. NNT : 2019GREAU019 . tel-03170195

**HAL Id: tel-03170195**

**<https://theses.hal.science/tel-03170195>**

Submitted on 16 Mar 2021

**HAL** is a multi-disciplinary open access archive for the deposit and dissemination of scientific research documents, whether they are published or not. The documents may come from teaching and research institutions in France or abroad, or from public or private research centers.

L'archive ouverte pluridisciplinaire **HAL**, est destinée au dépôt et à la diffusion de documents scientifiques de niveau recherche, publiés ou non, émanant des établissements d'enseignement et de recherche français ou étrangers, des laboratoires publics ou privés.

## **THÈSE**

Pour obtenir le grade de

**DOCTEUR DE LA**

**COMMUNAUTÉ UNIVERSITÉ GRENOBLE ALPES**

Spécialité : **Sciences de la Terre, de l'Univers et de l'Environnement (CESTUE)**

Arrêté ministériel : 25 mai 2016

Présentée par

**Gabriela Patricia FLORES AVILES**

Thèse dirigée par **Céline DUWIG**, Chargé de recherche et codirigée par **Yvan ROSSIER**, Enseignant-chercheur, UJF et **Marc Descloitres**, IRD

préparée au sein du Laboratoire **Institut de Geosciences de l'Environnement**  
dans l'**École Doctorale Terre-Univers-Environnement**

**Une approche multidisciplinaire des bassins d'eaux souterraines pour conceptualiser les écoulements souterrains et détecter les sources de contamination par le nitrate. Lac Titicaca, Bolivie**

**A groundwater basin multidisciplinary approach to conceptualize subsurface flow and trace nitrate contamination sources. Lake Titicaca, Bolivia**

Thèse soutenue publiquement le **27 Septembre 2019**,  
devant le jury composé de :

**Mr. Roger GUERIN**

Pr. Université Pierre et Marie Curie, Paris: Rapporteur

**Mr. Olivier RIBOLZI**

Directeur de Recherche IRD, GET: Rapporteur

**Mme. Elisa SACCHI**

Pr. Université de Pavie, Italie: Examinatrice

**Mr. Alvaro SORUCO**

Pr. Institut de Géologie et Environnement, UMSA, Bolivie: Examineur

**Mr. Laurent OXARANGO**

Pr. Université Grenoble Alpes, Président

**Thèse soutenue financièrement par l'État plurinational de Bolivie, administrée par le ministère de l'Éducation bolivien (MINEDU)**



*To my beloved, the One and Only, who supports, understands and encourages me always. Psalm 103:1-5*

## Preface

Managing water quality degradation and pollution processes in the Katari and Lago Menor Basin, towards the environmental remediation of Lake Titicaca, has become a national priority for the Plurinational State of Bolivia since 2004. Among the strategies to tackle with these water issues, the Bolivian government, has been promoting and establishing key areas of scientific research related to the “*Conservation and restoration of Natural Ecosystems*” in order to empower the Bolivian Scientific Sovereignty, Supreme Decree 2100, 1 September 2014.

The present study, promoted by the Plurinational State of Bolivia through the Bolivian Ministry of Water and Environment (MMAyA), has arisen as a concern to the lack of knowledge about the behaviour of large scale groundwater flow systems within the Katari and Lago Menor Basin, their related environmental phenomena and potential contribution to Lake Titicaca eutrophication processes. Particularity, the main concern was to cope with the lack of science-based information for the management and protection of groundwater resources, which are increasingly being exploited because of climate variability and population growth.

## Abstract

Water quality degradation, climate variability and population growth are among the factors that constrains water availability in the semi-arid Katari and Lago Menor region (6,350 Km<sup>2</sup>), leading to an increasingly exploitation of groundwater resources. This thesis aims to conceptualize subsurface flow and trace nitrate contamination sources in the groundwater system within the Katari and Lago Menor Region.

A multidisciplinary approach for field investigation was used in this study, including a regional groundwater source inventory and groundwater level measurements, geophysical investigation techniques (e.g. TDEM-Time Domain ElectroMagnetic soundings), piezometer construction and installation, and a regional sampling campaign and analysis for major ion chemistry and dual isotopes of  $\delta^{15}N_{NO_3}$  and  $\delta^{18}O_{NO_3}$ .

The results allowed identifying the limits of two different geological settings (Piedmont subsystem and Lacustrine plain), the geometry of the Quaternary porous geologic media and the bottom boundaries of the aquifer. The groundwater flow regime corresponds to a classical gravity-driven regional flow system. Six subdomains possessing different hydraulic properties were identified. A large portion of the aquifer presents an unconfined behaviour, particularly on the Piedmont, whereas it remains confined in the plain areas. The thickness of the unconfined portion varies from 50 to 150 meters. Values of hydraulic conductivity for the unconfined portion range from  $1.1 \times 10^{-4}$  to  $5.9 \times 10^{-8}$  m/sec, specific yield ranges from 0.16 to 0.20 and recharge values range from 118 to 382 mm/year. While for the confined part the transmissivity values range around  $6.0 \times 10^{-6}$  m<sup>2</sup>/sec with a storativity value of  $1.2 \times 10^{-2}$  to  $6.0 \times 10^{-3}$ .

In the high Piedmont areas, where the hydraulic heads are high, the low mineralization and the chemical and isotopic compositions showed that the groundwater source is of good quality. In contrast, in the lower sector of the Piedmont, the shallower water tables of the alluvial-fluvioglacial-lacustrine sequence, make this area more vulnerable to contamination. Chemical facies and the isotopic composition of the dissolved  $NO_3^-$  revealed that the main origin of this anion is related to nitrogen fertilizers towards the NW of the Piedmont and human/animal waste towards the SE. Moreover, natural nitrate attenuation processes occur mainly in the lower sector of the Piedmont, when groundwater

mixes with the reservoir of lacustrine origin. Groundwater flowing in the plain areas, present primarily Na(K)-Cl facies relating the presence of evaporites. In this area groundwater is prone to contamination, especially when the clay layer is absent and in places where a connection to the Piedmont is evidenced (subterranean channels). The contribution of groundwater to the current Lake Titicaca (Cohana Bay) appears to be retarded due to the presence of the clay layer.

This basin-scale conceptual groundwater flow model provides a good understanding of the aquifer functioning, and a guide to future data collection in order to improve the robustness of future groundwater flow numerical modeling. All the science-based information generated from this research was arranged into a GIS spatial database to support decision makers in the management and protection of groundwater resources. This science-based information also contributes to the environmental remediation of Lake Titicaca, a national priority for the Plurinational State of Bolivia.

## Résumé

La dégradation de la qualité de l'eau, la variabilité climatique et la croissance démographique font partie des facteurs limitant la disponibilité de l'eau dans les régions semi-arides de Katari et de Lago Menor (6,350 Km<sup>2</sup>), entraînant une exploitation croissante des ressources en eaux souterraines. Cette thèse a pour but de conceptualiser le système d'écoulement souterrains à grande échelle et de détecter les sources de contamination par les nitrates dans les régions de Katari et Lago Menor.

Dans cette étude, on a utilisé une approche multidisciplinaire comprenant un inventaire régional des sources d'eaux souterraines et des mesures du niveau piézométrique, des techniques d'investigation géophysique (sondages électromagnétiques à domaine temporel TDEM), la construction et l'installation de piézomètres, l'analyse chimique des ions majeurs et les isotopes de  $\delta^{15}N_{NO_3}$  et de  $\delta^{18}O_{NO_3}$ .

Les résultats ont permis d'identifier les limites de deux contextes géologiques différents (le sous-système du Piémont et la plaine lacustre), la géométrie du milieu géologique poreux du Quaternaire et les limites inférieures de l'aquifère. L'analyse régionale montre que les flux souterrains suivent le modèle classique d'écoulement basé sur la gravité. Six sous-domaines ont été identifiés possédant des propriétés hydrauliques différentes. Une grande partie de l'aquifère présente un comportement non confiné, en particulier sur le Piémont, alors qu'il reste confiné dans les zones de plaine. L'épaisseur de la portion non confinée varie de 50 à 150 mètres. Les valeurs de conductivité hydraulique pour la portion non confinée vont de  $1.1 \times 10^{-4}$  à  $5.0 \times 10^{-6} m/sec$ , le rendement spécifique de 0,16 à 0,20 et les valeurs de recharge vont de 118 à 382 mm/year. Tandis que pour la partie confinée, les valeurs de transmissivité se situent autour de  $6.0 \times 10^{-6} m^2/sec$  avec une valeur de stockage de  $1.2 \times 10^{-2}$  à  $6.0 \times 10^{-3}$ .

En particulier, dans les hautes régions du Piémont où se trouvent les fortes pressions hydrauliques, les compositions minérales, chimiques et isotopiques montrent que la source d'eau souterraine est de bonne qualité. En revanche, dans la partie inférieure du Piémont, les nappes phréatiques moins profondes de la séquence alluvial-fluvioglaciale-lacustre rendent cette zone plus vulnérable à la contamination. En fait, le faciès chimique et la composition isotopique du  $NO_3^-$  dissous - ont révélé que l'origine principale de cet anion est liée aux engrais azotés vers le nord-ouest du Piémont et aux déchets humaines /

animales vers le SE. De plus, les processus naturels d'atténuation du nitrate se produisent principalement dans le secteur inférieur du Piémont, lorsque les eaux souterraines se mélangent au réservoir d'origine lacustre.

En revanche, les eaux souterraines s'écoulant dans les plaines présentent principalement des faciès de Na (K) -Cl mettant en évidence la présence d'évaporites. Dans cette zone, les eaux souterraines sont sujettes à la contamination, en particulier lorsque la couche d'argile est absente et dans les endroits où une connexion au Piémont est mise en évidence (canaux souterrains). La contribution des eaux souterraines au lac Titicaca actuel (baie de Cohana) semble être retardée en raison de la présence de la couche d'argile.

Ce modèle conceptuel d'écoulement des eaux souterraines permet une bonne compréhension du fonctionnement de l'aquifère et fournit un guide pour la collecte future de données afin d'améliorer la robustesse d'une future modélisation numérique des flux d'eau souterrains. Toutes les informations scientifiques issues de cette recherche ont été rassemblées dans une base de données spatiales SIG pour aider les décideurs à gérer et à protéger les ressources en eaux souterraines. Ces informations scientifiques contribuent également à l'assainissement de l'environnement du lac Titicaca, une priorité nationale de l'État plurinational de Bolivie.

## Acknowledgments

The present study and my PhD education at the Institute of Environmental Geosciences (IGE) was undertaken with the financial support of the Plurinational State of Bolivia through the Project entitled “*100 Scholarships for Postgraduate Education within the Framework of Technological and Scientific Sovereignty*”, Supreme Decree 2100, 1 September 2014, administered by the Ministry of Education (MINEDU). The aim of these scholarships is to engage young Bolivian professionals for enhancing their capabilities in scientific research through offering opportunities in a range of countries and fields within the International Scientific Community, in order to promote and empower the Bolivian Scientific Sovereignty.

The field work carried out during this research was partly funded by LABEX OSUG@2020, ANR grant no.ANR-10-LABX-56 (financed by the Future Investments programme launched by the French government and implemented by the ANR).

I would like to extend my sincere gratitude to the following institutions and people for their help during the development of this research:

The Bolivian Ministry of Water and Environment (M.M.A.y.A, La Paz) for their logistical, technical support and for providing me with valuable data and information. Special thanks to the Cuenca Katari and Lago Menor Management Direction and to the local communities of the Municipalities of Pucarani, Batallas, Laja, Viacha, Puerto Pérez and El Alto.

The Institute de Recherche pour le Développement (IRD-in Bolivia since 1968) for their logistical support during the development of the field campaigns. Special thanks to Mr. Julio César.

The University of San Andres (UMSA, La Paz) for their logistical and technical support. Special thanks to Mayra Pérez who assisted me during the development of my different field campaigns.

IRD Associate Researcher Celine Duwig and UGA Associate Professor Yvan Rossier, for providing assistance with the field and laboratory work, and for providing guidance, oversight and their insightful commentary and advice with regards to the development of this thesis.

IRD Associate Researcher Marc Descloitres, for his considerable assistance with the geophysical investigation, for his insightful commentary with regards to the development of the geophysics manuscript, and for his valuable time and advice during my presentation within the International Scientific Community.

UNIPV (University of Pavia) Associate Professor Elisa Sacchi, for her considerable assistance with the isotopic and hydrochemical data interpretation, and for her valuable contributions to the nitrate manuscript.

Lorenzo Spadini, Joel Savarino, Nicolas Caillon and Ilan Bourgeois for their technical assistance and support during the analysis of my water samples. Special thanks to Joel Savarino and Lorenzo Spadini for their insightful commentary and contributions with regards to the hydrochemical and isotopic characterizations.

To conclude, I would also like to thank to my parents Víctor and Patricia for their advices, support, unconditional love and time. To my siblings, Víctor, Paola, Mariana, Valeria and to my gorgeous niece Samantha, because their joy and determination are always a deep encouragement for my life.

# Table of contents

---

<i>Preface</i> .....	3
<i>Abstract</i> .....	4
<i>Résumé</i> .....	6
<i>Aknowledgments</i> .....	8
<b>Chapter 1</b> .....	<b>15</b>
<b>Introduction</b> .....	<b>15</b>
1.1 Research Objectives .....	18
1.2 Limitations.....	19
1.3 Organization of the thesis .....	20
<b>Chapter 2</b> .....	<b>22</b>
<b>Regional Environmental Setting of the Study Site</b> .....	<b>22</b>
2.1 Location and description .....	22
2.2 Climate.....	22
2.2.1 Precipitation.....	24
2.2.2 Temperature and Evapotranspiration.....	25
2.3 Surface topography, drainage, wetland and alpine features .....	25
2.4 Geology and Paleohydrology .....	27
2.5 Population and Groundwater dependent sectors in the Basin .....	31
2.6 Potential environmental threats to groundwater resources in the Basin.....	32
2.7 Previous hydrogeological studies in the Basin .....	34
2.8 Previous Hydrochemical and Isotopic studies in the Basin.....	35
<b>Chapter 3</b> .....	<b>37</b>
<b>Methods and Techniques</b> .....	<b>37</b>
3.1 Introduction .....	37
3.2 Field work.....	40
3.2.1. Sampling campaign .....	40
3.2.2. Groundwater source inventory and water level measurements.....	42
3.2.3. Geophysical measurements .....	44
3.2.4. Piezometer construction and installation.....	44
3.3 Laboratory work .....	48
3.4 Data analysis methods .....	50
<b>Chapter 4</b> .....	<b>51</b>
<b>Regional geophysical characterization</b> .....	<b>51</b>
4.1 Introduction .....	51
4.2 Article I: <i>Insight into the Bolivian Lake Titicaca aquifer system, inferred from geophysical (TDEM), hydrogeological and hydrogeochemical data</i> .....	52
4.3 Conclusions .....	106

<b>Chapter 5</b> .....	<b>107</b>
<b>Basin-scale conceptual groundwater flow model</b> .....	<b>107</b>
5.1 Introduction .....	107
5.2 Article II: <i>Basin-scale conceptual groundwater flow model under natural conditions of the semi-arid, Bolivian Lake Titicaca Aquifer System</i> .....	108
5.3 Conclusions .....	151
<b>Chapter 6</b> .....	<b>152</b>
<b>Groundwater basin-scale hydrochemical and dual isotopic characterization</b> .....	<b>152</b>
6.1 Introduction .....	152
6.2 Article III: <i>Tracing nitrate contamination in a gravity-driven groundwater flow system of Lake Titicaca Basin, Bolivian Altiplano: influence on water chemistry and nitrogen isotopes</i> .....	153
6.3 Conclusions .....	201
<b>Chapter 7</b> .....	<b>202</b>
<b>Conclusions and perspectives</b> .....	<b>202</b>
References .....	211
<b>APPENDIX</b> .....	<b>227</b>
<b>APPENDIX A:</b> .....	<b>227</b>

# Tables

---

**Table 3.1.** Location and position of the new piezometers using the Universal Transverse Mercator (UTM) coordinate system. .... 45

# Figures

---

<b>Figure 2.1.</b> Geographical context of the Katari and Lago Menor Basin. Hypsometric colours represent the elevation in meters above the sea level (m a.s.l) of the terrain (DEM: SRTM 1-Arc-Second Global-N.A.S.A, 2000).....	23
<b>Figure 2.2.</b> Mean monthly precipitation at El Alto airport Station, recorded from 2009-2018 (data available at <a href="http://www.senamhi.gob.bo">http://www.senamhi.gob.bo</a> ). .....	24
<b>Figure 2.3.</b> Geological and Structural map of the basin, showing the M.M.A.y.A groudwater monitoring network and the available information (modified from geological data G.E.O.S.I.R.H-2017 and GEOBOL&Swedish Geological AB (1995)). .....	30
<b>Figure 2.4.</b> Hypsometric map showing ancient lake invasions and previous hydrogeological information in the Purapurani zone. Hypsometric colours represent the elevation in meters above the sea level (m a.s.l) of the terrain (DEM: SRTM 1-Arc-Second Global-N.A.S.A, 2000).....	36
<b>Figure 3.1.</b> General methodology for developing a basin-scale conceptual groundwater flow model for the Katari and Lago Menor region .....	38
<b>Figure 3.2.</b> General methodology for the application of the hydrogeochemical and dual isotopic approach within the Katari and Lago Menor Basin aquifer. ....	39
<b>Figure 3.3.</b> Some sampling sites and the equipment carried out into the field: a) Lagoon located in the upper part of the basin nearby the glaciated peaks, b) wetland located in the low Piedmont area, c) Deep well located in a Pumping station, d) Deep well presenting the artesianism phenomena, d) Shore of Lake Titicaca and e) Field equipment for measuring water quality parameters and alkalinity.....	41
<b>Figure 3.4.</b> Flowchart for Sampling groundwater monitoring points and performing geochemical field measurements.....	42
<b>Figure 3.5.</b> a) Device used for measuring the location of each inventoried groundwater source and example of groundwater level measurements performed in the field, b) deep well, c) well in a pumping house provided with a submersible pump and d) dug well. ....	43
<b>Figure 3.6.</b> a) TEMfast 48 equipment used for measuring resistivity parameters in the field and b) Example of setting the coincident loop configuration in the field.....	44
<b>Figure 3.7.</b> a) Location of the new piezometers and b) example of design and constructive details of piezometer P-1. Each piezometer consists of a 2 in PVC single-casing, single-screen for collecting water level data and water samples. ....	46
<b>Figure 3.8.</b> Drilling and piezometer completion in the Katari and Lago Menor Basin. a) On-site drilling equipment, b) detailed stratigraphic record, c) PVC casing screening and installation of the piezometer, d) water level measurement	

	after the development, f) Completion of the piezometer with a surface seal and a protective casing for providing piezometer security and e) piezometer development.....	48
<b>Figure 3.9.</b>	a) Samples for major ion analysis, b) materials for the preconcentration procedure, c) Samples (1 liter) were poured in the funnels and drained by gravity, d) preparation of the 10 ml eluted samples by the addition of bacteria in order to ensure 100 nmol of NO <sub>3</sub> and a matrix volume of NaCl, e) 12 hours of incubation, then NaOH was added for trapping nitrogen dioxide in each vial, and finally isotopic compositions were measure in the f) MAT 253 IRMS Mass Spectrometer.....	49
<b>Figure 7. 1.</b>	Location of the profile for the 3D cut. ....	205
<b>Figure 7.2.</b>	Conceptual groundwater flow model incorporating the results of the different investigation techniques. ....	206
<b>Figure 7.3.</b>	Map showing the current available information of the Katari and Lago Menor Basin aquifer after the present investigation. The red and yellow areas indicate the future work that might be performed following this study. ....	208
<b>Figure 7.4.</b>	Map showing the current available groundwater sampling points for measuring hydrogeochemical and isotopic information within the Katari and Lago Menor Basin aquifer after the present investigation. The red areas indicate the future work that might be performed following this study. ....	210

## Introduction

Globally, groundwater is a vital source for drinking and agricultural purposes, particularly in arid and semi-arid regions (van der Kamp & Hayashi, 2009; Wei et al., 2014; Yousif et al., 2015; Grizard et al., 2018). However, it is constrained to the investigation and conceptualization of groundwater flow systems at the scale of drainage basins (Tóth, 1995; Tóth, 1999; Tóth, 2010; Mádl-Szönyi et al., 2015).

Prior research around the world has thoroughly investigated basin-scale flow of groundwater and the factors controlling it. These studies have demonstrated that basin-scale gravity-driven groundwater flow systems are influenced by topography and the geological framework (Tóth, 1962; Tóth, 1963; Tóth, 1995; Navarro de León et al., 2005; Tóth et al., 2010; Zhou & Li, 2011).

In addition, these investigations agree that the most fundamental consequence of evaluating basin-scale groundwater flow systems is the understanding of a wide range of physical, chemical and ecological phenomena (Tóth, 1999; Navarro de León et al., 2005; Zhou & Li, 2011). However, the main limitation for building basin-scale groundwater flow models is usually the lack of sufficient data. In fact, several investigations around the world have documented that the application of one investigation technique is not sufficient for developing conceptual models of complex hydrogeological systems, becoming even

more difficult when hydrogeological data is limited. Geological, hydrogeological and geophysical surveys are required to construct physical 3D conceptual models (Lachaal et al., 2011; Turner et al., 2015; Saroli et al., 2017; Bayanzul et al., 2018). The continuous measurements of water budget components and groundwater levels are also necessary to create databases for the analysis of basin-scale flow systems to calibrate and validate regional transient groundwater models (Zhou & Li, 2011; Izady et al., 2015).

As a matter of fact, significant advances in groundwater flow modeling at the scale of drainage basins, have arisen due to the strong demand for predicting regional impacts of climate and human pressures on groundwater systems, and to formulate sustainable resources development scenarios. (Corbet, 2000; Michael et al., 2009; Passadore et al., 2009; Zhou & Li, 2011; Hu et al., 2015; Izady et al., 2015; Doble et al., 2017; Ebrahim et al., 2019).

In South America, only few studies attempted to build basin-scale numerical groundwater flow models (Varni et al., 1999; Araújo et al., 1999; Calderón et al., 2007; Jayne et al., 2016) due to the lack of or insufficient data. As a result, most of groundwater investigations conducted in South America are focused primarily in the development of local or regional groundwater conceptual models by means of the combination of multiple approaches that represent valuable input datasets for numerical groundwater modeling.

Several studies can be cited: in the Northern Chile, the multidisciplinary study conducted by Viguié et al. (2018) in the hyperarid Atacama Desert, the multi-method assessment performed by Oyarzún et al. (2014) in the semi-arid Limarí River basin, and the groundwater recharge assessment carried out in the arid Salar del Huasco basin (Uribe et al., 2015). Additionally, in Argentina, Mira et al. (2015) integrated geological and geophysical data to build a geological subsurface model for the Corrientes province aquifer. Maldonado et al. (2015) combined hydrogeochemical and groundwater level data to assess the deep aquifers from the Pampean plain (Maldonado et al., 2015). Furthermore, in Brazil, Fernandes et al. (2016) used physical and structural geology data to develop a preliminary conceptual model of groundwater flow for the Serra Geral basalt aquifer.

In Bolivia, local groundwater investigations mainly relate the application of geophysical techniques. For example, Guérin et al. (2001) used geophysical surveys and groundwater electrical conductivity measurements to identify saline groundwater in the semi-arid

Bolivian Altiplano. Gómez et al. (2019) performed electromagnetic soundings and electrical resistivity tomography to investigate the thickness of an alluvial aquifer and to delineate the relief of the bedrock. Gonzáles-Amaya et al. (2018) used hydrogeophysics to refine hydrogeological conceptual models in terms of layering and lateral variation and thickness in the Central part of Bolivia.

In the Katari and Lago Menor Basin, one of the most populated and deteriorated basins of the semi-arid Bolivian Altiplano (BID, 2016; Agramont et al., 2019), recent research has predicted that climate variability and population growth will most likely render to a water shortage after the mid-2020s (Kinouchi et al., 2019), which will lead to an increasingly exploitation of groundwater resources in order to meet this growing demand. Thus, the development of a basin-scale groundwater flow concept is compulsory for understanding groundwater natural flow processes, including lateral inflow and outflow boundaries, as well as sinks and sources mechanisms.

Previous investigation on the site showed local hydrogeological characterizations based on lithology, groundwater level measurements, hydrochemistry and stable isotopes of deuterium and oxygen 18 (MMAyA, 2016; Quino et al., 2019). Moreover, due to the lack of geophysical information it was not possible to identify neither regional hydraulic continuity, nor bottom boundaries or the spatial and vertical variation of the geologic media. The identification of regional hydraulic continuity is of vital importance for the correct interpretation of natural flow processes and phenomena (Tóth, 1995; Tóth, 1999; Mádl-Szönyi et al., 2015).

On the other hand, much is known about the current degradation of water quality of the rivers of the basin that discharge into the shallower Lake Titicaca (Lake Huiñamarca) (Fonturbel, 2005; Lazzaro et al., 2016; Guédron et al., 2017; Archundia et al., 2017; Archundia et al., 2018 ; Acha et al., 2018; Quino et al., 2019). However, little is known about the potential influence of sewage, waste disposal, farmland and mining activities into groundwater resources of the basin (M.M.A.y.A, 2016; Brienza et al., 2017; Quino et al., 2019). In fact, most of the rural communities in the basin's water supply relies mainly on groundwater either from wells, springs or wetlands. However, they lack of adequate disposals of sewage and human waste (M.M.A.y.A, 2014).

The available hydrogeological and hydrochemical data, resultant of the previous local research performed in the study area, are valuable for creating local hydrogeological databases. Moreover, a basin-scale investigation is compulsory for understanding the main physical, chemical and biological processes at the regional scales. Groundwater moving in gravity-driven groundwater flow systems at the scale of drainage basins, generally present water sources of high quality in recharge areas due to the high hydraulic heads, whereas the low hydraulic heads in the throughflow and discharge areas (Tóth, 1962; Tóth, 1963; Tóth, 1995; Zhou & Li, 2011) make this zones more vulnerable to degradation (Pilla et al., 2005).

The correct understanding of groundwater flow dynamics in the Katari and Lago Menor basin can improve the current comprehension of Lake Titicaca eutrophication processes, seeing that many studies around the world have shown that contaminated and/or nutrient-rich groundwater entering lakes has led to lake pollution and/or eutrophication (Shaw et al. 1990; Robertson et al. 2005; Özen et al. 2010) and revealed if groundwater resources in the basin are threatened by agricultural leaching, livestock production and/or by domestic wastewater.

A research to conceptualize subsurface flow and trace nitrate contamination sources at a basin-scale in the Katari and Lago Menor region, in the Bolivian Altiplano, had never been presented before. This particular high-altitude, gravity-driven conceptual groundwater flow model allowed the depiction of the geometry of the domain, the main flow paths and hydrochemical evolution patterns as well as nitrate fluxes and denitrification process from the recharge zones, along the groundwater flow system and towards the discharge areas.

## **1.1 Research Objectives**

This investigation aims to apply a multidisciplinary approach (geology, geophysics, hydrogeochemistry, GIS, isotopy and groundwater level data) to conceptualize subsurface flow within the Katari and Lago menor region. The proposed basin-scale conceptual groundwater flow model will allow evaluating the direction and magnitude of water flow, natural flow processes, boundaries of the groundwater system, as well as sink and sources mechanisms. Moreover, it will explain the factors responsible for the: i) natural and final groundwater hydrochemical compositions, ii) evolution patterns from the recharge zones towards the discharge zones of the aquifer, iii) the potential sources of nitrate

contamination, and iv) the potential nitrate contribution to the eutrophication of Lake Titicaca.

The specific aims are:

- To characterize the regional continuity, geometry and bottom boundaries (depth to the top of the Tertiary/Devonian sedimentary bedrock) of the Quaternary porous geologic media that fills up the Katari and Lago Menor Basin.
- To develop a basin-scale conceptual groundwater flow model considering the previous characterization, natural flow processes, aquifer hydraulic properties, boundary conditions and sources and sinks of the groundwater system, under natural conditions (pre-development conditions).
- To trace natural background levels of groundwater and nitrate contamination sources at a basin-scale, from the high Piedmont areas to the Lacustrine plain, by the application of hydrochemistry and dual isotopes  $\delta^{15}N_{NO_3}$  and  $\delta^{18}O_{NO_3}$ , considering the previous hydrogeological knowledge.
- To provide knowledge about hydrochemical evolution patterns and natural nitrate attenuation processes in a gravity-driven hydrogeological environment, from the recharge zones, along the groundwater flow system and towards the discharge areas.
- To provide with a regional hydrogeological database, using GIS tools, that will support decision makers and administrative units, to formulate policies for the management and protection of groundwater resources within the Katari and Lago Menor region. This science-based information will also contribute to the environmental remediation of Lake Titicaca.

## **1.2 Limitations**

The main limitations for developing the conceptual groundwater flow model in the Katari and Lago Menor region, relies on the difficulty of evaluating the hydrogeology of deep and thick flow domains due to the scarcity of data, high exploration costs and technical difficulties (Lemke et al., 2009; Mádl-Szőnyi et al., 2015; Zhou & Heralth, 2017).

Although the research associated to this study was achieved within some practical and financial constraints, the main limitations were the following:

- The lack of sufficient observation wells in order to establish a regional groundwater level monitoring network and obtain time series of groundwater levels for the regional flow system analysis.
- The scarcity of representative aquifer test data for the aquifer.
- The lack of available information about processes of exchange of surface water and groundwater within the basin.
- The lack of available information regarding the quantification of groundwater evapotranspiration in wetlands.
- The scarcity of spring discharge measurements in the groundwater system.

### **1.3 Organization of the thesis**

This manuscript is organized in seven chapters as follows:

1. General Introduction
2. Regional environmental setting of the study site: this chapter describes the climate, geology, and human and physical geography as well as previous research work performed in the domain of paleohydrology, hydrogeology and quality of water resources.
3. Methods and techniques: this chapter explains the field work campaigns, laboratory determination and data analysis methods in order to obtain the different physical parameters of the study domain and the state variables (pressure head and concentrations)
4. Regional geophysical characterization: this chapter is based on the first scientific article that is under revision in Journal of South America Earth Sciences. It relates the characterization of the aquifer domain by means of geophysical, geochemical tools and water level data.

5. Conceptual groundwater flow model: this chapter encompasses the second scientific article describing the conceptualization of the groundwater flow in the study area and the water balance, as well as the first attempt of numerical modelling of groundwater flow in 2D
6. Groundwater basin-scale hydrochemical and dual isotopic characterization: this is the third scientific article in preparation analyzing the main groundwater hydrogeochemical facies, nitrate source, flow and fate in the aquifer.
7. Final conclusions and perspectives.

# Regional Environmental Setting of the Study Site

## 2.1 Location and description

At a regional scale the study site is located within the Katari and Lago Menor Basin, in the semi-arid region of the Bolivian Altiplano.

The Katari and Lago Menor Basin is a high altitude sedimentary basin with an approximate area of 6,350  $Km^2$ . It is bounded by the high mountains of the Eastern Cordillera, the southeast of Lake Titicaca (Lake Huiñamarca) and the outcropping rock formations towards the Tiwanaku, Comanche and Colquencha Cities (Figure 2.1).

## 2.2 Climate

The climate in the Northern Bolivian Altiplano is described as South American Summer Monsoon (SASM) which means that greater than 80% of precipitation occurs in the austral summer (Condom et al., 2004; Placzek et al., 2011; Canedo et al., 2016). In the Katari and Lago Menor Basin the climate is cold and semi-arid with a marked '*Rainy season*' (October to March) and '*Dry season*' (April to September).

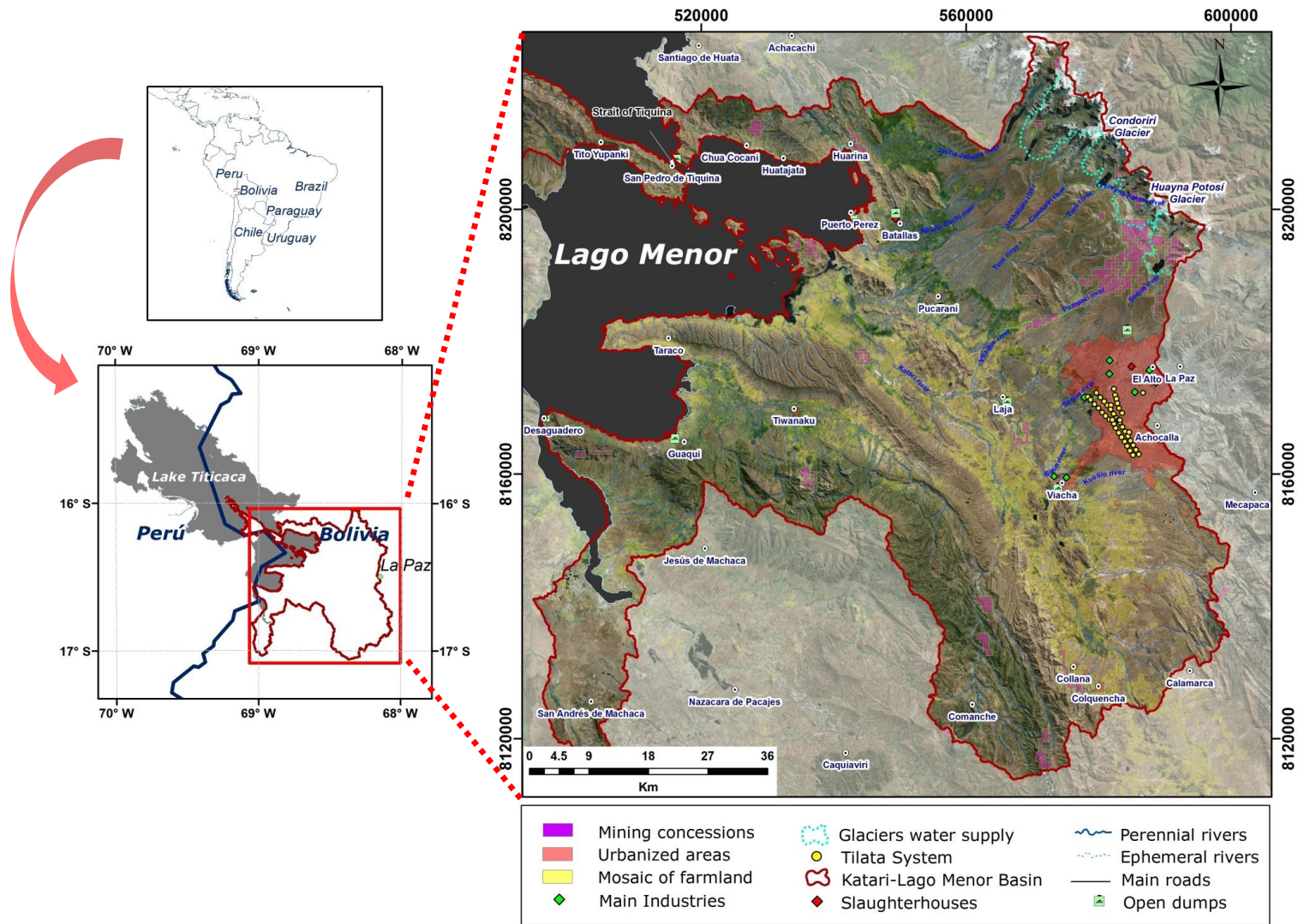


**Figure 2.1.** Geographical context of the Katari and Lago Menor Basin.

### 2.2.1 Precipitation

The precipitation in the Northern Altiplano originates from the east and falls predominantly in the summer months (Plackzec et al., 2011). The total precipitation in the Katari and Lago Menor Basin varies across the basin and depends on the local topography. For instance, in the high peak glaciated areas of the Eastern Cordillera, the mean annual precipitation varies from  $577$  to  $750 \text{ mm} \cdot \text{year}^{-1}$  (Rabatel et al., 2006; Veettil et al., 2018; Kinouchi et al., 2019) while in the low areas, along the shores of Lake Titicaca, reaches a maximum of  $800 \text{ mm} \cdot \text{year}^{-1}$  (Fritz et al., 2007; Delclaux et al., 2007; Pillco et al., 2019).

Figure 2.2, illustrates the long-term variation (2009-2018) of precipitation recorded at El Alto airport station. The total annual precipitation is  $614 \text{ mm} \cdot \text{year}^{-1}$ , average data from 2009 to 2018. About 84% of the total annual precipitation occurs from October through March. June presents the lowest mean monthly precipitation (8.2 mm) and January and February the highest ( $\sim 119.5 \text{ mm}$ ).

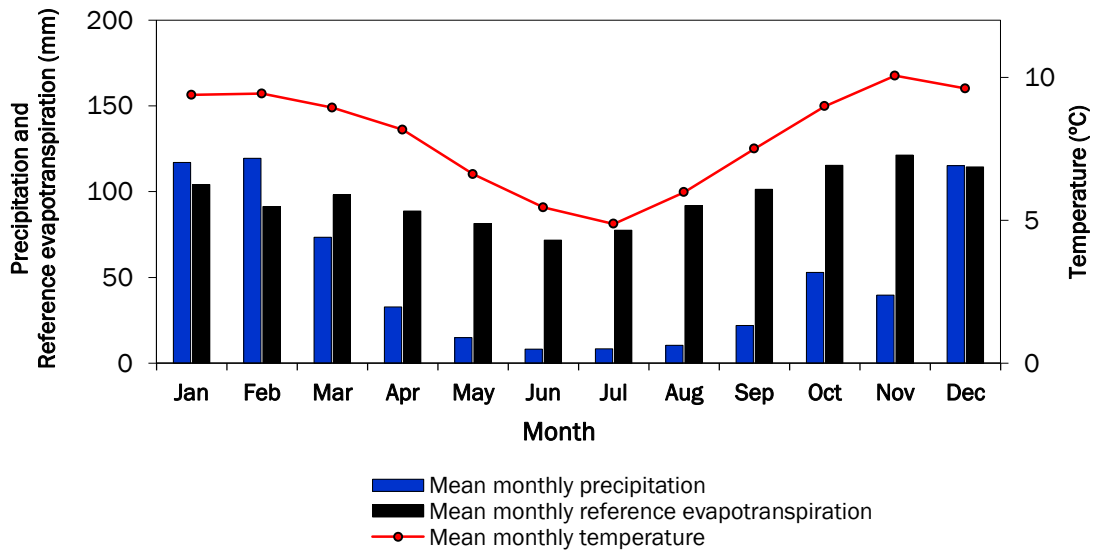


**Figure 2.** Mean monthly precipitation at El Alto airport Station, recorded from 2009-2018 (data available at <http://www.senamhi.gob.bo>).

### 2.2.2 Temperature and Evapotranspiration

Similarly as for precipitation, temperature and evapotranspiration vary across the basin and depending on the local topography.

In fact, the mean air temperature in the high glaciated areas oscillates from 1 to 5 °C (Veettil et al., 2018; Kinouchi et al., 2019). In addition, Kinouchi et al. (2013) demonstrated that sublimation and evaporation in these glaciated areas would account for  $222 \text{ mm} \cdot \text{year}^{-1}$ .

Furthermore, records from El Alto airport station (Fig.2.2) show that the maximum value of air temperature occurs in November (19.5°C) and the minimum in July (-9.0 °C) presenting a mean annual of 7.9 °C. Moreover, the mean monthly reference evapotranspiration computed with daily temperature records (Fig.2.2) show that the total annual reference evapotranspiration is about  $1,157.5 \text{ mm} \cdot \text{year}^{-1}$ .

Finally, in the lower areas, a mean air temperature ranging from 7.7 to 10.8 °C was reported by Pillco et al. (2019) over Lake Titicaca. These authors have also proven that the upper limit of annual Lake evaporation would account for a mean of  $1,700 \text{ mm} \cdot \text{year}^{-1}$ .

## 2.3 Surface topography, drainage, wetland and alpine features

### 2.3.1 Topography

The Katari and Lago Menor Basin presents a high sector of mountainous relief (~6,000 m a.s.l) and a depression sector with a gentler topography (~3,810 m a.s.l) (Figure 2.1).

In the high areas, the peaks comprised in the basin are glaciated (Chacaltaya, Huayna Potosí, Condoriri, Jisk'a Pata), even though most of the glaciers that have been investigated are currently in retreat (Rabatel et al., 2006; Fritz et al., 2007; Soruco et al., 2015; Kinouchi et al., 2013; Kinouchi et al., 2019). In addition, the current geomorphology of the basin show U-shaped deep valleys up-stream of the Seque, Tuni, Condoriri, Jachallani, Khullu Cachi and Jacha Jahuirra rivers, evidencing a glacio-fluvial origin. These valleys were most likely formed during the glacial-interglacial cycles of the Eastern Cordillera (Argollo et al., 2008).

The ancient behaviour of meltwater rivers is of vital importance for understanding groundwater flow dynamics as they could have formed permeable deposits in deep valleys eroded in the the Tertiary/Devonian sedimentary bedrock or in the glacial terrain. In fact, in glaciated terrains, buried valley aquifers are prevalent (Freeze and Cherry, 1979; Sauriol, 2016), they behave as tunnel valleys allowing melt-water drainage and recharging aquifers.

### 2.3.2 *Hydrology network*

Nowadays, the semi-arid climate in the basin, showing annual values of evapotranspiration exceeding precipitation, evidence that the amount of runoff in the study area, is not large enough to currently form integrated drainage networks. In fact, in the high sector, the mountainous relief favour the formation of short straight mountain streams whereas in the lower areas, the gentler topography allows the formation of longer rivers (Fig. 2.1).

Prior research highlighted that four main rivers flows through the southern part of the basin: the Seco, Seke, Pallina and Katari rivers (Fig.2.1). The Seke and Seco rivers flow from the high mountain ranges, above the Milluni Valley, towards El Alto City and discharge into the Pallina river. The Pallina river flows into the Katari river (Archundia et al., 2016). Many of these drainage systems are intermittent and are often dry. According to Archundia et al. (2016) waste-water discharge from El Alto city would be the main source contributing to these rivers's flow.

All the rivers of the Katari and Lago Menor basin discharges its waters directly in to the shallower Lake Huiñamarca which is part of Lake Titicaca (Cross et al., 2001; Fritz et al., 2007; Guédron et al., 2017; Archundia et al., 2017; Pillco et al., 2019).

### 2.3.3 *Wetland ecosystems*

The prevalence of wetland ecosystems in the lower sectors of the Katari and Lago Menor basin (Fig. 2.3) is most likely attributed to: underground barriers allowing groundwater flowing out, geologic phenomena occurring at the foot of hillslopes, or could relate the accumulation of precipitation with low infiltration rates due to the presence of clayey deposits.

Particularly in arid and semi-arid regions, wetland ecosystems are associated to discharge areas of regional gravity-driven groundwater flow systems (Foster et al., 2006; Tóth et al.,

1999). However, they could also be encountered at the perimeter of highly permeable alluvial fans (Woods et al., 2006), or overlying hard or impermeable subsurface layers (Melly et al., 2017).

#### 2.3.4 *Rock glaciers*

Prior research generally confirms that nowadays, in the Eastern Cordillera, rock glaciers are more abundant than glaciers (UNESCO, 2018). Indeed, active rock glaciers (currently moving) and inactive rock glaciers (no movement, but ice is present) were evidenced in the Tuni Condoriri valley and near the Huayna Potosí glacier (Rangecroft et al., 2014). Rangecroft et al. (2016) implicitly indicated that due to future climate warming, by the end of the century, today's intact rock glaciers would become relict forms. Relict rock glaciers are complex hydrogeological systems with high storage capacity (Winkler et al., 2016) that might act as relevant groundwater storages (Pauritsch et al., 2017).

The discharge behaviour of these alpine landforms is also of vital importance for understanding groundwater flow dynamics since they could have a connection with the groundwater system. Indeed, many investigations around the world (Jiráková et al., 2010; Grenier et al., 2012; Kane et al., 2013; Sterckx et al., 2018; Saltel et al., 2019) showed several examples of melt-water recharge or subglacial recharge to aquifers.

## **2.4 Geology and Paleohydrology**

The Katari and Lago Menor Basin consists of erosional landforms in Tertiary and Paleozoic rock formations that are filled up with Pleistocene to recent sediments (Fig. 2.3). These erosional landforms are linked to the Quaternary glaciation considered as the most outstanding dynamic processes carried out in the Eastern Cordillera (Argollo et al., 2008).

As a matter of fact, many well documented studies have been carried out between the Eastern Cordillera and Lake Titicaca region to understand the Quaternary glaciation and the paleo-hydrologic variations of the lake, by means of the application of different methods that includes the use of radiocarbon dating and other isotopic tracers, pollen fossil data analysis, sedimentological and palynological approaches, modelling and high resolution seismic data analysis (Servant and Fontes, 1978; Lavenu, 1992; Argollo et al., 2000; Cross et al., 2001; D'Agostino et al., 2002; Abbott et al., 2003; Heine, 2004; Condom

et al., 2004; Fritz et al., 2006; Fritz et al., 2007; Zech et al., 2007; Bush et al., 2010; Plackzec et al., 2011).

Some authors supported the hypothesis that periods of maximum lake expansion would correspond to the end of a glaciation event and occurred only due to the melting of glaciers (Servant & Fontes, 1978; Lavenu, 1992). However, this hypothesis was later questioned because humid climatic phases would not have been taken into account (Argollo et al. 1995).

Indeed, wet and cold conditions during the regional glacial advance (glacial cycles) and warm and dry conditions during the regional glacial retreat (interglacial cycles) (Fritz et al., 2007), are the main factors that favoured the formation of glacial and lacustrine landforms between the high mountains of the Eastern Cordillera and Lake Titicaca region (Argollo et al., 2000; Cross et al., 2001; Abbott et al., 2003; Fritz et al., 2006; Fritz et al., 2007; Zech et al., 2007; Bush et al., 2010; Plackzec et al., 2011; Quesada et al., 2015).

Therefore, the sediments that fill up the Katari and Lago Menor Basin are the result of erosional processes. Glacial erosion of Silurian and Devonian rock formations in the high mountain ranges and Lake expansion and evaporation processes in the lower areas (Ballivian, 1978; Lavenu, 1992; Argollo et al., 1995; Heine, 2004; Zech et al., 2007; Argollo et al., 2008).

#### *2.4.1 Quaternary stratigraphy*

The unconsolidated sediments that fill up the Katari and Lago Menor basin are classified as high altitude facies, glacial and interglacial deposits in the high peaks and on the piedmont, torrential fluvial deposits on the piedmont and high plain and lacustrine evaporite deposits in the plateau (Lavenu, 1992).

The recognized glacial-interglacial cycles that were taken place in the Bolivian Eastern Cordillera, during the Quaternary glaciation, are: Choqueyapu I, Choqueyapu II, Sorata/Choqueyapu interglacial, Sorata, Kaluyo/Sorata interglacial, Kaluyo, Calvario/Kaluyo interglacial and Calvario (from younger to older) (Ballivian 1978; Lavenu, 1992; Argollo et al., 2008). In addition, the recognized phases of Lake expansion in the northern Bolivian Altiplano, as a result of glacial-interglacial cycles, are: Lake Ballivian, Lake Cabana and Lake Mataro (from younger to older) (Ballivian, 1978;

Lavenu, 1992; Argollo, 2008; Fritz et al., 2004; Sánchez-Saldías et al., 2014). Lavenu (1992) reported that the most ancient deposits, called Mataro, is an ablation surface developed at a present-day altitude 3950 m a.s.l around Lake Titicaca Basin while the sediments of Lake Ballivian correspond to a water body situated at a present-day altitude of 3860 m a.s.l (see Fig. 2.4).

The lithostratigraphy related to the different Quaternary glaciation and tectonic units that make up the geological structure of the Katari and Lago Menor basin are shown in Fig.2.3 and are listed in Table 1 (Article I, Flores-Avilés et al., 2019).

The thickness of the Quaternary deposits, their spatial continuity in depth, and the bottom of these geologic media (depth to the sedimentary bedrock), is poorly known since preceding geological studies showed profiles with a vertical scale not adapted for hydrogeological assessments (Ballivian et al., 1978; GEOBOL & Swedish Geological AB, 1995).

#### *2.4.2 Sedimentary bedrock geology and mineralogy*

The composition of the sediment former rocks is of key importance for understanding the final hydrochemical composition of groundwater in the Katari and Lago Menor Basin.

In the high sector of the basin (Fig. 2.3), the Silurian sequence varies from the stratigraphically lowest Cancañiri Formation (~0-150 m thick), a poorly sorted dark-gray to green diamictite (glacial tillite), to the Uncia Formation (~850-1200m thick) mainly composed of shales, and the stratigraphically highest Catavi Formation (~500-800m thick) made of quartzite and shales, essentially composed of quartz ( $SiO_2$ ), siderite ( $FeCO_3$ ), hematite ( $Fe_2O_3$ ), apatite ( $Ca_5(PO_4)_3F_2$ ) associated with some amounts of pyrite, arsenopyrite, cassiterite, siderite and chlorite (Sugaki et al., 1988; Salvaderry et al., 2007; Murray et al., 2010; Zeballos et al., 2017) (Table 1, Article I). In addition, the Devonian sedimentary sequence comprises the Vila Vila Formation made of quartz sandstones and muscovite rich limolites (Zeballos et al., 2016) (Table 1, Article I).

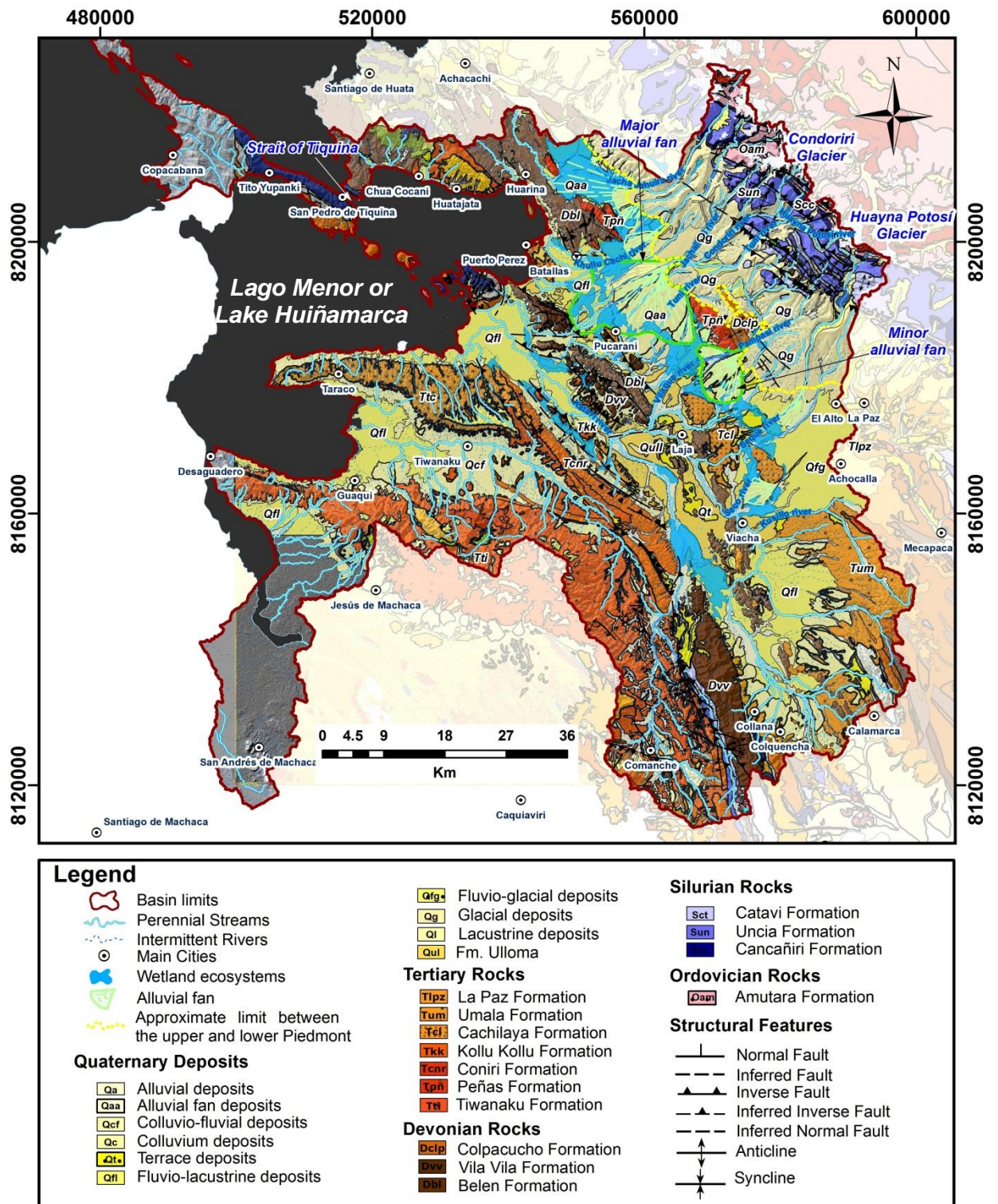


Figure 2. 3. Geological and Structural map of the basin, showing the M.M.A.y.A groundwater monitoring network and the available information (modified from geological data G.E.O.S.I.R.H-2017 and GEOBOL&Swedish Geological AB (1995)).

Furthermore, in the lower sector of the basin, the Devonian Vila Vila Formation is overlaid by the Belen Formation, also devonic in age and composed of siltstones, mudstones and

fine-grained sandstones composed of 55.52 wt% ( $SiO_2$ ); 19.93 wt.% ( $Al_2O_3$ ) (Zeballos et al., 2016). Finally, the Tertiary Kollu Kollu Formation is composed of evaporitic layers such as gypsum and limestone to the top, red shales and sandstones. This deposit is chemically composed of 52.50 wt.% ( $SiO_2$ ); 23.4350 wt.% ( $Al_2O_3$ ) (Zeballos et al., 2017) (Table 1, Article I).

### 2.4.3 *Tectonics*

The Katari and Lago Menor Basin is set within a larger structural basin with complex tectonic characteristics that are related to the Eastern Cordillera and Lake Titicaca domain (Lavenu, 1981; Roeder, 1988; Lamb et al., 1997; Murray et al., 2010).

Prior research substantiates the belief that two tectonic events could have influenced the actual geometry of the Quaternary deposits (Lavenu, 1992). Deposits aged from the upper Pliocene to the early Quaternary were subjected to tectonic compression (reverse faults as a result of a N-S shortening). After this episode of compression and up to now, all Quaternary deposits, in the Altiplano and Piedmonts, were influenced by tectonic extension due to a high topography effect (N-S to N20°E direction). In addition, Fritz et al. (2012) reported the influence of tectonics and geomorphic processes affecting lake-level trends, particularly in the older strata.

## **2.5 Population and Groundwater dependent sectors in the Basin**

The Katari and Lago Menor Basin primarily comprises the metropolitan Cities of El Alto, Viacha, Laja, Pucarani, Batallas and Puerto Pérez (Fig.2.1), being the Cities of El Alto and Viacha the largest cities by population (M.M.A.y.A, 2014).

Projections of population growth in the City of El Alto (I.N.E, 2017) predict that the human population is likely to keep growing, reaching an estimated of 943,558 inhabitants in 2020 while an approximate of 860,062 inhabitants was reached in 2017. Whereas, in the City of Viacha, the population in 2017 was 80,724 and projections predict that the human population will reach an estimated of 88,068 inhabitants in 2020.

In fact, approximately 10% of the Bolivian national population (1 million of inhabitants) inhabits the Katari and Lago Menor Basin, being one of the most populated and deteriorated basins in the country (B.I.D, 2016; Agramont et al., 2019).

### *2.5.1. Groundwater dependent sectors*

The main water uses in the basin are domestic drinking water supply, industry and irrigation (M.M.A.Y.A, 2014). Melted water from the high peak glaciers and groundwater withdrawals are both important sources of water supply for the population in the Katari and Lago Menor basin (M.M.A.Y.A, 2014; Kinouchi et al., 2019).

According to M.M.A.Y.A (2019), the drinking water coverage levels in the largest city of the basin (El Alto) were close to 81 per cent in 2012. About 20 per cent of this coverage level was supplied by groundwater from wells of the Tilata System (M.M.A.Y.A, 2014). Whereas in 2018, the drinking water coverage levels has extended to about 90 per cent, as a result of the Tilata System's expansion through the implementation of new groundwater wells. These new groundwater wells supply water for about 118,823 inhabitants (M.M.A.Y.A, 2019).

Furthermore, a large number of industries in the City of El Alto totally depend on groundwater, although the implementation of private wells for private purposes are not regulated (Bolivian Water Law of 1906, in force at the present; Nickson et al., 2002).

In the case of the City of Viacha, the drinking water coverage levels account for 88 per cent of the population and relies only on groundwater from wells (M.M.A.Y.A, 2014), and in the other cities of the Katari and Lago Menor Basin water supply relies mainly on groundwater either from wells, springs or wetlands.

## **2.6 Potential environmental threats to groundwater resources in the Basin**

### *2.6.1. Sanitation, sewage and waste disposal*

In regards with sanitation, about 95 per cent of the population of the City of El Alto has access to sewage sanitary networks (M.M.A.Y.A, 2019). Indeed, waste water is collected in to the sewage treatment plant (Puchukollo). Although, the Puchukollo plant has exceeded its capacity of collection and treatment facilities due to the accelerated increasing population size (M.M.A.y.A Environmental Audit, 2014; BID 2016; Archundia et al., 2017; Figure 1, Article 3).

Besides that, the City of El Alto operates a sanitary landfill (Villa Ingenio) since 1996, that dispose of leachate collection and bottom sealing systems. According to Barroso et al. (2010) the Villa Ingenio landfill would lie on glacial till materials with low hydraulic conductivities.

Moreover, most of the population in the other cities of the basin lack of adequate disposals of sewage and human waste, instead each house has poorly constructed latrines. On the other hand, they dispose their solid waste in open-air dumps (data available at <http://geosirh.riegobolivia.org>).

Therefore, municipal and industrial wastewater, as well as the inadequate disposal of solid waste, could represent a major environmental threat to groundwater resources in the basin.

#### *2.6.2. Farmland and livestock practices*

Weather and soil conditions benefit farming practices in the basin. Indeed, excluding the city of El Alto, considered as a major industrial city (Archundia et al., 2017), about 65 per cent of the total population in the basin are dedicated to agricultural and livestock activities. They cultivate primarily potatoes, onions, barley, beans and a variety of vegetables, and raise bovine, ovine and camelid cattle (M.M.A.y.A, 2014; Figure 1, Article 3).

The increasing demand of agricultural production due to population growth can result in a higher demand for the use of mineralised and organic fertilizers (F.A.O, 1999) representing also a threat to groundwater resources.

#### *2.6.3. Mining activities*

Mining is concentrated in the upper part of the basin, close to the Milluni lake (data available at <http://geosirh.riegobolivia.org>). Most of these mines presents environmental liabilities which mainly consists of rock dumps and tailing dams without proper management (M.M.A.y.A Environmental Audit, 2014). Even though that mining activities has stopped in the 90's, the impact of mining waste (Fe, Mn, Zn, As, Cd, Ob, Cu, Sn) on water quality remains a serious environmental problem (Salvaderry et al., 2008).

## 2.7 Previous hydrogeological studies in the Basin

Within the frame of the Katari “Pedagogic River Basin Programme” (M.M.A.y.A, 2010; Agramont et al., 2019), the Bolivian Ministry of Water and Environment (M.M.A.y.A), have been investigating and monitoring groundwater resources primarily in the largest cities of the basin (El Alto and Viacha). The zone of investigation known as Purapurani (Fig.2.4) has an approximately area of  $370 \text{ Km}^2$ . It was delimited according to a lithologic composition and stratigraphy of Quaternary sediments: fluvio-glacial and alluvial deposits (supposedly saturated) surrounded by glacial deposits to the north, and the Paleozoic and Paleogene rocks towards the west and south (M.M.A.y.A, 2014).

According to M.M.A.y.A (2016) the fluvio-glacial materials are mainly composed of sands, gravels and clays, and are considered as potential permeable layers with an hydraulic conductivity ranging from  $2.0 \times 10^{-4} - 1.3 \times 10^{-6} \text{ m/s}$ . Preliminary results in the Purapurani zone, based on long-term groundwater level monitoring data (50 observation wells), suggest that groundwater flow direction is coherent with the NE-SW surface topography. However, close to the east boundary, groundwater flow diverts towards the valleys of the City of La Paz.

Even though, the available lithology information of boreholes drilled at a depth of 60 meters (G.E.O.S.I.R.H, 2016) evidence layers of gravel origin with predominantly gravel materials that comprises: medium gravel granular materials varying from 60 to 80%, clay materials varying from 30% to 10% and fine sand materials (10%). There are no studies that report the thickness of these deposits (depth to the substratum) and their spatial continuity (hydraulic continuity). The geometry, bottom boundaries and spatial continuity of hydrogeological layers play a vital role in the development of groundwater investigations.

Furthermore, Barroso et al. (2010) conducted a detailed hydrogeological assesment in the Quaternary glacial deposits located to the north of the Purapurani zone. The aim of this assesment was to identify the level of risk that the “Villa Ingenio” sanitary landfill would possess to groundwater. This author concluded that the landfill had been placed over clayey Glacial-till materials of granite blocks, quartzite, quartzose and intermingled sand, with horizontal hydraulic conductivities ranging from  $1.2 \times 10^{-8} - 3.3 \times 10^{-7} \text{ m/s}$ .

## 2.8 Previous Hydrochemical and Isotopic studies in the Basin

The Ministry of Water and Environment (M.M.A.y.A) have been working at the implementation of monitoring programs of quantity and quality in the Purapurani zone since 2010 (M.M.A.y.A, 2016). In this context, they have been working in coordination with the IAEA (International Atomic Energy Agency), within the Project “Using Isotopes for Hydrogeological Assessment of Intensively Exploited Aquifers in Latin America (ARCAL CXXVII), and with the University of San Francisco Xavier de Chuquisaca (Master’s thesis).

They have conducted several sampling campaigns in this zone (Fig.2.4) and monitored around 50 points of groundwater (wells, springs) and surface water (rivers) sources, since 2010. Thus, major ion facies of water, stable isotopes of oxygen 18 and deuterium, and radioactive isotopes of carbon 14 and tritium information is available at M.M.A.y.A (2016).

Generally, groundwater in the Purapurani zone present  $Ca(Mg) - HCO_3^-$  and  $Na(K) - HCO_3^-$  facies. However, there are increasing trends of  $Cl^-$ ,  $NO_3^-$  and  $SO_4^{2-}$  in some sectors that could be related to anthropogenic and mining sources of contamination (Limpas et al., 2010; Gómez et al., 2012; M.M.A.y.A, 2016). In addition, isotopic results of deuterium and oxygen 18 in groundwater hosted in the Purapurani zone, showed values isotopically lighter suggesting that recharge of groundwaters were ancient and originated from rains or glacial melting of a different climatic regime (M.M.A.y.A, 2016).

Furthermore, Barroso et al. (2010) reported that groundwater hosted in the glacial-till materials present predominantly  $Ca(Mg) - HCO_3^-$  facies.

Finally, Quino et al. (2019) conducted a local hydrochemical assessment of groundwater hosted in plain area of the Katari and Lago Menor Basin (lower Katari). These authors concluded that  $Ca(Mg) - HCO_3^-$ ,  $Ca - Cl$  and  $Na - HCO_3^-$  groundwater facies were not clearly defined.

All the available hydrogeological and hydrochemical data, resultant of the previous local research performed in the study area, are valuable for creating a regional hydrogeological database. Moreover, a basin-scale investigation is compulsory for the correct interpretation

of natural flow processes and phenomena, and the comprehension of the final hydrochemical composition of groundwater.

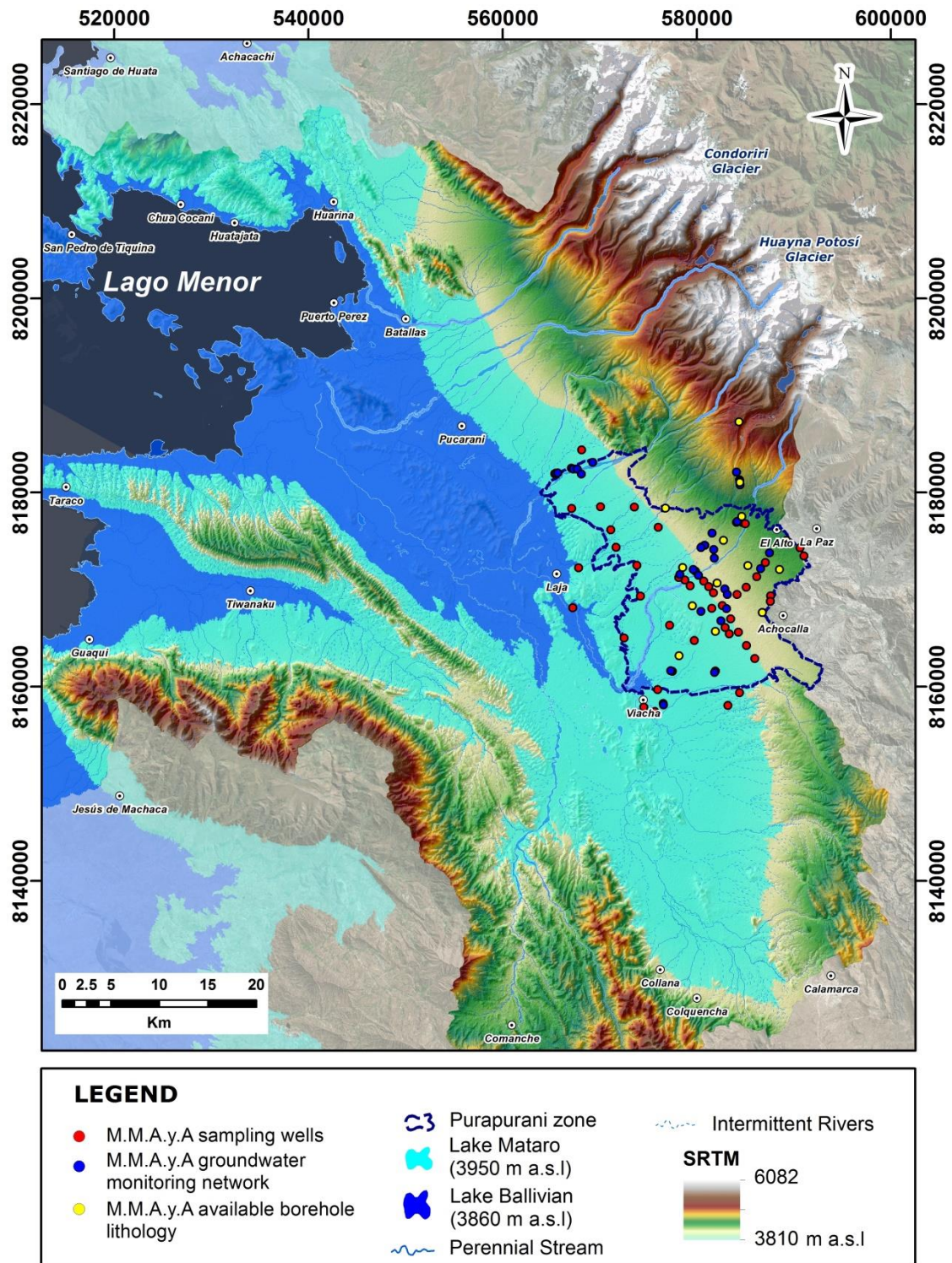


*Figure 2. 4. Hypsometric map showing ancient lake invasions and previous hydrogeological information in the Purapurani zone. Hypsometric colours represent the elevation in meters above the sea level (m a.s.l.) of the terrain (DEM: SRTM 1-Arc-Second Global-N.A.S.A, 2000).*

## Methods and Techniques

### 3.1 Introduction

The evaluation of basin-scale groundwater flow systems allows the understanding of a wide range of natural phenomena and processes that relates topography, geology and climate (Tóth, 1999; Navarro de León et al., 2005; Zhou & Li, 2011). Conceptual groundwater flow models are simplified versions of the real-world groundwater problem such that it captures the essential features of the real-world problem and that it can be described mathematically (Anderson, Woessner & Hunt, 2015). They are considered as the foundation of computer-based numerical groundwater flow modeling (Bredehoeft et al., 2005; Izady et al., 2015; Zhou & Heralth, 2017).

Regional conceptual groundwater flow models should include the major physical processes operating within a particular hydrogeologic environment and the generalized boundaries of the system (Tóth et al., 1999; Zhou & Li, 2011; Sahoo et al., 2017). The main components that control groundwater flow regime in a hydrogeologic environment are topography, geology and climate (Tóth et al., 1999; Navarro de León et al., 2010). The main limitations for developing conceptual groundwater flow models relies on the difficulty of evaluating regional hydraulic continuity and evaluating the hydrogeology of deep and thick flow

domains due to the scarcity of data, high exploration costs and technical difficulties (Tóth et al., 1995; Lemke et al., 2009; Mádl-Szőnyi et al., 2015; Zhou & Heralth, 2017).

In fact, several investigations around the world have documented that the application of one investigation technique is not sufficient for developing conceptual models of complex hydrogeological systems, becoming even more difficult when hydrogeological data is limited (Zhou & Li, 2011; Lachaal et al., 2011; Turner et al., 2015; Saroli et al., 2017; Bayanzul et al., 2018). A basin-scale investigation is necessary for the correct interpretation of natural flow processes and phenomena in the site. The first step for developing conceptual groundwater flow models in any study, consists of planning and designing strategies for field data collection using all the applicable methods (Bredehoeft, 2005; Zhou & Li, 2011).

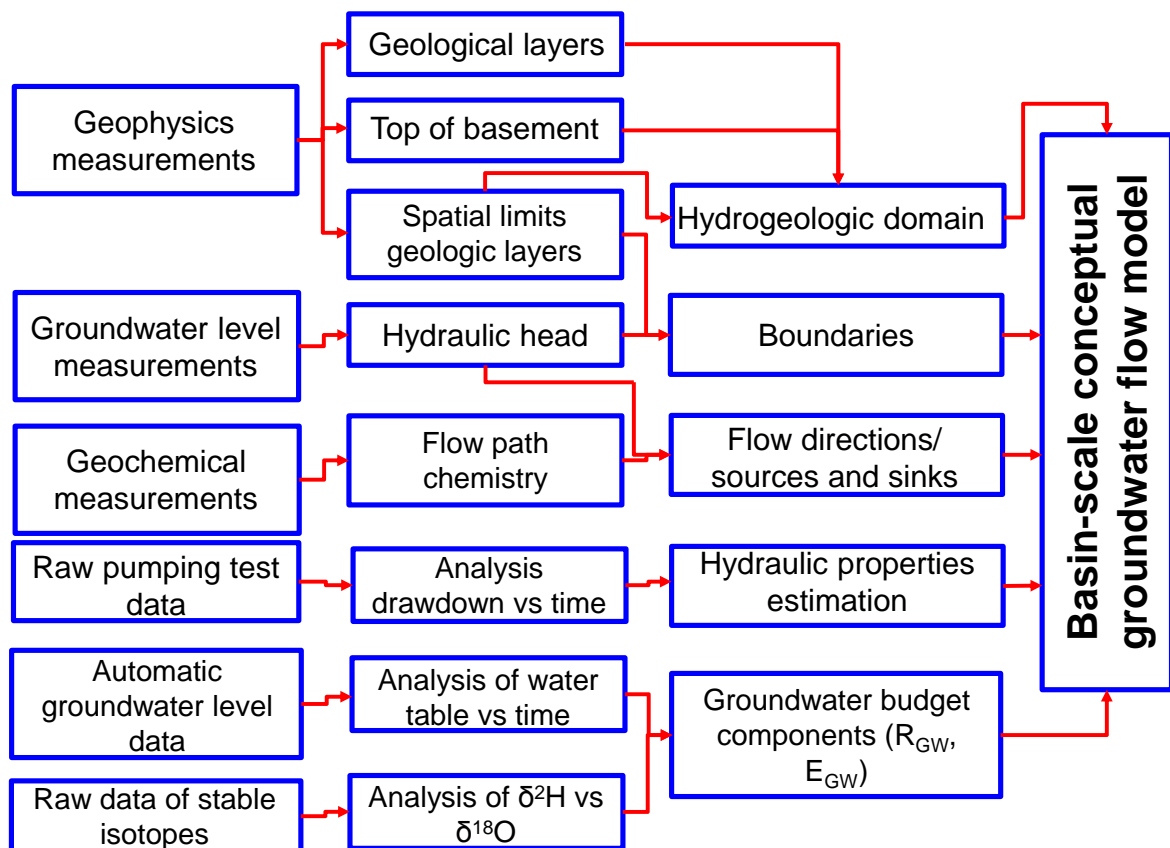


**Figure 3.1.** General methodology for developing a basin-scale conceptual groundwater flow model for the Katari and Lago Menor region

The flowchart in Figure 3.1 presents the general methodology for developing a basin-scale conceptual groundwater flow model. This methodology facilitated the compilation and

interpretation of hydrogeological results deduced from different investigation techniques. Initially, the available information of borehole lithology, spatial surface geology/structural map (G.E.O.S.I.R.H, 2017), and topography of the site (Digital Elevation Model (DEM) (Shuttle Radar Topography Mission 1 Arc-Second Global -SRTM-GL1) (NASA, 2000), allowed designing survey strategies for conducting a geophysical characterization, the design and construction of new piezometers, a groundwater source inventory and water level measurements and a regional sampling campaign for measuring geochemical and isotopic parameters.

The integrated spatial data permitted identifying the hydrogeologic domain, the boundaries of the aquifer, flow directions, sources and sinks, the estimation of hydraulic properties and some of the groundwater budget components. The basin-scale conceptual groundwater flow model allows explaining the subsurface flow movement at the scale of the basin.

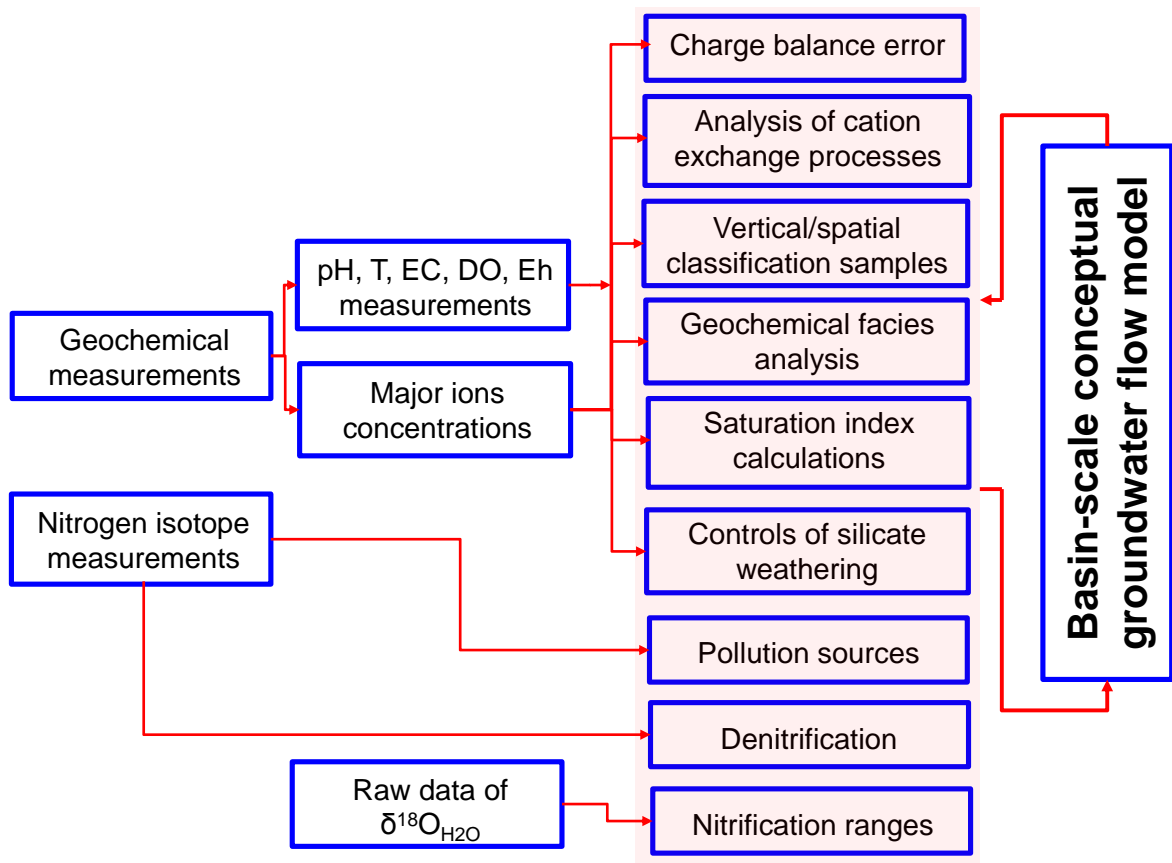


**Figure 3.2.** General methodology for the application of the hydrogeochemical and dual isotopic approach within the Katari and Lago Menor Basin aquifer.

Subsequently, flowchart 3.2 shows the methodology used for the application of the hydrogeochemical and dual isotopic approach.

In fact, geochemical and isotopic data allows explaining the factors responsible for the hydrochemical composition and evolution of groundwater, the potential sources of contamination and the potential nitrate contribution to the eutrophication of Lake Titicaca within the Katari and Lago Menor Basin-aquifer.

In this context, the research work associated with this study is subdivided in: fieldwork, laboratory work and data analysis. Several tasks are comprised within these categories and are addressed in the different manuscripts presented in Chapter 4, 5 and 6 (Article I, Article II and Article III).

## **3.2 Field work**

### *3.2.1. Sampling campaign*

A regional sampling campaign was conducted in the Katari and Lago Menor Basin during April and May of 2017, at the end of wet season. A total of 75 water samples were collected from groundwater and surface water sources for the analysis of major ion chemistry and dual isotopes of  $\delta^{15}N_{NO_3}$  and  $\delta^{18}O_{NO_3}$ . The main objectives for performing this campaign were to: i) verify and validate groundwater sources for the establishment of a regional groundwater monitoring network, ii) ascertain regional groundwater flow paths in the basin, iii) investigate the systematic changes of water's anion facies along flow systems and with depths, iv) identify the main sources of nitrate contamination, v) determine the possible processes (nitrification/denitrification) that could modify groundwater nitrate concentrations, and vi) evaluate its potential contribution to the eutrophication of Lake Titicaca.

Therefore, groundwater samples were collected from 52 deep wells (30–110 m b.g.l), 5 springs and 2 wetlands. Most of the wells were provided with electrical pumps or they presented the artesianism phenomena. Surface water were retrieved from rivers (8), lagoons (3) in the upper part of the glaciated peaks and from the shore of Lake Titicaca (5) (Figure 3.4).

The flowchart in Figure 3.4 display the general steps and procedures performed in the field to measure major ions and isotopic compositions. Samples for the analysis of major cations and anions were filtered in-situ using 0.45  $\mu\text{m}$  cellulose acetate siringe filters (millipore). Filtrate samples used for anion quantification were frozen in unwashed falcon tubes while filtrate samples for cation measurements were acidified with ultrapure 2%  $\text{HNO}_3$  and stored at 4°C until analysis. Total alkalinity was measured in the field by the titration method (HACH digital titrator method) and recalculated as bicarbonate.



**Figure 3.3.** Some sampling sites and the equipment carried out into the field: a) Lagoon located in the upper part of the basin nearby the glaciated peaks, b) wetland located in the low Piedmont area, c) Deep well located in a Pumping station, d) Deep well presenting the artesianism phenomena, d) Shore of Lake Titicaca and e) Field equipment for measuring water quality parameters and alkalinity.

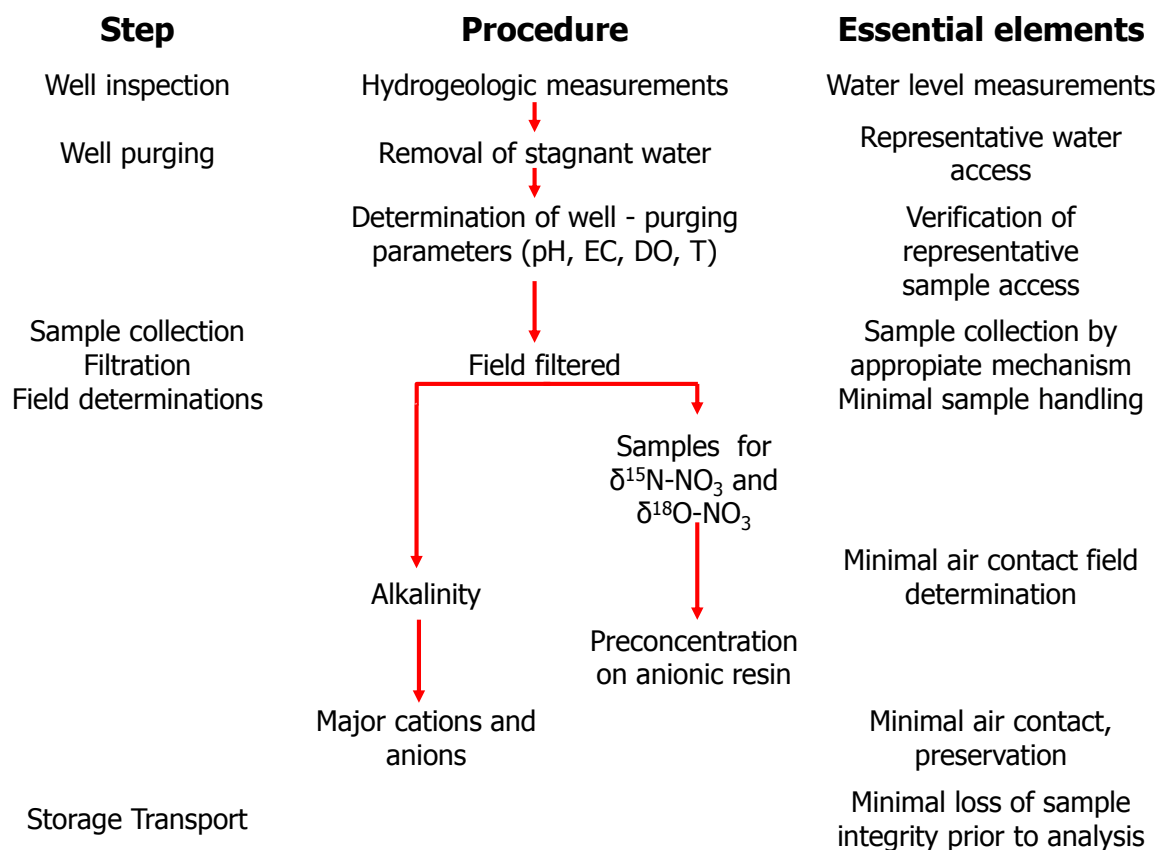


**Figure 3.4.** Flowchart for Sampling groundwater monitoring points and performing geochemical field measurements.

This sampling campaign was conducted following standard international guides, methods and procedures for sampling groundwater monitoring wells (ASTM D4448-0, 1994; Nielsen, 2006; Schwartz & Zhang, 2003; Mazor, 2004) for the proper sampling and geochemical field measurements to ensure high quality analysis, reliable interpretation of data and consistency for the incorporation in a regional hydrogeological database.

### 3.2.2. Groundwater source inventory and water level measurements

A regional field campaign, for inventorying groundwater sources and measuring groundwater levels, was carried out during August of 2017. A total of 97 sources were verified and validated in the field: 19 artesian wells, 36 deep wells, 32 dug wells, 8 springs and 2 wetlands (Fig.3.5). The main objectives for performing this regional field campaign were to: i) verify and validate groundwater sources for the establishment of a regional groundwater monitoring network, ii) construct a contour map of groundwater levels for

assessing lateral groundwater inflow and outflow and iii) propose a regional groundwater level monitoring network in order to obtain time series of groundwater levels, essential for the construction of regional transient groundwater models.

The groundwater source inventory consisted in the field verification of well conditions or groundwater sources (i.e. springs, wetlands). Each site was georeferenced, with a GPS Garmin Etrex 30 (position accuracy less than 15 meters and +/- 400 ft of height-based on an ellipsoid and not on a vertical datum). Groundwater level measurements were performed using a water level meter Solinst of 100 meters, graduated to millimeter.

The common difficulty experienced when measuring groundwater levels was that most of the wells were provided with submersible electrical pumps. Although it was ensured that the well was not pumped at least 48 hours before measuring groundwater levels, technical issues related to the water well system constrained the progress of this campaign. For this reason, the design, construction and installation of new piezometers were necessary for establishing a regional groundwater level monitoring network in the study site.



**Figure 3.5.** a) Device used for measuring the location of each inventoried groundwater source and example of groundwater level measurements performed in the field, b) deep well, c) well in a pumping house provided with a submersible pump and d) dug well.

### 3.2.3. Geophysical measurements

A regional field campaign, for performing Time Domain Electromagnetic measurements (TDEM) was conducted during June and July of 2017. The main objectives of conducting this campaign were to: i) investigate electrical resistivity parameters of Quaternary, Tertiary and Devonian rock formations, ii) investigate regional hydraulic continuity in the basin, iii) investigate the geometry (depth and thickness) of potential porous geologic media.

Therefore, a total of 187 TDEM (Time Domain ElectroMagnetic) soundings were performed in the field with a TEMfast 48 equipment (AEMR technology, The Netherlands) (Fig. 3.6). TDEM measurements were performed using a coincident loop configuration, a transmitter/receiver (Tx/Rx) loop of 100 x 100 m<sup>2</sup> and a 25 x 25 m<sup>2</sup> (or 50 x 50 m<sup>2</sup> loop when urban sites were surveyed). Detailed explanation about the TDEM method, survey strategy and data processing is presented in Chapter 4 (Article I).



**Figure 3.6.** a) TEMfast 48 equipment used for measuring resistivity parameters in the field and b) Example of setting the coincident loop configuration in the field.

### 3.2.4. Piezometer construction and installation

A total of five new piezometers were installed in the Katari and Lago Menor Basin during the first semester of 2018 (Table 3.1). These piezometers were installed in order to: i) investigate temporal variations of groundwater-lake interactions, ii) study the connection between the piedmont and plain areas through a buried channel, iii) investigate the behavior of temporal groundwater levels in a natural wetland area, iv) incorporate

observation wells in a regional groundwater level monitoring network and for v) monitoring groundwater quality.

**Table 3. 1.** Location and position of the new piezometers using the Universal Transverse Mercator (UTM) coordinate system.

Code	Diameter (in)	Depth of well from top of casing (m)	Casing stickup (m above ground surface)	UTM Easting (m)	UTM Northing (m)	Depth of well from surface (m a.s.l)
P-1	2	50	0.4	545835	8200738	3778.1
P-2	2	35	0.4	545348	8193806	3794.0
P-3	2	26	0.4	553770	8189721	3831.9
P-4	2	16	0.4	553530	8195571	3863.1
P-5	2	53	0.4	545039	8185793	3776.9

The design, construction and location of these piezometers were performed following the results of the geophysical investigation and groundwater source inventory. There were also taken into account the field considerations for designing and installing Groundwater Monitoring Wells reported by Nielsen (2006) and Sanders (1998).

Figure 3.7 displays the design and location of each piezometer. Piezometer design consisted of a 2 in PVC casing and a slotted casing screen of 20 meters of length wrapped with a nytex mesh of 500  $\mu\text{m}$ . The screen slot size of 0.020 in was manually performed in the field in order to retain the natural fine materials. According to geophysics, the lengths of these screens allow the study of two different flow domains in the groundwater system presenting different hydraulic properties and electrical conductivities.

C.O.F.A.D.E.N.A was contracted for drilling the boreholes and performing the piezometers installations. The direct mud rotary method was used for drilling 6 in boreholes at each site location. Basically, this method uses a drilling fluid that consists of water and bentonite and the hole is advanced by the rotational action of a drill string. This kind of drilling used tricone roller bits and allowed obtaining small cores every meter of drilling. Therefore, detailed stratigraphic descriptions were performed in the field. After completing the borehole drilling, C.O.F.A.D.E.N.A installed the piezometers.

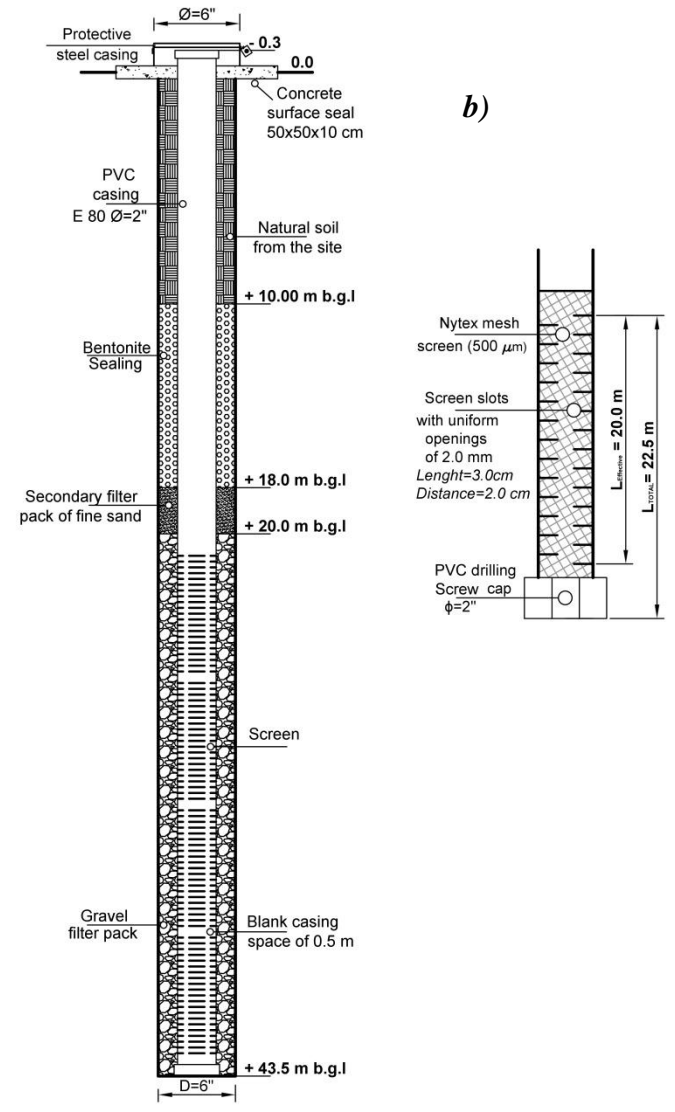
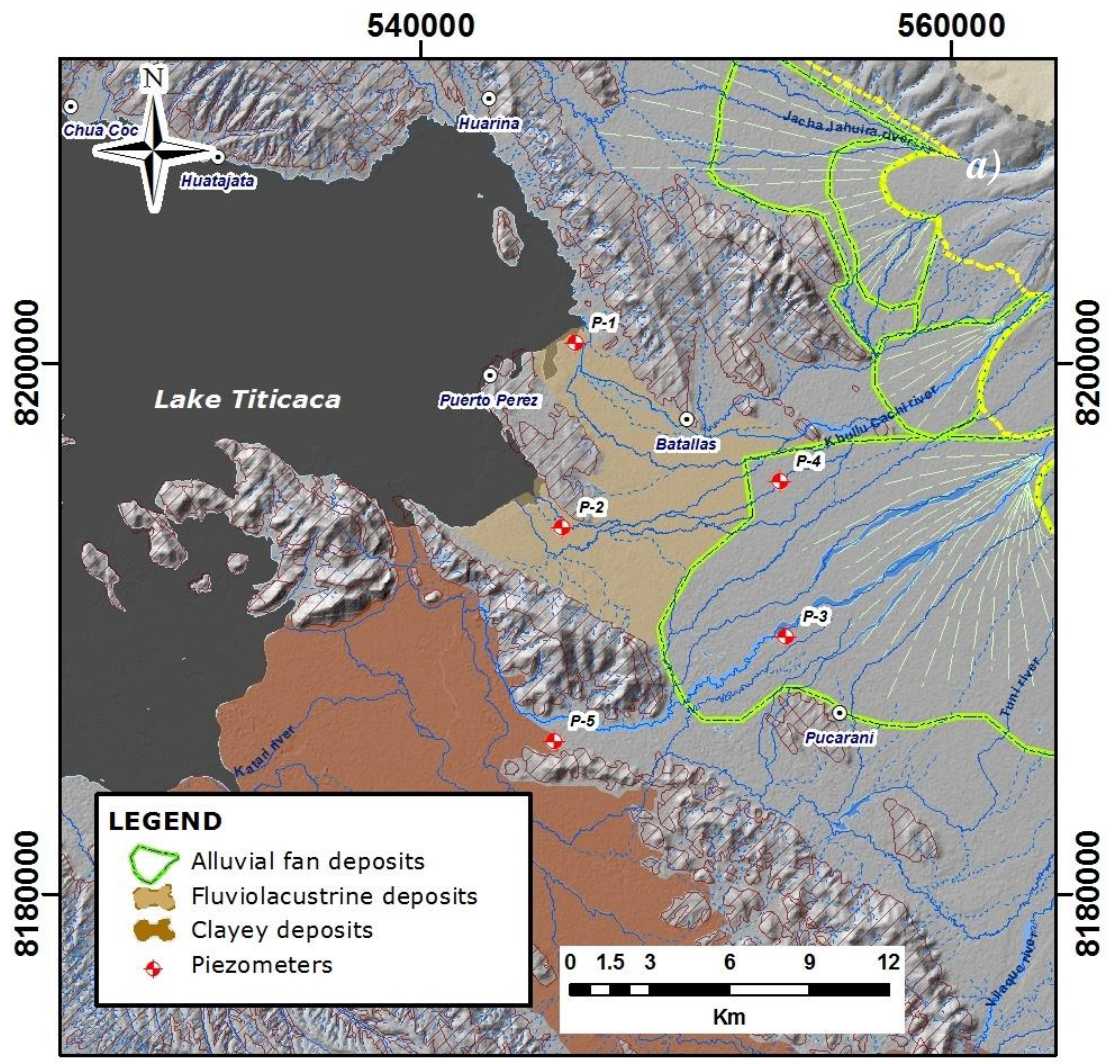


Figure 3.7. a) Location of the new piezometers and b) example of design and constructive details of piezometer P-1. Each piezometer consists of a 2 in PVC single-casing, single-screen for collecting water level data and water samples.

Afterwards, according to the design (Fig. 3.5) the filter pack that consisted of very well-sorted gravel materials of 0.125 *in* of size was extended 3 *ft* above the screen as recommended by Nielsen (2006). There were required 0.35  $m^3$  of gravel for each 6 *in* borehole. Then a secondary filter pack of fine-sand was placed to prevent bentonite grout infiltration through the primary filter pack. This secondary filter pack was extended 2 meters above the primary filter pack as depicted in Fig. 3.5.

Besides, an annular seal of bentonite grout (0.20  $m^3$ ) was placed above the secondary filter pack in order to avoid any potential vertical movement of water contaminants. Then, natural soil material, was used to fill up the borehole until reaching ground surface. Finally, a surface seal of concrete of 50 × 50 × 10 *cm* surrounding the piezometer casing extended at least 20*cm* above the surface (Fig. 3.5). Each piezometer was secured with an additional 6 *in* steel casing as displayed in the design figure.

After the piezometer installation was completed, development was performed by surging and pumping with compressed air for around 12 hours in order to remove the fine materials, stabilize the filter pack and maximize the hydraulic connection between the well and the adjacent formation material.

Figure 3.8 shows a summary of the procedure followed for drilling and completing each of the piezometers.

In addition, groundwater levels were measured manually and then four levelloggers (Solinst) were installed in the monitoring piezometers: P-1, P-2, P-3, and P-5 (Fig. 3.5). Levelloggers measure temporal variations of water pressure and electrical conductivity every hour. Besides, a Barologger (Solinst) was installed in the monitoring piezometer P-2, for measuring barometric fluctuations and compensating levelloggers measurements. Automatic water pressure measurements for the estimation of groundwater recharge were recorded between August of 2018 and March of 2019. Data processing and interpretation are explained in Chapter 4 (Article II and Appendix). Moreover, automatic water pressure measurements are still being recorded for evaluating groundwater level fluctuations changes and estimating groundwater recharge.



**Figure 3.8.** *Drilling and piezometer completion in the Katari and Lago Menor Basin. a) On-site drilling equipment, b) detailed stratigraphic record, c) PVC casing screening and installation of the piezometer, d) water level measurement after the development, f) Completion of the piezometer with a surface seal and a protective casing for providing piezometer security and e) piezometer development.*

### 3.3 Laboratory work

Samples for isotopic analyses ( $\delta^{15}N_{NO_3}$  and  $\delta^{18}O_{NO_3}$ ) were preconcentrated on an anionic resin (0.3mL AG 1-X8 resin, Bio-Rad) and eluted with 10 mL of a 1M NaCl solution (Bourgeois I et al., 2018; Erbland, 2012), during the regional sampling campaign, in the Chemical Institute Laboratory at the UMSA (University of San Andrés) (Fig. 3.7). After, isotopic compositions of  $\delta^{15}N_{NO_3}$  and  $\delta^{18}O_{NO_3}$  were quantified, at the IGE (Institut des

Géosciences de l'Environnement) Laboratory, using the bacterial denitrifier method (Sigman et al., 2001; Kendall et al., 2007) and conducted on a MAT 253 IRMS Mass Spectrometer (Kaiser et al., 2007).



**Figure 3.9.** a) Samples for major ion analysis, b) materials for the preconcentration procedure, c) Samples (1 liter) were poured in the funnels and drained by gravity, d) preparation of the 10 ml eluted samples by the addition of bacteria in order to ensure 100 nmol of  $\text{NO}_3$  and a matrix volume of NaCl, e) 12 hours of incubation, then NaOH was added for trapping nitrogen dioxide in each vial, and finally isotopic compositions were measure in the f) MAT 253 IRMS Mass Spectrometer.

Chemical analyses were also performed at the IGE laboratory. Major ion concentrations were measured by ion chromatography using the Metrohm 732/733 modular system, precision  $\pm 0.1 \text{ mg/L}$ , and calibrated with standard solutions Roth (5 to 40 mg/L range). The calibration procedure for the Ion cromathography is described in Spadini (2013).

### **3.4 Data analysis methods**

From the above mentioned field campaigns, a large quantity of new data was generated at a regional scale. The data vary primarily over space but also over time (automatic water pressure measurements). These data were analyzed in order to obtain meaningful interpretations. The data analysis process included statistical, graphical and the use of software packages such as TEM-RESearcher (A.E.M.R, 2012) for 1D inversion of TDEM soundings, AUTOCAD (Autodesk, 2019) for the analysis of Topographic profiles, Diagrammes (Simler, 2014) for the geochemical data processing. The results of these analysis are described in detail in Chapter 4, 5 and 6 (Article I, Article II and Article III).

Finally, all the data that were validated after the analysis process, were arranged into a spatial database using GIS tools (ESRI ArcMap 10.x). The integrated spatial data will help to obtain information regarding the hydrogeological layers, the aquifer system characteristics and the water quality conditions within the Katari and Lago Menor region.

# Regional geophysical characterization

## 4.1 Introduction

Prior investigations in the study area reported very local hydrogeological characterizations (~6 % of the total surface of the basin) based on lithology, groundwater level measurements, hydrochemistry, stable isotopes of deuterium and oxygen 18, and radioactive isotopes of tritium and carbon-14 (M.M.A.y.A, 2016; Quino et al., 2019). Moreover, due to the lack of geophysical information it was not possible to identify neither regional hydraulic continuity, nor bottom boundaries or the spatial and vertical variation of the porous geologic media. The recognition of regional cross-formational hydraulic communication and bottom boundaries is of vital importance for the correct interpretation of natural flow processes and phenomena (Tóth, 1995; Tóth, 1999; Mádl-Szőnyi et al., 2015).

This chapter explains the results of the regional geophysical characterization performed in the Katari and Lago Menor Basin. The results are presented following the basic structure of a typical scientific article which is under revision in the Journal of South American Earth Sciences. This article aims to characterize: i) the regional continuity and geometry of the Quaternary porous geologic media, ii) the bottom boundaries of the aquifer (depth to the top of the Tertiary/Devonian sedimentary bedrock) and couple groundwater level

measurements and geochemical data in order to iii) propose the groundwater flow dynamics at a basin-scale.

## **4.2 Article I: Insight into the Katari-Lago Menor Basin aquifer, Lake Titicaca-Bolivia, inferred from geophysical (TDEM), hydrogeological and geochemical data**

**Gabriela Patricia Flores Avilés<sup>1,2 a</sup>, Marc Descloitres<sup>1</sup>, Céline Duwig<sup>1</sup>, Yvan Rossier<sup>1</sup>, Lorenzo Spadini<sup>1</sup>, Anatoly Legchenko<sup>1</sup>, Álvaro Soruco<sup>3</sup>, Jaime Argollo<sup>3</sup>, Mayra Pérez<sup>3</sup>, Waldo Medinaceli<sup>4</sup>**

<sup>1</sup> Univ. Grenoble Alpes, IGE, IRD, CNRS, Grenoble-INP \*, 38000 Grenoble, France

<sup>2</sup> Ministerio de Educación Estado Plurinacional de Bolivia (Ministry of Education), La Paz, Bolivia

<sup>3</sup> University Mayor of San Andrés (UMSA), La Paz, Bolivia

<sup>4</sup> Ministerio de Medio Ambiente y Agua (Ministry of Water and Environment of Bolivia), La Paz, Bolivia

\* Institute of Engineering Univ. Grenoble Alpes

<sup>a</sup>gpfloresaviles@gmail.com

### *Abstract*

The increasing demand for water and irrigation in the semi-arid Bolivian Altiplano requires a better knowledge of the available resources, particularly groundwater. The aim of this study is to provide a first insight into the hydrogeological structure (0-200 m deep) and groundwater dynamics of the Katari-Lago Menor Basin aquifer located between the Eastern Cordillera and Lake Titicaca, Bolivia. This aquifer is studied using geophysical data (a total of 187 Time Domain Electromagnetic (TDEM) soundings), piezometric data (97 groundwater level measurements) and geochemical data (52 groundwater samples), combined with geological, lithological and topographical information.

The results allowed identifying stratigraphic models consistent with the Quaternary sediments being hydraulically connected and behaving as a single regional basin-aquifer. This basin-aquifer is delimited by the most ancient lake invasions towards the southern, western and northern sides and by the lower limit of rock glaciers towards the eastern side. A large portion of the aquifer presents an unconfined behaviour varying from 50 to 150 meters while the confined portion varies from 100 to 150 meters.

Groundwater flow within the Katari and Lago Menor Basin aquifer is composed of several interconnected groundwater flow systems. The main groundwater flow system starts in the

high mountain ranges of the Eastern Cordillera, follows the topographic Piedmont gradient (NE to SW) and discharges in a series of wetlands.

This multidisciplinary approach proved to be an appropriate method to derive a consistent picture of the hydrogeological functioning of the Katari-Lago Menor Basin aquifer.

**Keywords:** Katari-Lago Menor Basin aquifer, groundwater resources, Time-Domain Electromagnetic soundings

### *1. Introduction*

Water quality degradation, climate variability and population growth are among the factors that constrain water availability in the semi-arid Bolivian Altiplano (Coudrain et al., 1994; Guérin et al., 2001; Garcia et al., 2010; Archundia et al., 2017a, 2017b; Guédron et al., 2017; Quino et al., 2019; Gómez et al., 2019) and in the central parts of Bolivia (González-Amaya et al., 2018a, 2018b), leading to an increasing exploitation of groundwater resources.

In the Katari and Lago Menor Basin (Fig.1), one of the most populated and contaminated basins of the Bolivian Altiplano (BID, 2016; Agramont et al., 2019), melt water from the high peak glaciers of the Eastern Cordillera and groundwater withdrawals, are both important sources of water supply for domestic drinking, industry and irrigation purposes (M.M.A.yA, 2014; Soruco et al., 2015; Kinouchi et al., 2019). Recent research predicted that climate variability and population growth will most likely lead to a water shortage after the mid-2020s (Kinouchi et al., 2019) which could intensify groundwater exploitation in order to meet the growing demand.

To contribute to the sustainable management of groundwater resources within the Katari and Lago Menor Basin, the understanding of the main natural flow processes of the groundwater system at the basin scale is essential for developing numerical groundwater flow models, evaluating recharge, discharge, aquifer storage, and sustainable yield. Previous investigations on the site showed local-scale hydrogeological characterizations based on lithology, groundwater level measurements, hydrochemistry and stable isotopes of deuterium and oxygen 18 (M.M.A.yA, 2016; Quino et al., 2019). However, the lack of geophysical information did not allow the identification of vertical, lateral or spatial

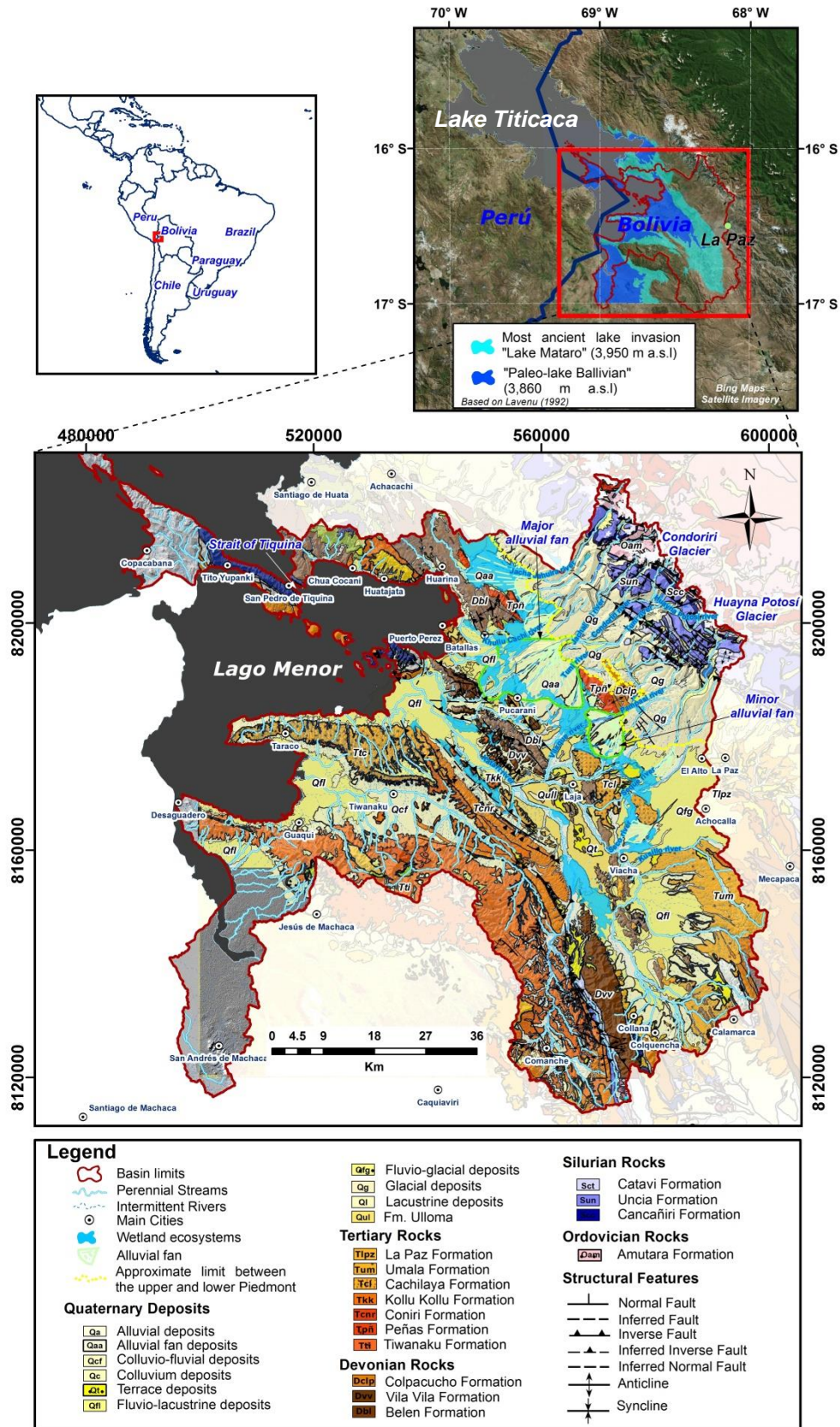


Figure 1. (Top left) Location of the study area in South America. (Top right and Bottom) Study area showing the Katari and Lago Menor Basin, situated at the southeast of Lake Titicaca. It also shows the Geological and Morphostructural features of the basin (Based on geological data from G.E.O.S.I.R.H (2017) and GEOBOL & Swedish Geological AB (1995)).

variation of the permeable Quaternary geologic media nor the bottom boundaries of the aquifer or aquifers (depth to bedrock).

Additionally, former geological studies showed profiles describing general geological formations to a depth of 1 km (Ballivian et al., 1978; GEOBOL & Swedish Geological AB, 1995). This vertical scale is not suitable for the assessment of shallow (0-200 m) groundwater investigations. Indeed, in this depth range, the thickness and lateral extent (geometry), hydraulic properties and hydrostratigraphic units of the aquifer are not known.

Moreover, little is known about the potential influence of sewage, waste disposal, farmland and mining activities on groundwater resources of the basin (Barroso, 2010; M.M.A.yA, 2016; Quino et al., 2019; Archundia et al., 2017b). Actually, most of the rural communities in the basin rely mainly on groundwater either from wells, springs or wetlands. However, they lack of adequate disposals of sewage and human waste (M.M.A.yA, 2014). A basin-scale groundwater investigation is necessary for understanding the main physical, chemical and biological processes.

The understanding of the main natural flow processes of the groundwater system requires the delimitation of the domain, the determination of the boundaries and initial conditions, and the physical characteristics of the porous media. A combination of tools is needed to adequately characterize the aquifers in this region. Previous research across the world, including South America, have shown that the application of multidisciplinary studies can contribute to the understanding of the functioning of complex hydrogeological systems (Guerin et al., 2001; Ramos et al., 2014; Mira et al., 2015; Gómez et al., 2016; Gómez et al., 2019; Gonzales Amaya et al., 2018a, 2018b; Maldonado et al., 2018; Viguier et al., 2018).

The aim of this study is to provide a first characterization of the aquifer at the scale of the Katari and Lago Menor Basin. To achieve, this objective, we conducted a multidisciplinary study (geology, geophysics, geochemistry, and groundwater level measurements). The specific objectives were to determine: i) the spatial limits of the aquifer, ii) the vertical and lateral variation of the Quaternary geologic media, iii) the bottom boundaries of the aquifer (depth to the top of the Tertiary/Devonian bedrock), and to characterize iv) the groundwater flow dynamics at the scale of the Katari-Lago Menor Basin.

Finally, we propose a 3D conceptual model of the aquifer structure and its functioning as a basis for assessing the current knowledge of groundwater resources, possible development of numerical models and therefore development of future groundwater management strategies in the Bolivian Lake Titicaca region.

## *2. Background information on the study area*

The study site is located within the Katari and Lago Menor Basin, in the semi-arid region of the Bolivian Northern Altiplano. The Katari and Lago Menor Basin is a sedimentary basin with an approximate area of  $6350 \text{ km}^2$  and it is bounded by the high mountains of the Eastern Cordillera, the southeast of Lake Titicaca (Lago Menor or Lake Huiñamarca) and the outcropping rock formations towards the Tiwanaku, Comanche and Colquencha Cities (Fig.1).

Previous studies have documented that Lake Titicaca comprises two, nearly separated basins connected by the strait of Tiquina: (i) the Lago Menor (also called in some studies Huiñamarca) Basin (Fig.1) averaging  $1428 \text{ km}^2$  and 9 m depth (up to 40 m depth) and (ii) the Lago Grande Basin averaging  $7131 \text{ km}^2$  and 125 m depth (up to 284 m depth) (Cross et al., 2001; Fritz et al., 2006; Fritz et al., 2007).

### *2.1 Geology*

The Katari and Lago Menor Basin consists of erosional landforms in Tertiary and Paleozoic sedimentary rock formations that are filled up with Pleistocene to Holocene sediments (Fig. 1). These landforms were influenced by Quaternary glaciations of different ages and extensions. These Quaternary glaciations are related to the Andes Cordillera uplift and large-scale climatic patterns (Argollo and Iriondo, 2008; Araos et al., 2017; Emmer et al., 2019). Indeed, wet and cold conditions during regional glacial advance (glacial cycles) and warm and dry conditions during regional glacial retreat (interglacial cycles) (Fritz et al., 2007), are the main climatic patterns that favoured the formation of glacial and lacustrine landforms between the high mountains of the Bolivian Eastern Cordillera and Lake Titicaca region (Argollo and Mourguiart, 2000; Cross et al., 2001; Abbott et al., 2003; Fritz et al., 2006; Fritz et al., 2007; Zech et al., 2007; Bush et al., 2010; Plackzec et al., 2011; Quesada et al., 2015).

Therefore, the deposits that fill up the Katari and Lago Menor basin result from glacial erosion of the Paleozoic (Silurian/ Devonian) sedimentary sequence from the high mountain ranges, and lake expansions and evaporation processes in the lower sectors (Ballivian, 1978; Lavenu, 1992; Argollo and Mourguiart, 1995; Heine, 2004; Zech et al., 2007; Argollo and Iriondo, 2008). Lavenu (1992) classified these deposits as: i) glacial and interglacial deposits in the high peaks and on the piedmont, ii) torrential fluvial deposits on the piedmont and high plain, and iii) lacustrine evaporite deposits in the plateau. Additionally, the occurrence of alluvial fan deposits in the study area is controlled by topography. They are formed close to steep sided mountains or hills (waved glacial deposits) flanked by areas of low relief (Fig.1).

In this paper, we propose to describe our results considering two major geomorphological domains: the “Piedmont subsystem” and the “Lacustrine plain”.

The “Piedmont subsystem” starts from the outcropping Silurian formations (in the high mountain ranges of the upper eastern area) and reaches the outcropping Devonian formations (i.e. Dvv and Dbl) to the southwest (towards Pucarani, Laja and Viacha Cities) (Fig.1). The Piedmont subsystem is subdivided into the upper and lower Piedmont areas (Fig.1). The upper Piedmont area corresponds to a significant accumulation of glacial and fluvioglacial outwash deposits (Ballivian, 1978; Lavenu, 1992; Argollo and Mourguiart, 2000; Argollo and Iriondo, 2008), whereas the lower Piedmont area is characterized by fluvial-alluvial and/or fluvioglacial outwash deposits sometimes overlying ancient lacustrine deposits. Additionally, the occurrence of two alluvial fans formed at the mouths of the Tuni and Condoriri rivers in the NW and the Sorechata and Pampasi rivers in the SE, are denominated as major and minor alluvial fans, respectively (Fig.1).

The “Lacustrine plain” is bounded by those Devonian formations (i.e. Dvv and Dbl) and the Tertiary formations (i.e. Tkk, Tcn and Ttc) outcropping between the Taraco, Collana and Colquencha Cities (Fig.1). The Lacustrine plain is characterized by the presence of lacustrine deposits that are related to the ancient lake invasions. According to Lavenu (1992), the present Lake Titicaca overlays deposits from Paleo-lake Ballivian “Ulloma Formation, Qull” (Fig.1) which hosts vast clay resources (Zeballos et al., 2017), while deposits from the most ancient Paleo-lakes Mataro and Cabana underlying the Ulloma Formation are series of fluvial detrital deposits (Table 1).

Generally, the thickness of these Quaternary deposits, their spatial continuity, and the depth to bedrock, are poorly known. Preceding geological studies showed profiles with a vertical scale (1 km) not suited for hydrogeological assessments (Ballivian et al., 1978; GEOBOL & Swedish Geological AB, 1995). The Quaternary glaciation history indicates that the permeable Quaternary geologic sediments could be associated with: Early-Pleistocene glacial deposits, Late-Pleistocene fluvioglacial outwash deposits, or Late-Pleistocene lacustrine deposits (Table 1).

Furthermore, the Tertiary/Devonian/Silurian sedimentary sequence is dominated by shales and sandstones (Salvaderry-Aranguren et al., 2008; Murray et al., 2010; Zeballos et al., 2017). These sedimentary units are rich in ore and clay minerals and are extracted for the mining and ceramic industries (Sugaki, 1988; Salvaderry-Aranguren et al., 2008; Zeballos et al., 2017). However, there is no evidence that they are significant aquifers with exploitable groundwater. In this study, these Tertiary and Paleozoic sedimentary formations are assumed to be the impervious bottom of the Quaternary geologic media containing water.

Considering the recognized glacial-interglacial cycles and lake expansions between the Bolivian Eastern Cordillera and the Bolivian Northern Altiplano, the lithostratigraphy and geological structure that make up the Katari and Lago Menor Basin, are shown in Figure 1 and listed in Table 1 (from younger to older) (Ballivian, 1978; Lavenue, 1992; GEOBOL & Swedish Geological AB, 1995; Suárez-Soruco and Díaz-Martínez, 1996; Argollo and Mourguiart, 2000; Heine, 2004; Argollo and Iriondo 2008; Fritz et al., 2004; Salvaderry et al., 2008; Murray et al., 2010; Sánchez-Saldías et al., 2014; Zeballos et al., 2016 ; Zeballos et al., 2017).

## 2.2 *Climate*

The climate in the Katari and Lago Menor region could be described as South American Summer Monsoon reported in several studies for the Northern Altiplano (Condom et al., 2004; Placzek et al., 2011; Canedo et al., 2016). It presents a cold and semi-arid climate with a marked 'Rainy season' (October to March) and 'Dry season' (April to September). The annual precipitation and evapotranspiration also varies across the basin and depends mainly on the local topography.

In the high peak glaciated areas (Huayna Potosí, Condoriri glaciers) of the Eastern Cordillera (Fig.1), the mean annual precipitation varies from 577 to 750  $mm\ year^{-1}$  (Rabatel et al., 2006; Veetil et al., 2018; Kinouchi et al., 2019) while the sublimation and evaporation in these glaciated areas accounts for 222  $mm\ year^{-1}$  (Kinouchi et al., 2013). Additionally, on the piedmont, daily long-term variations (2009-2018) of precipitation recorded at El Alto airport station (Fig.1) showed that the mean annual precipitation reaches 614  $mm\ year^{-1}$  and the mean annual potential evapotranspiration 1158  $mm\ year^{-1}$ . Finally, in the lower sectors, long-term variations of precipitation reported by Geerts et al. (2009), at the Huarina station (Fig.1), showed that the mean annual precipitation reaches up to 513  $mm\ year^{-1}$ , whereas the estimated actual crop evapotranspiration for quinoa cultivation would vary around for 350 to 500  $mm\ year^{-1}$ .

### *2.3 Hydrogeological setting of the study area*

Previous local-scale research has investigated and monitored groundwater resources primarily in the two largest cities of the Katari and Lago Menor Basin (El Alto and Viacha, Fig.1) (M.M.A.yA, 2016). M.M.A.yA (2014) delimited the Purapurani zone (370  $Km^2$ ) (Fig.2) according to the lithology and general stratigraphy of the Quaternary deposits: fluvio-glacial and alluvial deposits surrounded by glacial deposits to the north, and the Paleozoic rocks towards the west and south.

The lithological information of several boreholes drilled in the Purapurani zone to a depth of 60 to 110 meters (GEOSIRH, 2017) indicated that the Quaternary geologic media is saturated. However, there are no studies that reported the total thickness of these deposits (depth to bedrock) or their spatial continuity (hydraulic continuity).

Field data from two pumping tests performed by M.M.A.yA established that fluvio-glacial materials in the Purapurani zone behave as potential permeable layers with a hydraulic conductivity ranging from  $1.3 \times 10^{-6}$  to  $2.0 \times 10^{-4}$   $m/s$ . Moreover, long-term groundwater level monitoring data (50 observation wells) have shown that groundwater flow direction, towards NE to SW in this zone, is consistent with flow from the high surface elevations to the low elevations. Close to the east boundary, groundwater flow diverts in the SE direction, towards the valleys of the City of La Paz (M.M.A.yA, 2016).

Barroso (2010) conducted a detailed hydrogeological assessment in the location of El Alto Sanitary landfill (Fig.2), towards the NE of the Purapurani zone. This author concluded

that the landfill had been placed over clayey glacial-till materials of granite blocks, quartzite, quartzes and intermingled sand, with horizontal hydraulic conductivities ranging from  $1.2 \times 10^{-8}$  to  $3.3 \times 10^{-7}$  m/s.

Table 1. Lithostratigraphy of the study area (literature review Ballivian, 1978; Lavenu, 1992; GEOBOL & Swedish Geological AB, 1995; Suárez-Soruco and Díaz-Martínez, 1996; Argollo and Mourguiart, 2000; Heine, 2004; Argollo and Iriondo 2008; Fritz et al., 2004; Salvaderry et al., 2008; Murray et al., 2010; Sánchez-Saldías et al., 2014; Zeballos et al., 2016 ; Zeballos et al., 2017).

System	Epoch	Piedmont subsystem <sup>1</sup>				Lacustrine plain		
		Quaternary Glaciations	Formation/Deposit	Symbol	Lithology	Formation/Deposit	Symbol	Lithology
Quaternary	Holocene		Alluvial deposits	Qaa*	Pebbles, gravels, sand and silt	Fluvio lacustrine deposits	Qfl	Gravels, sands, silt and clay
			Low Terrace			Deposits (Lake Titicaca)	Ql	Silts, clays and sands
			High Terrace	Qt	Pebbles, gravel, sand, silt and clay	<i>Erosion surface</i>		Evaporites
	Upper Pleistocene	Choqueyapu Glaciation (Stage 2)	Choqueyapu II Formation	Qg	(Frontal moraines)	Deposits (Paleo-lake Tauca)		No influence in the Northern Altiplano
		Choqueyapu Glaciation (Stage 1)	Choqueyapu I Formation	Qg	(Lateral moraines)	Deposits (Paleo-Lake Minchin)		No influence in the Northern Altiplano
			<i>Ablation surface</i>		Gravels and soils (fluvial erosion)	<i>Erosion surface</i>		Alluvial/Colluvial - Dunes deposits
		Sorata Glaciation	Sorata Formation	Qg	Moraine ridges and flow-tills (clasts and blocks of quartzites, shales and granites in a clayey matrix)	Ulloma Fm.(Deposits from Pale-lake Ballivian)	Qull	Well stratified fine sands with an alternation of clayey and silty layers
			<i>Ablation Surface</i>		Gravel and soils (red horizon with iron accumulations)*			
	Lower Pleistocene	Kaluyo Glaciation	Kaluyo Formation	Qg	Tills composed of striated rock blocks with an intercalation of fluvio-glacial gravels	Paleo-lacustrine deposits (Paleo-lake Cabana)		Clay and sand laminae with banks of gravels and sands ~50m thickness (presence of halite/gypsum evaporites)
		Purapurani Formation	Qfg	Conglomerates with rounded elements (Upper part) and gravels in a clayey matrix with paleo-soil levels and clayey intercalations (Lower part)		Qcb-mt		
Calvario glaciation		Calvario Formation	Qg	Tills of gravels and blocks (mainly granites) in a silty-sandy matrix. The upper part of this till presents fluvial gravels	Paleo-lacustrine deposits from Paleo-lake Mataro		Alternation of clay-sandy banks and sand-gravelly layers ~50m thickness (presence of halite/gypsum evaporites)	
		Precalvarian Deposits		Gravels				
		<i>Erosion Surface</i>		Red paleo-soil				

\* Alluvial fan deposits (Qaa) could also represent a significant accumulation of Pre-Sorata gravels (Argollo and Iriondo, 2008)

<sup>1</sup> Ancient lake invasions could have reached the lower Piedmont area (Lavenu, 1992). Therefore, paleo-lacustrine deposits could underlay Pleistocene glacial and/or fluvio-glacial eposits.

Table 1, continued

<b>Tertiary</b>	Pliocene	La Paz Formation	Tlp Fm.	Clay-sandy well stratified deposits with different levels of cinerita tuff	Taraco Formation	Ttc	Red-orange conglomerates and sandstones
	Upper Miocene	Cachilaya Formation	Tcl Fm.	Polymictic conglomerates, claystones with tuff levels			
	Lower Miocene-Upper Oligocene	Kollu Kollu Formation	Tkk Fm.	Series of gypsum-bearing sandstones and claystones of lacustrine facies (evaporitic layers to the top)	Kollu Kollu Formation	Tkk	Series of gypsum-bearing sandstones and claystones of lacustrine facies (evaporitic layers at the top of the Formation)
		Peñas Formation	Tpñ Fm.	Reddish polymorphic conglomerates and sandstones	Coniri Formation	Tcnr	Reddish polymorphic conglomerates and sandstones
<b>Devonian</b>	Late-Middle	Colpacucho Formation	Dclp Fm.	Shales and finely stratified siltstones and powerful sandstone banks			
	Early	Belen Formation	Dbl Fm.	Alternation of fine-grained sandstone and shabby grayish-black shales	Belen Formation	Dbl	Alternation of fine-grained sandstone and shabby grayish-black shales
		Vila Vila Formation	Dvv Fm.	Sandstones and quartzite banks of medium grain with crossed stratification (highly weathered siltstones)	Vila Vila Formation	Dvv	Sandstones and quartzite banks of medium grain with crossed stratification (highly weathered siltstones)
<b>Silurian</b>	Pridoli	Catavi Formation	Sct Fm.	Black shales and sandstones deformed by faults and folds			

The wetland ecosystems are other significant features that could be part of the groundwater system. Several investigations around the world have shown that in arid and semi-arid regions, wetland ecosystems can be associated with discharge areas of regional gravity-driven groundwater flow systems (Foster et al., 2006; Tóth et al., 1999). In the study area, the wetlands located in the lower sectors of the Piedmont subsystem (Fig. 1) are associated with groundwater discharges controlled by the topography and geology (i.e. large alluvial fans). Another type of wetlands, formed over impermeable subsurface layers (i.e. clay deposits), are encountered in the Lacustrine plain. According to Melly et al. (2017) these type of wetlands, overlying hard or impermeable subsurface layers are called “perched wetlands”.

Finally, the presence of active or inactive rock glaciers located in the upper part of the basin, in the Tuni Condoriri valley and near the Huayna Potosí glacier (Rangecroft et al., 2014), could also be linked to the regional groundwater system as a recharge source for the aquifer. Rangecroft et al. (2016) demonstrated that these rock glaciers would become relict forms, by the end of the century, due to future climate warming. Relict rock glaciers are complex hydrogeological systems with high storage capacity (Winkler et al., 2016; Harrington et al., 2018) that might act as relevant groundwater storages (Pauritsch et al., 2017; Jones et al., 2019).

### *3. Materials and Methods*

In this study, the general methodology that facilitated the interpretation and compilation of hydrogeological results are deduced from the application of a multidisciplinary approach (geology, geophysics, geochemistry, and groundwater level measurements). This approach was proved to be useful in other groundwater systems in South America (Guerin et al., 2001; Ramos Ramos, 2014; Mira et al., 2015; Gómez et al., 2016; Gómez et al., 2019; Gonzales Amaya et al., 2018a, 2018b; Maldonado et al., 2018; Viguier et al., 2018).

For instance, several studies can be cited in the northern Chile such as the multidisciplinary study conducted by Viguier et al. (2018) in the hyperarid Atacama Desert, the multi-method assessment performed by Oyarzún et al. (2014) in the semi-arid Limarí River basin, and the groundwater recharge assessment carried out in the arid Salar del Huasco basin (Uribe et al., 2015). Additionally, in Argentina, Mira et al. (2015) integrated geological and geophysical data to build a geological subsurface model for the Corrientes province aquifer. Maldonado et al. (2015) combined hydrogeochemical and groundwater

level data to assess the deep aquifers from the Pampean plain (Maldonado et al., 2015). Furthermore, in Brazil, Fernandes et al. (2016) used physical and structural geology data to develop a preliminary conceptual model of groundwater flow for the Serra Geral basalt aquifer.

In Bolivia, local groundwater investigations mainly relate the application of geophysical techniques. For example, Guérin et al. (2001) used geophysical surveys and groundwater electrical conductivity measurements to identify saline groundwater in the semi-arid Bolivian Altiplano. Gómez et al. (2019) performed electromagnetic soundings and electrical resistivity tomography to investigate the thickness of an alluvial aquifer and to delineate the relief of the bedrock. Gonzáles Amaya et al. (2018a) used hydrogeophysics to refine hydrogeological conceptual models. Additionally, these authors (Gonzales Amaya et al., 2018b) used transient electromagnetic soundings for mapping saline water zones in the semiarid Punata alluvial fan, in the Central part of Bolivia. Following those approaches, we used a combination of geophysical, groundwater levels and geochemical measurements.

### *3.1 Time Domain Electromagnetic (TDEM) soundings*

#### *3.1.1 TDEM principle*

Time Domain Electromagnetic (TDEM) is a geophysical sounding method based on the investigation of the electrical resistivity of rocks. Resistivity is a well-known parameter in hydrogeophysics. For our study, electrical resistivity is a well adapted parameter because our objective is to discriminate permeable formations from more clayey formations, possibly identify conductive brackish groundwater close to the lake (if any) or any lateral variations of groundwater electrical conductivity. Previous studies have demonstrated the usefulness of TDEM for groundwater investigations in arid and semi-arid areas, as highlighted by Descloitres et al. (2013) in the semiarid Lake Chad Basin (Niger), Viguiet et al. (2018) in the hyperarid Atacama Desert (Northern Chile), or by Guérin et al. (2001) and Gonzales Amaya et al. (2018) in the semiarid Altiplano (Bolivia).

Basically TDEM uses a large transmitter (Tx) square loop (typically 50x50m<sup>2</sup> or 100x100m<sup>2</sup>) and a receiver loop (Rx) both laid out on the surface. Rx can be either a small coil at the centre of Tx (central loop system), or be the same cable as Tx (coincident loop system, as used in our study). A direct current is injected in Tx creating a primary static magnetic field that diffuses into the ground. Once the primary magnetic field is

established, the current is abruptly turned-off creating a decreasing flux with time. Due to the induction principle, eddy currents are then created in the soil immediately below Tx cable. As the time elapse, and because the primary magnetic field no longer exists, the eddy current are decreasing with time and further current loops are created deeper and expand laterally in the sub-surface, as smoke rings. Each eddy current loop creates a secondary magnetic field (with the same polarity that the primary magnetic field) also decreasing with time, creating an induced current in Rx loop. The result (the decreasing voltage with time) is then analysed to derive the basic information given by TDEM: the sounding curve, i.e the variation of apparent resistivity with time. Field data are then fitted to simulated data curves, using a layered resistivity model of the ground by means of an automatic adjustment (inversion) of a starting 1-D model with a minimum of layers (usually 3). If the RMS calculated after the inversion remains high (i.e. above 2-3 %) one or two additional layers are introduced to smooth the model and decrease the RMS. The final results are interpreted as a 1-D (layered) model of the resistivity with depth, which can be related to the geology and related aquifers. Further information can be found in the comprehensive review of TDEM for groundwater exploration published by Fitterman and Stewart (1986).

### *3.1.2 TDEM survey strategy and interpretation*

The locations of the TDEM profiles were chosen in order to investigate the different outcropping formations (Tertiary/Devonian substratum) and the different Quaternary deposits (alluvial fan, fluvio-glacial, glacial, paleo-lacustrine and fluvio-lacustrine deposits). The locations of these profiles are presented in Figure 2.

Profile 1 is 44 km long (75 soundings, Table 2), and has a NE-SW direction. It stretched from the Eastern Cordillera to the Piedmont subsystem and the Lacustrine plain. This profile investigated also Devonian and Tertiary formations perpendicular to their main structural direction. It crosses Quaternary glacial and fluvio-glacial deposits, alluvial fan deposits, and paleo-lacustrine deposits.

Profile 2 is 33 km long (32 soundings, Table 2), and has a SE-NW direction. It is perpendicular to profile 1 is used to explore Quaternary fluvio-glacial, alluvial fan and paleo-lacustrine deposits.

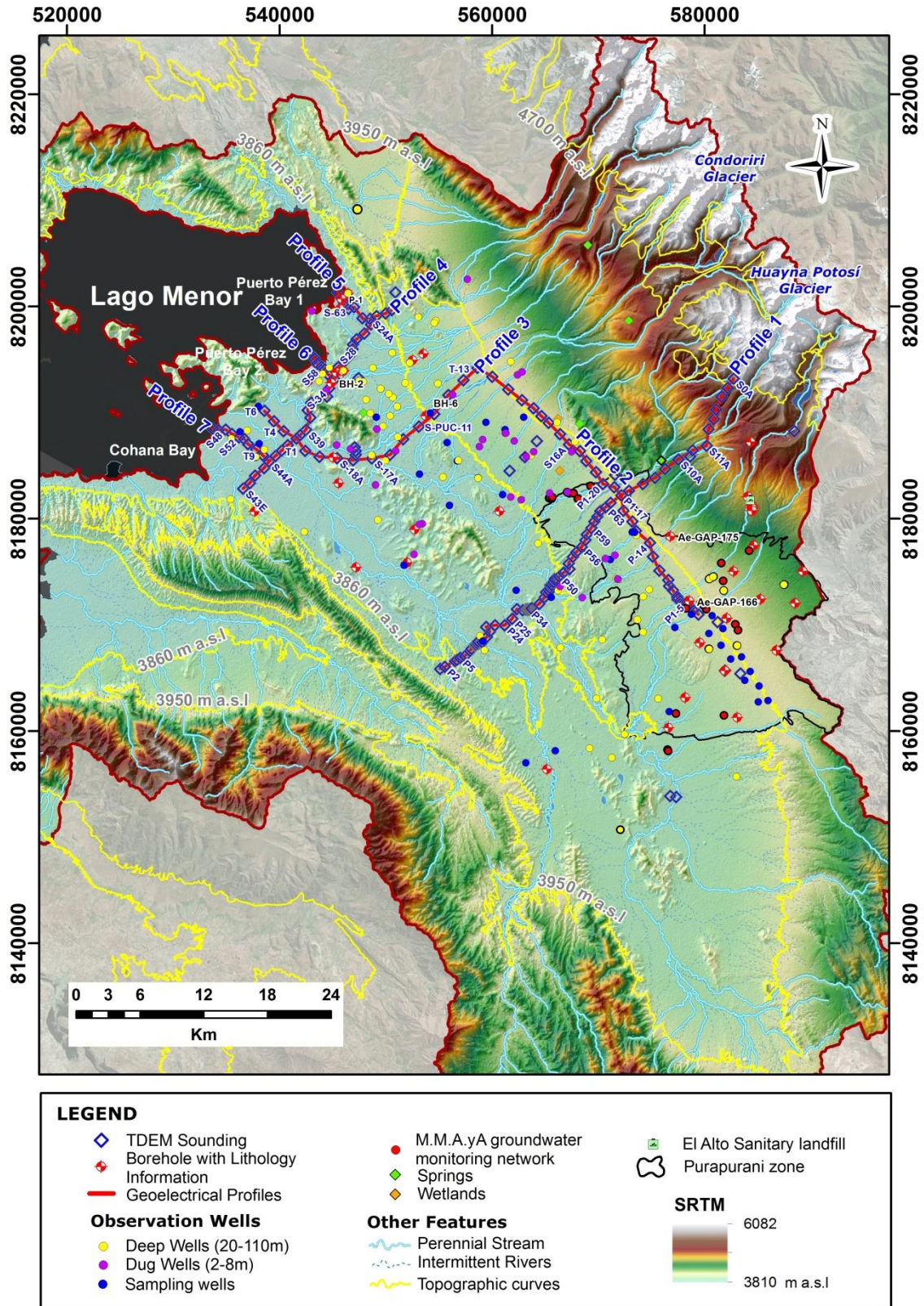


Figure 2. Map of geophysical, groundwater level and geochemical measurements performed within the Katari and Lago Menor Basin. Hypsometric colours represent the elevation in meters above the sea level (m a.s.l) of the terrain (DEM: SRTM 1-Arc-Second Global-N.A.S.A, 2000).

Profile 3 of 26 km long (16 soundings, Table 2), located between the lake (Cohana Bay) and the lower Piedmont area, investigates paleo-lacustrine and alluvial fan deposits. It also explores a zone where we hypothesised the presence of a subterranean channel for groundwater flow interconnecting the Piedmont subsystem and Lacustrine plain.

Profile 4 was 24 km long (30 soundings, Table 2), has a NE-SW direction. This profile was designed to perpendicularly cross Devonian and Tertiary formations as well as Quaternary fluvio-lacustrine deposits close to Lake Titicaca.

Profiles 5, 6 and 7 (6 km, 3 km and 6km long, respectively) have a NW-SE direction and included 7 to 10 soundings each (Table 2). They are located on the shores of Lake Titicaca (Cohana and Puerto Perez Bays) to understand the geometry of Quaternary paleo-lacustrine deposits, that interact directly with Lago Menor.

Additional TDEM soundings were performed near boreholes (Fig.2). All in all, TDEM soundings are located close to 30 boreholes from the geodatabase of MMAyA/VRHR/PDCK (M.M.A.yA, 2014) with available lithological logs.

Along the profiles, the initial sampling interval was a spacing of 500 m. This distance was considered to be the minimum length required to describe relevant aquifer heterogeneity. As no major heterogeneity was discovered within the first 10 km of the profile, the distance between the soundings was then increased to 1.5 km separation. A total of 187 TDEM soundings (Table 2) were performed with the TEM-FAST 48 equipment (AEMR technology, The Netherlands). The soundings were performed using a coincident loop configuration, a transmitter/receiver (Tx/Rx) loop of 100 x 100 m<sup>2</sup> and when urban sites were surveyed, using a 25 x 25 m<sup>2</sup> coincident receiver loops. Measurements were performed using the maximum possible Tx current (2.1 A). At each location, a set of 200 to 260 individual sounding curves have been recorded and stacked to reduce the electromagnetic noise. An acquisition time was adjusted from few micro-seconds to 400 or even 4000  $\mu$ s according to the level of noise and subsurface TDEM response. An automatic filtering option has been chosen (including 50 Hz removal). Ambient electromagnetic noise was also recorded daily to provide the necessary information to remove noisy points from the sounding curve. 1-D inversion was performed with TEM-RES software, developed by AEMR technology.

Table 2. Location of TDEM soundings and investigated formations. The location is based on the UTM WGS84 zone 19S coordinate system. The altitude values are based on SRTM-GL1-30m. Coincident loop configuration  $T_x=R_x$  : (loop size in meters).

	ID	Easting (m)	Northing (m)	Surface Altitude SRTM (m a.s.l.)	Tx (m)	Rx (m)	Investigated formations
<b>Profile 1</b>							
1	S0-A	582720	8193215	4658	100	100	
2	S3-A	582153	8192355	4609	100	100	
3	S5-A	581576	8191530	4511	100	100	
4	S2-A	581074	8190309	4411	100	100	
5	S4-A	580869	8189419	4379	100	100	
6	S1-A	580356	8188442	4312	100	100	
7	S11-A	580188	8186907	4222	100	100	Glacial/ fluvioglacial deposits
8	S8-A	578872	8186472	4187	100	100	
9	S8-B	578629	8185885	4160	100	100	
10	S10-A	577521	8185608	4121	100	100	
11	S7-A	576258	8184721	4077	100	100	
12	S9-A	575328	8183866	4041	100	100	
13	S-PUC-07	574191	8183280	4009	100	100	
14	S-PUC-06	573081	8182707	3982	100	100	
15	<b>P1-17</b>	572142	8182223	3957	100	100	
16	P64	571147	8181522	3938	100	100	
17	P63	570674	8181093	3922	100	100	
18	P62	570169	8180758	3914	100	100	
19	P61	569904	8180227	3907	100	100	Alluvial/ paleo-lacustrine deposits
20	P60	569607	8179763	3899	100	100	
21	P59	569324	8179153	3893	100	100	
22	P58	568901	8178541	3885	100	100	
23	P57	568776	8178016	3884	100	100	
24	P56	568427	8177333	3878	100	100	
25	P55	567885	8176845	3906	100	100	
26	P54	567607	8176423	3921	100	100	
27	P53	567188	8175795	3886	100	100	Tertiary Formation (Tcl)
28	P52	567284	8175262	3902	100	100	
29	P51	566727	8174943	3883	100	100	
30	P50	566304	8174582	3868	100	100	
31	P49	565880	8174310	3849	100	100	
32	P48	565785	8174042	3851	100	100	
33	P47	565602	8173791	3852	100	100	
34	P46	565461	8173765	3851	100	100	
35	P45	565458	8173493	3852	100	100	Paleo-lacustrine deposits
36	P44	565388	8173200	3853	100	100	
37	P43	565079	8173092	3858	100	100	
38	P42	564938	8172616	3852	100	100	
39	S-LJ-01	564441	8171993	3844	100	100	
40	P39	563690	8171570	3878	25	25	
41	P38	563640	8171541	3876	25	25	Devonian Formation (Dbl)
42	P37	563600	8171526	3873	25	25	
43	P36	563513	8171503	3856	25	25	
44	P34	563468	8171486	3847	25	25	
45	P32	563377	8171464	3845	25	25	Paleo-lacustrine deposits
46	P31	563340	8171481	3843	25	25	

Table 2, Continued

ID	Easting (m)	Northing (m)	Surface Altitude SRTM (masl)	Tx (m)	Rx (m)	Investigated Formations	
<b>Profile 1</b>							
47	P30	563283	8171501	3839	25	25	
48	P29	563185	8171473	3842	25	25	
49	P27	562890	8171391	3845	100	100	
50	P26	562323	8171504	3846	50	50	
51	P25	561881	8170585	3867	100	100	
52	P24	561170	8169978	3854	100	100	
53	P23	560260	8169988	3856	100	100	Paleo-lacustrine deposits
54	P22	559434	8169828	3858	100	100	
55	S-LJ-04	559507	8168884	3856	100	100	
56	P21	559793	8169370	3856	100	100	
57	P20	559060	8168386	3843	100	100	
58	P19	558692	8168452	3842	25	25	
59	P18	558683	8168402	3843	25	25	
60	P17	558646	8168280	3843	25	25	
61	P16	558665	8168232	3842	100	100	
62	P15	558603	8168230	3841	25	25	
63	P14	558483	8168183	3841	25	25	
64	P13	558430	8168169	3841	25	25	
65	P12	558421	8168156	3841	100	100	Paleo-lacustrine deposits
66	P11	558391	8168139	3840	25	25	
67	P10	558348	8168110	3841	25	25	
68	P8	558051	8167758	3848	100	100	
69	P7	557924	8167574	3860	100	100	
70	P6	557455	8167072	3856	100	100	
71	P5	556978	8166905	3859	100	100	
72	P4	556683	8166718	3883	100	100	Tertiary Formation (Tkk)
73	P3	556515	8166626	3907	100	100	
74	P2	555528	8166074	3869	100	100	Paleo-lacustrine deposits
75	P1	555105	8165863	3894	100	100	Tertiary Formation (Tcnr)
<b>Profile 2</b>							
76	T-13	558610	8194231	3933	100	100	
77	T-14	560008	8193393	3941	100	100	
78	T-15	561508	8192215	3951	100	100	
79	P1-23	562806	8191192	3956	100	100	
80	S13	563888	8190422	3965	100	100	Alluvial deposits (Major alluvial fan)
81	S-PUC-21	564641	8189691	3960	100	100	
82	S14	565312	8189056	3953	100	100	
83	S15	566385	8187983	3941	100	100	
84	S16	567231	8187014	3929	100	100	
85	P1-22	568256	8186391	3930	100	100	
86	S-PUC-20	568813	8185391	3919	100	100	Alluvial deposits (Thin layer)
87	P1-21	569757	8184397	3927	100	100	

Table 2, Continued

ID	Easting (m)	Northing (m)	Surface Altitude SRTM (masl)	Tx (m)	Rx (m)	Investigated Formations	
<b>Profile 2</b>							
88	P1-20	570437	8183297	3937	100	100	
89	P1-18	571497	8182989	3952	100	100	
	<b>P1-17</b>	572142	8182223	3957	100	100	Alluvial fan deposits (Minor alluvial fan)/Paleolacustrine deposits
90	P1-16	572365	8180766	3946	100	100	
91	P1-15	573208	8179750	3943	100	100	
92	S-LJ-02	573570	8178439	3932	100	100	
93	P1-14	574857	8177747	3939	100	100	
94	P1-13	575137	8176467	3929	100	100	
95	P1-12	575736	8175139	3922	100	100	
96	P1-11	576576	8174245	3925	100	100	
97	P1-10	576656	8173686	3923	100	100	
98	P1-9	577001	8173274	3925	25	25	
99	P1-8	577409	8172672	3924	100	100	Fluvioglacial/Paleolacustrine deposits
100	P1-7	577447	8172433	3923	100	100	
101	P1-6	577693	8172260	3924	100	100	
102	P1-5	578320	8172160	3933	100	100	
103	P1-4	578380	8171931	3933	100	100	
104	P1-3	578644	8171743	3934	100	100	
105	P1-2	578939	8171345	3931	100	100	
106	P1-1	579413	8170996	3936	100	100	
<b>Profile 3</b>							
	<b>T-13</b>	558610	8194231	3933.459754	100	100	
107	T12	557290	8193070	3909.535871	100	100	
108	S-PUC-12	555858	8191672	3880.6	100	100	Alluvial (Major alluvial fan)/Paleo-lacustrine deposits
109	S-PUC-04	554545	8189869	3859.112097	100	100	
110	S-PUC-11	553088	8188696	3851.8	100	100	
111	S-PUC-10	551617	8187506	3840.8	100	100	
112	S-PUC-09	550373	8186042	3838.5	100	100	
113	S17A	548678	8185697	3832	100	100	
114	S22A	546926	8185522	3831	100	100	
115	S18A	545412	8185735	3827	100	100	
116	S-PUC-14	543751	8185848	3826	100	100	Paleo-lacustrine deposits
117	T1	542396	8186425	3823.369384	100	100	
118	T2	541601	8187585	3828.299101	100	100	
119	T4	540372	8188270	3826.258777	100	100	
120	T5	539454	8189198	3824.454618	100	100	
121	T6	538579	8190210	3825.368	100	100	
<b>Profile 4</b>							
122	S43E	536563	8182865	3826	100	100	Paleo-lacustrine deposits
123	S43D	537202	8183360	3824	100	100	
124	S43B	537682	8184071	3825	100	100	
125	S43A	538555	8184799	3826	100	100	

Table 2, Continued

	ID	Easting (m)	Northing (m)	Surface Altitude SRTM (masl)	Tx (m)	Rx (m)	Investigated Formations
126	<b>S44A</b>	539000	8185410	3826	100	100	
127	S45A	539618	8185927	3826	100	100	
128	T8	540205	8186431	3826	100	100	
129	T7	540750	8186936	3827	100	100	Paleo-lacustrine deposits
130	T2	541601	8187585	3828	100	100	
131	T3	541910	8187882	3826	100	100	
132	S39	542485	8188390	3826	100	100	
133	S40	542879	8189551	3828	100	100	
134	S41	542627	8190246	3839	100	100	
135	S42	542962	8190975	3863	100	100	Devonian Formation (Dbl)
136	S33	544451	8191530	3874	100	100	
<b>Profile 4</b>							
137	S34	544671	8192305	3834	100	100	
138	<b>S36</b>	545172	8193157	3825	100	100	Paleo-lacustrine deposits (Puerto Pérez bay 2)
139	S37	545348	8193806	3829	100	100	
140	S28	545468	8194296	3826	100	100	
141	S29	546048	8194788	3859	100	100	
142	S30	546661	8195431	3837	100	100	Tertiary Formations (Tcl, Tkk)
143	S31	546839	8195990	3844	100	100	
144	S32	546902	8196459	3850	100	100	
145	S32A	547239	8196936	3835	100	100	
146	S23	547959	8197459	3839	100	100	Paleo-lacustrine deposits (Puerto Pérez bay 1)
147	<b>S24</b>	548600	8198331	3838	100	100	
148	S24A	548495	8198865	3838	100	100	
149	S25	549100	8199117	3866	100	100	
150	S26	549969	8199364	3925	100	100	Devonian Formation (Dbl)
151	S26A	550563	8199673	3870	100	100	
<b>Profile 5</b>							
152	S62A	545446	8201362	3824	100	100	
153	S63	545811	8200792	3826	100	100	
154	S65	546029	8200404	3825	100	100	
155	S67	546123	8200060	3829	100	100	
156	S69	546507	8199800	3827	100	100	Paleo-lacustrine deposits
157	S-BT-07	547002	8199955	3829	100	100	
158	S-BT-08	547782	8198906	3833	100	100	
	<b>S24</b>	548600	8198331	3838	100	100	
<b>Profile 6</b>							
159	S56C	543187	8195247	3825	100	100	
160	S56B	543261	8195106	3823	100	100	
161	S56	543519	8194610	3826	100	100	
162	S58	543937	8194342	3825	100	100	Paleo-lacustrine deposits
163	S60	544249	8194091	3824	100	100	
164	S61	544535	8193631	3827	100	100	
	<b>S36</b>	545172	8193157	3825	100	100	

Table 2, Continued

ID	Easting (m)	Northing (m)	Surface Altitude SRTM (masl)	Tx (m)	Rx (m)	Investigated Formations	
<b>Profile 7</b>							
165	S48C	533688	8188494	3824	100	100	
166	S48B	534247	8188382	3825	100	100	
167	S48	534923	8188411	3823	100	100	
168	S50	535488	8188024	3824	100	100	
169	S52	536172	8187698	3830	100	100	
170	S54	536673	8187527	3828	100	100	Paleo-lacustrine deposits
171	T11	537011	8187048	3824.103133	100	100	
172	T10	537779	8186563	3827.660935	100	100	
173	T9	538426	8186018	3827.537339	100	100	
	<b>S44A</b>	539000	8185410	3826	100	100	
<b>Other Soundings</b>							
174	PC-1	583359	8165430	3929	25	25	
175	PC-2	581907	8165700	3923	25	25	Fluvioglacial deposits
176	PC-3	581232	8170281	3938	25	25	
177	SITE-1	576765	8153899	3861	100	100	Paleolacustrine deposits
178	SITE-2	588442	8188267	4464	100	100	Glacial deposits
179	SITE-3	577321	8153803	3863	100	100	Paleolacustrine deposits
180	SCH	547412	8193268	3835	100	100	Paleolacustrine deposits
181	S12B	564213	8187341	3916	100	100	Alluvial (Major alluvial fan)/Paleo-lacustrine deposits
182	T-16	563078	8185821	3896	100	100	
183	S12A	561646	8184526	3877	100	100	
184	S27	550889	8201358	3887	100	100	Devonian Formation (Dbl)
185	S19A	547143	8186039	3833	100	100	
186	S21A	547156	8186379	3831	100	100	Paleolacustrine deposits
187	S20A	547064	8186754	3833	100	100	

For inversion, several considerations were taken into account. We used 1-D (layered) models to fit the data. The 1-D hypothesis is considered as reasonable in the context of a sedimentary aquifer at the scale of one TDEM sounding (lateral investigation limited to few tens of meters laterally away from the loop of the cable). In a second step, for several TDEM soundings close to boreholes, we tested inversions using: a) three or four resistivity model layers and b) a smooth multilayer resistivity models with 10 to 20 layers. Both, the 3-4 layers and smooth multilayer models, gave acceptable RMS values not greater than 1 to 2 %. We chose to use the simplest resistivity models to easier link geological formations to a unique range of resistivity. Eventually, we chose to conduct a 1-D inversion for each sounding, and not to use a Laterally Constrain Inversion –LCI- procedure (Auken et al, 2005). In our case, even if LCI could be considered in some parts of the survey with a first layer that characterizes a unique geological pattern along long sections (as in the alluvial fans for example), the resistivity of second and third deeper layers greatly vary laterally especially where paleo-valleys or buried Tertiary formations are present. In those areas, no lateral correlations between layers are possible since some models have low resistive layers in the deep section and others have high resistive layers and are close together (few hundreds of meters). In such complicated geology, a LCI procedure would have required a smaller distance between sounding points. For future large surveys, for example for airborne TDEM survey that allows a shorter distance between sounding points, LCI could be considered, taking advantage of our ground results to adapt the convenient lateral sampling interval between two TDEM soundings.

### *3.2 Piezometric and geochemical measurements*

#### *3.2.1 Groundwater level measurements*

The field measurements of water levels were undertaken for a subset of wells/boreholes and groundwater sources in the vicinity of the study area. A total of 97 groundwater sources were validated in the field during August of 2017: 55 deep wells, 32 dug wells, 8 springs and 2 wetlands (Fig.1). Measurements corresponding to water level depths were converted to hydraulic head using sea level as the reference datum. Hydraulic head elevations were used to assess groundwater flow direction and horizontal hydraulic gradients in the study area. The vertical reference, altitude above sea level (m a.s.l), are based on the SRTM-GL1-30 m (Shuttle Radar Topography Mission 1 Arc-Second Global, approximately 30 m resolution, N.A.S.A, 2000) digital elevation model (DEM). The

accuracy of this DEM over the Altiplano was tested by Satgé et al. (2016). These authors state that the SRTM-GL1-30 m DEM has a more precise elevation and relative height-pixel accuracy than SRTM-v4 and GDEM-v2, based on STD and RMSE values and bias analysis.

### *3.2.2 Geochemical sampling and analysis*

Groundwater samples were collected from 52 deep wells, 20 to 110 m b.g.l (meters below ground level), mostly by electrical pumps (Fig.1). The sampling strategy was defined in accordance with the TDEM survey, considering the spatial and vertical distribution of the main permeable Quaternary formations. These wells were selected to characterize the geochemical facies of the groundwater and to ascertain the regional groundwater circulation patterns in the basin.

Major ion concentrations ( $\text{Ca}^{2+}$ ,  $\text{Mg}^{2+}$ ,  $\text{Na}^+$ ,  $\text{K}^+$ ,  $\text{HCO}_3^-$ ,  $\text{Cl}^-$ ,  $\text{SO}_4^{2-}$ ,  $\text{NO}_3^-$ ) were quantified, at the IGE (Institut des Géosciences de l'Environnement) Laboratory, using the Metrohm 732/733 ion chromatograph modular system, precision  $\pm 0.1$  mg/L, and calibrated with standard solutions Roth (5 to 40 mg/L range). Blanks consisted of ultrapure, (Milli-Q) water. Total alkalinity was measured in the field by titration (HACH digital titrator method) and recalculated as bicarbonate. A piper diagram, performed with DIAGRAMMES (Simler, 2014), was used to point out the typical groundwater facies of the Katari-Lago Menor aquifer.

## *4. Results*

### *4.1 Hydraulic head contour map and electrical conductivity variations*

Figure 3 displays hydraulic head contours and general flowpaths from the groundwater system. From this figure, five flow systems can be distinguished where recharge mainly comes from the upper Piedmont and from effective infiltration from precipitation.

In the first flow system groundwater moves to the SW and flows into Lake Titicaca (Puerto Pérez Bays) in the northwest (e.g. flowpath 1). In the second flow system groundwater moves into the Lacustrine plain through breaks or channels between the bedrock outcrops and is illustrated by flowpaths 2, 4 and 6. The outlet of this second flow system is probably Lake Titicaca at the level of Cohana Bay. In the third flow system groundwater moves to the SW discharging in a series of wetlands (e.g. flowpath 3) or uplifts into the surface due

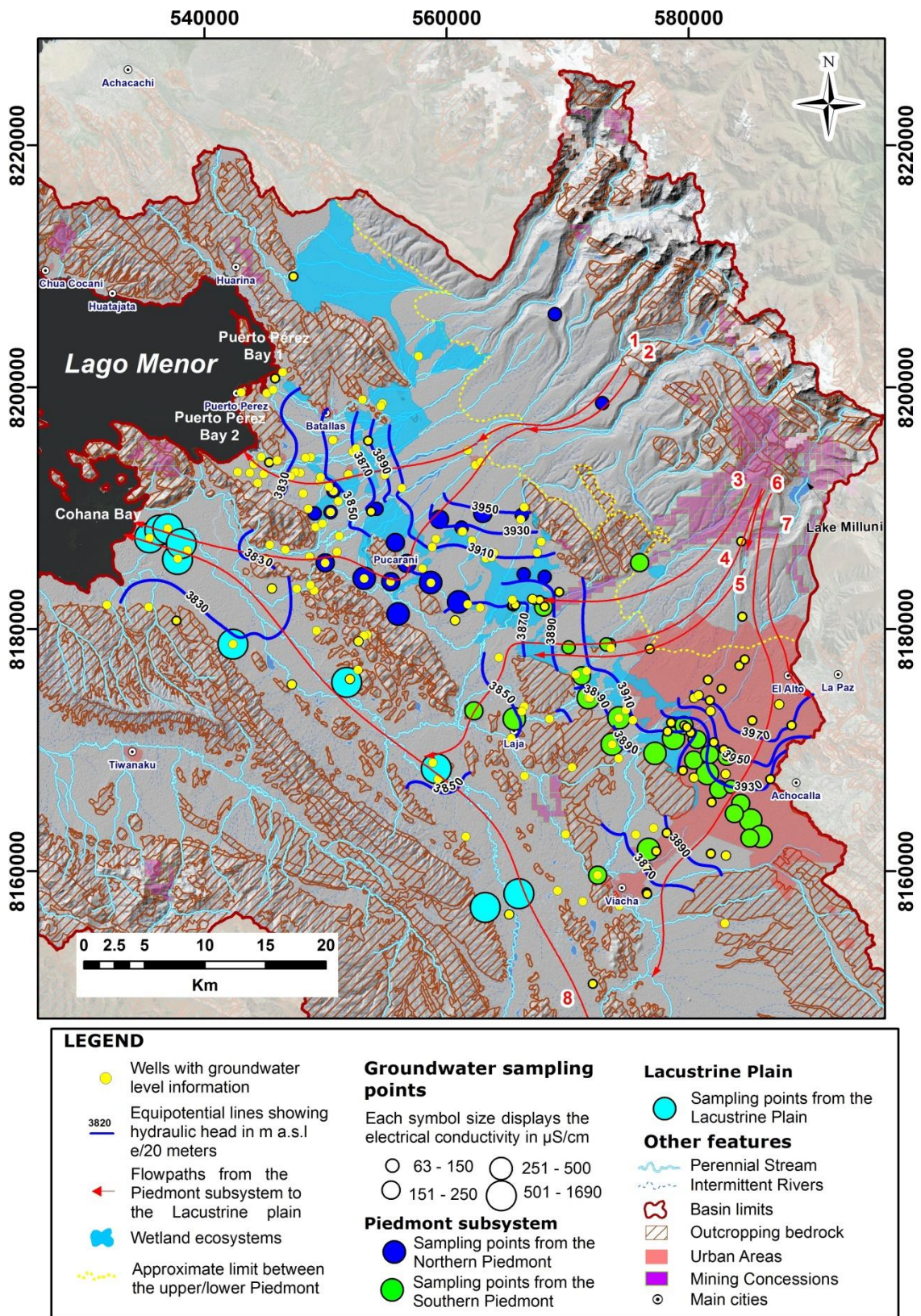


Figure 3. Hydraulic head contour map and groundwater electrical conductivity variations.

to the hydraulic barriers of bedrock outcrops, forming also wetlands (e.g. flowpath 5). In the fourth flow system groundwater moves towards the southeast discharging in springs and seepages in the El Alto-La Paz-Achocalla area (e.g. flowpath 6). And finally, the fifth flow system is illustrated by flowpath 8 where groundwater moves slowly to the NW, mainly due to the low hydraulic head gradient (flat slope) and probably due to limited recharge from the Piedmont subsystem.

Figure 3 also depicts groundwater electrical conductivity measurements (EC in  $\mu S/cm$ ) which vary within both geomorphological domains. Indeed, in the Piedmont subsystem, groundwater electrical conductivity values range between 63 to 416  $\mu S/cm$  towards the NW (blue circles) and between 86 to 433  $\mu S/cm$  towards the SE (green circles). Groundwater samples from the Piedmont subsystem are differentiated in colors because the southern zone appears to be more prone to contamination due to mining concessions and the urbanized city of El Alto. In contrast, in the Lacustrine plain groundwater electrical conductivity values range from 530 to 1700  $\mu S/cm$  (cyan circles).

## *4.2 TDEM interpretation*

### *4.2.1. TDEM comparison with boreholes and outcropping geological formations*

In order to be able to correlate TDEM resistivity profiles and geology, we conducted as a first step, an analysis of the TDEM soundings performed near boreholes and over the outcropping Tertiary/Devonian formations (i.e. Tcl, Tkk and Dbl, Table 1) (Fig.2).

TDEM soundings were performed between 250 m to 2 km of distance from boreholes (Fig.2) due to the presence of villages/houses. Consequently, the correspondence of thicknesses between TDEM and borehole is sometimes poor due to possible lateral changes.

Figure 4 displays field data from five representative TDEM soundings and their locations are shown in Figure 2. The layered resistivity TDEM model is presented as a color log beside the borehole log. Groundwater electrical conductivity measured for the majority of the boreholes varies over a relatively narrow range (i.e. between 80 and 200  $\mu S/cm$ ) (Fig.3). Therefore, resistivity variations can generally be attributed to changes in geology, not to groundwater electrical conductivity variations.

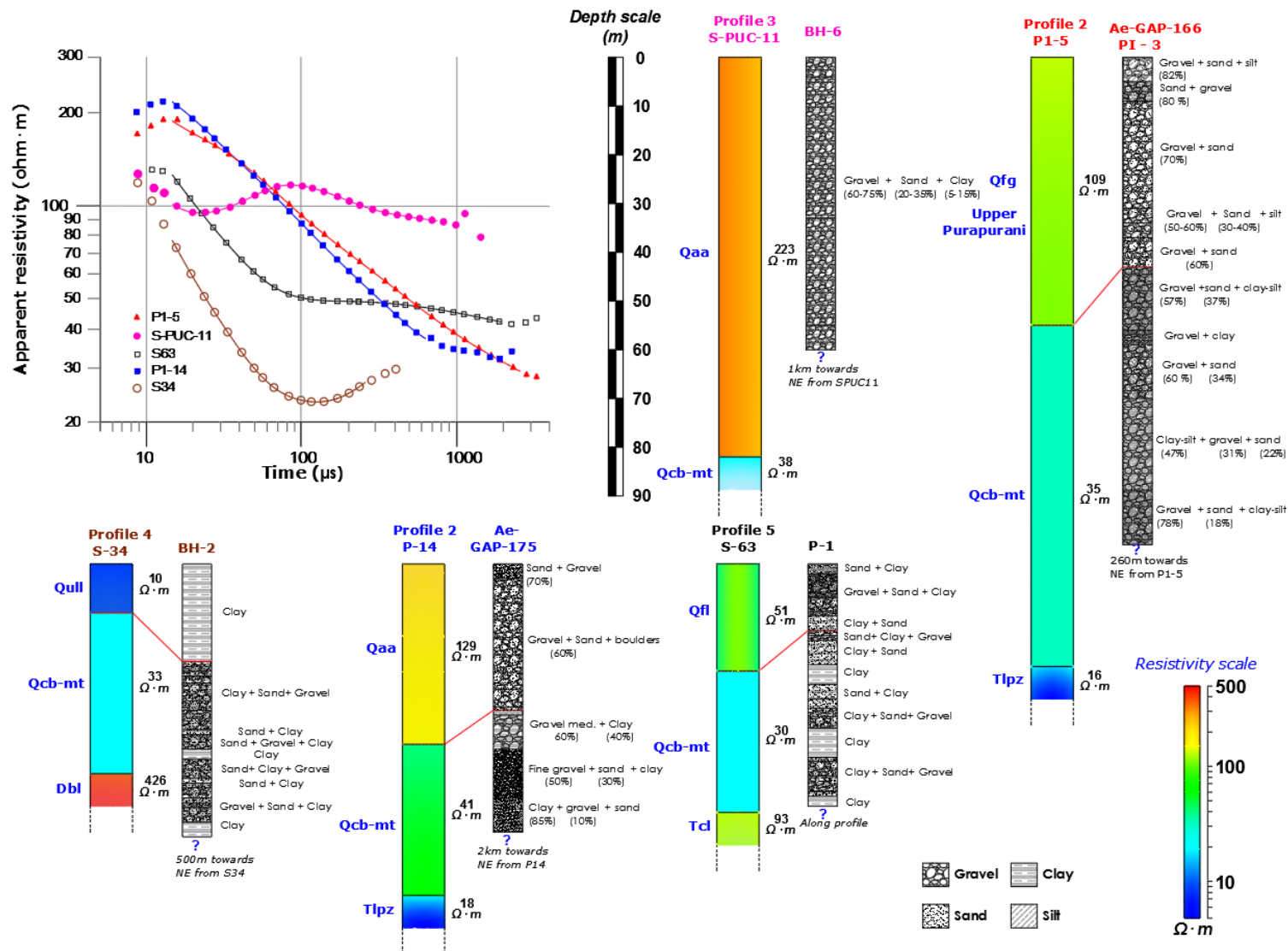


Figure 4. Example of five representative TDEM sounding curves (see location in Fig.2) and their corresponding 1D interpretation. The three or four layer model curves that fit the data are drawn as continuous colored lines. The red dashed line represents an approximate limit of correlation between resistivity and borehole lithology.

however care should be taken close to the lake, because groundwater conductivity is sometimes increasing (up to 600-1300  $\mu\text{S}/\text{cm}$ ) indicating a connection with Lake Titicaca ( $\sim 1000$   $\mu\text{S}/\text{cm}$ ) (Fig.3) or an influence of the evaporitic nature of the paleo-lacustrine formations (i.e. Qcb-mt formation, Table 1).

TDEM sounding S-34 (borehole BH-2, 500 m away,  $\text{EC} \sim 106$   $\mu\text{S}/\text{cm}$ ) investigates a shallow clay layer appearing as a unique resistivity layer of 10  $\Omega\cdot\text{m}$ . Deeper, TDEM model shows a second layer with resistivity values of 33  $\Omega\cdot\text{m}$  characteristic of an alternation of sand and gravel with thin clayey layers. Then, TDEM shows a more resistive layer, 426  $\Omega\cdot\text{m}$  not seen in the borehole.

TDEM sounding P1-14 (borehole Ae GAP 175, 2 km away,  $\text{EC} \sim 86$   $\mu\text{S}/\text{cm}$ ) investigates a shallow massive sand and gravel formation as a unique resistivity layer of 129  $\Omega\cdot\text{m}$ . Deeper, TDEM model shows a second layer with resistivity values of 41  $\Omega\cdot\text{m}$  characteristic of an alternation of sand and gravel with thin clayey layers. Then, TDEM shows a more conductive layer, 18  $\Omega\cdot\text{m}$  not seen in the borehole.

TDEM sounding S-PUC-11 (borehole BH-6, 1km away,  $\text{EC} \sim 142$   $\mu\text{S}/\text{cm}$ ) investigates gravel and sand deposits with a limited fraction of clay ( $\sim 5\%$ ) appearing as a unique resistivity layer of 233  $\Omega\cdot\text{m}$ . Deeper, TDEM model shows a third layer with resistivity values of 38  $\Omega\cdot\text{m}$  attributed to more silty or clayey layer not seen in the borehole log.

TDEM sounding S-63 (borehole P-1, 50 m away,  $\text{EC} \sim 600$   $\mu\text{S}/\text{cm}$ ) investigates a fluvio-lacustrine deposit. The first layer is an alternation of thin sand and clay layers as a unique resistivity layer of 51  $\Omega\cdot\text{m}$ . Deeper, TDEM model shows a second layer with resistivity values of 30  $\Omega\cdot\text{m}$  while clay layers are becoming more frequent. Then, TDEM shows a more resistive layer, 93  $\Omega\cdot\text{m}$  not seen in the borehole log.

TDEM sounding P1-5 (borehole Ae-GAP-166 PI3, 250m away,  $\text{EC} \sim 230$   $\mu\text{S}/\text{cm}$ ; Fig.2), investigates fluvio-glacial deposits with shallow layers of gravels and sands appearing as a unique resistivity layer of 109  $\Omega\cdot\text{m}$ . Below, clay-silt layers present a resistivity value of 35  $\Omega\cdot\text{m}$ . Deeper, TDEM model shows a third layer with resistivity values of  $\sim 16$   $\Omega\cdot\text{m}$  attributed to more clayey layers not seen in the borehole log.

This comparison analysis illustrates two major facts: first, the geology of the area as described by boreholes exhibits most of the time a complicated interstratified medium.

Secondly, it illustrates the lack of TDEM resolution of thin, interstratified medium. This well-known limitation of the method arose in our study: fine intercalations of thin, clayey or loamy layers with thin sandy layers at depth cannot be delineated, as confirmed by Descloitres et al. (2013) for a clayey sand aquifer. Therefore, the stratified resistivity model derived from TDEM must be interpreted as a model representing thick geological units only. The resistivity value of those thick units varies with clay content, the greater the number of clayey layers are, the less the resistivity is. This information is a valuable indication for the hydrogeological potential of the aquifer.

The comparison with boreholes allows us to derive resistivity ranges for the Quaternary deposits (i.e. glacial, fluvioglacial, alluvial and paleo-lacustrine deposits). However, none of the borehole information investigates the substratum (i.e. Tertiary or Devonian sedimentary rocks). To evaluate the resistivity range for this substratum we performed some TDEM soundings directly on the outcropping formations (Fig.2). Figure 5 summarizes resistivity ranges for both Quaternary (boreholes) and Tertiary/Devonian (outcrops) and can be used as a guideline to conduct the entire TDEM profile interpretation.

From Figure 5 analysis, in the Lacustrine plain, paleo-lacustrine deposits are either clayey (5-15  $\Omega\cdot\text{m}$ ) or clay sandy-gravel layers with intermediate resistivity range (30-40  $\Omega\cdot\text{m}$ ). Within the Piedmont subsystem, the resistivity ranges from intermediate values (30-120  $\Omega\cdot\text{m}$ ) and can reach more resistive range (120-300  $\Omega\cdot\text{m}$ ) for alluvial fans and glacial deposits.

The substratum underlying the Quaternary geologic media, both within the Piedmont subsystem and Lacustrine plain, are resistive (up to ~300  $\Omega\cdot\text{m}$ ) except for the Kollu Kollu Formation (Tkk ~40  $\Omega\cdot\text{m}$ ) due to the presence of gypsum and for the Cachilaya Formation (Tcl ~150  $\Omega\cdot\text{m}$ ) a claystone formation with layers of tuff.

#### *4.2.2 TDEM profiles*

The lateral variations of resistivity along TDEM profiles are displayed in Figures 6 and 7. The descriptions of the results are based on the main geomorphological domains, i.e. the Piedmont subsystem and Lacustrine plain. For each domain, the stratigraphic interpretations are based on the interpretations illustrated in Figure 5.

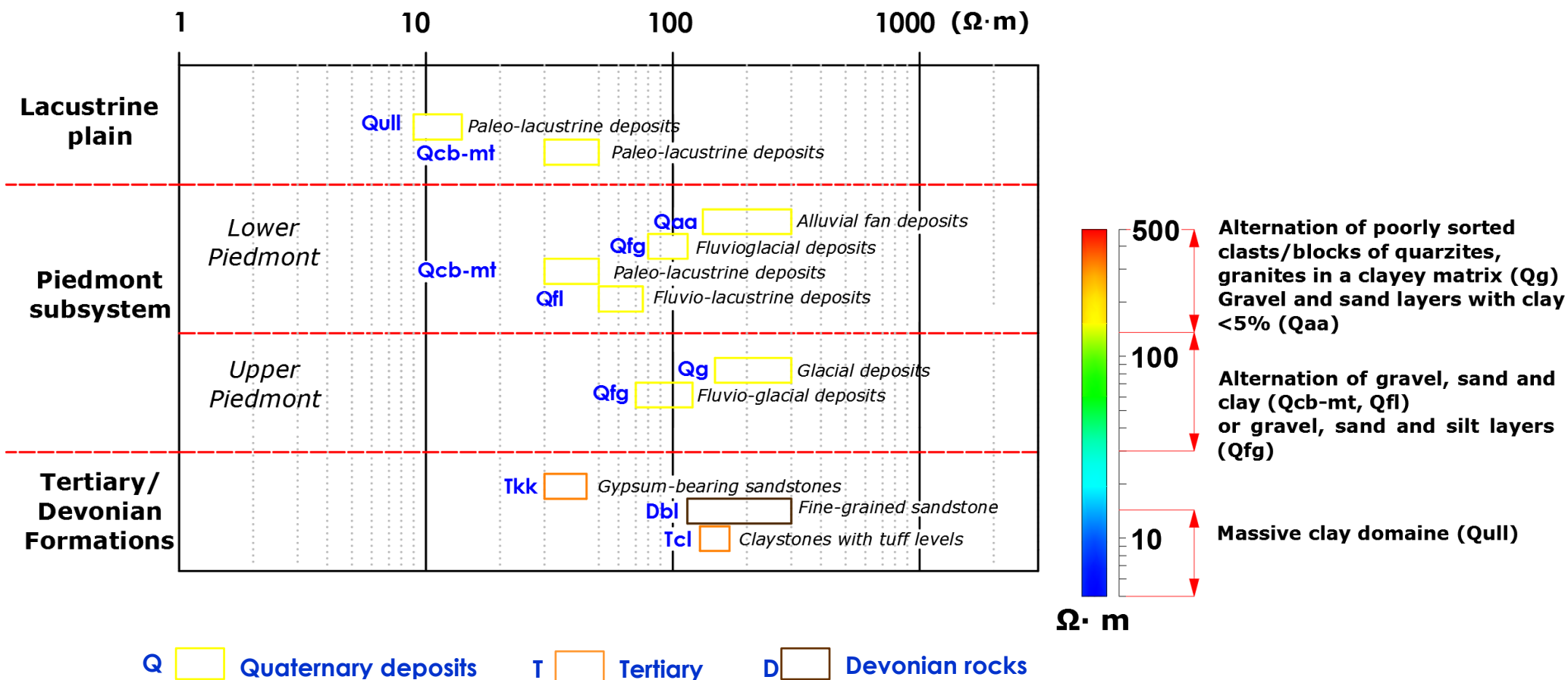


Figure 5. Resistivity ranges and associated geological formation derived from comparison between boreholes and TDEM soundings, and from TDEM soundings performed over outcropping Tertiary/Devonian rocks.

#### 4.2.2.1 Piedmont subsystem

##### *Profile 1*

The upper Piedmont area in Profile 1 (Fig.2, Fig.6) shows, from surface to depth, a first layer composed of two parts: one is found above 4260 m a.s.l (between TDEM soundings “S0A” and “S1A”) and show resistivity values of  $\sim 100$  to  $170 \Omega \cdot \text{m}$  and a thickness of 60 to 150 m. This part is attributed to glacial deposits (geological Formation, “Qg”) probably from the Sorata glaciation (Table 1). Then, a second part (below 4260 m a.s.l) between soundings S11A-S10A, shows more resistive values ( $\sim 300 \Omega \cdot \text{m}$ ) and a thickness of  $\sim 125$  m, is also attributed to glacial deposits (flow-tills) from the same formation (Qg-Sorata Fm.). From borehole information nearby this second part is composed of poorly sorted clasts/blocks of quartzite, shales and granites in a clayey matrix.

Below this first resistive layer, a second layer between soundings S0A and S10A, shows resistivity values of  $\sim 60$  to  $120 \Omega \cdot \text{m}$  and a thickness of 60 to 120 m. This layer may belong to deposits from a non-differentiated interglacial/glacial cycle, possibly the fluvio-glacial (Qfg) Purapurani Formation or the glacial (Qg) Calvario Formation, composed of gravel with silt layers or tills and fluvial gravels (Table 1). The same layer is found between soundings S7A and S-9A, showing resistivity values up to  $\sim 80 \Omega \cdot \text{m}$  and a thickness of 60 to 150 m.

Below the above layers, the pattern of the top of the substratum (underlying Quaternary deposits) is found similar to the actual topography of the closest rocky outcrops, located about 2 km from the profile in a NW direction. This noticeable correspondence is a strong indication of a sharp, bedrock topography at the base of the Quaternary deposits, as seen in the section between soundings S8A and S-PUC-07 (Profile 1, Fig.6). This bedrock topography could be the result of the tectonic deformations associated to the Eastern Cordillera and the Altiplano region (i.e. structural features, Fig.1).

In the lower Piedmont area (Fig.2, Fig.6), the section between soundings S-PUC-07 to P56 shows an uppermost layer with resistivity values of  $\sim 250$  to  $115 \Omega \cdot \text{m}$  and a thickness of 40 to 75 m, revealing the geometry of the minor alluvial fan deposits (Qaa) (Fig.1, Table 1). From borehole information nearby, these deposits consist of gravels, sands and clays.

Then, below the alluvial fan deposits, a second layer between soundings P63-P59 and P58-P56, shows resistivity values of  $\sim 30 \Omega \cdot m$  and a thickness of 50 to 130 m. These sections display paleo-valley geometries with deposits that may be attributable to the ancient Lakes Cabana and Mataro (Table 1) remaining as a unique non-differentiated formation (Qcb-mt) in this interpretation. From borehole information nearby, it comprises clayey sandy and gravelly sand intercalations.

In addition, sections P49-SLJ01 and P34-P25 show a first layer with resistivity values of  $\sim 40$  to  $60 \Omega \cdot m$  and a thickness up to 100 m, which may be attributed to fluvio-lacustrine deposits (Qfl), comprised of gravel and sand materials with clay and silt content (Table 1). A deeper, second layer, found in section P49-S-LJ-01 with resistivity values  $\sim 30$  to  $40 \Omega \cdot m$  and a thickness of 40 to 100 m, may belong to deposits from the (Qcb-mt), both layered formations indicating fluvial conditions, with alternation of clay, sand and gravel deposits (Table 1).

The vertical resistivity variations in section P49 –S-LJ-01 (from 60 to  $30 \Omega \cdot m$ ) rather than being different geological formations (i.e. Qfl and Qcb-mt) may also be due to change in groundwater electrical conductivity.

### *Profile 2*

From Profile 2 (Figure 2, Figure 7), we learn additional information about the lower Piedmont area. From NW to SE, Profile 2 shows the transverse geometry of the major alluvial fan deposit separated by the rocky formation (Tpñ), outcropping 1 km towards the NE (Fig. 1, Table 1), as well as the minor alluvial fan deposit in transition with fluvio-glacial deposits (Fig. 1).

Towards the NW, the section between soundings T-13 and S16A shows an upper layer with resistivity values  $\sim 270$  to  $370 \Omega \cdot m$  and a thickness up to 85 m, revealing a thick accumulation of alluvial deposits (Qaa), probably Pre-Sorata gravels (Table 1), that are mainly composed of sandy gravel and medium and fine gravels, as evidenced in borehole BH-6.

The section between soundings P1-22 and P1-21 (Fig. 7) shows a first layer with resistivity values of  $\sim 140 \Omega \cdot m$  and a maximum thickness of  $\sim 20$  m, which is attributed as a thin layer of alluvial deposits (Figure 4).

Towards the SE, section P1-20–P1-14 displays a first layer with resistivity values of ~140 to 240  $\Omega\cdot\text{m}$  and a thickness of 20 to 50 m, which is attributed to deposits from the minor alluvial fan (Qaa), consisting of gravels, sands and clays. Subsequently, the section between soundings P1-13 and P1-1 depicts a first layer with resistivity values of ~100  $\Omega\cdot\text{m}$  and a thickness of 30 to 70 m, attributed to fluvio-glacial outwash sediments (Qfg) from the upper Purapurani Formation (Table 1), which mainly comprises gravel, sand and silt sediments (borehole Ae-GAP-166, Figure 4).

Then, a deeper second layer with resistivity values of ~30 to 40  $\Omega\cdot\text{m}$  and a thickness of 20 to 50 m is found along the whole section between soundings P1-18 and P1-1, that is attributed to deposits from the ancient Lake Cabana and Mataro (Qcb-mt) (Table 1) composed of alternating clay, sand and gravel deposits. The Purapurani Formation seen below the city of El Alto has outcropping lacustrine deposits at its base, with a lithology similar to the La Paz Formation (Tlp) (Table 1).

### *Profile 3*

Profile 3 (Fig.2, Fig.7) also investigates the lower Piedmont area. Between soundings T13 and S-PUC-10 (aligned in a NE-SW direction), we can investigate the longitudinal section of the major alluvial fan (Fig. 1). Underlying this section, from soundings S-PUC-12 to S-PUC-10, we can follow a sequence that could be attributed to deposits from the ancient's lake invasions.

The major alluvial fan (Qaa) shows a layer with resistivity values of ~ 450 to 130  $\Omega\cdot\text{m}$  and a thickness up to 90 m. This layer is composed of two parts: one is found between TDEM soundings “T13” and “S-PUC-04” showing resistivity values of ~450  $\Omega\cdot\text{m}$  and a thickness of up to 90 m, attributed to deposits from the middle part of the fan comprised of gravel and sand materials. The second part, located between soundings S-PUC-11 and S-PUC-10, shows resistivity values of ~200  $\Omega\cdot\text{m}$  and a thickness of up to 90 m, are attributed as alluvial deposits from the distal part of the fan, consisting of sands and clays.

Below this layer, section S-PUC-12–S-PUC-10 shows a second layer with resistivity values of ~40-70  $\Omega\cdot\text{m}$  and a thickness of ~60 to 130 m. This layer probably corresponds to deposits from the ancient Cabana and Mataro Lakes (Table 1). Higher values of resistivity (~70  $\Omega\cdot\text{m}$ ) might be attributed to the Mataro deposits, which are a series of fluvial, detrital deposits showing alternating beds of clayey sand and gravelly sand (Table 1).

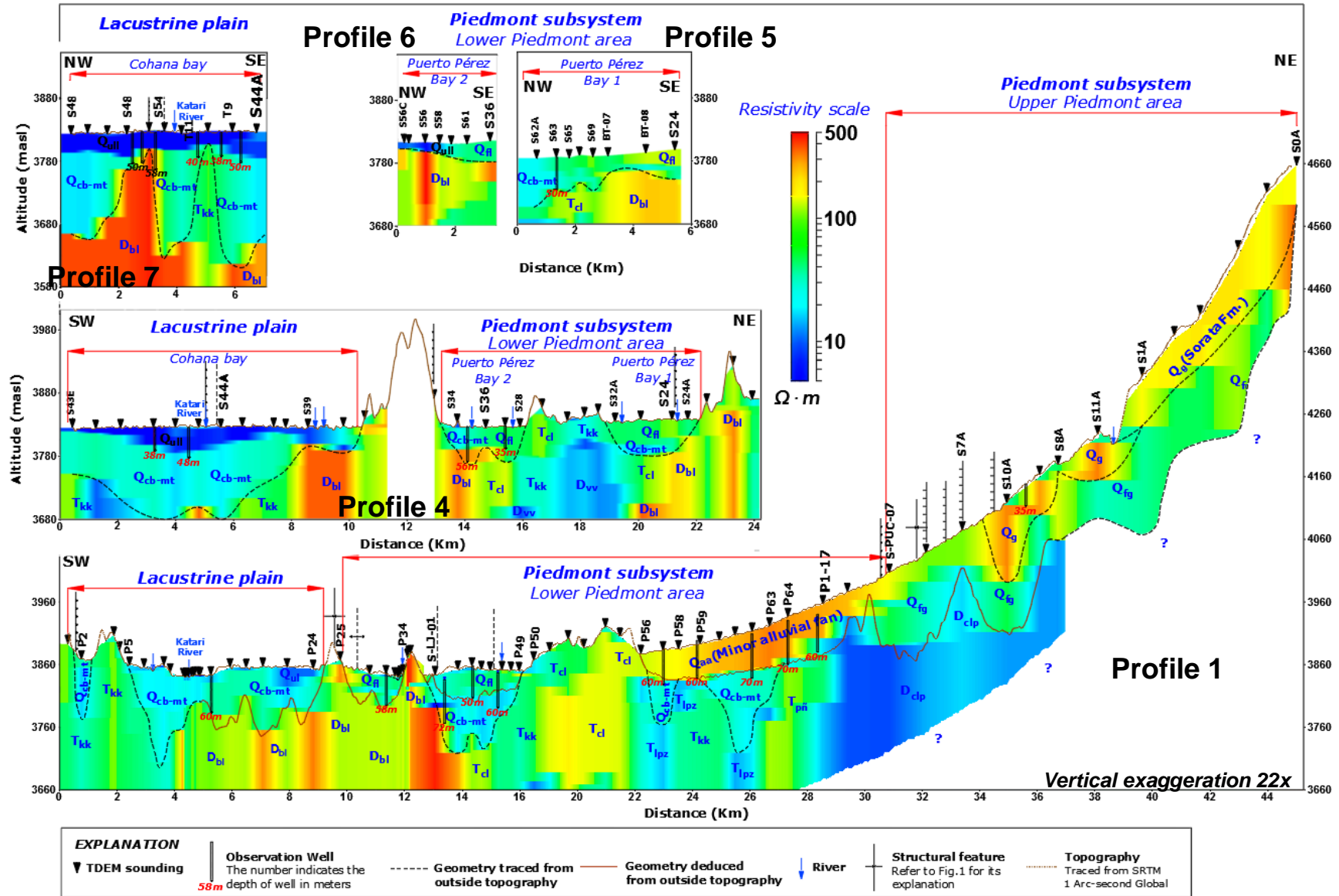


Figure 6. Geoelectrical profiles 1, 4, 5, 6 and 7, derived from TDEM soundings and overlaid by the geological formations found in the study area (Table 1, Fig.1 and Fig.2).

#### *Profile 4*

In Profile 4 (Fig.2, Fig.6), the sections located at ‘Puerto Perez Bay 1’ (i.e. soundings S24A to S32A) and at ‘Puerto Perez Bay 2’ (Fig. 6) provide more information about deposits from ancient lake invasions in the lower Piedmont area.

Sections located between soundings S24A-S32A and S28-S36 are characterized by a first layer with resistivity values of  $\sim 60$  to  $100 \Omega \cdot \text{m}$  and a thickness of 25 to 60 m, attributed to fluvio-lacustrine deposits (Qfl), which from borehole information corresponds to thin layered sequences comprising medium to coarse sand materials with clay content. A second layer is observed between soundings S24 and S23 ( $\sim 20$  to  $40 \Omega \cdot \text{m}$ ) and a thickness of 20 m, that might correspond to deposits from the Mataro and Cabana Lakes (Table 1).

Additionally, a change in resistivity values is observed immediately after section “S28-S36”. TDEM sounding S34 shows a first layer of resistivity of  $\sim 10 \Omega \cdot \text{m}$  and a thickness of  $\sim 10$  m, attributed to deposits from the Ballivian Lake, which from a nearby borehole is comprised of clay deposits (BH-2, Fig. 4). Below this first layer, a second layer with a resistivity value of  $\sim 30 \Omega \cdot \text{m}$  and a thickness of  $\sim 30$  m, is attributed to the non-differentiated Qcb-mt Formation (Table 1).

#### *Profiles 5 and 6*

Section S24A-S63 from Profile 5 (Fig.2 and Fig.6) shows additional information from the lower Piedmont area. It shows resistivity values of  $\sim 60$  to  $100 \Omega \cdot \text{m}$  and a thickness of  $\sim 20$  to 40 m, which are attributed to fluvio-lacustrine deposits (Qfl). Below this first layer, a second layer with resistivity values of  $\sim 30$  to  $40 \Omega \cdot \text{m}$  and a thickness of  $\sim 20$  m, is attributed as the non-differentiated Qcb-mt Formation. The same layer (Qcb-mt) is observed in TDEM sounding S62A but with a thickness of  $\sim 80$  m.

In addition, Profile 6 (Fig.2 and Fig.6) shows a first layer with resistivity values of  $\sim 60 \Omega \cdot \text{m}$  and a thickness of 20 to 40m, attributed to fluvio-lacustrine deposits (Qfl). Immediately after, section S58-S56C, shows a layer with resistivity values of  $\sim 10$  to  $20 \Omega \cdot \text{m}$  and a thickness of  $\sim 7$  to 20 m, which corresponds to clay deposits from the Ballivian Lake (Qull) (Table 1).

The Tertiary or Devonian bedrock underlying the Quaternary deposits has conductive values ( $T_{lpz} \sim 20\Omega\cdot m$ ;  $T_{pñ} \sim 50\Omega\cdot m$ ;  $D_{clp} \sim 15\Omega\cdot m$ ) suggesting clay content and/or fracturing for the Peñas ( $T_{pñ}$ ) and Vila Vila Formations ( $D_{vv}$ ), respectively (Table 1).

#### 4.2.2.2 Lacustrine plain (lake invasions)

##### *Profile 1*

Profile 1 (Fig.2, Fig.6) shows important information from the Lacustrine plain. From NE to SW, ancient lakes invasions are illustrated in section P24-P2. In section P24-P5, we find a first layer with resistivity values  $\sim 15\Omega\cdot m$  and a thickness varying from 2 to 30 m, which correspond to deposits from Paleo-lake Ballivian “Ulloma Formation” (Qull) (Table 1). From borehole information, consists of fine sands with clayey and silty layers. The resistivity value of  $15\Omega\cdot m$  suggests that the clay content is significant.

A deeper second layer, found in sections (P24-P5) with resistivity values  $\sim 30$  to  $40\Omega\cdot m$  and a thickness of 40 to 100 m, may belong to deposits from the ancient Lakes Cabana and Mataro, remaining as a unique non-differentiated formation (Qcb-mt) in this interpretation. Both formations are layered grounds with fluvial indications (alternating clay, sand and gravel deposits) (Table 1).

##### *Profile 3, 4 and 7*

Additional information from the lacustrine plain is depicted in Profile 3 (Fig.2, Fig.7). The subterranean channel, investigated in section S-PUC-09–S-18A (E-W direction, Figure 7) shows resistivity values of  $\sim 40$ - $70\Omega\cdot m$  and a thickness of  $\sim 40$  to 90 m, and is attributed to deposits from the ancient Cabana and Mataro Lakes, Qcb-mt (Table 1). This channel shows deposits with lateral continuity interconnecting the Piedmont subsystem and the Lacustrine plain.

Section S-PUC-14–T6 (SE-NW direction) depicts a first layer with resistivity values of  $\sim 10\Omega\cdot m$  and a thickness of 5 to 30m, attributed to deposits from Paleo-lake Ballivian (Qull). Then, a second layer with resistivity values of  $\sim 45\Omega\cdot m$  and a thickness of  $\sim 100$  m is shown in section S-PUC-14–T4; this layer is attributed to the non-differentiated Qcb-mt deposits from the ancient Lakes Cabana and Mataro (Table 1).

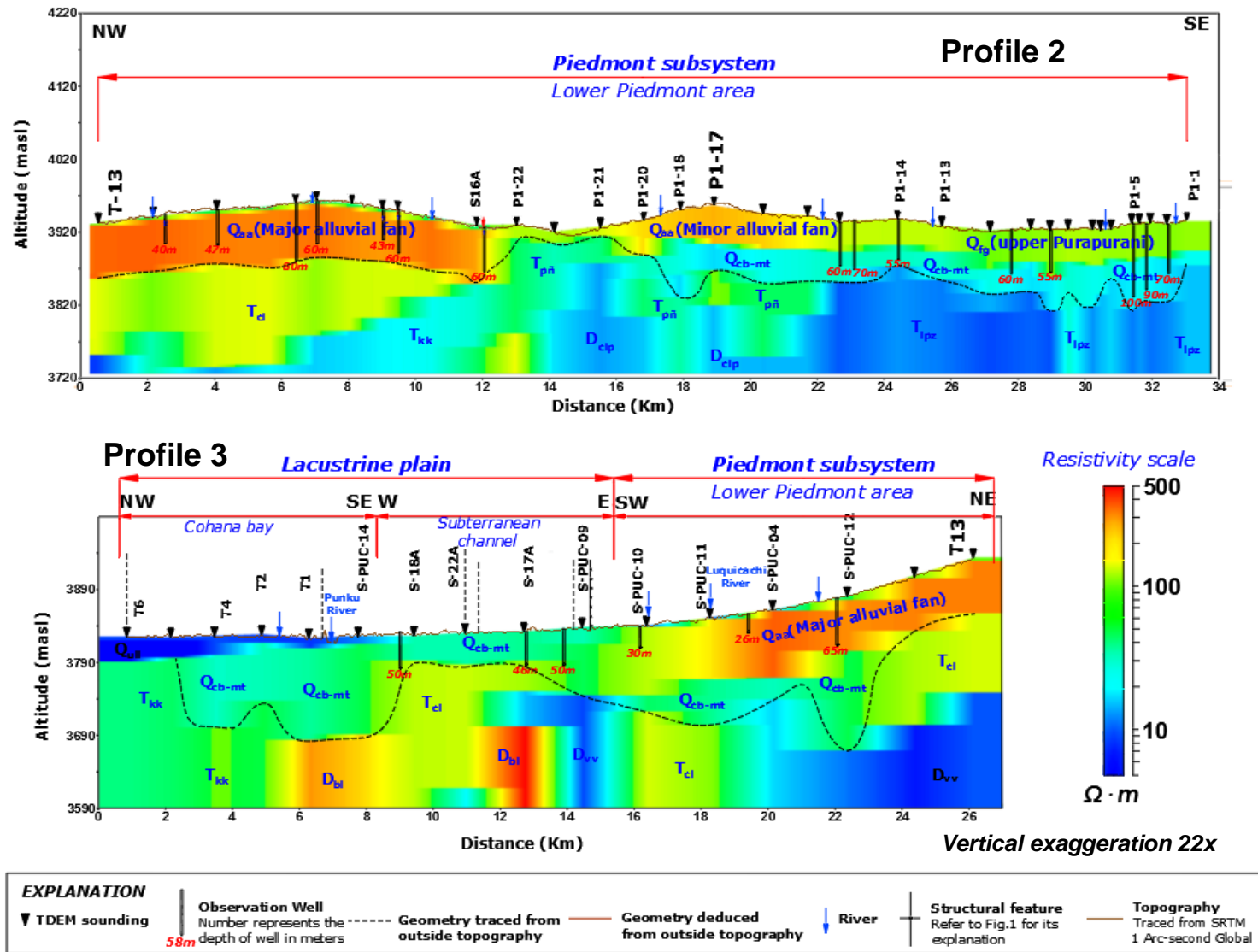


Figure 7. Geoelectrical profiles 2 and 3, derived from TDEM soundings and overlaid by the geological formations found in the study area (Table 1, Fig.1 and Fig.2).

The Lacustrine plain is also depicted in Profile 4 (Fig.6). Section S39-S43E shows a first layer with resistivity values of  $\sim 5$  to  $10 \Omega \cdot m$  and a thickness of  $\sim 7$  to  $45$  m, attributed to deposits from Paleo-lake Ballivian (Qull), composed of clayey and silty layers (Table 1). Then, a second layer with resistivity values of  $\sim 35$  to  $45 \Omega \cdot m$  and a thickness of  $\sim 40$  to  $140$  m may belong to the non-differentiated Qcb-mt Formation.

Profile 7 (Fig.6) provides more information from the Lacustrine plain. Section S44A-S48C shows a first layer with resistivity values of  $\sim 5$  to  $10 \Omega \cdot m$  and a thickness of  $\sim 30$  to  $45$  m and is attributed to deposits from the ancient Ballivian Lake, Qull (Table 1). Below, a second layer is observed in sections S44A-T9, T11-S54, S48-S48C with resistivity values of  $\sim 30$  to  $45 \Omega \cdot m$  and a thickness of  $20$  to  $150$  m, that may correspond to deposits from the non-differentiated Cabana and Mataro Lakes (Qcb-mt).

Similarly to what was found for the Piedmont subsystem, the Quaternary paleo-lacustrine deposits overlay the Tertiary or Devonian bedrock. Resistivity values (Tcl  $\sim 150 \Omega \cdot m$ ; Tkk  $\sim 40 \Omega \cdot m$ ; Dvv  $\sim 20 \Omega \cdot m$ ; Dbl  $\sim 500 \Omega \cdot m$ ) are considered to be the bottom of the paleo-lacustrine geologic media.

#### 4.2 Hydrogeochemical characteristics

Groundwater in the Piedmont subsystem (blue and green circles, Fig.3 and Fig.8) presents predominantly bicarbonate dominance with a noticeable increase of : i)  $Ca(Mg)$  relative to  $Na(K)$  facies with  $EC \sim 63 - 250 \mu S/cm$ , and ii)  $Na(K)$  relative to  $Ca(Mg)$  facies with  $EC \sim 251 - 500 \mu S/cm$ .

The  $Ca(Mg) - HCO_3^-$  facies relate silicate weathering from the Devonian/Silurian sedimentary bedrock in the ancient fluvial-alluvial and glacial sedimentary environments, while the  $Na(K)$  enrichments result from groundwater mixing. Indeed, TDEM results show that in the lower Piedmont fluvioglacial and alluvial layers (Qfg, Qaa) overlay paleo-lacustrine layers (Qcb-mt). Therefore, groundwater hosted in the Qfg, Qaa layers enriched in  $Ca(Mg) - HCO_3^-$  flushes the evaporite enriched water in exchangeable  $Na^+$  hosted in the Qcb-mt layers.

Notably, enrichment trends of  $SO_4^{2-}$  and  $Cl^-$  facies with mixed  $Na(K)$  and  $Ca(Mg)$  contributions are attributed to: i) seepage from influent rivers, i.e. sulphate-rich upstream

waters locally influenced by environmental liabilities from inactive mines (Fig. 3), or to ii) anthropogenic contamination from the urbanized areas of the city of El Alto (Fig. 3).

Finally, groundwater in the lacustrine plain (cyan circles, Fig.3, Fig.8) is for some sampling points enriched in  $Na(K) - Cl^-$  facies ( $EC \sim 1690 \mu S/cm$ ). These high conductivity waters stand for the presence of evaporites originated from past evaporation processes of lacustrine origin. Relatively high  $HCO_3^-$  and  $SO_4^{2-}$  concentrations ( $EC \sim 500$  to  $700 \mu S/cm$ ) are recorded for some samples located nearby the outcropping bedrock, especially those close to the Kollu-Kollu Formation (Tkk; Fig.1, Table 1).

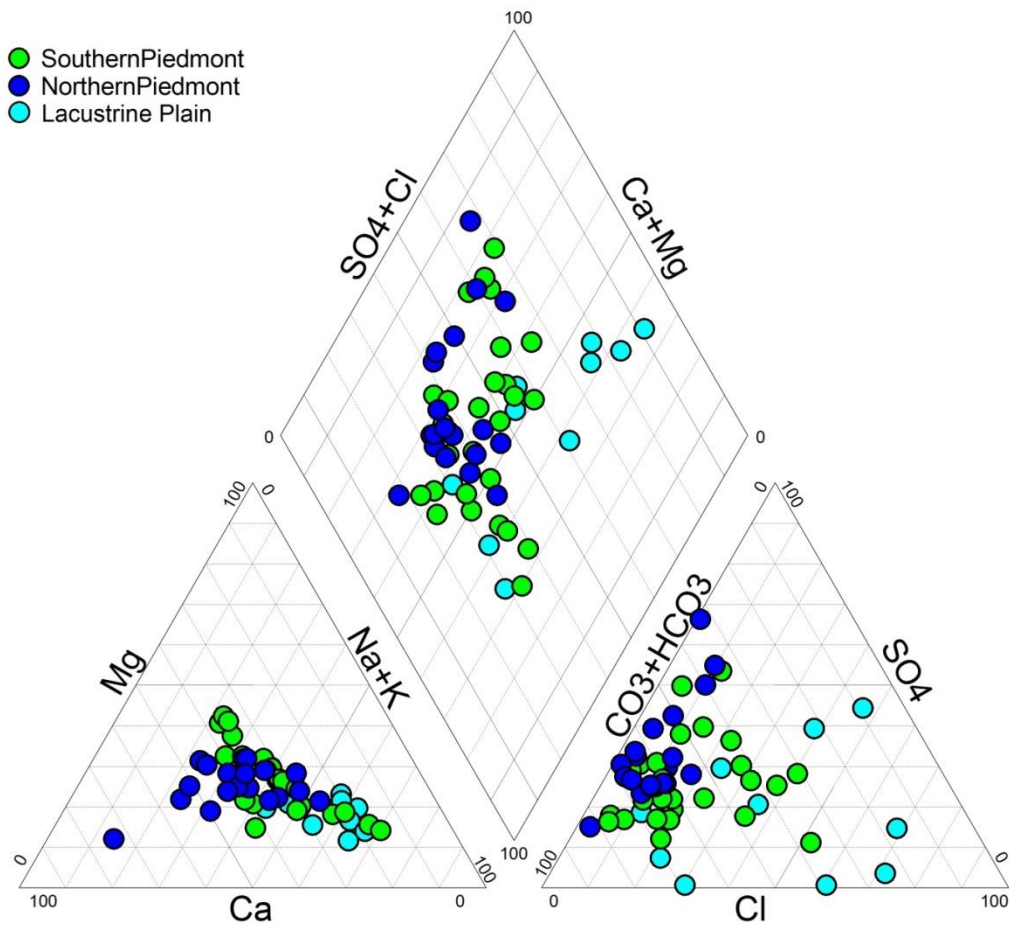


Figure 8. Piper diagram showing geochemical facies of groundwater within the Piedmont subsystem and Lacustrine plain. Refer to Fig.3 for the geographical location of this groundwater sampling points.

## 5. Discussion

### 5.1 Extension and physical properties of the aquifer

The aquifer extends from the Eastern Cordillera and is delimited by the most ancient lake invasion “Lake Mataro” towards the southern, western and northern sides of the Katari and Lago Menor Basin (Fig.9). According to Lavenu (1992) the top of the Mataro deposits would be an ablation surface developed at a present-day altitude of 3,950 m a.s.l around the paleo-basin (see Fig.1 and topographic curves of Fig.2). The limit of the aquifer towards the eastern side is delineated by the lower limit of rock glaciers defined to be at approximately 4700 m a.s.l by Rangecroft et al. (2014) (Fig. 2). More field work is required in the Achacachi region (Fig.1, Fig.2) because besides glacial erosion, the topographic curve of 3,950 m a.s.l also suggests the influence of ancient lake invasions and therefore could be part of the regional groundwater system.

The stratigraphic models presented in the results section are consistent with the Quaternary sediments being hydraulically connected and behaving as a single regional aquifer system. Continuity is locally disrupted when the substratum (Tertiary or Devonian Formations) outcrops inside the domain.

The aquifer comprises: i) glacial (Qg) and fluvioglacial (Qfg) outwash layers of ~200 m of thickness (above 4100 m a.s.l), in the upper Piedmont area, ii) fluvioglacial (Qfg) and paleo-lacustrine layers (Qcb-mt), ranging from ~50 to 150 m of thickness, in the lower Piedmont area, and iii) paleo-lacustrine layers (Qcb-mt) of ~40-150 m thickness in the Lacustrine plain. A clay aquitard (Ulloma Formation, Qull), overlaying the paleo-lacustrine layers (Qcb-mt) in the Lacustrine plain, presents a thickness of ~45 meters close to Lake Titicaca (Cohana bay) and decreases in thickness when far away from the Lake (Fig.9, Fig.10).

In fact, a large portion of the aquifer presents an unconfined behaviour whereas it remains confined below the Ulloma Formation (Fig.9, Fig.10). The thickness of the unconfined portion varies from 50 to 150 meters and that of the confined from 100 to 150 meters. Values of hydraulic conductivity for the unconfined portion range from  $1.1 \times 10^{-4}$  m/sec (alluvial fan deposits, Qaa),  $2.5 \times 10^{-6}$  m/sec (fluvioglacial deposits, Qfg) to  $5.9 \times 10^{-8}$  m/sec (glacial deposits, Qg) (JICA, 1987; M.M.A.yA, 2016 ; Barroso, 2010),

while for the confined part transmissivity values range around  $6.0 \times 10^{-6} \text{ m}^2/\text{sec}$  (paleo-lacustrine deposits, Qcb-mt) (JICA, 1987).

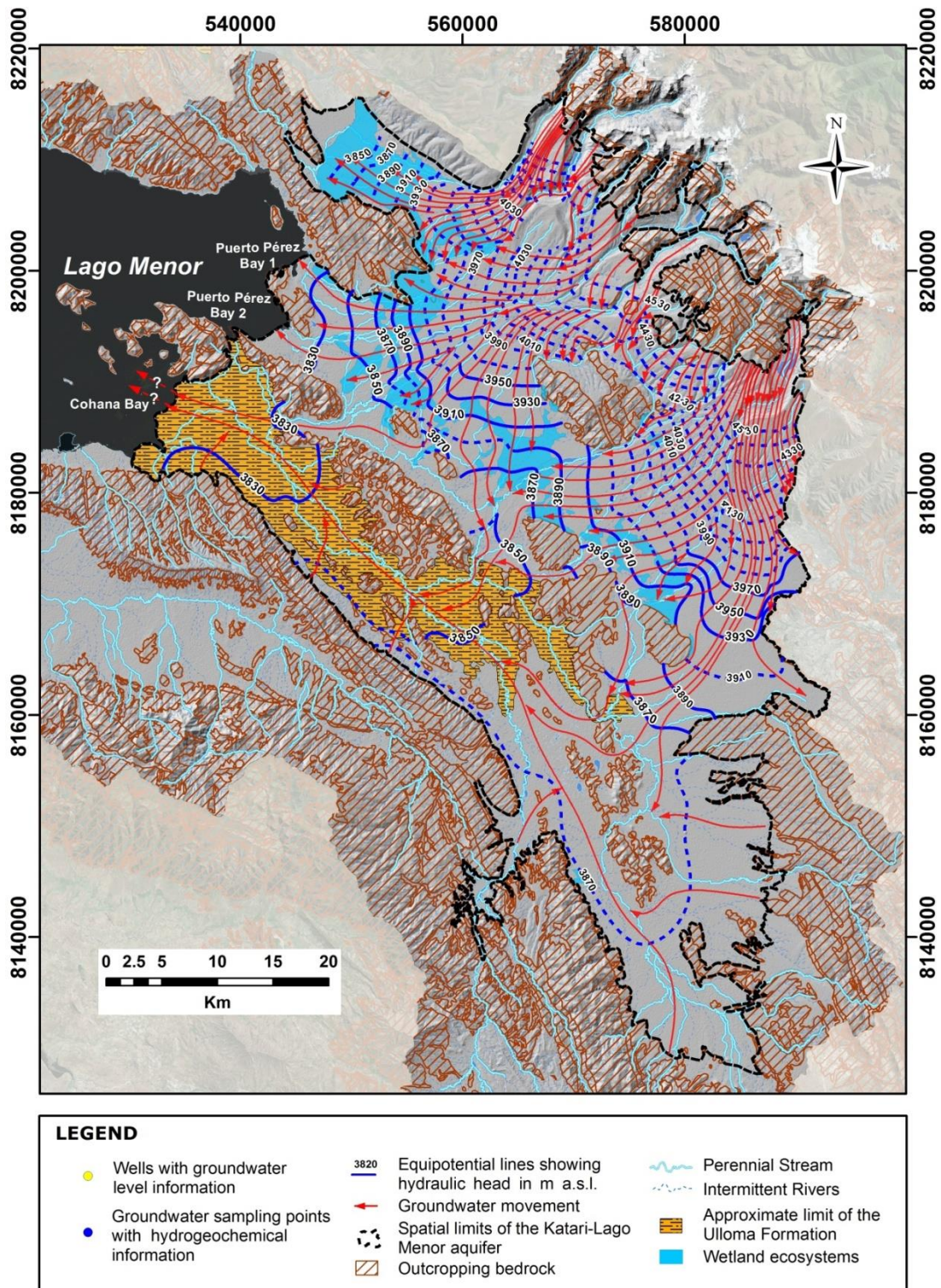


Figure 9. Groundwater flow map of the Katari-Lago Menor Basin aquifer under natural conditions (prior to any large scale withdrawal). Dashed blue equipotential lines are derived from the combination of the interpreted geological, TDEM, landscape, hydraulic head and geochemical data.

## 5.2 Regional hydrogeological and geochemical functioning

The groundwater flow system displayed in Fig.9 corresponds to a classical gravity-driven regional groundwater flow (Tóth, 1999; Navarro de León et al., 2005; Tóth and Hayashi, 2010; Mádl-Szönyi et al., 2015). Regions with dashed potentiometric contours were inferred from the combination of the interpreted geological, TDEM, landscape and groundwater hydrochemical data.

Groundwater flow within the Katari and Lago Menor Basin is composed of several interconnected groundwater flow systems (Fig.9). The main groundwater flow system starts in the upper Piedmont (high mountain ranges of the Eastern Cordillera) and follows the topographic Piedmont gradient (NE to SW) (Fig. 9 and Fig.10). Most groundwater recharge results from the infiltration of precipitation and runoff on the high mountain ranges. Indeed, groundwater circulating in the Piedmont layers (Qg, Qfg, Qaa) show bicarbonate dominance with an enrichment of  $Ca(Mg)$  facies (Fig.10). However, when this type of water mixes with the evaporite enriched water of lacustrine origin,  $Na(K)$  is released.

The outcrops of the Devonian and Tertiary Formations within the Piedmont subsystem (Fig.9 and Fig.10) act as underground barriers that deviate the flow to generate individualised groundwater flow systems. Most of these groundwater flow systems enter directly into Lake Titicaca (Puerto Perez Bays) and others reach the Lacustrine plain. In contrast, the interruption of Quaternary deposits in the southern limit due to the topographic depression (west of La Paz and Achocalla Cities) generates a natural outflow of groundwater towards the hillsides of La Paz and Achocalla Cities.

The outcropping rock formations between the Piedmont subsystem and Lacustrine plain, act as barriers that constrain the direction of the water flow, resulting in different types of groundwater discharge in the lower Piedmont, particularly wetlands (Fig.9 and Fig.10), where a large stock of groundwater is evaporated. According to Tóth (1999) and Tóth and Hayashi (2010) these typical hydrologic features also result from the action of groundwater moving in basin-scale gravity-flow systems.

Finally, the groundwater flow systems that reach the Lacustrine plain and the groundwater flow system starting in the Collana limit (Fig.1, Fig.9) follow the SE-NW topographic gradient towards Lake Titicaca (Cohana Bay). Groundwater hosted in the Qcb-mt layers

probably moves further since the present Lake Titicaca overlays deposits from Paleo-lake Ballivian “Ulloma Formation, Qull” (Fig.9 and Fig.10) and these deposits overlay the Qcb-mt deposits.

In the Lacustrine plain, groundwater hosted in the paleo-lacustrine layers (Qcb-mt), underlying the clay aquitard (Qull, Ulloma Formation) presents predominantly  $Na(K) - Cl^-$  facies relating the presence of evaporites. The presence of this aquitard may retard dissolution processes of these soluble minerals due to low infiltration rates of meteoric waters or any contaminants as it is attested by the high electrical conductivity values in this area ( $\sim 1690 \mu S/cm$ ). Additionally, the increases of  $HCO_3^-$  and  $SO_4^{2-}$  anions can relate to ancient processes that favoured the erosion of Tertiary Formations containing evaporitic rocks such as the Kollu-Kollu Formation (Tkk ; Table 1) which is composed of evaporitic layers (limestone and gypsum) at the top of the formation (Zeballos et al., 2017). In fact, Quino et al. (2019) reported the same hydrogeochemical patterns in groundwater samples located close to the Tkk Formation.

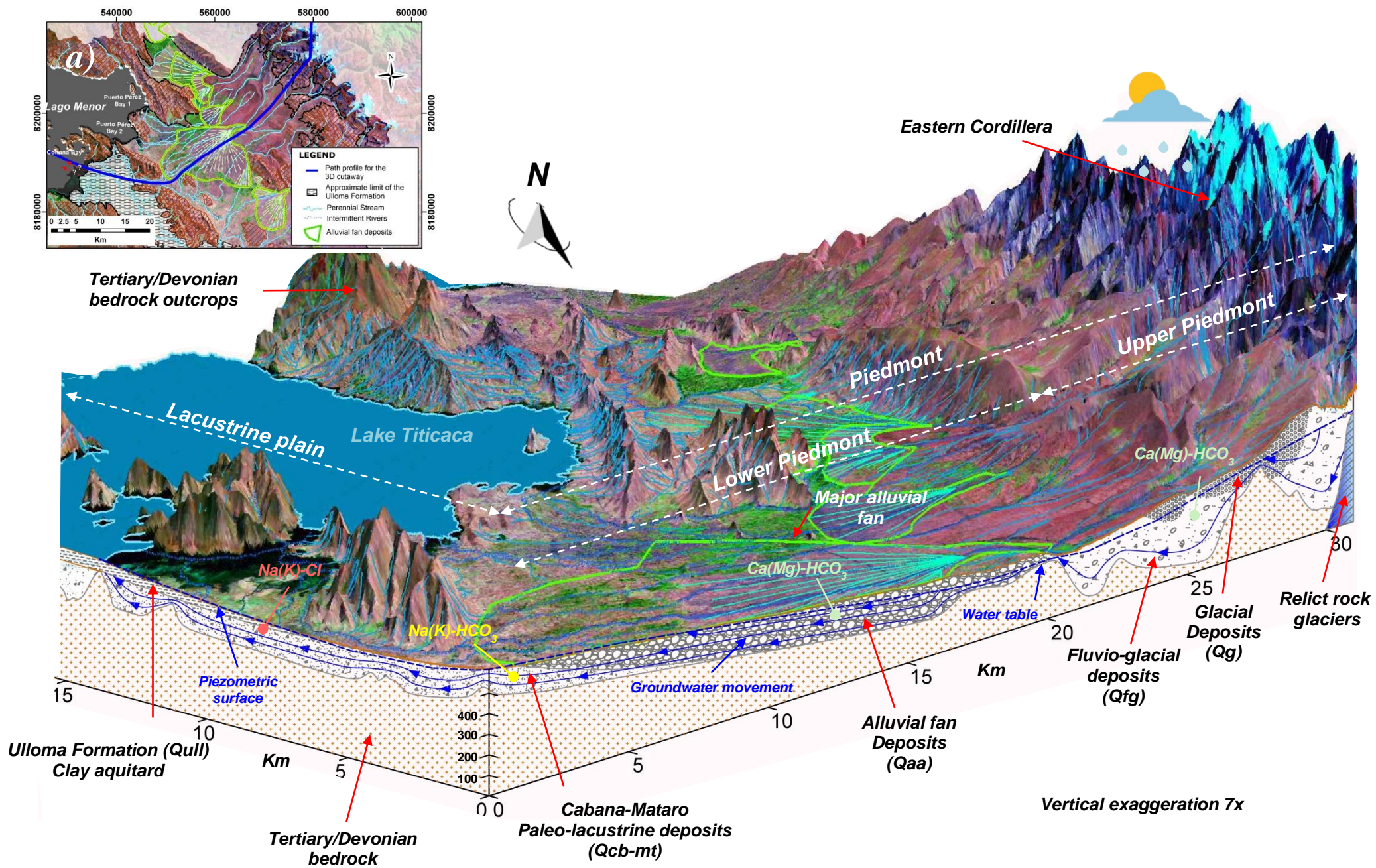


Figure 10. a) Location of the path profile for the 3D cut, and b) 3D conceptual model of the aquifer structure and its hydrogeological functioning.

## *6. Conclusions and final recommendations*

This paper presents a multidisciplinary study using geology, geophysics (TDEM), geochemistry, and groundwater level measurements for the assessment of a large scale aquifer within the Katari and Lago Menor Basin, located in the semi-arid Altiplano, between the Eastern Cordillera and the south-east of Lake Titicaca. This study gives a first insight of the 3D geometry and the geochemical and hydrogeological functioning of the Katari-Lago Menor Basin aquifer. Some of the necessary information for further sustainable management of this aquifer, such as geometry and extent of the domain, physical parameters and boundary conditions, are now available.

Time Domain Electromagnetics (TDEM) was found as an efficient method for identifying the subsurface structure of the different geological formations present in the study area, within the range of 0 to 200 m depth. Resistivity profiles combined with geology, borehole lithology, topography as well as additional groundwater level and geochemical measurements, were helpful in resolving the spatial limits of the aquifer, the vertical and lateral continuity of the Quaternary porous geologic media, the shape and position of the bottom of the aquifer (depth to the bedrock, i.e. Tertiary or Devonian Formations), and revealed a general overview of the natural dynamic behaviour of the aquifer at the scale of the Katari and Lago Menor Basin.

The stratigraphic models were consistent with the Quaternary sediments being hydraulically connected and behaving as a single regional aquifer system. The main groundwater flow system starts in the upper Piedmont, follows the topographic Piedmont gradient (NE to SW) and discharges in a series of wetlands. Part of the groundwater flow that reaches the Lacustrine plain follows the SE-NW topographic gradient towards Lake Titicaca (Cohana Bay).

The next step is the development of a 3D numerical groundwater flow model to improve the understanding of the whole groundwater flow system in this aquifer. The building of this model also could be facilitated by denser electromagnetic TDEM surveys (ground based or airborne). This model will be a powerful tool for the sustainable management of groundwater resources. Such type of model will help in evaluating and quantifying the groundwater resources and test different groundwater development scenarios including pollution problems.

## *Acknowledgments*

*The present study was undertaken with the financial support of the Plurinational State of Bolivia provided through the Program “100 Scholarships for Postgraduate Education within the Framework of Technological and Scientific Sovereignty”, Supreme Decree 2100 (1 September 2014) and administered by the Ministry of Education (MINEDU). And partly funded by LABEX OSUG@2020, ANR grant no.ANR-10-LABX-56 (financed by the Future Investments programme launched by the French government and implemented by the ANR). We would like to thanks to the Ministry of Environment and Water (M.M.A.yA, La Paz) and the University of San Andres (UMSA, La Paz) for their logistical and technical support. Special thanks to Marizol Flores, Elise Levasseur, Enrique and Mr. Julio César Salinas for their assistance in the field work, to the IGE laboratory for their technical assistance and support during the analysis of the water samples, and to the local communities of the Municipalities of Pucarani, Batallas, Laja, Viacha, Puerto Pérez and El Alto for their support during the field work.*

## *References*

- Abbott, M.B., Wolfe, B.B., Wolfe, A.P., Seltzer, G.O., Aravena, R., Mark, B.G., Polissar, P.J., Rodbell, D.T., Rowe, H.D., Vuille, M., 2003. Holocene paleohydrology and glacial history of the central Andes using multiproxy lake sediment studies. *Palaeogeography, Palaeoclimatology, Palaeoecology* 194, 123-138.
- Achá, D., Guédron, S., Amouroux, D., Point, D., Lazzaro, X., Fernandez, P.E., Sarret, G., 2018. Algal Bloom Exacerbates Hydrogen Sulfide and Methylmercury Contamination in the Emblematic High-Altitude Lake Titicaca. *Geosciences* 8, 438.
- Agramont, A., Craps, M., Balderrama, M., Huysmans, M., 2019. Transdisciplinary Learning Communities to Involve Vulnerable Social Groups in Solving Complex Water-Related Problems in Bolivia. *Water* 11, 385.
- Araos, J.M., Le Roux, J.P., Gutierrez, N.M., 2017. Relict glacial landscape in the Sierra Baguales Mountain Range (50°-51° S): evidence of glaciation dynamics and types in the eastern foothills of the southern Patagonian Andes. *J. Mt. Sci.* 14(2): 282-295.
- Archundia, D., Duwig, C., Spadini, L., Uzu, G., Guedron, S., Morel, M.C. 2017a. How Uncontrolled Urban Expansion Increases the Contamination of the Titicaca Lake Basin (El Alto, La Paz, Bolivia). *Water Air And Soil Pollution* 228, 44.
- Archundia, D., Duwig, C., Lehembre, F., Chiro, n S., Morel, M.C., Prado, B., Bourdat-Deschamps, M., Vince, E., Flores Aviles, G., Martins, J.M.F., 2017b. Antibiotic pollution in the Katari subcatchment of the Titicaca Lake: major transformation products and occurrence of resistance genes. *Science of the Total Environment* 576, 671–682.
- Argollo, J., Mourguiart, P. 1995. Los Climas Cuaternarios de Bolivia. *Cambios Cuaternarios en América del Sur*. In: JArgollo, J., Mourguiart, P. (Eds.), *Climas Cuaternarios en América del Sur*. ORSTOM-UMSA, 135-155.
- Argollo, J., Mourguiart, P., 2000. Late Quaternary climate history of the Bolivian Altiplano. *Quaternary International* 72, 37-51.

- Argollo J, Iriondo M (2008) *El Cuaternario de Bolivia y Regiones vecinas*. Ed.: Moglia (ISBN 9872463700), 280 pages.
- Auken, E., Christiansen, A. V., Jacobsen, B.H., Foged, N., Sørensen, K.I., 2005. Piecewise 1D laterally constrained inversion of resistivity data, 2005. *Geophysical Prospecting* 53 (4), 497-506.
- Ballivian, O., Bles, J.E., Servant, M., 1978. El Plio-Cuaternario de la Región de La Paz (Andes Orientales, Bolivia). *Cah. O.R.S.T.O.M. sér. Géol.* 10 (1), 101–113.
- Barroso, C.A., 2010. Delimitación de la contaminación del agua subterránea por lixiviados en un till glacial del relleno sanitario “Villa Ingenio”: El Alto-Bolivia. Universidad Mayor Real Pontificia de San Francisco Xavier de Chuquisaca. Tesis de Posgrado.
- B.I.D., 2016. Programa de Saneamiento del Lago Titicaca (Cuenca Katari, Bahía Cohana) BO-L1118. Marco de Gestión Ambiental y Social (MGAS), 87 pp.
- Bush, M.B., Hanselman, J.A., Gosling, W.D., 2010. Nonlinear climate change and Andean feedbacks: an imminent turning point? *Global Change Biology* 16 (12), 3223-3232.
- Canedo, C., Pillco, Z.R., Berndtsson, R., 2016. Role of Hydrological Studies for the Development of the TDPS System. *Water* 8(4), 144.
- Condom, T., Coudrain, A., Dezetter, A., Brunstein, D., Delclaux, F., Sicart, J.E., 2004. Transient modelling of lacustrine regressions: two case studies from the Andean Altiplano. *Hydrol. Process.* 18, 2395–2408.
- Cross, S., Baker, P., Seltzer, G., Fritz, S., Dunbar, R., 2001. Late Quaternary Climate and Hydrology of Tropical South America Inferred from an Isotopic and Chemical Model of Lake Titicaca, Bolivia and Perú. *Quaternary Research* 56(1), 1-9.
- Coudrain-Ribstein, A., Olive, P., Quintanilla, J., Sondag, F., Cahuaya, D., 1995. Salinity and isotopic dynamics of the groundwater resources on the Bolivian Altiplano. *Application of Tracers in Arid Zones Hydrology, Proceedings of the Vienna Symposium*. IAHS Publ. 232, 267-276.
- Descloitres, M., Chalikakis, K., Legchenko, A., Moussa, A.M., Genthon, P., Favreau, G., Le Coz, M., Boucher, M., Oï, M., 2013. Investigation of groundwater resources in

the Komadugu Yobe Valley (Lake Chad Basin, Niger) using MRS and TDEM methods. *Journal of African Earth Sciences* 87, 71–85.

- Emmer, A., Juřicová, A., Veettil, B.K., 2019. Glacier retreat, rock weathering and the growth of lichens in the Churup Valley, Peruvian Tropical Andes. *J. Mt. Sci.* 16(7), 1485-1499.
- Fernandes, A.J., Maldaner, C.H., Negri, F., Rouleau, A., Wahnfried, I.D. 2016. Aspects of a conceptual groundwater flow model of the Serra Geral basalt aquifer (Sao Paulo, Brazil) from physical and structural geology data. *Hydrogeol. J.* 24, 1199–1212.
- Fitterman, D.V., Stewart, M.T., 1986. Transient electromagnetic sounding for groundwater. *Geophysics* 51(4), 995-1005.
- Foster, S., Koundouri, P., Tuinhof, A., Kemper, K., Nanni, M., Garduno, H., 2006. Groundwater dependent ecosystems: the challenge of balanced assessment and adequate conservation. GW Mate briefing note series; no. 15. Washington, DC: World Bank. <http://documents.worldbank.org/curated/en/407851468138596688>
- Fritz, S.C., Baker, P.A., Lowenstein, T.K., Seltzer, G.O., Rigsby, C.A., Dwyer, G.S., Tapia, P.M., Arnold, K.K., Ku, T.L., Luo, S., 2004. Hydrologic variation during the last 170,000 years in the southern hemisphere tropics of South America. *Quaternary Research* 61, 95– 104.
- Fritz, S.C., Baker, P.A., Tapia, P., Garland, J., 2006. Spatial and temporal variation in cores from Lake Titicaca, Bolivia/Peru during the last 13,000 years. *Quaternary International* 158(1), 23-29.
- Fritz, S.C., Baker, P.A., Seltzer, G.O., Ballantyne, A., Tapia, P., Cheng, H., Edwards, R.L., 2007. Quaternary glaciation and hydrologic variation in the South American tropics as reconstructed from the Lake Titicaca drilling project. *Quaternary Research* 68 (3), 410-420.
- Garcia, M.E., Bengtsson, L., Persson, K.M., 2010. On the distribution of saline groundwater in the Poopó Basin, Central Bolivian Highland. *Journal of Water Management and Research* 66, 199–203.

- Geerts, S., Raes, D., Garcia, M., Taboada, C., Miranda, R., Cusicanqui, J., Mhizha, T., Vacher, J., 2009. Modeling the potential for closing quinoa yield gaps under varying water availability in the Bolivian Altiplano. *Agricultural Water Management* 96, 1652–1658.
- GEOSIRH, 2017. Infraestructura de Datos Espaciales. Plan Director de la Cuenca Katari y Lago Menor del Titicaca. Ministerio de Medio Ambiente y Agua. Viceministerio de Recursos Hídricos y Riego. <http://geosirh.riegobolivia.org/layers/geosirh>.
- GEOBOL, 1995. Geological sheets Calamarca N° 5943, Jesús Macha N° 5843, Tiahuanacu N°5844, La Paz N°5944, Achacachi N°5845 and Milluni N°5945 Escala 1:100000, Servicio Geologico de Bolivia (GEOBOL) and Geological Swedish AB (eds).
- Gómez, E., Barmen, G., Rosberg, J., 2016. Groundwater Origins and Circulation Patterns Based on Isotopes in Challapampa Aquifer, Bolivia. *Water* 8, 207.
- Gómez, E., Larsson, M., Dahlin, T., Barmen, G., Rosberg, J.E., 2019. Alluvial aquifer thickness and bedrock structure delineation by electromagnetic methods in the highlands of Bolivia. *Environmental Earth Sciences* 78, 84.
- Gonzales Amaya, A., Ortiz, J., Durán, A., Villazón, M., 2018a. Hydrogeophysical methods and hydrogeological models: basis for groundwater sustainable management in Valle Alto (Bolivia) . *Sustainable Water Resources Management* 5(3), 1179-1188.
- Gonzales Amaya, A., Mardh, J., Dahlin, T., 2018b. Delimiting a saline water zone in Quaternary fluvial–alluvial deposits using transient electromagnetic: a case study in Punata, Bolivia. *Environmental Earth Sciences* 77,46.
- Guédron, S., Point, D., Acha, D., Bouchet, S., Baya, P.A., Tessier, E., Monperrus, M., Molina, C.I., Groleau, A., Chauvaud, L., Thebault, J., Amice, E., Alanoca, L., Duwig, C., Uzu, G., Lazarro, X., Bertrand, A., Bertrand, S., Barbraud, C., Delord, K., Gibon, F.M., Ibanez, C., Flores, M., Fernandez Saavedra, P., Ezpinoza, M.E., Heredia, C., Rocha, F., Zepita, C., Amouroux, D., 2017. Mercury contamination level and speciation inventory in Lakes Titicaca & Uru-Uru (Bolivia): Current status and future trends. *Environmental Pollution* 231, 262-270.

- Guérin, R., Descloitres, M., Coudrain, A., Talbi, A., Gallaire, R., 2001. Geophysical surveys for identifying saline groundwater in the semi-arid region of the central Altiplano, Bolivia. *Hydrological Processes* 15, 3287–3301.
- Harrington, J.S., Mozil, A., Hayashi, M., Bentley, L.R., 2018. Groundwater flow and storage processes in an inactive rock glacier. *Hydrological processes*. doi: 10.1002/hyp.13248.
- Heine, K., 2004. Late Quaternary Glaciations of Bolivia. *Quaternary Glaciations-Extent and Chronology 2(C)*, 83–88.
- JICA, 1987. Final Report for the Study on groundwater development Project on El Alto district in La Paz city. Japan International Cooperation Agency. Republic of Bolivia.
- Jones, D.B., Harrison, S., Anderson, K., Whalley, W.B., 2019. Rock glaciers and mountain hydrology: A review. *Earth-Science Reviews*, 193, 66-90.
- Kinouchi, T., Liu, T., Mendoza, J., Asaoka, Y., 2013. Modeling glacier melt and runoff in a high-altitude headwater catchment in the Cordillera Real, Andes. *Hydrol. Earth Syst. Sci. Discuss.*, 10, 13093–13144.
- Kinouchi, T., Nakajima, T., Mendoza, J., Fuchs, P., Asaoka, Y., 2019. Water security in high mountain cities of the Andes under a growing population and climate change: A case study of La Paz and El Alto, Bolivia. *Water Security* 6, 100025.
- Lamb, S., Hoke, L., 1997. Origin of the high plateau in the Central Andes, Bolivia, South America. *Tectonics* 16(4), 623-649.
- Lavenu, A., 1992. Formation and geological evolution. In: Dejoux, C., Iltis, A. (Eds.), *Lake Titicaca: A Synthesis of Limnological Knowledge*, Kluwer Academic Publishers, pp. 3-13.
- Mádl-Szönyl, J., Tóth, Á., 2015. Basin-scale conceptual groundwater flow model for an unconfined and confined thick carbonate region. *Hydrogeol. J.* 3, 1359–1380.
- Maldonado, L., Bécher, F., Cabrera, A., Blarasina, M., Lutria, V., Matteoda, E., Giuliano, J., 2018. Hydrogeochemical features and groundwater renewal rate estimates from

- deep aquifers in the Pampean plain, Córdoba province, Argentina. *Journal of South American Earth Sciences* 85, 126–134.
- Melly, B.L., Schael, D.M., Gama, P.T., 2017. Perched wetlands: An explanation to wetland formation in semi-arid areas. *Journal of Arid Environments* 141, 34-39.
- Mira, A., Veroslavsky, G., Rossello, E., Vives, L., 2015. Subsurface geological modeling of Corrientes province (NE Argentina) and its relationships with the Guaraní Aquifer system function. *Journal of South American Earth Sciences* 62, 148-163.
- Murray, B.P., Horton, B.K., Matos, R., Heizler, M.T., 2010. Oligocene–Miocene basin evolution in the northern Altiplano, Bolivia: Implications for evolution of the central Andean backthrust belt and high plateau. *GSA Bulletin* 122(9/10), 1443–1462.
- M.M.A.yA., 2014. Plan Maestro Metropolitano de Agua Potable y Saneamiento La Paz - El Alto, Bolivia. Ministerio de Medio Ambiente y Agua, Viceministerio de Recursos Hídricos y Riego, La Paz, Bolivia, 932 pp.
- M.M.A.yA., 2016. Plan de Manejo Preliminar de los Acuíferos de Purapurani y Viacha. Ministerio de Medio Ambiente y Agua, Viceministerio de Recursos Hídricos y Riego, La Paz, Bolivia, 184 pp.
- Navarro de León, I., Gárfias-Soliz, J., Mahknecht, J., 2005. Groundwater flow regime under natural conditions as inferred from past evidence and contemporary field observations in a semi-arid basin: Cuenca de la Independencia, Guanajuato, México. *Journal of Arid Environments* 63, 756–771
- N.A.S.A, 2000. Shuttle Radar Topography Mission (SRTM) 1 Arc-Second Global, project from the National Aeronautics and Space Administration. Available at <http://dds.cr.usgs.gov/ee-data/coveragemaps/shp/ee/srtm/srtm.zip>
- Pauritsch, M., Wagner, T., Winkler, G., Birk, S., 2017. Investigating groundwater flow components in an Alpine relict rock glacier (Austria) using a numerical model. *Hydrogeol. J.* 25, 371–383.
- Placzek, C.J., Quade, J., Patchett, P.J., 2011. Isotopic tracers of paleohydrologic change in large lakes of the Bolivian Altiplano. *Quaternary Research* 75, 231–244.

- Oyarzún, R., Barrera, F., Salazar, P., Maturama, H., Oyarzún, J., Aguirre, E., Alvarez, P., Jourde, H., Kretschmer, N., 2014. Multi-method assessment of connectivity between surface water and shallow groundwater: the case of Limarí River basin, north-central Chile. *Hydrogeol. J.* 22, 1857–1873.
- Quesada, B., Sylvestre, F., Vimeux, F., Black, J., Paillès, C., Sonzogni, C., Alexandre, A., Blard, P.H., Tonetto, A., Mazur, J.C., Bruneton, H., 2015. Impact of Bolivian paleolake evaporation on the  $\delta^{18}\text{O}$  of the Andean glaciers during the last deglaciation (18.5-11.7 ka): diatom-inferred  $\delta^{18}\text{O}$  values and hydro-isotopic modeling. *Quaternary Science Reviews* 120, 93-106.
- Quino, L.I., Ormachea, M.M., Ramos Ramos, O.E., Bhattacharya, P., Quispe, C.R., Quintanilla, A.J., Sracek, O., 2019. Hydrochemical assessment with respect to arsenic and other trace elements in the Lower Katari Basin, Bolivian Altiplano. *Groundwater for Sustainable Development* 8, 281–293.
- Rabatel, A., Francou, B., Soruco, A., Gomez, J., Caceres, B., Ceballos, J.L., 2013. Current state of glaciers in the tropical Andes: a multi-century perspective on glacier evolution and climate change. *Cryosphere* 7(1), 81–102.
- Ramos Ramos, O.E., 2014. Geochemistry of trace elements in the Bolivian Altiplano- Effects of natural processes and anthropogenic activities. PhD Thesis, Royal Institute of Technology in Stockholm, Universidad Mayor de San Andrés La Paz, 68 pp.
- Rangecroft, S., 2014. Rock glaciers, water security and climate change in the Bolivian Andes. PhD thesis, University of Exeter, 318 pp.
- Rangecroft, S., Suggitt, A.J., Anderson, K., Harrison, S., 2016. Future climate warming and changes to mountain permafrost in the Bolivian Andes. *Climatic Change* 137 (1-2), 231-243.
- Salvaderry - Aranguren, M.M., Probst, A., Roulet, M., Isaure, M.P., 2008. Contamination of surface waters by mining wastes in the Milluni Valley (Cordillera Real, Bolivia): Mineralogical and hydrological influences. *Applied Geochemistry* 23(5), 1299-1324.

- Sánchez-Saldías, A., Fariña, R.A., 2014. Palaeogeographic reconstruction of Minchin palaeolake system, South America: The influence of astronomical forcing. *Geoscience Frontiers* 5, 249-259.
- Satge, F., Denezine, M., Pillco, R., Timouk, F., Pinel, S., Molina, J., Garnier, J., Seyler, F., Bonnet, M.P., 2016. Absolute and relative height-pixel accuracy of SRTM-GL1 over the South American Andean Plateau. *ISPRS Journal Photogrammetry and Remote Sensing* 121, 157–166.
- Simler, R., 2014. Manuel d'utilisation DIAGRAMMES. Pages 1-42
- Soruco, A., Vincent, C., Rabatel, A., Francou, B., Thibert, E., Sicart, J., & Condom, T. (2015). Contribution of glacier runoff to water resources of La Paz city, Bolivia (16° S). *Annals of Glaciology*, 56(70), 147-154.
- Suárez-Soruco, R., Díaz-Martínez, E., 1996. Léxico Estratigráfico de Bolivia. *Revista Técnica de Yacimientos Petrolíferos Fiscales Bolivianos*, 17(1-2), 3-227.
- Sugaki, A., Kitakaze, A., 1988. Tin-bearing Minerals from Bolivian Polymetallic Deposits and their Mineralization Stages. *Mining Geology* 38(5), 419-435.
- Tóth, J., 1999. Groundwater as a geologic agent: An overview of the causes, processes, and manifestations. *Hydrogeol. J.* 7, 1–14.
- Tóth, J., Hayashi M., 2010. The theory of basinal gravity flow of groundwater and its impacts on hydrology Japan. *J. Groundwater Hydrol.* 52, 335-354.
- Uribe, J., Muñoz, J.F., Gironás, J., Oyarzún, R., Aguirre, E., Aravena, R., 2015. Assessing groundwater recharge in an Andean closed basin using isotopic characterization and a rainfall-runoff model: Salar del Huasco basin, Chile. *Hydrogeol. J.* 23: 1535–1551.
- Viguié, B., Jourde, H., Yáñez, G., Lira, E., Leonardi, V., Moya, C., García-Pérez, T., Maringue, J., Lictevout, E., 2018. Multidisciplinary study for the assessment of the geometry, boundaries and preferential recharge zones of an overexploited aquifer in the Atacama Desert (Pampa del Tamarugal, Northern Chile). *J. South Am. Earth Sci.* 86, 366–383.

- Veettil, B.K., Wang, S., Simões, J.C., Ruiz Pereira, S.F., 2018. Glacier monitoring in the eastern mountain ranges of Bolivia from 1975 to 2016 using Landsat and Sentinel-2 data. *Environ. Earth Sci.* 77, 452.
- Winkler, G., Wagner, T., Pauritsch, M., Birk, S., Kellerer-Pirklbauer, A., Benischke, R., Leis, A., Morawetz, R., Schreilechner, M.G., Hergarten, S., 2016. Identification and assessment of groundwater flow and storage components of the relict Schöneben Rock Glacier, Niedere Tauern Range, Eastern Alps (Austria). *Hydrogeol. J.* 24, 937–953.
- Zeballos, A., Weihd, P., Blanco, M., Machaca, V., 2016. Geological, mineralogical and chemical characterization of Devonian kaolinite-bearing sediments for further applications in the ceramic (tiles) industry in La Paz, Bolivia. *Environ. Earth Sci.* 75, 546.
- Zeballos, A., Weihd, P., Blanco, M., Machaca, V., 2017. Characterization of some nonmetallic resources in Bolivia: an overview of their potentiality and their application in specialized formulations. *Environ. Earth Sci.* 76, 754.
- Zech, R., Kull, C., Kubik, P.W., Veit, H., 2007. LGM and Late Glacial glacier advances in the Cordillera Real and Cochabamba (Bolivia) deduced from  $^{10}\text{Be}$  surface exposure dating. *Clim. Past*, 3, 623–635.

### 4.3 Conclusions

Results from the regional geophysical characterization confirmed that the Quaternary porous geologic media in the Katari and Lago Menor Basin behaves as one single complex entity, hydraulically connected. In addition, the systematic changes in the water's anion facies from  $HCO_3^-$  through  $SO_4^{2-}$  to  $Cl^-$  reflects that groundwater is moving in basinal gravity-flow systems (Tóth, 1999; Mádl-Szönyi, 2015).

Therefore, the “Bolivian Lake Titicaca” aquifer is a complex and multilayered sequence of glacial and fluvioglacial layers (~200 m thick) in the upper part of the Piedmont; alluvial, fluvioglacial and lacustrine layers (~50 to 150 m thickness) in the lower sector of the Piedmont; and lacustrine layers (~40 to 150 m thickness) in the plain area.

The regional hydrogeological functioning of the aquifer is understood. However, further geophysical investigations will be required to evaluate: i) the thickness of glacial and fluvioglacial layers on the NE sector of the upper Piedmont (area influenced by tectonics), ii) the actual extent and thickness of the paleo-lacustrine clay layer (Ulloma formation), and iii) the extent and thickness of the paleo-lacustrine Cabana and Mataro formation (Qcb-mt) towards the south of Viacha.

# Basin-scale conceptual groundwater flow model

## 5.1 Introduction

This chapter explains the results of the basin-scale conceptual groundwater flow model developed for the Katari and Lago Menor region. These results are presented following the basic structure of a typical scientific article.

The basin-scale conceptual model considers the previous regional geophysical characterization, natural flow processes, aquifer hydraulic properties, boundary conditions and sources and sinks of the groundwater system.

This basin-scale conceptual groundwater flow model provides a good understanding of the aquifer functioning, and a guide to future data collection in order to improve the robustness of future groundwater flow numerical modeling.

## **5.2 Article II: Basin-scale conceptual groundwater flow model under natural conditions of the semi-arid, Bolivian Lake Titicaca Aquifer System**

**Gabriela Patricia Flores Avilés<sup>1,2,a</sup>, Yvan Rossier<sup>1</sup>, Céline Duwig<sup>1</sup>, Marc Descloitres<sup>1</sup>, Mayra Perez<sup>3</sup>, Anatoly Legchenko<sup>1</sup>, Álvaro Soruco<sup>3</sup>, Jaime Argollo<sup>3</sup>, Waldo Medinaceli<sup>4</sup>**

<sup>1</sup> Univ. Grenoble Alpes, IGE, IRD, CNRS, Grenoble-INP \*, 38000 Grenoble, France,

<sup>2</sup> Ministerio de Educación Estado Plurinacional de Bolivia (Ministry of Education), La Paz, Bolivia

<sup>3</sup> University Mayor of San Andrés (UMSA), La Paz, Bolivia

<sup>4</sup> Ministerio de Medio Ambiente y Agua (Ministry of Water and Environment of Bolivia), La Paz, Bolivia

\* Institute of Engineering Univ. Grenoble Alpes

<sup>a</sup>gpfloresaviles@gmail.com

### *1. Introduction*

Globally, groundwater is a vital source for drinking and agricultural purposes, particularly in arid and semi-arid regions (van der Kamp & Hayashi, 2009; Wei et al., 2013; Yousif et al., 2015; Grizard et al., 2018). Moreover, it is restricted to the careful investigation and conceptualization of subsurface flow systems (Tóth, 1995; Tóth, 1999; Tóth, 2010; Mádl-Szönyi et al., 2015).

As a matter of fact, much attention has been drawn to the development of accurate conceptual models because they are considered as the foundation of groundwater numerical modeling (Bredehoeft, 2005; Izady, 2013). Indeed, discussions regarding groundwater models have denominated various sources of uncertainties. Those uncertainties generally relate to parameter values, boundary conditions, model structure and hydrogeological stresses (Zhou & Heralth, 2017; Samani et al., 2017). However, recent investigations indicate that the largest prediction uncertainty may come from the conceptualization of hydrogeological systems (Bredehoeft, 2005; Nettasana et al., 2010; Izady et al., 2015; Zhou & Heralth, 2017). Therefore, an adequate characterization of hydrogeological systems should be the first challenge to achieve before the development of groundwater flow numerical models.

The main limitation for developing groundwater flow concepts relies on the available data and information. In fact, several investigations around the world have documented that the application of one investigation technique is not sufficient for developing conceptual models of complex hydrogeological systems, becoming even more difficult when hydrogeological data is limited (Zhou & Li, 2011; Lachaal et al., 2011; Turner et al., 2015;

Saroli et al., 2017; Bayanzul et al., 2018). Over-simplification of real systems can lead to the development of a model with lack of information and conversely detailed characterizations of hydrogeological systems may result in costly models (Lemke et al., 2009; Zhou & Heralth, 2017).

In South America, Herrera et al. (2007) combined hydrogeological, chemical and isotopical data to assess recharge and advance in the conceptual hydrogeological model of volcanic Easter Island (Chile). Besides, Fernandes et al. (2016) developed a preliminary conceptual model of groundwater flow for the Serra Geral basalt aquifer in order to assess the recharge to the underlying sandstone Guarani Aquifer System in Brasil. Herrera et al. In Bolivia Gonzales-Amaya (2018) presented 2D hydrogeological conceptual models refined by geophysics in terms of layering, lateral variation and thicknesses of two alluvial fans located in Valle Alto (Bolivia).

A previous research in the study area combined geological, geophysical, piezometric and hydrochemical data as a first step towards a better knowledge of the Bolivian Lake Titicaca aquifer system (Flores-Avilés et al. 2019). As a follow-up from this study, this paper aims to develop a basin-scale groundwater flow concept for such spatially complex aquifer system, considering in addition to the previous hydrogeological knowledge, flow processes, aquifer hydraulic properties, boundary conditions and sinks and sources of the groundwater system. This conceptual model will establish an advanced understanding of the groundwater flow dynamics under natural conditions and will provide a guide to future data collection in order to improve the robustness of future groundwater flow numerical modeling.

## *2. Background information of the study site*

### *Hydrogeological framework*

Prior research in the study area evidenced that the Katari and Lago Menor Basin aquifer had been set under two different geological settings allowing the formation of the “Piedmont subsystem” and the “Lacustrine plain”, both behaving hydraulically as “one aquifer”. For instance, Fig.1 show the different geological layers identified for the Piedmont subsystem.

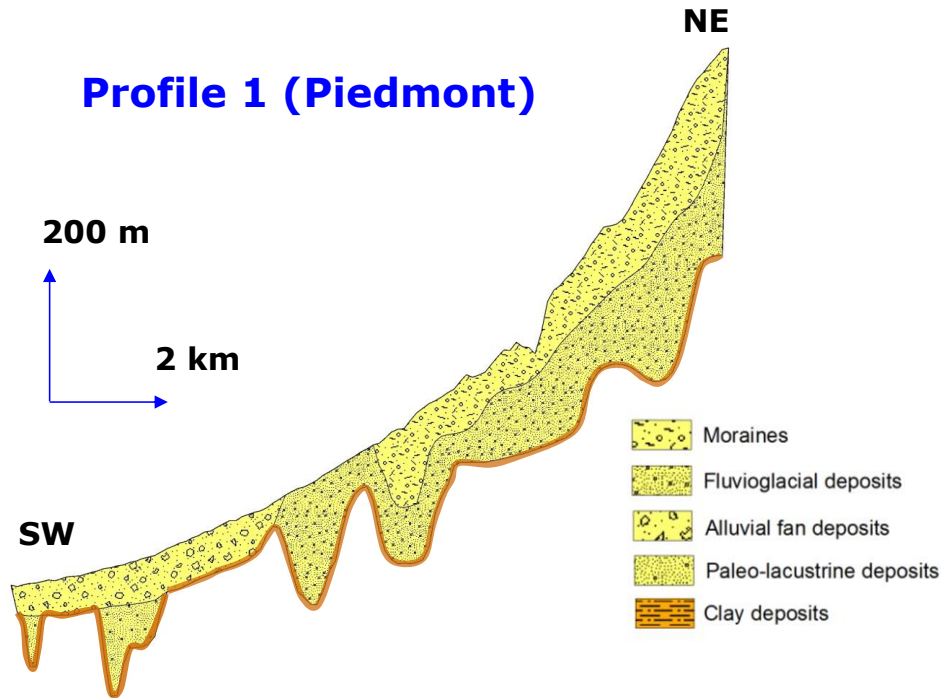


Figure 1. Geological layers identified for the Piedmont subsystem (Flores Avilés et al., 2019)

The basin-aquifer is complex due to its spatial lithological variability. Indeed, six geological layers (Table 1) derived from geophysical measurements, their geometry and the depth to the impervious layer, were identified and validated by means of the integration of geological, geophysical, piezometric and hydrochemical data (Flores-Avilés et al., 2019). This information will be the basis for the creation of a hydrogeological framework.

Table 1. Summary of the different geological layers, derived from resistivity measurements, identified in the Bolivian Lake Titicaca Aquifer System (After Flores-Avilés et al., 2019).

Geological Layer	Unconsolidated Quaternary deposits	Lithology	Thickness (meters)
Layer 1	Moraines	Tills (clasts/blocks of quartzites, shales and granites, with significant content of clay)	60 to 150 m (upper Piedmont)
Layer 2	Fluvioglacial outwash deposits/Purapurani formation	Gravel with silt layers-tills and fluvial gravels/ Gravels with silt layers-clay, sand and gravels	60-150 m (upper Piedmont) 30-70 m (SE lower Piedmont)
Layer 3	Alluvial fan deposits	Sandy gravel and medium to fine gravels	85-100 m (NW lower Piedmont) 20-50 m (SE lower Piedmont)
Layer 4	Fluvio-lacustrine deposits	Thin layered sequences that comprises medium to coarse sand materials and clay	15-60-m (NW close to Lake Titicaca)
Layer 5	Lacustrine deposits (Cabana-Mataro Formation)	Fluviatile detrital deposits alternating layers of clayey sand and gravelly sand	20-50 m to 40-100 m (Piedmont Subsystem) 40-140 m (Lacustrine plain)
Layer 6	Lacustrine deposits(Ulloma Formation)	Fine sands with clayey and silty layers (significant clay content)	2-45 m (Lacustrine plain)

### *3. Materials and Methods*

The main steps for developing a numerical groundwater-flow model are presented in the flowchart of Figure 2. The modeling steps involves: data acquisition, groundwater flow conceptualization, model setup, model calibration and model application (Domenico & Schwartz, 1990; Pham et al., 2017; Sahoo et al., 2017).

In this study, there were considered only the data acquisition and model conceptualization steps from Figure 2, in order to develop a basin-scale conceptual ground water flow model for the Lake Titicaca aquifer system.

#### *3.1 Data acquisition*

The dataset acquired during 2017 includes topographic, geological (borehole lithology), geophysical (Time Domain Electromagnetic soundings), hydrogeological and hydrogeochemical data, and is reported in Flores-Avilés et al. (2019).

In addition, automatic water pressure measurements were recorded between August of 2018 and March of 2019, in coordination with the Ministry of Water and Environment (MMAyA). There were installed four levelloggers (Solinst) for measuring water pressure and electrical conductivity, in the monitoring piezometers: P-1, P-2, P-3, and P-5 (Fig. 2). An additional Barologger (Solinst) was installed in the monitoring well P-2, for measuring barometric fluctuations and compensating levelloggers measurements. These piezometers were installed in coordination with the M.M.Ay.A during the first semester of 2018, to: i) investigate temporal variations of groundwater-lake interactions, ii) study the connection between the piedmont and plain areas through a buried channel, iii) investigate the behavior of temporal groundwater levels in a natural wetland area, iv) incorporate observation wells in a regional groundwater level monitoring network and for v) monitoring groundwater quality.

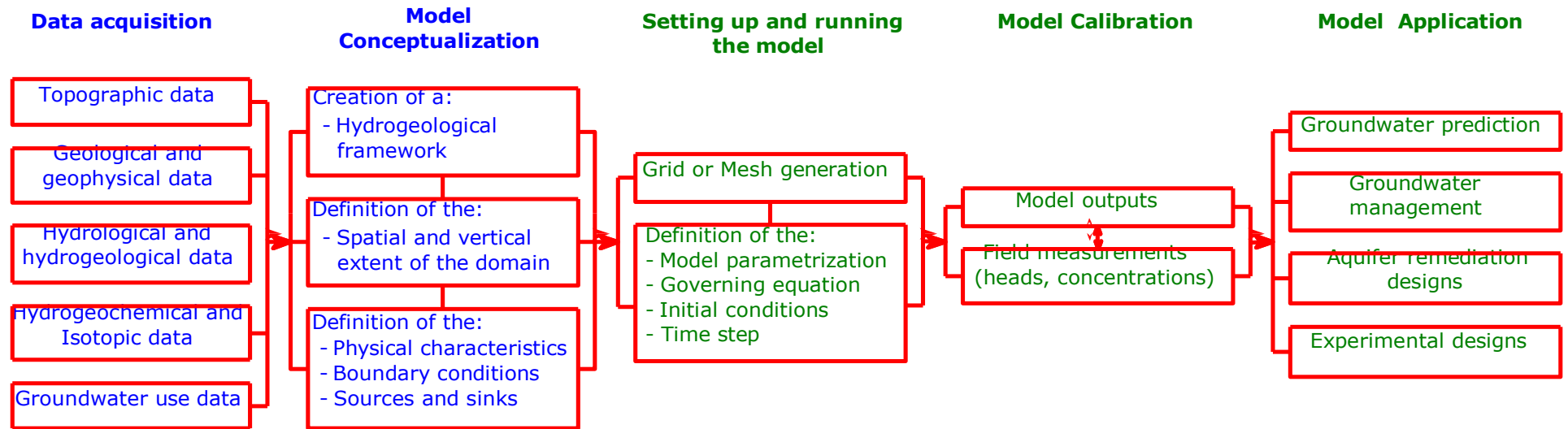


Figure 2. Flow chart for developing a groundwater-flow model, from the model conceptualization to the design of the numerical model (modified after Pham et al., 2017)

Besides, there was retrieved raw available data of automatic water pressure measurements recorded by the Ministry of Water and Environment (MMAyA) between December of 2010 and February of 2015. The Ministry installed ten Mini-Divers (DI501-[www.swstechnology.com](http://www.swstechnology.com)) for measuring water pressure in the monitoring wells: P-233, P-524, P-514, P-085, P-084, P-100, P-509, P-667, P-092 and P-192 (Fig. 2). A Baro-Diver (DI500-[www.swstechnology.com](http://www.swstechnology.com)) was also installed at monitoring well P-084 for measuring barometric fluctuations. These monitoring wells belong to the M.M.A.y.A Purapurani Groundwater Monitoring Network.

All automatic water pressure measurements were compensated by the barometric pressure fluctuations (Pa) in order to obtain the hydraulic head (meters). Then, monthly manual measurements and depth of deployment of the devices were used for computing the depth to water table (meters) and estimating water level rises for calculating groundwater recharge.

Furthermore, additional information of daily precipitation and temperature recorded at El Alto Station from January 2009 to April 2019 (available at <http://www.senamhi.gob.bo>) was retrieved for analyzing groundwater recharge.

Raw field data from two Pumping tests performed by MMAyA during March of 2013 were available at MMAyA geodatabase and used for estimating the hydraulic properties of the aquifer in specific zones.

### *3.2 Development of the aquifer model conceptualization*

#### *3.2.1 Spatial and vertical extent of the Domain*

The spatial and vertical extent of the domain was defined as a result of the previous hydrogeological framework performed in the study area (Flores-Avilés et al., 2019). The maximum extent of the domain, towards the southern, western and northern sides, is defined by the most ancient Paleolake invasion developed at a current altitude of 3950 m a.s.l (Flores-Avilés et al., 2019). It has an approximate total extension of 3500  $Km^2$  as illustrated in Figure 3. However, in this study the Achacachi zone ( $\sim 670 Km^2$ ) was not considered as there is no available information of any type and is excluded from the current Hydrosocial limits of the Katari and Lago Menor Basin (Fig.3).

In addition, the domain was subdivided into six subdomains. Each of these subdomains, besides their unique lithological characteristics are considered to possess a unique set of hydraulic properties that will be detailed later. The physical characteristics and extension of these subdomains are presented in Table 4 and Figure 4.

On the other hand, there were considered the following assumptions in order to define outside boundary conditions along the six sides of the domain.

*Assumptions:*

- Along the eastern side of the domain, nearby to the high glaciated peak areas, it is hypothesized that Relict forms of rock glaciers represent a groundwater inflow to the aquifer. The lower limit of rock glaciers was approximated to be at 4700 masl (Rangecroft et al., 2016).
- Along part of the southern side, towards the depression of La Paz, Achocalla and Mecapaca cities, the disruption of quaternary deposits produce that a natural outflow of groundwater. These discharges are evidenced by springs.
- Along part of the southern side and the western side of the domain, the limit of paleolacustrine deposits, represents the maximum extension of the domain. This limit reaches the outcropping impermeable barriers (Tertiary or Devonian rock formations).
- Along the northern side of the domain, it is hypothesized that the aquifer naturally discharges towards Lake Titicaca (Seepage into the effluent Lake Titicaca).
- The unconsolidated Quaternary deposits lie on Tertiary or Devonian rock formations considered as impermeable formations. The top of these impervious formations represent the bottom of aquifer.
- The top of the aquifer under natural conditions is defined by the water table, in the portion where it presents an unconfined behaviour. Semipervious boundaries (leakage out overlying layers) should be defined over particular subdomains. However, when developing a groundwater numerical model the top of the aquifer under variably saturated conditions will be defined by the ground surface.

### *3.2.3 Physical characteristics*

Raw field data from two multi-well Pumping tests conducted by MMAyA during March of 2013, were analyzed and interpreted considering the solution of Neuman (1975) and the Theis recovery method (Kruseman & de Ridder, 1990), using residual drawdowns. Therefore, the horizontal hydraulic conductivity, vertical hydraulic conductivity and elastic early-time storativity were determined. The specific yield was not determined because the duration of the pumping tests was not long enough to display the late-time response of the aquifer as displayed in the curves of the solution of Neuman (1975). At early pumping times water is instantaneously released from storage, however, under late-time conditions water is released by dewatering of the aquifer (Kruseman & de Ridder, 1991).

In addition, available information of horizontal hydraulic conductivity values were retrieved from previous works that conducted single Pumping tests (JICA, 1987; EPSAS, 2017) and slug tests (Barroso et al., 2010). These results were classified according to their location in the domain and the representative layer for which the hydraulic properties were measured.

### *3.2.4 Sinks and Sources inside the domain (under natural conditions)*

#### *3.2.4.1 Evapotranspiration of groundwater*

In arid and semi-arid regions, a significant quantity of groundwater is evapotranspired due to shallow water levels (Luo et al., 2009; McMahan et al., 2013; Sanderson et al., 2008). Indeed, one of the main mechanisms of groundwater loss in the Bolivian Lake Titicaca Aquifer System is due to evapotranspiration, particularly, in the lower Piedmont where water table is at the ground surface (wetland ecosystems) (Flores-Avilés et al., 2019). In this study, groundwater evapotranspiration is hypothesized to occur primarily in the lower sectors of the Piedmont, due to shallow water levels evidenced in field. However, an extinction depth should be calculated in order to define the water table depth beyond which evapotranspiration rates drops to negligible values.

#### *3.2.4.2 Evaporation loss during groundwater recharge (Isotopic analysis)*

Stable hydrogen and oxygen 18 isotopic compositions of surface water and groundwater reported by MMAyA (2016) were used to estimate an average of groundwater evaporative loss for year 2013. This value was estimated considering the local “evaporation slope”

adopted from surface water data. Then, the fractional water loss from evaporation can be modelled according to a Rayleigh distillation (Clark and Fritz, 1997):

$$\delta^{18}O_{gw} - \delta^{18}O_{prec} = \varepsilon^{18}O_{total} \cdot \ln f \quad (4)$$

where  $\delta^{18}O_{gw}$  is the delta oxygen 18 of groundwater [‰],  $\delta^{18}O_{prec}$  is the delta oxygen 18 of precipitation,  $\varepsilon^{18}O_{total}$  is the overall enrichment for evaporation [‰], and  $f$  is the residual water fraction.  $\delta^{18}O_{gw} - \delta^{18}O_{prec}$  is graphically determined according to the local “evaporation slope” and  $\varepsilon^{18}O_{total} = \varepsilon^{18}O_{l-v} + \Delta\varepsilon^{18}O_{bl-v}$ ;  $\varepsilon^{18}O_{l-v}$  is the fractionation factor for equilibrium water-vapour exchange for  $^{18}O$  and is a function of temperature [‰], and  $\Delta\varepsilon^{18}O_{bl-v}$  is the kinetic effect as a function of humidity [‰]. All these factors were estimated using the already computed values reported in Clark and Fritz. (1997).

### 3.2.4.3 Groundwater recharge

The quantification of groundwater recharge is of vital importance, in semi-arid and arid regions (Scanlon et al., 2002; Sophocleus, 2005; Manghi et al., 2009; Izady et al., 2015; Xu et al., 2019). In this study groundwater recharge was determined by means of the application of saturated-zone techniques when data was available. Groundwater recharge estimated from saturated-zone techniques provides evidence of *actual recharge* because water reaches the water table (Scanlon et al., 2002; Healy et al., 2001). Conversely, recharge estimated from unsaturated-zone and surface-water techniques could or could not reach the water table due to unsaturated-zone processes or the ability of the saturated zone to accept recharge.

#### 3.2.4.3.1 Saturated-Zone Techniques (Water-Table Fluctuation Method-WTF)

The Water-Table fluctuation method (WTF) establishes that rises in groundwater levels of unconfined aquifers are the result of recharge water that arrives at the water table. This method requires the identification of water-level rises that occur in response to individual storms. Water levels prior to rises should be extrapolated to their expected position as if there were not any source of recharge. Then, water level rises are estimated as the difference between the peak level and the extrapolated antecedent level. And recharge is determined by the following equation:

$$R = \Delta S^{gw} = S_y \cdot \frac{\Delta H}{\Delta t} \quad (5)$$

Where  $\Delta S^{gw}$  is the change in groundwater storage,  $S_y$  is the specific yield (a physical characteristic of unconfined aquifers),  $H$  is the water table height, and  $t$  is the time. This equation assumes that water that arrives at the water table goes immediately into storage and that all the other components of recharge, such as, change in groundwater storage, seepage from influent or effluent surface sources, and evapotranspiration from groundwater, are zero. Determining a representative value for specific yield is one of the difficulties for the application of this method (Scanlon et al., 2002; Healy and Cook, 2002; Matengu et al., 2019).

The computed results from the available automatic water pressure measurements were used to plot hydrographs of daily depth to water table fluctuations, estimate water level rises and determine the groundwater recharge when data was available. The WTF was applied over the portion of the domain presenting an unconfined behaviour.

In regions where the domain presented a confined behaviour only groundwater level fluctuations were analyzed.

## 4. Results and discussion

### 4.1 Boundary conditions

#### 4.1.1 Eastern side of the domain (Neumann-Type 2)

A boundary condition of groundwater inflow (Type 2) was defined along the eastern side of the domain (Fig.3). This boundary was delineated following the topographic curve (4700 m a.s.l) considered as the lower limit of Rock glaciers in the Bolivian Andes (Rangecroft et al., 2014; Rangecroft et al., 2016). Relict rock glaciers are complex hydrogeological systems with high storage capacity (Winkler et al., 2016) that might act as relevant groundwater storages (Pauritsch et al., 2017).

Furthermore, many investigation around the world (Jiráková et al., 2010; Grenier et al., 2012; Kane et al., 2013; Sterckx et al., 2018; Saltel et al., 2019) showed several examples of melt-water recharge or subglacial recharge to aquifers. For instance, Jirakova et al. (2010) characterised at the European scale the recharge conditions since the late

Pleistocene by means of the application of stable isotopes and radioisotopes. This author put the most recent findings about permafrost relics (rock glaciers) and ice sheet extension in order to explain recharge features. It has been proved that in permafrost-free areas (relicts forms) recharge has probably occurred continuously without any hiatus. However, more complicated recharge or even lack of it is expected as a consequence of ice covered or frozen ground.

#### *4.1.2 Southern side of the domain (Cauchy-Type 3)*

A boundary condition of groundwater outflow (Cauchy Type 3) was delineated along part of the southern side of the domain (Fig.3). As reported by Flores-Avilés et al. (2019), there is a natural outflow of groundwater towards the depression of La Paz, Achocalla and Mecapaca Cities caused by the disruption of the unconsolidated Quaternary deposits.

Moreover, no flow boundary conditions (Type 2) were also defined along the southern side of the domain (towards the southeast of the City of Viacha) (Fig.3). In this area, the extent of Paleolacustrine deposits reaches the outcropping Tertiary rock formations (impervious barriers).

#### *4.2.3 Western side of the domain (Neumann-Type 2)*

No flow boundary conditions (Type 2) were defined along the western side of the domain (Fig.3). In this area, the maximum extent of Paleolacustrine deposits (3950 m a.s.l) also reaches the outcropping Tertiary formations (Impervious barriers).

#### *4.2.4 Northern side of the domain (Cauchy-Type 3 and Neumann-Type 2)*

Head-dependant flow conditions (Type 3) were defined along part of the northern side of the domain (Fig. 3). In this area groundwater leaves the aquifer by seepage into the effluent Lake Titicaca at Cohana bay and the Puerto Pérez bays (Flores-Avilés et al., 2019). It should be noted that depending on the seasonal station “Rainy” and “Dry” seasons, water from Lake Titicaca could enter or leave the aquifer. It might enter the aquifer most likely during the “Rainy” season.

Furthermore, no flow boundary conditions were also defined along this side following the location of the outcropping impervious barriers (Tertiary and Devonian formations). An additional Neumann condition (Type 2) was defined along this side as depicted in Fig.2.

This boundary reflects the groundwater inflow that may enter into the aquifer from the excluded Achacachi zone (Figure 2).

#### *4.2.5 Bottom of the Domain (Neumann Type 2)*

No flow boundary conditions (Type 2) were defined over the bottom of the domain (Fig.10), as the plio-Quaternary unconsolidated deposits lie on Tertiary or Devonian rock formations, considered as impervious formations (Flores-Avilés et al., 2019).

#### *4.2.6 Top of the Domain (Dirichlet Type 1 and Neumann Type 2)*

The top of the domain is defined by the water table in regions where the aquifer presents an unconfined behaviour (Fig.10). However, semipervious boundaries were defined above Layer 5. It was assumed that leakage out into Layer 6 represents water that may leave the aquifer (Fig.10). In fact, Lacustrine clay deposits (Layer 6), are widely accepted to be common aquitards. It should be noted that in an aquitard groundwater flow is assumed to be predominantly vertical (Gerber et al., 2001; Timms et al., 2014; Timms et al., 2016) and that the horizontal flow could be neglected.

These top boundaries should be set under saturated conditions when developing a groundwater numerical model. Moreover, they could also be set under variably saturated conditions, where the top of the domain will be defined by the ground surface.

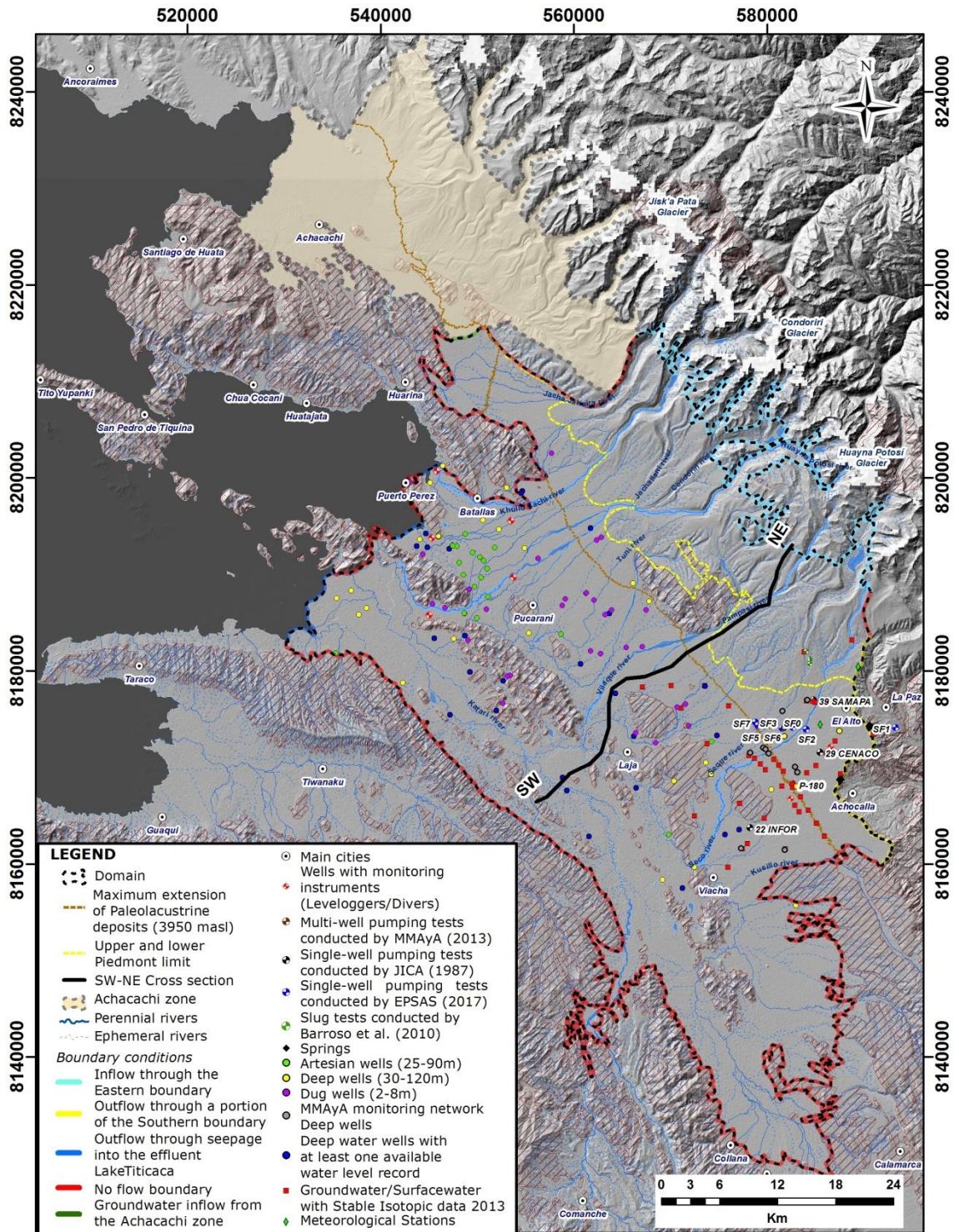


**Figure 3.** Conceptual model of Lake Titicaca Aquifer System showing the spatial extension of the domain and its boundaries along the Eastern, Western, Northern and Southern sides. It also shows the location of the monitoring wells where water pressure measurements were recorded and the monitoring points where pumping tests were conducted.

## 4.2 Physical characteristics

Table 2 shows a summary of the aquifer properties obtained from the analysis of raw data from aquifer tests (Multi-well Pumping tests) conducted by MMAyA (2013). The physical characteristics obtained from both pumping tests are representative values for Layer 2 (Fluvioglacial deposits) and show that this portion of the domain presents an unconfined behaviour. These properties will be used later for estimating recharge by the WTF (Water Table fluctuation method).

In the first case, the location of the monitoring well P-180 suggests that this borehole could have also traversed Layer 5 (Table 1). Indeed, by analyzing the depth of the well (~3831 masl from surface) and the approximate altitude of Paleolacustrine deposits evidenced by geophysics ~3853 masl (Flores-Avilés et al., 2019), it was obtained that Layer 2 present a thickness of ~100 m and Layer 5, a thickness of ~22 m. This could evidence that hydraulic properties are representative of Layer 2.

In the second case, the monitoring well P-525 is far from the limit of Paleolake. It presents a depth of ~3910 masl from surface. Thus, low hydraulic conductivity values could suggest that Layer 3 (Alluvial fan deposits) in this area presents a thin thickness or that the screen of the well was installed along Layer 2.

**Table 2.** Summary of aquifer properties obtained from the analysis of Multi-well pumping tests performed during March of 2013 at monitoring wells P-180, OW-1, OW-2 and P-525, P-524 (raw field data is available at MMAyA geodatabase).

Layer	Horizontal Hydraulic conductivity, $K_h$ (m/sec)	Vertical Hydraulic conductivity, $K_v$ (m/sec)	Elastic storativity, $S_A$ (**)	Specific yield, $S_y$ (**)	Storativity, $S$ (**)
Layer 2 + Layer 5 (P-180)	$2.5 \times 10^{-6}$	$5.09 \times 10^{-5}$	0.016	~0.16*	0.144
Layer 3 + Layer 2 (P-525)	$3.5 \times 10^{-6}$	$1.3 \times 10^{-6}$	0.008	–	–

\* Assumed from literature considering its glacial origin and predominantly gravel composition (Kruseman & De Ridder, 1990)

\*\* Dimensionless

– Not able to estimate because the duration of the pumping test was not enough longer to display the late-time response of the aquifer

Additional information of horizontal hydraulic conductivity values reported by JICA (1987) and EPSAS (2017) are summarized in Table 3. This information was analyzed regarding its location and the Layers (Table 1) that the monitoring wells would have traversed when drilled.

**Table 3.** Summary of horizontal hydraulic conductivities reported from Single-well pumping tests performed by JICA (1987) and EPSAS (2017).

Layer	Monitoring well	Diameter (in)	Depth of well from top of casing (m)	Casing stickup (m above ground surface)	Easting (m)	Northing (m)	Depth of well from surface (masl)**	Horizontal Hydraulic conductivity, K (m/s)
Layer 2	39 SEMAPA *	8	40	0.5	584796	8176994	4014.0	1.2E-05
Layer 2	29 CENACO *	6	64	0.5	585472	8171589	3943.6	8.2E-06
Layer 3 +Layer 5	22 INFOR *	8	52	0.5	578217	8163749	3839.8	5.0E-06
Layer 2	SF0	8	111	0.4	584037	8173935	3898.3	2.4E-05
Layer 2	SF2	8	91	0.4	582651	8174164	3899.8	2.1E-05
Layer 3	SF3	8	94	0.8	581550	8174067	3888.4	1.1E-04
Layer 3 +Layer 2	SF5	8	104	0.5	579724	8174291	3860.0	5.5E-05
Layer 2	SF6	8	94	0.8	579076	8174325	3862.0	4.3E-05
Layer 2	SF7	8	97	0.4	578788	8174710	3855.5	1.2E-05

\* Single – well pumping tests performed by JICA (1987)

\*\*Depth of well were normalized to a reference datum. The reference datum used was the Digital Elevation Model (DEM)- Shuttle Radar Topography Mission 1 Arc-Second Global

Most of the monitoring points reported in Table 3 are located far from the limit of Paleolake invasion (Fig.2). However, SF6 and SF7 appearing to be the closest to the mentioned limit, present depth altitudes higher than 3853 masl (maximum altitude of Paleolacustrine deposits). Only the monitoring well 22 INFOR appears to be traversing Layer 5 (Lacustrine deposits) besides Layer 3 (Alluvial fan deposits). Indeed, a depth of ~3840 masl (Table 3) suggest that in this point, Layer 3 would present a thickness of 38 meters and Layer 5, 13 meters. Moreover, the low horizontal hydraulic conductivity, suggest that the screen of this well was installed most likely along Layer 5 which comprises a layered sequence of clayey sand and gravelly sand materials (Table 1).

Furthermore, monitoring well SF-3 (875 meters SE away from P-525) present a hydraulic conductivity of  $1.1 \times 10^{-4} \text{ m/sec}$ , value coherent for unconsolidated gravel materials in a sandy matrix, characteristic of the Alluvial fan deposits (Layer 3). Drilling reports (EPSAS, 2017) confirmed that very coarse materials (gravels and sands) were traversed up to a depth of 90 meters.

As manifested before, each of the subdomains in the domain, besides their unique lithological characteristics, would also possess a unique set of physical characteristics (Fig. 4). Table 4, summarize the different subdomains, their assumed behaviour (unconfined or confined) according to the boundary conditions already defined (top conditions), and their hydraulic properties. It should be noted that groundwater flow through Layer 6 (Fig.3, Fig.4) is assumed to be predominantly vertical yielding a confined behaviour below Subdomain 6.

**Table 4.** Summary of the different subdomains identified in the Bolivian Lake Titicaca Aquifer System.

Subdomain	Unconsolidated Quaternary deposits	Aquitard		Unconfined behaviour		Confined behaviour	
		$K_v$ (m/sec)	$C$ (day)	$K_h$ (m/sec)	$S_y$	$T$ (m <sup>2</sup> /sec)	$S$
Subdomain 1	Moraines			$5.9 \times 10^{-8}$	0.16*		
Subdomain 2	Fluvioglacial outwash deposits			$2.5 \times 10^{-6}$	0.16*		*
Subdomain 3	Alluvial fan deposits			$1.1 \times 10^{-4}$	0.20*		
Subdomain 4	Fluvio-lacustrine deposits			$5.0 \times 10^{-6}$	0.18*		
Subdomain 5	Paleo-lacustrine deposits (Cabana-Mataro Formation)			$5.0 \times 10^{-6}$	0.18*	$6.0 \times 10^{-6}$ *	$6.0 \times 10^{-3}$ *
Subdomain 6	Lacustrine deposits (Ulloma Formation)	$3.0 \times 10^{-9}$	115,740				

Note:  $K_h$  horizontal hydraulic conductivity in the subdomain,  $S_y$  specific yield,  $K_v$  horizontal hydraulic conductivity in the subdomain,  $C$  hydraulic resistance,  $T$  transmissivity, and  $S$  storativity coefficient

\* Values estimated or assumed from literature

Table 4, considers the following assumptions:

- Horizontal hydraulic conductivity across Subdomain 1 was defined using few available information from slug tests performed in the Glacial-Till deposits, reported by Barroso et al. (2010). And compared regarding its lithology (till materials), with large scale field determinations reported by Gerber et al. (2001), Timms et al. (2016) among others. The specific yield was assumed regarding its lithology, sandy and gravelly till materials ( Kruseman & De Ridder, 1990)
- Vertical hydraulic conductivity across Subdomain 6 was assumed regarding its lithology, clayey-silt materials (Timms et al., 2014).

- The hydraulic resistance ( $K_v/D$ ), defined as the resistance of an aquitard to vertical flow, across Subdomain 6, was estimated considering a mean saturated thickness ( $D$ ) of ~30 meters for Layer 6 (Table 1).
- The mean thickness of Layer 2 below Subdomain 1 was assumed to be ~150 meters and the mean depth of Layer 5 below Subdomain 6, ~120 meters (Table 1).
- Storativity values, for the confined portion (below Subdomain 6), were estimated considering a specific storage value for dense sandy gravel materials,  $1.0 \times 10^{-4} m^{-1} - 5.0 \times 10^{-5} m^{-1}$  (Domenico et al., 1965).
- The specific yield value for Subdomain 5 was assumed regarding its lithology, layered sequence of clayey sand and gravelly sand materials (Healey and Cook, 2002).
- Even though that geophysical properties across Subdomain 4 (~100  $\Omega \cdot m$ ) and Subdomain 5 (~45  $\Omega \cdot m$ ) are different (Flores-Avilés et al., 2019). The hydraulic properties across Subdomain 4 and 5, are assumed to be the same. In regards with the borehole lithology information that showed thin layered sequences comprising medium to coarse sand materials with clay content in both subdomains.

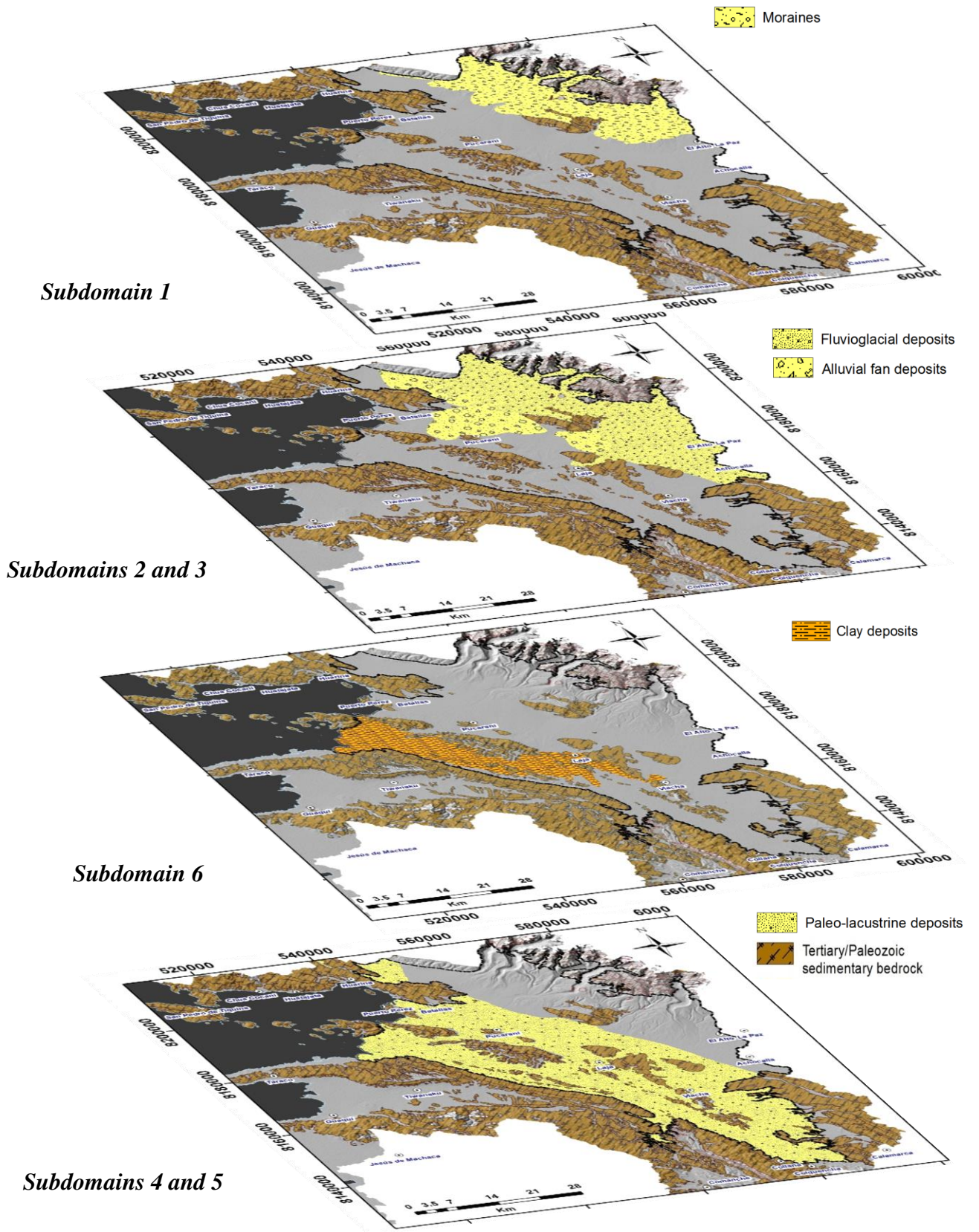


Figure 4. Corresponding subdomains for aquifer properties as described in Table 4.

### 4.3 Sinks and sources inside the domain (under natural conditions)

#### 4.3.1 Estimation of evaporation during recharge over Subdomain 3 (Isotopic Data 2013)

Figure 5 displays the isotopic composition of  $\delta^2H$  ‰ and  $\delta^{18}O$  ‰ from groundwater and surface water at the Purapurani zone reported by MMAyA (2016).

According to MMAyA (2016), values lying below the meteoric line of local precipitation should reflect the presence of ancient waters that were originated in a different climatic regime.

Indeed, isotopically lighter values (more negative, blue squares) coincide with the location of groundwater primarily hosted across Subdomain 5 (Paleolacustrine deposits related to Paleolake invasion). Besides, red squares, show groundwater hosted across Subdomain 2 (fluvioglacial deposits) or in some cases a mixing of waters (Flores-Avilés et al., 2019) as boreholes could traverse Layer 2 and Layer 5 (Table 1).

Although representing a mixture of waters and also of recharge events, this second type of waters (red squares) also reflects secondary fractionation by evaporation prior to infiltration. This could be evidenced by the samples following the local “evaporation slope”, showing that groundwater have experienced evaporative enrichment (Fig. 5).

Based on the local evaporation slope ( $s = 5$ ) and the mathematical basis of Gonfiantini (1986), it was possible to estimate an average of evaporative loss during recharge of the aquifer over Subdomain 3. Therefore, the overall enrichment for  $^{18}O$  was estimated to be  $\varepsilon^{18}O_{total} = -14.25$  ‰ and the fractional water loss from evaporation yielded a residual water fraction of  $f = 0.81$  and an average of evaporative loss of 19%.

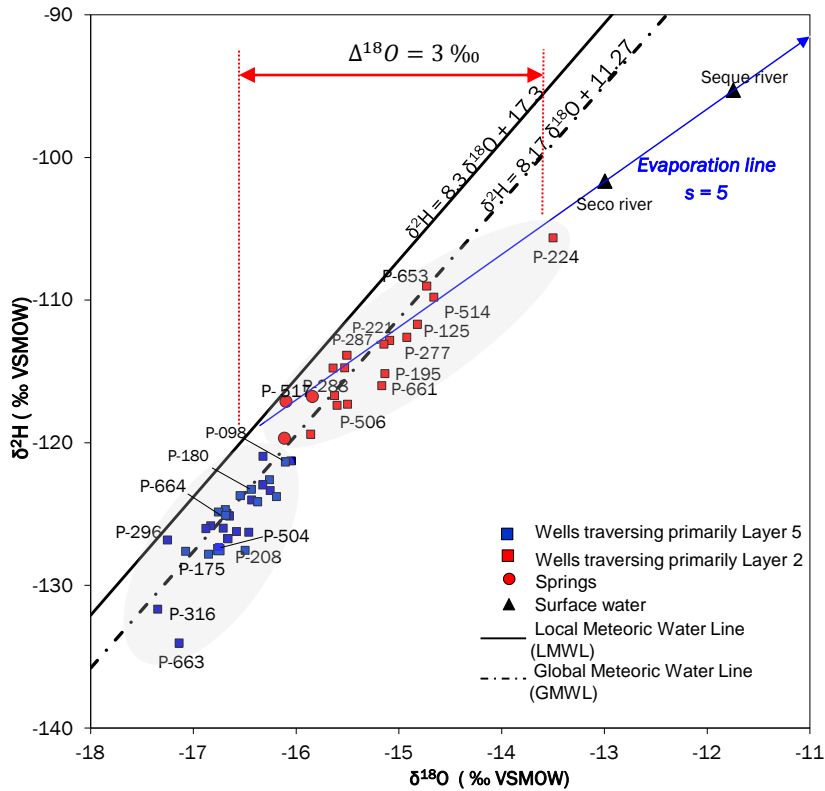


**Figure 5.** Stable hydrogen and oxygen isotopic composition of surface water and groundwater at the Bolivian Lake Titicaca aquifer system (Purapurani Zone) Field Sampling Campaign July (2013), modified after MMAyA (2016).

#### 4.3.2 Groundwater level fluctuations and Groundwater recharge

The Water Table Fluctuation method (WTF) was used to estimate groundwater recharge only over the portion of the aquifer presenting an unconfined behaviour. Moreover, groundwater level fluctuations were analyzed over regions presenting a confined behaviour.

##### 4.3.2.1 Subdomain 2 (Unconfined behaviour)

Figure 6 shows the location and hydrographs of water level fluctuations for monitoring wells situated inside Subdomain 2. Generally, the response of the aquifer to precipitation in this Subdomain show groundwater levels receding during April to September. Punctual water table rises during this period could be attributed to the influence of the Seque River (P-514; P524). Then, during October and November, the aquifer response to precipitation is slow, showing small rises of water level.

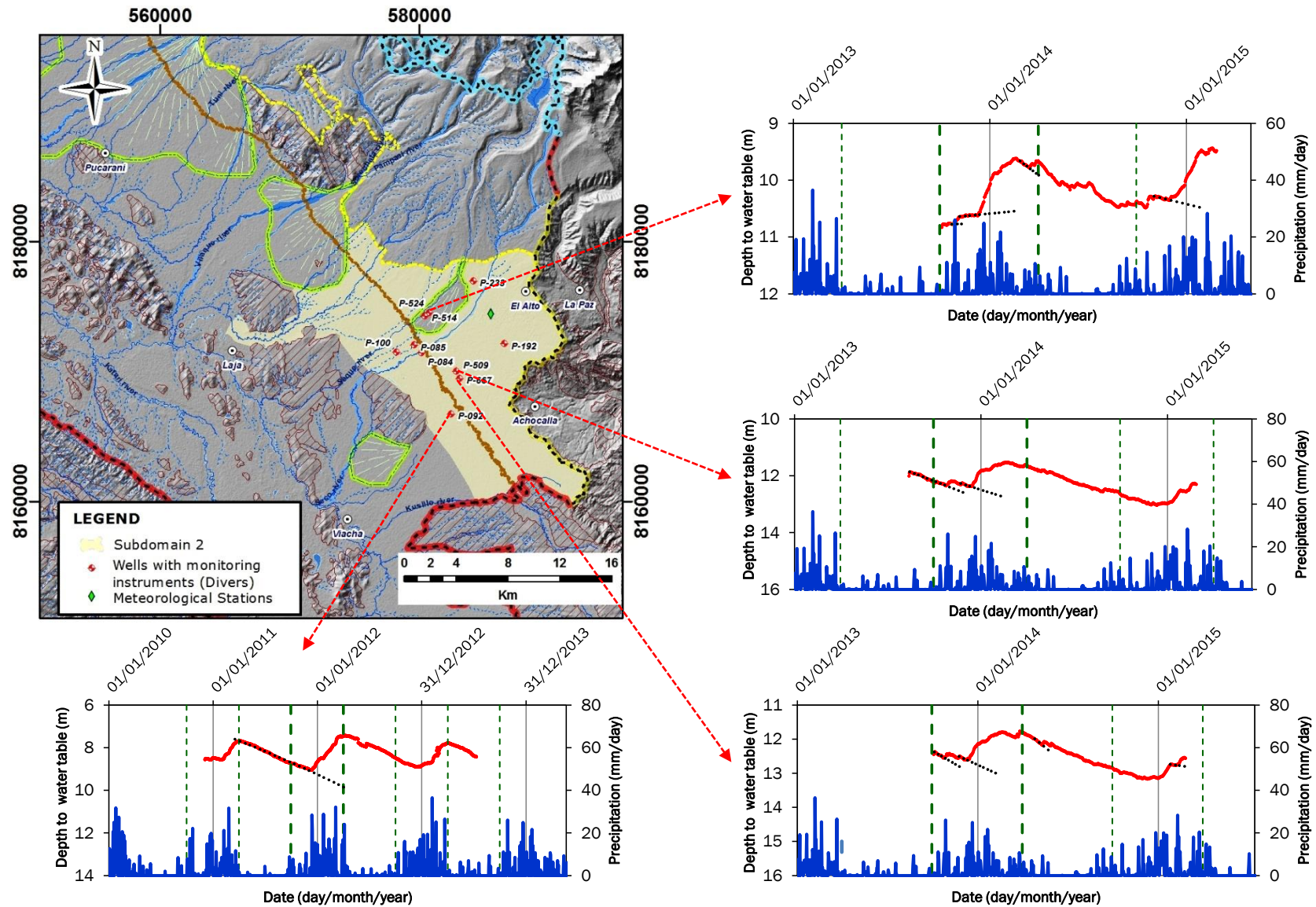


Figure 6. Hydrographs of water level fluctuations (red line) for wells located at Subdomain 2 and bar graphs of daily average precipitation (blue line) from El Alto Station. Gray lines represent the end of a hydrological year. Green dashed lines represent seasonal limits (01/04 to 30/09 – “Dry season”) and (01/10 to 31/03 “Wet season”). Black dotted lines represent the hypothetical extrapolated recession curves for WTF (Water table fluctuation) analysis.

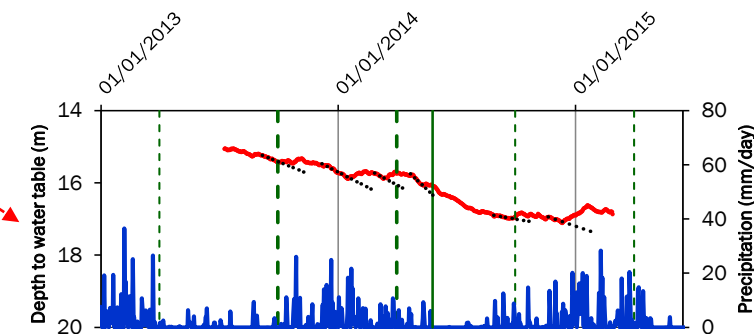
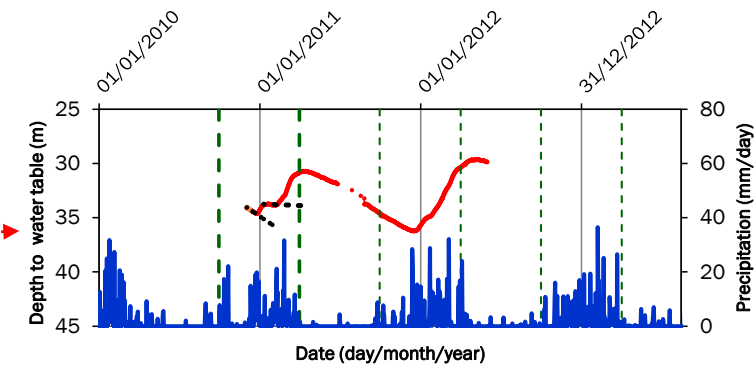
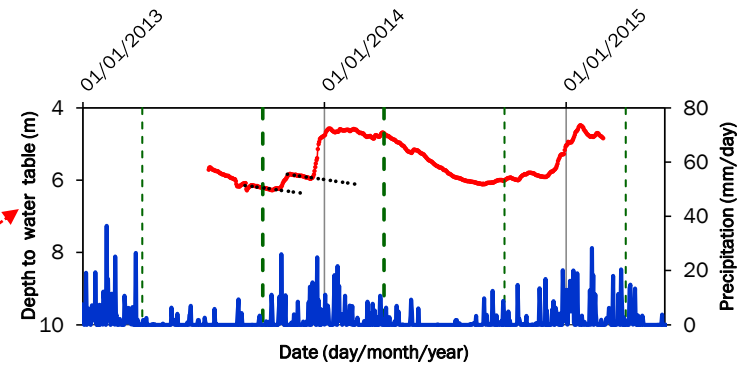
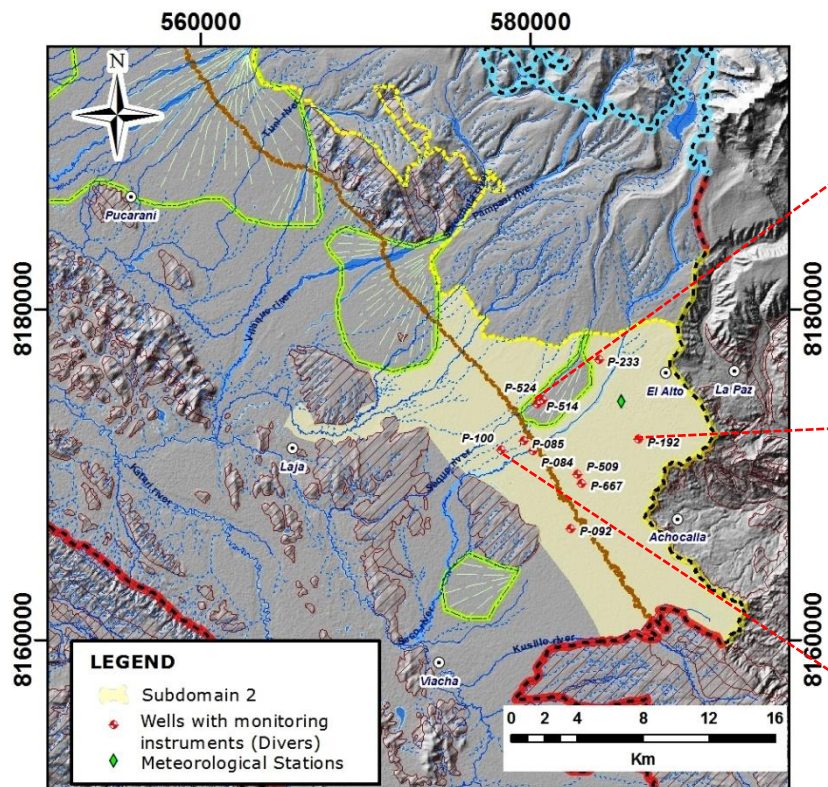


Figure 6. (continued)

After, water table gradually rises from December to March reaching its maximum peak level by the middle of February (P-514; P524; P-509; P-667; P-092; P-192).

Groundwater recharge over this Subdomain was estimated by the Water Table Fluctuation Method (WTF) considering a specific yield value of 0.16 (Table 4). In fact, a total water level rise of 1.4 meters was estimated for the period of 10/2013 to 03/2014, at monitoring point P-514 (Table 5), accounting for a total recharge of 230 mm and representing around 64 % of the total precipitation for that period. Besides, total water level rises of ~1.5 meters were estimated from 10/2013 to 02/2014 at monitoring points P-509, P-667, accounting for a total recharge of 246 mm, representing 71 % of the total precipitation (Table 5). And rises of 2.4 meters were estimated from 12/2011 to 03/2012 accounting for a total recharge of 382 mm, representing 76 % of the total precipitation (P-092). Additionally, it was evidenced that shallower water tables present higher level rises. For instance, at monitoring point P-524 water level rises were estimated to be 1.9 m from 10/2013 to 01/2014, accounting for a total recharge of 302 mm, representing over 98% of the total precipitation.

In the case of deeper water tables (29.7-34.3 m) evidenced at P-192, the response of the aquifer to precipitation show the same behaviour of level fluctuations. Moreover, estimations of water level rise from 12/10 to 03/2011, accounts for a total rise of 4.7 meters, meaning a total of 744 mm of recharge. This value surpasses the total precipitation of 340 mm, suggesting that in addition to the natural replenishment, water level rises could account for other source of recharge (Table 5).

Even though that monitoring points P-084, P-085 and P-100 are located inside Subdomain 3, near the wetland ecosystems and close to the Seco River, the different response of the aquifer evidenced by the hydrographs confirms the influence of very close pumping wells. However, at monitoring point P-100 (Fig.6), it was still possible to evidence water level rises in response to precipitation considering a constant pumping rate (MMAyA, 2014). Indeed, water level rises were estimated to be 1.09 meters from 10/2013 to 04/2014 accounting for a total recharge of 174 mm and representing 69 % of the total precipitation (Table 5).

Table 5. Change in water level and groundwater recharge for the Bolivian Lake Titicaca aquifer system over Subdomain 3, Subdomain 4, Subdomain 2 and Subdomain 6. Daily precipitation corresponds to data recorded in El Alto airport station.

	Monitoring point	Easting (m)	Northing (m)	Surface Altitude (masl)	Depth of well from Surface (masl)	Period	Time (days)	Total Precipitation (mm)	Change in water level, $\Delta H(m)$	Specific yield, Sy	Recharge (mm)	Percentage of Total Precipitation (%)
Subdomain 2	P-514	580445	8174329	3968	3889.0	21/10/2013 04/11/2013	15	59	0.22	0.16	36	60
						06/12/2013 11/02/2014	68	282	0.97	0.16	155	55
						08/03/2014 27/03/2014	20	52	0.25	0.16	40	76
	P-509	582901	8170054	3964	3876.6	14/10/2013 30/10/2013	17	55	0.23	0.16	37	68
						06/12/2013 15/02/2014	72	288	1.31	0.16	209	72
	P-667	583155	8169502	3962	3862.3	14/10/2013 29/10/2013	16	53	0.24	0.16	38	72
						02/12/2013 15/02/2014	76	290	1.30	0.16	208	72
	P-092	582487	8166770	3941	3851.0	01/12/2011 20/03/2012	111	502	2.39	0.16	382	76
	P-524	580812	8174537	3978	3945.8	08/10/2013 06/11/2013	30	80	0.48	0.16	77	97
						05/12/2013 24/01/2014	51	228	1.40	0.16	224	98
P-192	586590	8172156	4025	3906.1	08/12/2010 07/01/2011	31	133	1.59	0.16	254		
					03/02/2011 27/03/2011	53	207	3.06	0.16	490		
					01/10/2013 31/10/2013	31	70	0.33	0.16	52	75	
P-100	578253	8171541	3927	3869.7	12/01/2014 08/02/2014	28	114	0.43	0.16	68	60	
					07/03/2014 18/04/2014	43	76	0.33	0.16	53	71	
Subdomain 4	P-1	545835	8200738	3828	3778.1	12/10/2018 09/11/2018	29	82	0.18			
						02/01/2019 19/01/2019	18	48	0.13			
						29/01/2019 24/02/2019	27	127	0.41			
P-2	545348	8193806	3829	3794.0	11/10/2018 26/10/2018	16	78	0.13				
					13/12/2018 07/01/2019	26	151	0.14				
						28/01/2019 26/02/2019	30	139	0.19			
Subdomain 3	P-3	553770	8189721	3858	3831.9	11/10/2018 06/11/2018	27	90	0.15	0.2	29	32
						14/12/2018 04/01/2019	22	140	0.21	0.2	41	30
						28/01/2019 16/02/2019	20	130	0.24	0.2	48	37
Subdomain 6	P-5	545039	8185793	3829	3776.9	01/10/2018 18/10/2018	18	45	0.08			
						15/11/2018 22/11/2018	8	9	0.03			
						11/12/2018 19/12/2018	9	70	0.03			
						24/12/2018 28/12/2018	5	6	0.04			
						27/01/2019 02/02/2019	7	37	0.08			
					04/02/2019 20/02/2019	17	72	0.12				

Overall, groundwater recharge estimated over one hydrologic year (12/2011 to 03/2012 and 10/2013 to 03/2014) at Subdomain 2, represents around 64% to 76% of the total precipitation for that periods. An exception was evidenced when shallower (4.7 to 5.7 meters; P-524) and with deeper water tables (29.7-34.3 meters; P-192).

Therefore, considering the hydrologic year “2013-2014”, from the total precipitation ( $\sim 575 \text{ mm year}^{-1}$ ), water that reached the water table would have accounted for 174 to 302  $\text{mm year}^{-1}$  and the total average evaporative loss of groundwater would have accounted for  $\sim 33 \text{ mm year}^{-1}$  to 58  $\text{mm year}^{-1}$ .

#### 4.3.2.2 Subdomain 4 (*Confined behaviour*)

Figure 7 displays the location and hydrographs of hourly water level fluctuations for monitoring wells situated inside Subdomain 4 (P-1; P-2). The WTF was not applied because borehole lithology at both points evidenced a covering layer of clay materials from 2 to 4 meters of thickness. In fact, water level rises in this area are most likely attributed to seepage from the influent Lake Titicaca. This has been confirmed by electrical conductivity records (P-1), showing clear increases in response to high intensity precipitation events. This reflects that during precipitation events, Lake Titicaca water levels rise and may recharge the aquifer (Fig.7; Fig.8).

Total water level rises of 72 cm were estimated from 10/2018 to 02/2019 at monitoring point P-1 (Table 5) and 46 cm at monitoring point P-2 for the same period (Table 5). The lower value at P-2 accounts for its distance of location, being 2000 meters SE away of Lake Titicaca.

#### 4.3.2.3 Subdomain 3 (*Unconfined behaviour*)

The location and hydrograph of hourly water level fluctuations for monitoring well P-3 (situated inside Subdomain 3) is also displayed in Figure 7.

Groundwater level fluctuations present a delayed response to high-intensity precipitation events. This delay could be attributed to the slow drainage of the thin soil layer that from field observations may comprise a significant amount of clay materials. Groundwater recharge over this Subdomain was estimated considering a specific yield value of 0.20 (Table 4). Therefore, a total water level rise of 60 cm was estimated for the period of 10/2018 to 02/2019, accounting for a total net recharge 118 mm,

representing around 33 % of the total precipitation for that period (Table 5). In addition, electrical conductivity records at this monitoring point, showed values oscillating around 60.6 to 65  $\mu\text{S}/\text{cm}$ .

Furthermore, for the hydrologic year “2018-2019” from the total precipitation (up to may/2019) ( $\sim 577 \text{ mm year}^{-1}$ ), water that reached the water table would have accounted for 118  $\text{mm year}^{-1}$ .

#### *4.3.2.4 Subdomain 5 (Confined behaviour)*

The location and hydrograph of water levels for the monitoring well P-5 is also illustrated in Fig. 7. This point is situated inside Subdomain 6, evidencing a first layer of 15 meters of clay materials and 38 meters of clayey sandy and gravelly sand materials (Borehole lithology). Even though that WTF method was not applied, water level rises were also evidenced (Fig. 7e).

In fact, a total water level rise of 37 cm was estimated for the period of 10/2018 to 02/2019 (Table 5). Water level rises at this point may account for groundwater lateral drainage across Subdomain 5, arriving from the northeast. These water level rises could evidence the connection between the Piedmont subsystem and Lacustrine plain indicated by Flores-Avilés et al. (2019). In addition, electrical conductivity records oscillate between 150.6  $\mu\text{S}/\text{cm}$  (31/08/2018) to 150.1  $\mu\text{S}/\text{cm}$  (19/03/2019).

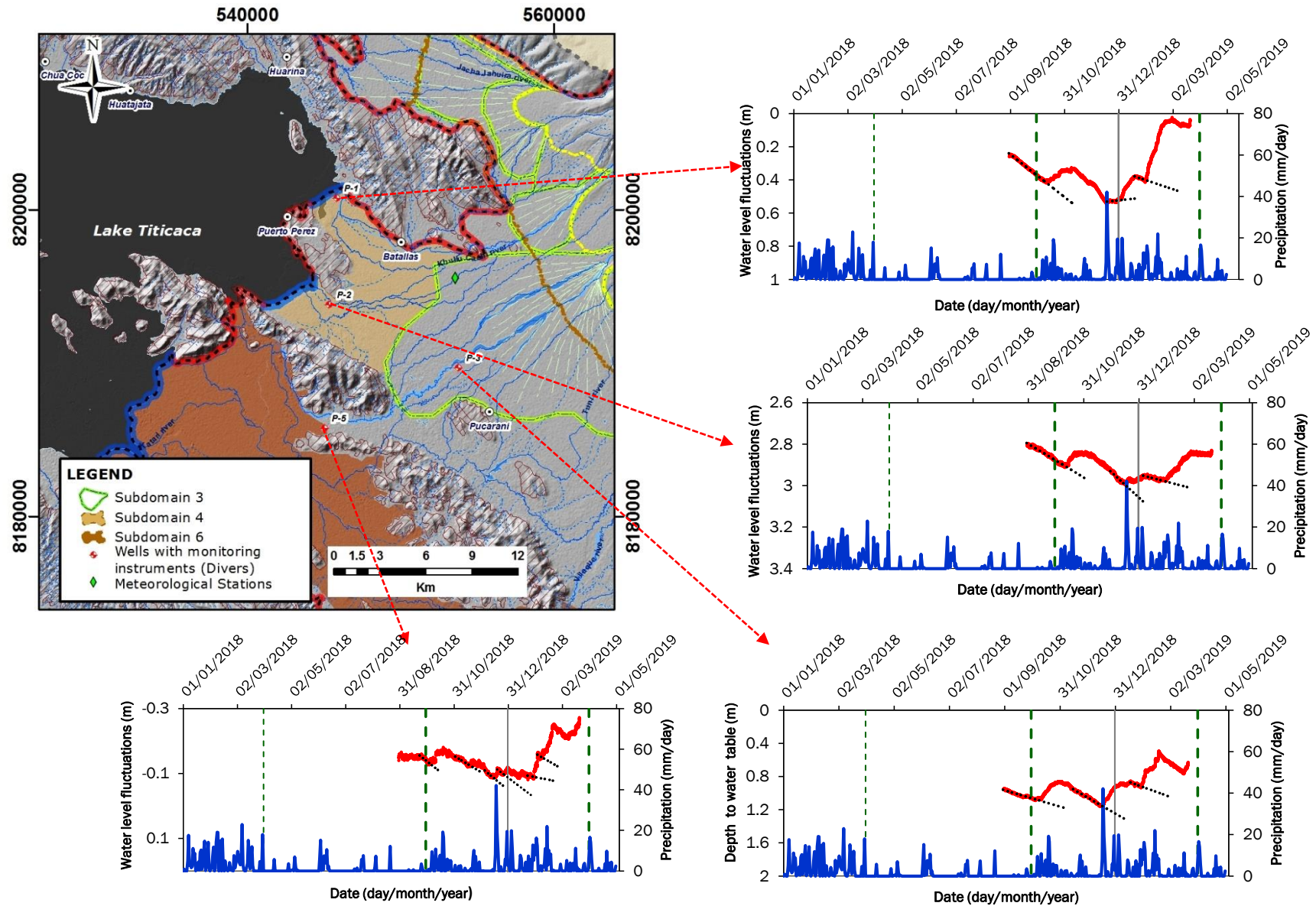
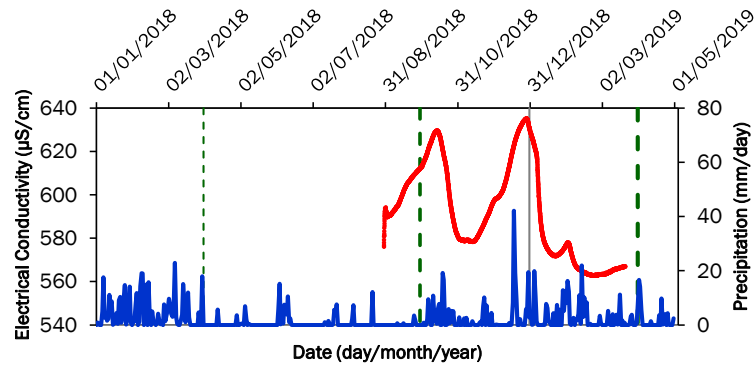


Figure 7. Hydrographs of water level fluctuations (red line) for wells located at Subdomain 3, 4 and 6 and records of daily average precipitation (blue line). Gray lines represent the end of a hydrological year. Green dashed lines represent seasonal limits (01/04 to 30/09 – “Dry season”) and (01/10 to 31/03 “Wet season”). Black dotted lines represent the hypothetical extrapolated recession curves for WTF (Water table fluctuation) analysis.



**Figure 8.** *Electrical conductivity measurements recorded at monitoring point P-1 and records of daily average precipitation (blue line).*

#### 4.4 Seepage from influent/effluent rivers inside the domain

Quaternary deposits comprised in the Bolivian Lake Titicaca Aquifer System were formed by or in association with Glaciers, during the Pleistocene Glaciation and Deglaciation (Lavenu, 1992; Argollo et al., 2008; Flores-Avilés et al., 2019). In glaciated terrains, buried valley aquifers and buried esker aquifers in particular are prevalent (Freeze and Cherry, 1979; Sauriol, 2016).

The current geomorphology of the study area evidence deep valleys in the domain relating a glacio-fluvial origin. For instance, up stream the U-shaped valley of the Seque river, nearby Lake Milluni, Quaternary deposits show ~90 meters of Moraine deposits laying over fluvio-glacial deposits. The same U-shaped valleys are observed up stream the Tuni, Condoriri, Jachallani, Khullu Cachi and Jacha Jahuira rivers. These valleys were most likely formed by glacial meltwater when the Huayna Potosí, Condoriri and Jisk'a Pata glaciers were retreating. Indeed, Flores-Avilés et al. (2019) have shown that downstream, towards the SE, the topography of Tertiary/Devonian bedrock present valley shapes. We believe that these meltwater rivers could have formed permeable deposits in deep valleys eroded in the glacial terrain or in the Tertiary/Devonian sedimentary bedrock. That nowadays may behave as tunnel valleys allowing melt-water drainage and recharging the aquifer (Fig.8).

Furthermore, nowadays the semiarid climate in the study area, showing annual values of evapotranspiration exceeding precipitation, evidence that the amount of runoff in the study area is not large enough to currently form integrated hydrographic networks.

#### 4.5 Regional groundwater flow concept for the Domain

The groundwater flow concept under natural conditions (pre-development conditions), corresponds to a classical gravity-driven regional flow (Tóth, 1962; Tóth, 1963; Tóth, 1995; Tóth, 1999; Tóth, 2010; Mádl-Szönyi) and is illustrated in Fig.9.

Firstly, a continuous inflow of water from Relict Rock Glaciers and meteoric water enter into the aquifer across the Eastern boundary. Then water flows through Subdomain 2 following the high topographic slope (NE-SW). During this travel, there are different ways of how water leaves the aquifer: i) an amount of water is lost by spring discharge through a portion of the Southern boundary, ii) other amount leaves the aquifer through the Northern boundary by seepage into the effluent Lake Titicaca (at Puerto Pérez Bays), iii) other amount is lost by evapotranspiration, mainly in the lower sector of the Piedmont (shallow water tables), and finally iv) an amount of water is lost by seepage into the effluent Seco, Pampasi, Sorechata, Vilaque, Huayna Potosí and Khullukhachi rivers.

Although groundwater is lost by the above mentioned ways, it also is renewed mostly by natural replenishment but also by seepage from the influent Seque, Huayna Potosí and Jachallani rivers. After, a significant amount of water flows an approximate distance of 35 Km and crosses to the plain area through deep subterranean channels formed by the outcropping impervious barriers. During this travel, the porous media in which water flows vary spatially and vertically, that means that firstly water flows through Subdomain 2, then through Subdomain 3, sometimes through Subdomain 2 and 5 and finally through Subdomain 5.

Under natural conditions, the velocity ( $v$ ) of the fluid movement is calculated by dividing Darcy's law by the effective porosity ( $s_v$ ), assuming the representative gradients ( $i$ ) from Figures 3 and 9. Calculations through Subdomain 2, Subdomain 3 and Subdomain 5 are summarized in table 6.

Table 6. Summary of velocity fluid movement through subdomains 2, 3 and 5, estimated by Darcy's law based on tables 2, 3 and 4, and figures 3 and 9.

Subdomain	$K_h$ (m/sec)	$S_y$	$\Delta H$ (m)	$\Delta L$ (m)	$i$	$q$ (m/year)	$v$ (m/year)
Subdomain 2	$1.2 \times 10^{-5}$	0.16	200	4000	0.05	18.9	118.2
	$2.5 \times 10^{-6}$	0.16	200	4000	0.05	3.9	24.6
Subdomain 3	$1.1 \times 10^{-4}$	0.20	100	10000	0.01	34.7	173.4
	$5.5 \times 10^{-5}$	0.20	100	10000	0.01	17.3	86.7
Subdomain 5	$5.0 \times 10^{-5}$	0.18	20	17000	0.001	1.9	1.0
	$5.0 \times 10^{-6}$	0.18	20	17000	0.001	0.2	10.3

From Figure 3 groundwater travels  $\sim 14$  Km through Subdomain 2 and  $\sim 10$  Km through Subdomain 3, from the high Eastern boundary before reaching the plain. Therefore the time of travel is estimated to range between 234 to 626 years.

Water from the high areas that reaches the plain area, flows mainly through Subdomain 5. In this area a major part of water is stored in Subdomain 5 and another amount flows following the low topographic slope (SE-NW), is lost by seepage into the effluent Lake Titicaca (Cohana bay) and by leakage into the overlying Subdomain 6. Groundwater is also renewed by natural replenishment.

Under natural conditions, the time of travel from the far Southern boundary (neaby Collana City) to Lake Titicaca ( $\sim 76$  Km) is estimated to range between 7374 to 73744 years.

The natural groundwater balance input and output components necessary to construct a steady state regional groundwater numerical model, might consider:

$$\begin{aligned} \Delta S^{gw} = & Q_{RelictRockGlaciers} + Q_{AchacachiZone} + Q_{Recharge} + Q_{influentRivers} \\ & \pm Q_{OverlyingSubdomains} - Q_{effluentLakeTiticaca} - Q_{effluentRivers} \\ & - Q_{SpringDischarge} - Q_{EvapotranspWetlands} \end{aligned}$$

Inputs

- Groundwater inflow through the aquifer boundaries (Inflow from relict rock glaciers, inflow from the Achacachi zone) ( $Q_{RelictRockGlaciers}$ ,  $Q_{AchacachiZone}$ )
- Recharge over Subdomains 2, 3, 4 and 5 ( $Q_{Recharge}$ )
- Seepage from the influent rivers (Seque, Huayna Potosí and Jachallani rivers) ( $Q_{InfluentRivers}$ )

#### Outputs

- Seepage into the effluent Lake Titicaca ( $Q_{EffluentLakeTiticaca}$ )
- Seepage into the effluent rivers (Seco, Pampasi, Sorechata, Vialque, Huayna Potosí and Khullukhachi rivers) ( $Q_{EffluentRivers}$ )
- Leakage out into the overlying Subdomain 6 (Clay aquitard) ( $Q_{OverlyingLayers}$ )
- Seepage into the effluent disruption zone ( $Q_{SpringDischarge}$ )
- Evapotranspiration from shallow water tables (i.e. wetland ecosystems) over a portion of Subdomain 2, Subdomain 3 and Subdomain 5 ( $Q_{EvapotranspWetlands}$ )

From the natural groundwater balance, the discharge from the Aquifer into the effluent Lake Titicaca could be estimated graphically from Figure 9.

At Puerto Pérez bays, the vertical resolution of the Time Domain Electromagnetic method (TDEM) reported in Flores-Avilés (2019) didn't allow identifying the very thin clay, evidenced by the analysis of groundwater level fluctuations. However it is hypothesized that groundwater in this zone leaves the aquifer by discharging into Lake Titicaca.

Therefore, from Fig.9 assuming a  $\kappa_h = 5.0 \times 10^{-6} \text{ m/sec}$  for Subdomain 5 (Layer 5), according to table 7 groundwater discharge at Puerto Pérez bays would range between 212 to 436  $\text{m}^3/\text{sec}$ . Aquifer tests are compulsory over this subdomain and the others, in order to determine its hydraulic properties.

Table 7. Summary of calculations of groundwater discharge into Lake Titicaca estimated graphically from the flow net map (Figure 9).

Lake Titicaca bay	$K_h$ (m/sec)	$i$	$B$ (m)	$W$ (m)	$A$ (m <sup>2</sup> )	$Q$ (m <sup>3</sup> /day)
Puerto Pérez	$5.0 \times 10^{-5}$	0.006	50	1700	85000	2117
Bay 1	$5.0 \times 10^{-6}$	0.006	50	1700	85000	212
Puerto Pérez	$5.0 \times 10^{-5}$	0.006	50	3400	170000	4360
Bay 2	$5.0 \times 10^{-6}$	0.006	50	3400	170000	436
Cohana Bay	$5.0 \times 10^{-5}$	0.001	150	8647	1297050	6592
	$5.0 \times 10^{-6}$	0.001	150	8647	1297050	659

Note:  $B$  is the thickness of Layer 5 at Subdomain 5, estimated from Flores Aviles et al. (2019)  
 $W$  is the width of the bay,  $Q$  is the discharge estimated with Darcy's law  $Q = q \cdot A$

At the Cohana bay, TDEM evidenced a very thick clay layer ( $\sim 45$  m). According to Quaternary glaciation history, the current Lake Titicaca would be overlying the clay layer from the Ballivian Paleolake expansion (Flores-Avilés et al., 2019). As a result, in this zone it is hypothesized that groundwater flow would be retarded due to this thick clay layer. Therefore, assuming a  $\kappa_h = 5.0 \times 10^{-6}$  m/sec for Subdomain 5 (Layer 5), according to table 7 groundwater discharge at Cohana bay would range around 659 m<sup>3</sup>/sec.

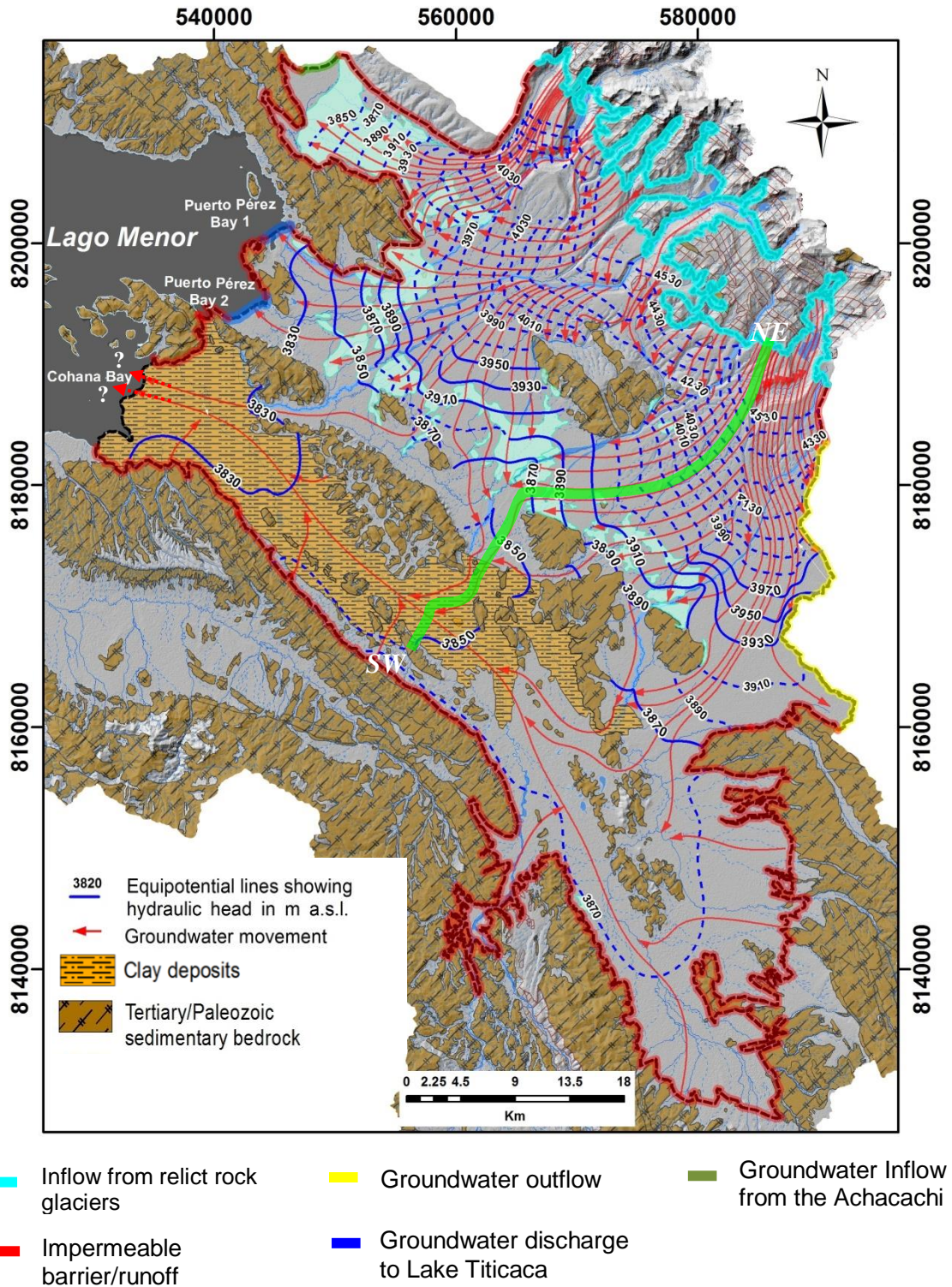


Figure 9. Conceptual model showing the regional groundwater flow dynamics under natural conditions and assuming steady state.

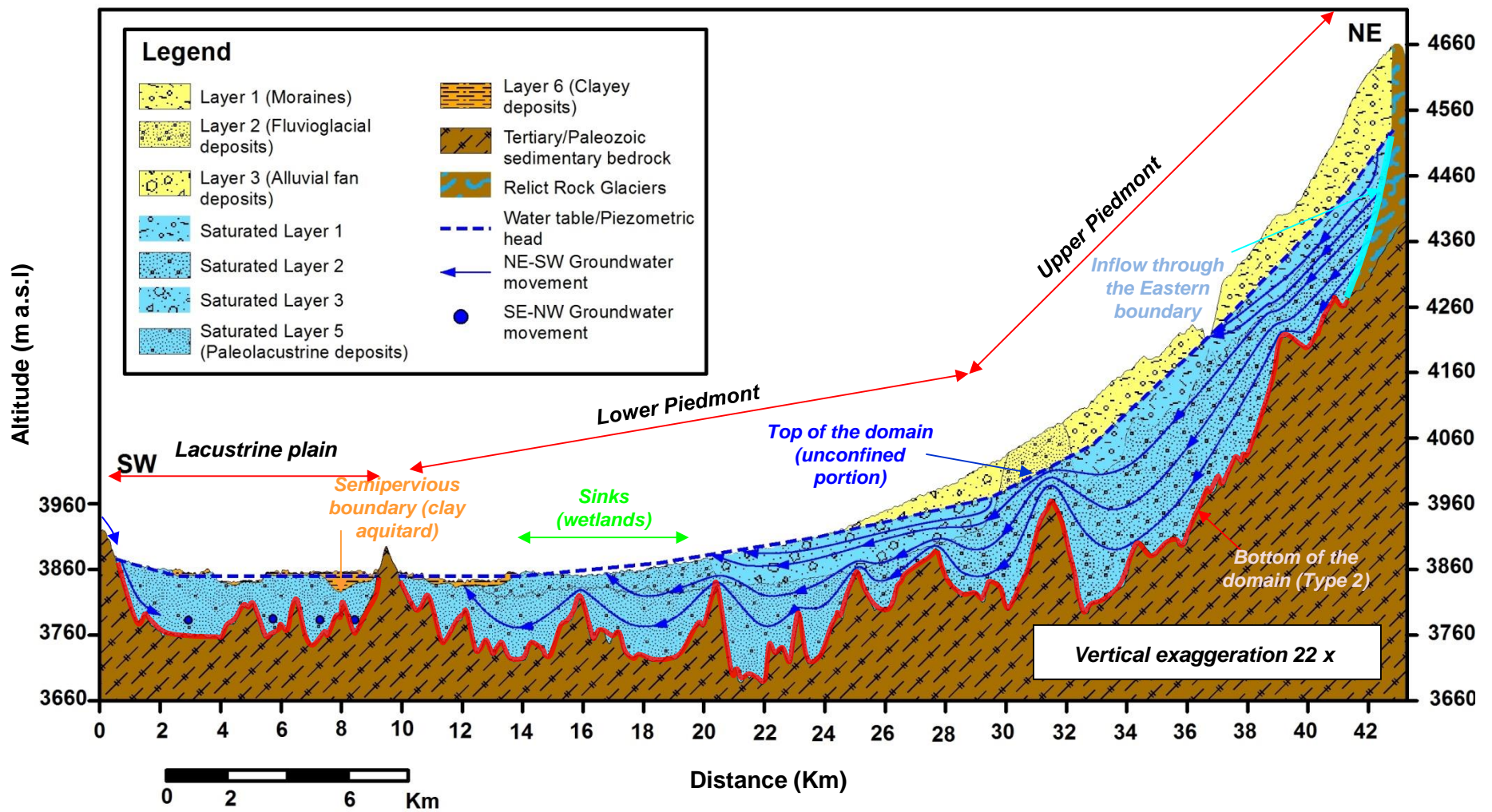


Figure 10. Conceptual groundwater flow model of the domain along the SW-NE cross section.

## 5. Summary and conclusions

A basin-scale conceptual groundwater flow model was developed for the Lake Titicaca aquifer system. The conceptual model considers all relevant contributions to groundwater flow, including lateral inflow and outflow through boundaries, as well as sinks (discharge) and sources (recharge) mechanisms inside the domain. This conceptual model was developed using detailed analysis of hydrogeologic data and field investigations when available.

The groundwater flow concept under natural conditions corresponds to a classical gravity-driven regional groundwater flow system (GDRGF). The porous geologic media in which water flows vary spatially and vertically. There were identified six Subdomains (regions possessing different hydraulic properties). A large portion of the aquifer presents an unconfined behaviour (Subdomain 1, 2, 3, 4, 5) whereas it remains confined below Subdomain 6. The thickness of the unconfined portion varies from 50 to 150 meters and that of the confined from 100 to 150 meters. Values of hydraulic conductivity for the unconfined portion range from  $1.1 \times 10^{-4}$  to  $5.9 \times 10^{-8} \text{ m/sec}$  and specific yield ranges from 0.16 to 0.20. While for the confined part transmissivity values range around  $6.0 \times 10^{-6} \text{ m}^2/\text{sec}$ , with a storativity values of  $1.2 \times 10^{-2} - 6.0 \times 10^{-3}$ .

Results of groundwater recharge (water that arrives at the water table) over a hydrologic year, at Subdomain 2 and Subdomain 3, estimated with the Water Fluctuation Method (WTF), showed that recharge would vary from 174 to 302  $\text{mm year}^{-1}$  and the total average evaporative loss of groundwater accounts for  $\sim 33 \text{ mm year}^{-1}$  to 58  $\text{mm year}^{-1}$ . Furthermore, groundwater level rises over a hydrologic year at Subdomain 4 vary from 46 to 72 cm (10/2018 to 02/2019) accounting most likely for seepage from the influent Lake Titicaca. Besides, groundwater level rises of 37 cm estimated over Subdomain 6 (10/2018 to 02/2019) mostly accounts for lateral inflow through Subdomain 5 arriving from the Northeast.

The findings from this study provide an advanced understanding of the groundwater flow dynamics under natural conditions and a guide to future data collection in order to improve the robustness of future groundwater flow numerical modeling. The methodology for the development of the conceptual model presented in this study can

be directly applied to other basins in Bolivia with similar hydrogeologic conditions provided that sufficient data is available. Furthermore, it is necessary to refine and improve the robustness of this conceptual model by means of the quantification of the natural groundwater balance components.

#### *Acknowledgments*

*The present study was undertaken with the financial support of the Government of the Plurinational State of Bolivia through the Program “100 Scholarships for Postgraduate Education within the Framework of Technological and Scientific Sovereignty”, administered by the Ministry of Education (MINEDU) and partly funded by LABEX OSUG@2020, ANR grant no.ANR-10-LABX-56 (financed by the Future Investments programme launched by the French government and implemented by the ANR). Special thanks to the Ministry of Environment and Water (M.M.A.Y.A, La Paz) and the University of San Andres (UMSA, La Paz) for their logistical and technical support.*

## References

- Allen RG, Pereira LS, Raes D, Smith M (1998) Crop evapotranspiration-Guidelines for computing crop water requirements-FAO Irrigation and drainage paper 56 (available at <http://www.fao.org/docrep/X0490E/X0490E00.htm#Contents>)
- Barroso Chulve A, Garfias Soliz J (2010) Delimitación de la contaminación del agua subterránea por lixiviados en un till glacial del relleno sanitario “Villa Ingenio”: El Alto-Bolivia. Universidad Mayor Real Pontificia de San Francisco Xavier de Chuquisaca. Tesis de Posgrado
- Bayanzul B, Nakamura K, Machida I, Watanabe N, Komai T (2018) Construction of a conceptual model for confined groundwater flow in the Gunii Khooloi Basin, Southern Gobi Region, Mongolia. *Hydrogeology Journal*. <https://doi.org/10.1007/s10040-019-01955-8>
- Bredehoeft J (2004) The conceptualization model problem—surprise. *Hydrogeol J* (2005) 13:37–46
- Clark I, Fritz P (1997) *Environmental Isotopes in Hydrogeology*. CRC Press, p. 28, p.43, p.87.
- Domenico PA, Mifflin MD (1965) Water from low- Permeability Sediments and Land Subsidence. *Water Resources Research*. Vol. 1, N°4.
- Ebrahim GY, Villholth KG, Bolous M (2018) Integrated hydrogeological modelling of hard-rock semi-arid terrain: supporting sustainable agricultural groundwater use in Hout catchment, Limpopo Province, South Africa. *Hydrogeology Journal*. <https://doi.org/10.1007/s10040-019-01957-6>
- EPSAS SA (2017) Informe Pozos Perforación del Proyecto: “Suministro de rápida implementación de agua potable en el Sistema El Alto-San Felipe de Seke y Tilata (Fase 2). Empresa Pública de Saneamiento Básico.
- Fernandes AJ, Maldaner CH, Negri F, Rouleau A, Wahnfried ID (2016) Aspects of a conceptual groundwater flow model of the Serra Geral basalt aquifer (Sao Paulo,

- Brazil) from physical and structural geology data. *Hydrogeol J* (2016) 24:1199–1212. DOI 10.1007/s10040-016-1370-6
- Flores-Avilés GP, Descloitres M, Duwig C, Rossier Y, Spadini L, Leghchenko A, Soruco A, Argollo J, Pérez Mayra, Medinaceli W (2019) Insight into the Bolivian Lake Titicaca aquifer system, inferred from geophysical (TDEM), hydrogeological and hydrogeochemical data. *Under Revision*
- Gómez E, Barmen G, Rosberg J (2016) Groundwater Origins and Circulation Patterns Based on Isotopes in Challapampa Aquifer, Bolivia. *Water* 2016, 8, 207; doi:10.3390/w8050207.
- Gerber RE, Boyce JI, Howard KWF (2001) Evaluation of heterogeneity and field-scale groundwater flow regime in a leaky till aquitard. *Hydrogeology Journal* (2001) 9:60–78. DOI 10.1007/s100400000115
- Grenier C, Régnier D, Mouche E, Benabderrahmane H, Costard F, Davy P (2013) Impact of permafrost development on groundwater flow patterns: a numerical study considering freezing cycles on a two-dimensional vertical cut through a generic river-plain system. *Hydrogeology Journal* (2013) 21: 257–270. DOI 10.1007/s10040-012-0909-4
- Hargreaves GH, Samani ZA (1985) Reference crop evapotranspiration from temperatura. *Applied Eng. In Agric.*, 1(2): 96-99
- Healy RW, Cook PG (2002) Using groundwater levels to estimate recharge. *Hydrogeology Journal* (2002) 10:91–109. DOI 10.1007/s10040-001-0178-0
- Herrera C, Custodio E (2008) Conceptual hydrogeological model of volcanic Easter Island (Chile) after chemical and isotopic surveys. *Hydrogeology Journal* (2008) 16: 1329–1348. DOI 10.1007/s10040-008-0316-z
- Izady A, Davary K, Alizadeh A, Ziaei AN, Alipoor A, Joodavi A, Brusseau ML (2013) A framework toward developing a groundwater conceptual model. *Arab J Geosci.* DOI 10.1007/s12517-013-0971-9

- Izady A, Davary K, Alizadeh A, Ziaei AN, Akhavan S, Alipoor A, Joodavi A, Brusseau ML (2015) Groundwater conceptualization and modeling using distributed SWAT based recharge for the semi-arid agricultural Neishaboor plain, Iran 2015. *Hydrogeology Journal* (2015) 23: 47–68. DOI 10.1007/s10040-014-1219-9
- JICA (1987) Final Report for the Study on groundwater development Project on El Alto district in La Paz city. Japan International Cooperation Agency. Republic of Bolivia.
- Jiráková H, Huneau F, Celle-Jeanton H, Hrkal Z, Le Coustumer P (2010) Insights into palaeorecharge conditions for European deep aquifers. *Hydrogeology Journal* (2011) 19: 1545–1562. DOI 10.1007/s10040-011-0765-7
- Kane DL, Yoshikawa K, McNamara JP (2012) Regional groundwater flow in an area mapped as continuous permafrost, NE Alaska (USA). *Hydrogeology Journal* (2013) 21: 41–52. DOI 10.1007/s10040-012-0937-0
- Lachaal F, Mlayah A, Anane M, Bédir M, Tarhouni J, Leduc C (2011) Comprehension and hydrogeological conceptualization of aquifer in arid and semi-arid regions using integrated hydrogeological information system: case of the deep aquifer of Zéramdine-Béni Hassen (east-central Tunisia). *Arab J Geosci*. DOI 10.1007/s12517-011-0498-x
- Lemke LD, Cypher JA (2009) Postaudit evaluation of conceptual model uncertainty for a glacial aquifer groundwater flow and contaminant transport model. *Hydrogeology Journal* (2010) 18: 945–958. DOI 10.1007/s10040-009-0554-8
- Luo YF, Peng SZ, Khan S, Cui YL, Wang Y, Feng YH (2009) A comparative study of groundwater evapotranspiration functions. 18th IMACS World Congress MODSIM09 Proceedings, 3095–3101, 2009
- Kruseman GP, de Ridder NA (1992) Analysis and Evaluation of Pumping Test Data. ILRI Publication 47, p. 99, p.196
- Mádl-Szőnyl J, Tóth Á (2015) Basin-scale conceptual groundwater flow model for an unconfined and confined thick carbonate region. *Hydrogeology Journal* (2015) 23: 1359–1380. DOI 10.1007/s10040-015-1274-x

- Manghi F, Mortazavi B, Crother C, Hamdi MR (2009) Estimating Regional Groundwater Recharge Using a Hydrological Budget Method. *Water Resour Manage* (2009) 23:2475–2489. DOI 10.1007/s11269-008-9391-0
- Matengu B, Xu Y, Tordiffe E (2019) Hydrogeological characteristics of the Omaruru Delta Aquifer System in Namibia. *Hydrogeology Journal* (2019) 27:857–883. <https://doi.org/10.1007/s10040-018-1913-0>
- McMahon TA, Peel MC, Lowe L, Srikanthan R, McVicar TR (2013) Estimating actual, potential, reference crop and pan evaporation using standard meteorological data: a pragmatic synthesis. *Hydrol. Earth Syst. Sci.*, 17, 1331–1363, 2013 [www.hydrol-earth-syst-sci.net/17/1331/2013/](http://www.hydrol-earth-syst-sci.net/17/1331/2013/). doi:10.5194/hess-17-1331-2013
- M.M.A.y.A (2014) Plan Maestro Metropolitano de Agua Potable y Saneamiento La Paz-El Alto Bolivia. Ministerio de Medio Ambiente y Agua/Viceministerio de Recursos Hídricos y Riego, La Paz, Bolivia, 276 pages.
- M.M.A.y.A (2016) Plan de Manejo Preliminar de los Acuíferos de Purapurani y Viacha. Ministerio de Medio Ambiente y Agua/Viceministerio de Recursos Hídricos y Riego, La Paz, Bolivia, 184 pages.
- Nettasana T, Craig J, Tolson B (2012) Conceptual and numerical models for sustainable groundwater management in the Thaphra area, Chi River Basin, Thailand. *Hydrogeology Journal* (2012) 20: 1355–1374. DOI 10.1007/s10040-012-0887-6
- Pauritsh M, Wagner T, Winkler G, Birk S (2017) Investigating groundwater flow components in an Alpine relict rock glacier (Austria) using a numerical model. *Hydrogeol J* (2017) 25:371–383. DOI 10.1007/s10040-016-1484-x
- Pham HV, Tsai FT (2017) Modeling complex aquifer systems: a case study in Baton Rouge, Louisiana (USA). *Hydrogeol J*. DOI 10.1007/s10040-016-1532-6
- Rangecroft S, Harrison S, Anderson K (2014) Rock glaciers, water security and climate change in the Bolivian Andes. University of Exeter as a thesis for the degree of Doctor of Philosophy in Physical Geography, Oct 2014

- Rangecroft S, Suggitt AJ, Anderson K, Harrison S (2016) Future climate warming and changes to mountain permafrost in the Bolivian Andes. *Climatic Change*. DOI 10.1007/s10584-016-1655-8
- Rosenberry DO, Stannard DI, Winter TC, Martinez ML (2004) Comparison of 13 equations for determining evapotranspiration from a prairie wetland, Cottonwood Lake area, North Dakota, USA. *WETLANDS*, Vol. 24, No. 3, September 2004, pp. 483–497
- Sahoo S, Jha MK (2017) Numerical groundwater-flow modeling to evaluate potential effects of pumping and recharge: implications for sustainable groundwater management in the Mahanadi delta region, India. *Hydrogeol J* (2017) 25:2489–2511. DOI 10.1007/s10040-017-1610-4
- Saltel M, Rebeix R, Thomas B, Franceschi M, Lavielle B, Bertran P (2019) Paleoclimate variations and impact on groundwater recharge in multi-layer aquifer systems using a multi-tracer approach (northern Aquitaine basin, France). *Hydrogeology Journal*. <https://doi.org/10.1007/s10040-019-01944-x>
- Samano S, Moghaddam AA, Ye M (2017) Investigating the effect of complexity on groundwater flow modeling uncertainty. *Stoch Environ Res Risk Assess*. DOI 10.1007/s00477-017-1436-6
- Sanderson JS, Cooper DJ (2008) Ground water discharge by evapotranspiration in wetlands of an arid intermountain basin. *Journal of Hydrology* (2008) 351, 344– 359
- Saroli M, Lancia M, Albano M, Casale A, Giovinco G, Petitta M, Zarlenga F, dell’Isola M (2017) A hydrogeological conceptual model of the Suio hydrothermal area (central Italy). *Hydrogeol J* (2017) 25:1811–1832. DOI 10.1007/s10040-017-1549-5
- Sauriol J (2016) Provenance of buried esker groundwater: the case of Vars-Winchester esker aquifer, Eastern Ontario, Canada. *Hydrogeol J* (2016) 24:123–139. DOI 10.1007/s10040-015-1327-1
- Scanlon BR, Healy RW, Cook PG (2002) Choosing appropriate techniques for quantifying groundwater recharge. *Hydrogeology Journal* (2002) 10:18–39. DOI 10.1007/s10040-0010176-2

- Sterckx A, Lemieux JM, Vaikmäe R (2018) Assessment of paleo-recharge under the Fennoscandian Ice Sheet and its impact on regional groundwater flow in the northern Baltic Artesian Basin using a numerical model. *Hydrogeology Journal* (2018) 26:2793–2810. <https://doi.org/10.1007/s10040-018-1838-7>
- Tóth J (1962) A theory of Groundwater Motion in Small Drainage Basins in Central Alberta, Canadá. *Journal of Geophysical Research*, Vol.67, N°11
- Tóth J (1963) A theoretical Analysis of Groundwater Flow in Small Drainage Basins. *Journal of Geophysical Research*, Vol.68, N°16
- Tóth J (1995) Hydraulic Continuity in large Sedimentary Basins. *Hydrogeology Journal*, v.3, no 4, 1995
- Tóth J (1999) Groundwater as a geologic agent: An overview of the causes, processes, and manifestations. *Hydrogeology Journal* (1999) 7:1–14
- Tóth J (2010) The theory of basinal gravity flow of groundwater and its impacts on hydrology Japan. *Special Issue Review* 335-354 (2010)
- Timms WA, Crane R, Anderson DJ, Bouzakkalos S, Whelan M, McGeeney D, Rahman PF, Acworth RI (2016) Accelerated gravity testing of aquitard core permeability and implications at formation and regional scale. *Hydrol. Earth Syst. Sci.*, 20, 39–54, 2016 [www.hydrol-earth-syst-sci.net/20/39/2016/](http://www.hydrol-earth-syst-sci.net/20/39/2016/) doi:10.5194/hess-20-39-2016
- Timms WA, Crane R, Anderson DJ, Bouzakkalos S, Whelan M, McGeeney D, Rahman PF, Guinea A, Acworth RI (2014) Vertical hydraulic conductivity of a clayey-silt aquitard: accelerated fluid flow in a centrifuge permeameter compared with in situ conditions. *Hydrol. Earth Syst. Sci. Discuss.*, 11, 3155–3212, 2014 [www.hydrol-earth-syst-sci-discuss.net/11/3155/2014/](http://www.hydrol-earth-syst-sci-discuss.net/11/3155/2014/). doi:10.5194/hessd-11-3155-2014
- Turner RJ, Mansour MM, Dearden R, Dochartaigh BEO, Hughes AG (2015) Improved understanding of groundwater flow in complex superficial deposits using three-dimensional geological-framework and groundwater models: an example from Glasgow, Scotland (UK). *Hydrogeology Journal* (2015) 23: 493–506. DOI 10.1007/s10040-014-1207-0

Winkler G, Wagner T, Pauritsch M, Birk S, Kellerer-Pirklbauer A, Benischke R, Leis A, Morawetz R, Schreilechner MG, Hergarten S (2016) Identification and assessment of groundwater flow and storage components of the relict Schöneben Rock Glacier, Niedere Tauern Range, Eastern Alps (Austria). *Hydrogeol J* (2016) 24:937–953. DOI 10.1007/s10040-015-1348-9

Xu Y, Beekman HE (2019) Review: Groundwater recharge estimation in arid and semi-arid southern Africa. *Hydrogeology Journal* (2019) 27:929–943. <https://doi.org/10.1007/s10040-018-1898-8>

Zhou Y, Li W (2011) A review of regional groundwater flow modeling. *GEOSCIENCE FRONTIERS* 2(2) (2011) 205e214 available at [www.sciencedirect.com](http://www.sciencedirect.com)

Zhou Y, Heralth HMPD (2017) Evaluation of alternative conceptual models for groundwater modelling. *Geoscience Frontiers* 8 (2017) 437e443

### **5.3 Conclusions**

The findings of the basin-scale conceptual groundwater flow approach provides an advanced understanding of the groundwater flow dynamics under natural conditions and a guide to future data collection in order to improve the robustness of 3D future groundwater flow numerical modeling. However, future work following this study might be directed towards collecting hydrogeological data in order to quantify the natural groundwater balance components for setting up and running a 3D basin scale groundwater flow numerical model.

Therefore, in order to refine and improve the robustness of future 3D groundwater flow numerical modeling, it is essential to: i) define a regional groundwater level monitoring network to provide time series of groundwater levels for the calibration of groundwater numerical models, ii) conduct multi-well pumping tests at least at each defined Subdomain to obtain physical parameters, iii) quantify groundwater inflow towards the Eastern boundary, iv) measure the seepage from influent rivers or seepage into effluent rivers, v) quantify groundwater evapotranspiration, vi) quantify the spring discharge along a portion of the Southern boundary.

Time series information would allow the development and validation of a transient numerical model which would be useful for management purposes (e.g. definition of pumping wells location or production wells, and protection zones), and to study future modeling scenarios. Thus, the next step in the perspective of groundwater flow numerical model, is to test all the boundary conditions in 3D, according to Article II.

# Groundwater basin-scale hydrochemical and dual isotopic characterization

## 6.1 Introduction

This chapter explains the results of the basin-scale hydrochemical and dual isotopic (nitrogen and oxygen) characterization of the Katari and Lago Menor region. These results are presented in the third scientific article. This article aims to trace the natural background levels of groundwater in the Katari and Lago Menor region, as well as the nitrate sources and fluxes. These results allowed evaluating if the groundwater resources are threatened by agricultural leaching, livestock production and/or by domestic wastewater.

The particular high-altitude, gravity-driven hydrogeological environment, allowed the depiction of hydrochemical evolution patterns and denitrification process, from the recharge zones, along the groundwater flow system and towards the discharge areas.

## **6.2 Article III: Tracing nitrate contamination in a gravity-driven groundwater flow system of Lake Titicaca Basin, Bolivian Altiplano: influence on water chemistry and nitrogen isotopes**

**Gabriela Patricia Flores Avilés<sup>1,2 a</sup>, Céline Duwig<sup>1</sup>, Elisa Sacchi<sup>3</sup>, Joel Savarino<sup>1</sup>, Lorenzo Spadini<sup>1</sup>, Oswaldo Ramos<sup>2</sup>, Maira Pérez<sup>4</sup>, Waldo Medinaceli<sup>5</sup>**

<sup>1</sup> Univ. Grenoble Alpes, IGE, IRD, CNRS, Grenoble-INP \*, 38000 Grenoble, France

<sup>2</sup> Ministerio de Educación Estado Plurinacional de Bolivia (Ministry of Education), La Paz, Bolivia

<sup>3</sup> Department of Earth and Environmental Sciences, University of Pavia, via Ferrata 1, 27100 Pavia, Italy

<sup>4</sup> University Mayor of San Andrés (UMSA), La Paz, Bolivia

<sup>5</sup> Ministerio de Medio Ambiente y Agua (Ministry of Water and Environment of Bolivia), La Paz, Bolivia

\* Institute of Engineering Univ. Grenoble Alpes

<sup>a</sup>gpfloresaviles@gmail.com

### 1. Introduction

One of the environmental effects and conditions associated to groundwater moving in gravity-driven flow sedimentary basins (Tóth, 2010), is chemistry, mineralogy (Tóth, 1995; Tóth, 1999) and isotopic compositions. The relatively high hydraulic heads in recharge areas represent a water source of high quality, whereas the low hydraulic heads in the throughflow and discharge areas (Tóth, 1962; Tóth, 1963; Tóth, 1995; Zhou et al., 2011) make this zones more vulnerable to degradation (Pilla et al., 2005).

Prior investigations around the world have demonstrated typical hydrochemical and isotopic patterns occurring in gravity-driven groundwater flow systems (Pilla et al., 2005; Mahlknecht et al., 2006; Tóth, 2010; Zhai et al., 2012). For instance, in the semi-arid Independence basin, in Mexico, groundwater from the main siliciclastic aquifer showed Ca-HCO<sub>3</sub> facies in the recharge areas, evolving to Na-HCO<sub>3</sub> facies along the groundwater flow system, towards the discharge areas (Mahlknecht et al., 2006). The same hydrochemical pattern was evidenced in the Quaternary aquifer system of Beijing Plain in China (Zhai et al., 2012). Groundwater presenting low mineralization in areas with high hydraulic heads were evidenced in the Po plain aquifer system, in Italy. In the same aquifer, the lowland areas characterized by a higher mineralization and more prone to contamination due to the shallower water tables (Pilla et al., 2005).

In Bolivia, in the Katari and Lago Menor Basin, one of the most populated and depressed basins of the semi-arid Bolivian Altiplano (BID, 2016; Agramont et al., 2019), prior research has thoroughly investigated the current degradation of surface

water quality of the rivers from the basin that discharge into the shallower Lake Titicaca (Lake Huiñamarca) (Fonturbel, 2005; Lazzaro et al., 2016; Guédron et al., 2017; Archundia et al., 2017a,2017b; Acha et al., 2018). However, little is known about the potential influence of sewage, waste disposal, farmland and mining activities into groundwater resources of the basin (MMAyA, 2016, Quino et al., 2019).

The use of mineral fertilizers, domestic sewage discharges, animal manure application to land, are among the anthropogenic activities that can greatly enrich  $NO_3^-$ , which is naturally present in groundwater at moderate concentrations of c.a 10 mg L<sup>-1</sup>. The analysis of N and O isotopic ratios of  $NO_3^-$  has been successfully applied in several surface water and groundwater studies around the world for providing detailed information of the sources and potential transformations of  $NO_3^-$  (i.e. Pauwels et al., 2000; Tang C et al., 2004; Sacchi et al., 2013; Delconte et al., 2014; Re et al., 2017; Martinelli et al., 2018; Spalding et al., 2019). Nevertheless, much less is known about the behaviour of nitrogen in groundwater-dominated watersheds in South America (Griffiths et al., 2015).

A regional geophysical characterization coupled with groundwater level measurements validated the occurrence of a gravity-driven groundwater flow system in the basin, named Lake Titicaca aquifer system (Flores-Avilés et al., 2019). The Quaternary porous geologic media that makes up Lake Titicaca aquifer system was identified as Piedmont and Lacustrine layers, both behaving hydraulically as “one aquifer”. Quaternary glaciation was responsible of the current geometry of Quaternary deposits in this aquifer. Glacial erosion of Silurian and Devonian rock formations in the high mountain ranges of the Eastern Cordillera and Lake expansion and evaporation processes in the lower areas (Ballivian, 1978; Lavenu, 1992; Argollo et al., 1995; Heine, 2004; Zech et al., 2007; Argollo et al., 2008).

Approximately 10% of the national Bolivian population (1 million of inhabitants) lives in this basin. Excluding to the city of El Alto, considered as a major industrial city (Hardy et al., 2015), around 65 percent of the population are dedicated to agricultural and livestock activities (M.M.A.y.A, 2015). As a consequence, the increasing demand of agricultural production due to population growth can result in a higher demand for the use of mineralised and organic fertilizers (FAO, 1999), leading to a suspension of the use of traditional application of manure to farmlands. On the other hand, most of

the population lack of adequate disposals of sewage and solid waste, instead each house has poorly constructed latrines. Therefore, agricultural, municipal and industrial wastewater, as well as the inadequate disposal of solid waste, could represent a major environmental threat to groundwater resources in the basin.

Assessing groundwater quality of Lake Titicaca aquifer system is necessary for distinguishing between natural mineralization processes (i.e. geology, water-rock interaction, residence time of groundwater) and anthropogenic impacts (e.g. ore extraction, urban and industrial pollution, agriculture). Determining the sources of groundwater contamination is an important step for the implementation of remediation measures aiming at improving groundwater quality. Furthermore, the correct understanding of hydrochemical evolution and isotopic compositions of groundwater in the basin can improve the current comprehension of Lake Titicaca eutrophication processes, seeing that many studies around the world have shown that contaminated and/or nutrient-rich groundwater entering lakes has led to lake pollution and/or eutrophication (Shaw et al. 1990; Robertson et al. 2005; Özen et al. 2010).

Although previous investigation on the site showed local hydrogeological characterizations based on lithology, groundwater level measurements, hydrochemistry and stable isotopes of deuterium and oxygen 18 (MMAyA, 2016; Quino et al., 2019). A research about a regional hydrochemical characterization, the determination of nitrate origin and dynamics in groundwater of Lake Titicaca aquifer system had been never presented before.

This paper aims to trace natural background levels and nitrate contamination in this basin-scale gravity-driven aquifer system, from the high Piedmont areas to the Lacustrine plain, by the application of hydrochemistry and dual isotopes  $\delta^{15}N_{NO_3}$  and  $\delta^{18}O_{NO_3}$ , considering the previous hydrogeological knowledge.

The main objectives are to:

- i) Distinguish between natural mineralization processes (i.e. geology, water-rock interaction, residence time of groundwater) and anthropogenic impacts (e.g. ore extraction, urban pollution, agriculture) from the Piedmont to the Lacustrine plain.

- ii) Understand the behaviour of nitrates in groundwater, from the recharge zones, along the groundwater flow system and towards the discharge areas.
- iii) Identify, localize and quantify the processes of nitrate attenuation processes in the groundwater flow system
- iv) Identify the potential sources of contamination.

The results of this investigation will indicate the natural backgrounds of groundwater quality and evaluate if groundwater resources are threatened by agricultural leaching, livestock production and/or by domestic wastewater. Moreover, the particular high-altitude hydrogeological environment of this basin-scale gravity-driven aquifer system, may allow the depiction of hydrochemical evolution and denitrification processes, along the groundwater flowsystem.

## *2.Site description*

### *2.1 Geography and climate*

The study site is located within the Katari and Lago Menor Basin, in the semi-arid region of the Bolivian Altiplano. The Katari and Lago Menor Basin is a high altitude sedimentary basin with an approximate area of  $6,350 \text{ Km}^2$ . It is bounded by the high mountains of the Eastern Cordillera, the southeast of Lake Titicaca (Lake Huiñamarca) and the outcropping rock formations towards the Tiwanaku, Comanche and Colquencha Cities (Figure 1). The climate in this basin is cold and semi-arid with a marked “wet season” (October- March) and “dry season” (April - September).

In the high peak glaciated areas of the Eastern Cordillera, air temperature oscillates from 1 to  $5^\circ\text{C}$ , with a total annual precipitation nearby  $750 \text{ mm} \cdot \text{year}^{-1}$  (Rabatel et al., 2006; Veettil et al., 2018), and sublimation and evaporation accounts for  $222 \text{ mm} \cdot \text{year}^{-1}$  (Kinouchi et al., 2013). Close to the shores of Lake Titicaca air temperature ranges from 7.7 to  $10.8^\circ\text{C}$  (Pillco et al., 2019), with a total annual precipitation varying from varies from 577 to  $750 \text{ mm} \cdot \text{year}^{-1}$  (Veettil et al., 2018; Kinouchi et al., 2019), and an annual Lake evaporation of  $1,700 \text{ mm year}^{-1}$  (Pillco et al., 2019).

The main municipalities which belong to the hydrogeological basin are: El Alto, the north of Viacha, south west of Batallas, Puerto Perez, Pucarani and the east of Laja. Excluding to the city of El Alto, a major industrial city (Hardy et al., 2015), around 65 percent of the population each municipality is dedicated to agricultural and livestock activities. They produce potatoes, barley, quinoa, wheat and raise bovine, ovine and camelid cattle and do not only use manure as fertilizers but as well urea and diamonium phosphate (MMAyA, 2015; FAO, 1999).

Most of the population in the basin has water access but lack of sanitary sewage systems; instead each house has poorly constructed latrines. About 70% of the Municipality of El Alto is connected to sanitary sewage systems (INE, 2015), and its waste water is treated in the water Puchukollo plant which discharges its treated waters into the Seco River (Archundia et al., 2017). Puchukollo has exceeded its capacity of collection and treatment facilities due to the accelerated increasing population size (MMAyA Environmental Audit, 2014; BID 2016). On the other hand, each municipality disposes their solid waste in open –air dumps (data available at <http://geosirh.riegobolivia.org>). There is a sanitary landfill (Villa Ingenio) located in El Alto city, in the middle upper part of the basin, which presents leachate and bottom sealing systems. According to Barroso et al. (2013) the Villa Ingenio landfill lies on a glacial till with low horizontal hydraulic conductivities ( $5.9 \times 10^{-8}$  m/sec ).

Most of the mining concessions are concentrated in the upper part of the basin (high mountain ranges), close to the Milluni lake (data available at <http://geosirh.riegobolivia.org>). Most of these mines present environmental liabilities which mainly consists of rock dumps and tailing dams without proper management (MMAyA Environmental Audit, 2014).

## *2.2 Geology and Hydrogeology*

The Katari and Lago Menor Basin consists of erosional landforms in Tertiary and Paleozoic rock formations that are filled up with Pleistocene to recent sediments. These erosional landforms are linked to the Quaternary glaciation.

Wet and cold conditions during the regional glacial advance (glacial cycles) and warm and dry conditions during the regional glacial retreat (interglacial cycles) (Fritz et al., 2007), are the main factors that favoured the formation of glacial and lacustrine

landforms between the high mountains of the Eastern Cordillera and the high-altitude Lake Titicaca region (Argollo et al., 2000; Cross et al., 2001; Abbott et al., 2003; Fritz et al., 2006; Fritz et al., 2007; Zech et al., 2007; Bush et al., 2010; Plackzec et al., 2011; Quesada et al., 2015).

A regional geophysical investigation coupled with groundwater level measurements validated the occurrence of an aquifer system in the basin, the Bolivian Lake Titicaca Aquifer System (Flores-Avilés et al., 2019). The results of this study showed two different hydrogeological settings: the Piedmont subsystem and Lacustrine plain. It also validated regional hydraulic continuity, the geometry and the bottom boundaries of Quaternary porous geologic media.

Thus, the aquifer system is comprised of: i) glacial and fluvioglacial outwash layers of ~200 m of thickness (above 4100 masl) in the upper Piedmont, ii) fluvioglacial and paleolacustrine layers, ranging from ~50 to 150 m of thickness, in the lower Piedmont (Fig.1), and iii) paleolacustrine layers of ~40-150 m thickness in the plain. In addition, a clay layer present primarily in the Lacustrine plain, behaves as a barrier for the infiltration of contaminants. It has a thickness of ~45 meters close to Lake Titicaca and decreases in thickness when far away from the Lake (Fig.1). Here on

Silicate minerals are predominantly in the matrix of glacial and fluvioglacial outwash layers. The Silurian sequence in the high mountain ranges encompasses the stratigraphically lowest Cancañiri formation, a poorly sorted dark-gray to green diamictite (glacial tillite), to the Uncia Formation composed of shales (~850-1200m thick) and the stratigraphically highest Catavi Formation, made of quartzite and shales (~500-800m thick). The latter is deformed by faults and folds which allowed mineralisation including some amounts of pyrite, arsenopyrite, cassiterite, siderite and chlorite. The Devonian Vila Vila Formation, comprises quartz sandstones and muscovite rich limolites (Sugaki et al., 1988; Salvaderry et al., 2007; Murray et al., 2010; Zeballos et al., 2017).

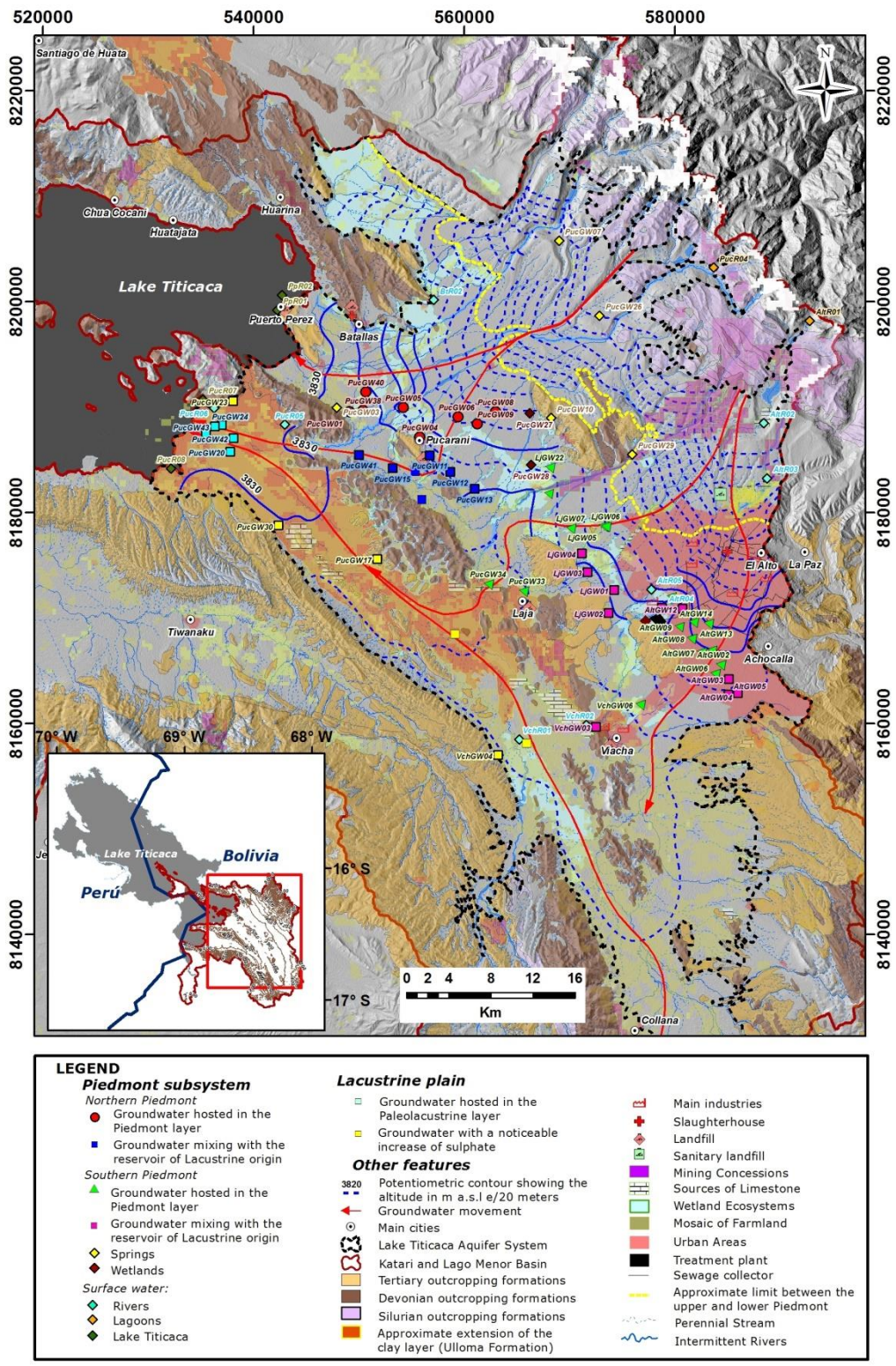


Figure 1. Location of the study area showing Lake Titicaca Aquifer System, regional groundwater movement, and samples retrieved in wells, springs, wetlands, rivers, lagoons and Lake). Each symbol represents samples located on the Piedmont subsystem or in the Lacustrine plain.

On the other hand, evaporites and silicate minerals compose dominantly paleolacustrine layers, originating from Tertiary and Devonian rock formations, currently outcropping in this plain. For instance, the Tertiary Kollu Kollu Formation is composed of evaporitic layers such as gypsum and limestone to the top, red shales and sandstones. Besides the Belen Formation, devonic in age is composed of siltstones, mudstones and fine-grained sandstones.

Regional groundwater flow in this aquifer follows the topographic NE to SW gradient on the Piedmont. It naturally discharges towards Lake Titicaca (Puerto Pérez Bays 1 and 2) in the northern side and flows out to springs when Quaternary deposits are disrupted (to the west of La Paz and Achocalla). In addition, a large part of the stock of groundwater is evaporated through wetlands located in the lower Piedmont area. These wetland ecosystems are associated to discharge areas of regional gravity-driven groundwater flow systems. Moreover, another amount of the groundwater stock reaches the western lacustrine plain, through deep subterranean channels, formed by the impervious barriers sometimes outcropping. Finally, in the lacustrine plain, groundwater flows follows the topographic SE to NW gradient, entering finally into Lake Titicaca (Cohana Bay).

### *3.Methods*

A total of 77 water samples, including groundwaters and surface waters, were collected during April and May of 2017, at the end of the wet season. Groundwater samples were collected from 52 deep wells (30–110 m b.g.l), mostly provided by electrical pumps, 5 springs and 2 wetlands, these last considered as natural discharge areas of Lake Titicaca aquifer system. Additional samples from surface water were collected from rivers (8), lagoons (3) in the upper part of the mountains and from the shore of Lake Titicaca (5). The sampling strategy was defined in accordance with the TDEM investigation (Flores Avilés et al., 2019) considering the spatial and vertical distribution of the main quaternary permeable formations and their connection regarding the Piedmont and Lacustrine subsystems.

Field measurements of pH, redox potential (Eh), electrical conductivity (EC), dissolved oxygen (DO) and temperature (T), were performed using a CONSORT C5010

multimeter. Total alkalinity was measured in the field by the titration method (HACH digital titration method) and recalculated as bicarbonate.

Samples for major elements were filtered in-situ using 0.45  $\mu\text{m}$  cellulose acetate siringe filters (millipore) and stored in pre-cleaned vials (burnt borosilicate vials). Filtrate samples used for anion quantification were frozen in unwashed falcon tubes while filtrate samples for cation measurements were acidified with ultrapure 2%  $\text{HNO}_3$  and stored at 4°C until analysis.

Chemical and isotopic analysis were performed at the IGE (Institut des Géosciences de l'Environnement) Laboratory. Major ion concentrations were measured by ion chromatography using Metrohm 732/733 modular system precision of  $\pm 0.1\text{mg/L}$  and calibrated using commercial reference solutions (Roth, 5 to 40  $\text{mg/L}$  range). Blanks consisted of ultrapure millipore water.

Samples for isotopic analysis ( $\delta^{15}\text{N}_{\text{NO}_3}$  and  $\delta^{18}\text{O}_{\text{NO}_3}$ ) were concentrated on an anionic resin (0.3mL AG 1-X8 resin, Bio-Rad) and eluted with 10 mL of a 1M NaCl solution (Bourgeois I et al., 2018). They were analyzed using the bacterial denitrifier method (Sigman et al., 2001; Kendall et al., 2007) and conducted on a MAT 253 IRMS Mass Spectrometer (Kaiser et al., 2007).

#### *4. Results and discussion*

##### *4.1 Hydrogeochemical characteristics of Lake Titicaca Aquifer System*

The Quaternary porous geologic media that makes up Lake Titicaca aquifer system are identified as Piedmont layers (glacial, fluvioglacial and alluvial deposits) and Lacustrine layers (paleolacustrine deposits), both behaving hydraulically as “single aquifer” (Flores-Avilés et al., 2019).

Generally, groundwater electrical conductivity ranges from 63 to 433  $\mu\text{S/cm}$  on the Piedmont and from 108 to 1700  $\mu\text{S/cm}$  in the Lacustrine plain (Table S1 of the Supplementary material SM). In addition, major ion concentrations on the Piedmont vary from 5 to 34  $\text{mg} \cdot \text{L}^{-1}$  for  $\text{Ca}^{2+}$ , 0.5 to 26  $\text{mg} \cdot \text{L}^{-1}$  for  $\text{Mg}^{2+}$ , 1.6 to 122  $\text{mg} \cdot \text{L}^{-1}$  for  $\text{Na}^+$ , 0.6 to 11.8  $\text{mg} \cdot \text{L}^{-1}$  for  $\text{K}^+$ , 8.5 to 143  $\text{mg} \cdot \text{L}^{-1}$  for  $\text{HCO}_3^-$ , 2 to 180  $\text{mg} \cdot \text{L}^{-1}$  for  $\text{SO}_4^{2-}$ , 0.1 to 177.5  $\text{mg} \cdot \text{L}^{-1}$  for  $\text{Cl}^-$  and 0.01 to 35.6  $\text{mg} \cdot \text{L}^{-1}$  for  $\text{NO}_3^-$ . Whereas

in the Lacustrine plain, ion concentrations range from 22.4 to 52  $mg \cdot L^{-1}$  for  $Ca^{2+}$ , 10.7 to 25  $mg \cdot L^{-1}$  for  $Mg^{2+}$ , 34 to 170  $mg \cdot L^{-1}$  for  $Na^+$ , 3.6 to 14.8  $mg \cdot L^{-1}$  for  $K^+$ , 37.4 to 416  $mg \cdot L^{-1}$  for  $HCO_3^-$ , 0.5 to 221.1  $mg \cdot L^{-1}$  for  $SO_4^{2-}$ , 18.7 to 409  $mg \cdot L^{-1}$  for  $Cl^-$  and 0.8 to 17.8  $mg \cdot L^{-1}$  for  $NO_3^-$  (Table S1, SM).

A piper diagram, plotted in rectangular coordinates (Fig.2) was used to point out the typical groundwater facies of Lake Titicaca aquifer system.

On the northern Piedmont, in the upper part, groundwater from springs show predominantly  $Ca(Mg) - HCO_3^-$  facies (PucGW26, PucGW10). A change in the anion's facies from  $HCO_3^-$  to  $SO_4^{2-}$  (PucGW07) suggest a local influence of environmental liabilities from inactive mines (yellow diamonds Fig. 1 and 2). Furthermore, in the lower Piedmont, groundwater present  $Ca(Mg) - HCO_3^-$  facies (EC~180  $\mu S/cm$ ) (red circles, Fig. 1 and 2). This typical facies may be attributed to the naturally occurring carbonate minerals in the matrix of the Quaternary Piedmont layers, that are related to fluvial-alluvial and glacial sedimentary environments. The enrichment trend of  $SO_4^{2-}$  could be attributed to seepage from influent rivers, as hydrochemical information from surface waters in lagoons close to the high peak glaciated areas (Fig.1) present  $Ca(Mg) - SO_4^{2-}$  facies with EC~150  $\mu S/cm$  (red diamonds, Figure 1 and 2).

In contrast, boreholes located in the flat areas of the Piedmont (blue squares) (~50 m b.g.l) show groundwater with bicarbonate dominance (EC~300  $\mu S/cm$ ) and a noticeable increase of  $Na(K)$  relative to  $Ca(Mg)$  (Fig.2). Indeed, groundwater circulating in the Piedmont layers enters into layers of paleolacustrine origin. Suggestively, groundwater with  $Ca(Mg) - HCO_3^-$  facies mix with the reservoir of lacustrine origin contact clay enriched in exchangeable  $Na^+$  originating from past evaporation sequences or mix with waters from such reservoirs. The expected  $Ca^{2+}$  versus  $Na^+$  cation exchange and/or mixing leads to the evolution from the  $Ca(Mg) - HCO_3^-$  to the  $Na(K) - HCO_3^-$  facies (Fig. 1, 2 red circles versus blue squares). These symbols do the level off from the cation exchange line in Figure 3, which suggest a predominance of cation exchange versus mixing processes (Re et al. 2017).

On the southern Piedmont, in the upper part, groundwater from springs (PucGW29) present high concentrations of sulphate (58  $mg \cdot L^{-1}$ ) even higher than in the northern zone (17  $mg \cdot L^{-1}$ ) (Table S1-SM). This indicates contributions from waters flowing

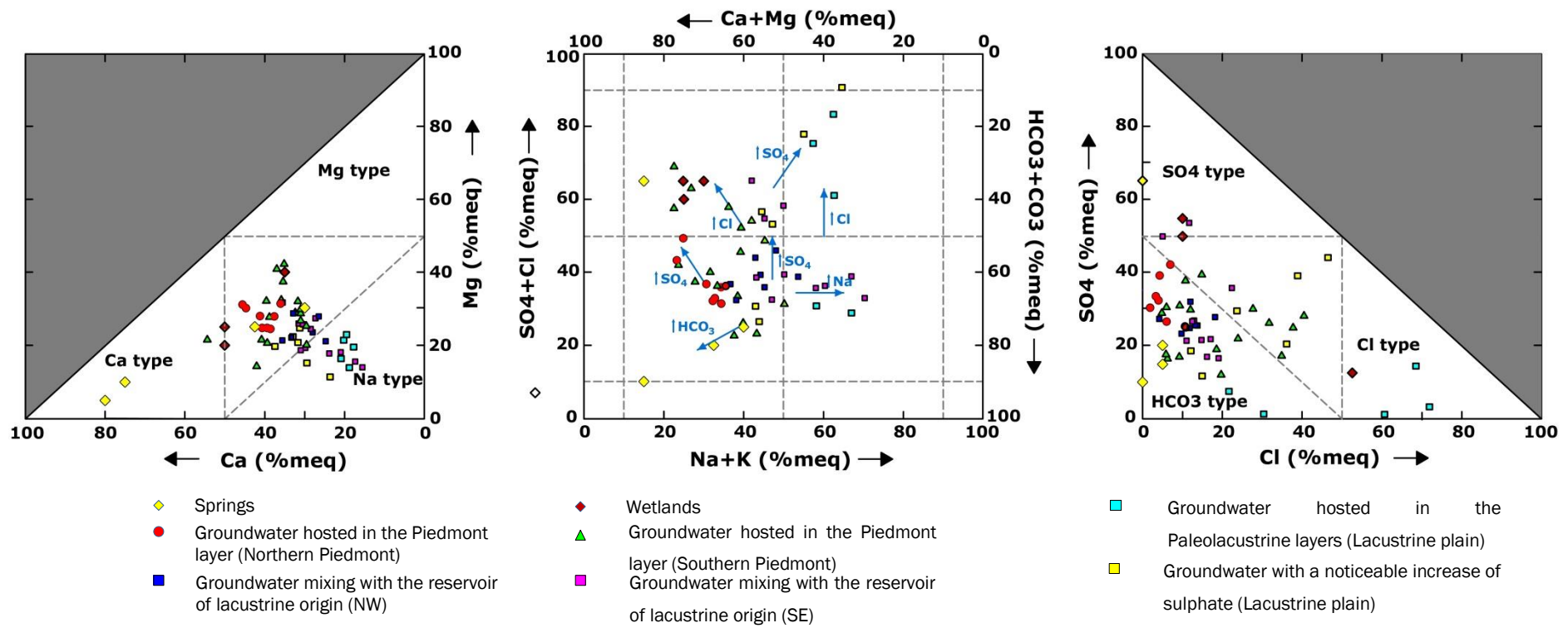


Figure 2. Piper diagram plotted in rectangular coordinates (Modif. After Ray and Mukherjee, 2008). Each symbol represents samples located in the Piedmont subsystem or Lacustrine plain.

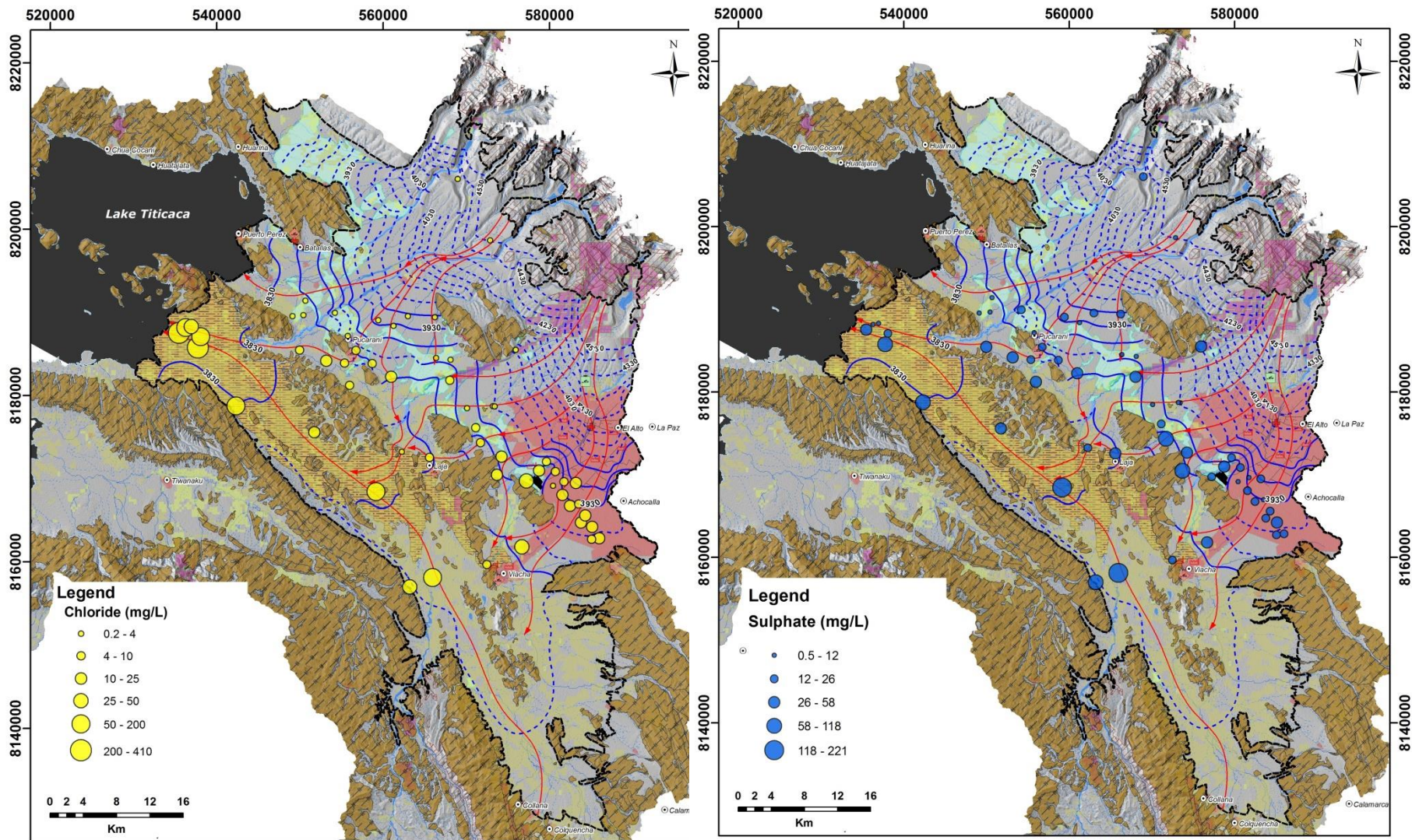


Figure 3. Maps showing chloride and sulphate spatial concentrations within the Katari and Lago Menor Basin aquifer from the Piedmont subsystem to the Lacustrine plain.

through rock dumps, galleries and tailing dams from mining activities, where insoluble sulphides from ores transform to soluble sulfate (Fig.1, 2 and 3).

In the lower sector of the southern Piedmont, we expect groundwater circulating in the Piedmont layers to have  $Ca(Mg) - HCO_3^-$  (EC~90-167  $\mu S/cm$ ) facies as in the northern zone. This facies is indeed attested for some of the waters sampled in these areas (some of the green diamonds, Fig. 1 and 2). These samples were all retrieved downstream the urbanized El Alto area. An enrichment trend of chloride is observed in several samples, it likely relates to anthropogenic contamination from the urbanization areas (Figure 3).

More downstream in this southern zone, similarly to the northern zone, a general increase of  $Na(K)$  relative to  $Ca(Mg)$ , suggest a  $Ca^{2+}$  versus  $Na^+$  cation exchange process in the Piedmont layers entering paleolacustrine layers (pink squares versus green triangles, Figures 1 and 2). The alignment of the points on the cation exchanger line in Figure 4 supports once more a predominance of a cation exchanger process over mixing processes. Mixing processes with other waters would not lead to waters of equal charge before and after mixing, which would result in a consequent levelling off of the cation exchanger line in Figure 4.

In the western Lacustrine plain, in the domain of the Ulloma clay formation (Fig.1) a shift from  $Ca(Mg) - HCO_3^-$  to  $Na(K) - SO_4^{2-}$  facies are evidenced in some samples located nearby the Tertiary sedimentary bedrock (yellow squares, Figures 1 and 2). Increasing trends of sulphate and bicarbonate are evidenced in some samples located nearby the Tertiary sedimentary bedrock (yellow squares, Figures 1 and 2). This could relate ancient processes that favoured the erosion of Tertiary Formations such as the Kollu-Kollu Formation (Tkk) which is composed of evaporitic layers to the top such as limestone and gypsum (Zeballos et al., 2017). In fact, Quino et al. (2019) reported the same hydrogeochemical pattern in groundwater samples located close to the Tkk Formation.

The cyan squares, originating from waters sampled bellow the Ulloma clay formation just before the entrance in Lake Titicaca (Figure 1) are for most of them highly enriched in  $Na(K) - Cl^-$  facies (EC~600-1700  $\mu S/cm$ ). These waters stand for the probable presence of evaporitic rocks related to ancient Paleolake expansion. Possibly the

impervious Ulloma formation in conjunction with the low water fluxes in that region (Flores-Avilés et al., 2019) ensures the presence of a salt stock and the associated enrichment of the groundwater up to date along specific flow lines.

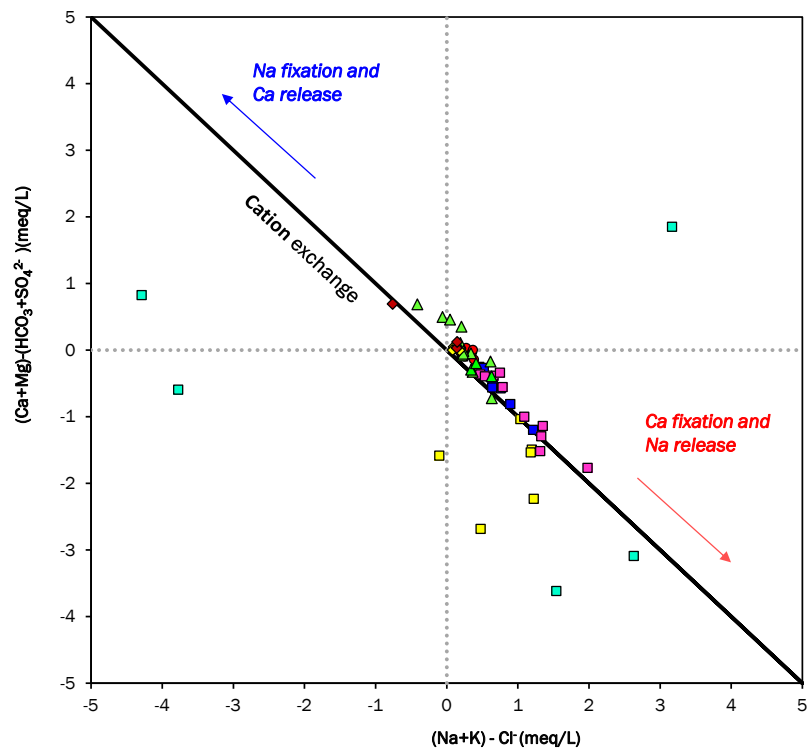
In fact for example when comparing sulphate versus chloride concentrations (Fig.3) groundwater in the Piedmont subsystem influenced by former mine sites show increased sulphate concentrations with no increase in chloride, while in the Lacustrine plain groundwater show both an increase in chloride and sulphate concentrations.

In summary, groundwater circulating in the Piedmont layers present  $Ca(Mg) - HCO_3^-$  facies in the high areas, reflecting the natural background composition of groundwater. Owing that besides the higher hydraulic heads in the recharge areas, the low horizontal hydraulic conductivities of glacial deposits ( $5.9 \times 10^{-8}$  m/sec) overlying fluvio-glacial deposits, may retard vertical flow and contaminants infiltration. Moreover, a noticeable enrichment trend of sulphate and chloride is evidenced downgradient, in the lower southern sector of the Piedmont. This could be related to anthropogenic contamination. Then, when groundwater mixes with the reservoir of lacustrine origin, it is transformed into  $Na(K) - HCO_3^-$  facies. Finally, groundwater in the Lacustrine plain, present predominantly  $Na(K) - Cl^-$  facies relating the presence of evaporites.

#### *4.2 Groundwater natural mineralization processes and anthropogenic impacts*

Saturation indexes for calcite, dolomite and gypsum versus electrical conductivity, displayed in Figure 5, were plotted in order to distinguish between natural mineralization processes and anthropogenic impacts. The saturation index zone representing equilibrium is  $\pm 0.4$  for calcite (5% of  $\log K_{\text{calcite}}$ ),  $\pm 0.85$  for dolomite (5% of  $\log K_{\text{dolomite}}$ ) and  $\pm 0.23$  for gypsum (5% of  $\log K_{\text{gypsum}}$ ).

In general, groundwater circulating in the Piedmont layers is undersaturated with respect to the carbonate minerals and gypsum. This suggests that groundwater may not have had sufficient time to equilibrate with these minerals, or for calcite, for which equilibration is rapid, that not enough solid carbonated rocks are present to reach saturation. Clear trends of increasing carbonate and gypsum saturation, from the higher to the lower areas of the Piedmont, are evident with an increasing electrical conductivity.



- |   |   |
|---|---|
| ◆ Springs   | ◆ Wetlands  |
| ● Groundwater hosted in the Piedmont layer (Northern Piedmont)        | ▲ Groundwater hosted in the Piedmont layer (Southern Piedmont)          |
| ■ Groundwater mixing with the reservoir of lacustrine origin (NW)     | ■ Groundwater mixing with the reservoir of lacustrine origin (SE)       |
| ■ Groundwater hosted in the Paleolacustrine layers (Lacustrine plain) | ■ Groundwater with a noticeable increase of sulphate (Lacustrine plain) |

Figure 4. Plot of  $(Ca + Mg) - (HCO_3 + SO_4^{2-})$  versus  $(Na+K)-Cl$ . The black line (negative slope -1:1) represents cation exchange. Each symbol represents samples located on the Piedmont subsystem or in the Lacustrine plain.

In addition, Figure S1 (SM) shows the molar ratios of  $Ca/Na$  vs  $HCO_3/Na$  as possible indicators of silicate versus carbonate weathering (Clark, 2015). Silicate weathering is dominant in groundwater circulating in the Piedmont layers, from the high areas (yellow and brown diamonds) towards the low areas (red circles and green triangles). In fact,  $Ca^{2+}/Na^+$  ratios are  $> 0.3 - 4$  and  $HCO_3^-/Na^+ \sim 1 - 3$  (Figure S1-SM). Moreover, when groundwater mix with the reservoir of Lacustrine origin (blue and pink squares), a decrease  $Ca^{2+}/Na^+$  ratios from (0.3 to 0.1) is evidenced. The excess of sodium

following the same pattern as evaporites suggest both silicate weathering and evaporites dissolution.

In the Lacustrine plain (EC~600-1700  $\mu S/cm$ ), groundwater is in equilibrium with respect to carbonate minerals (Fig.5). This confirms the presence of both minerals in the paleolacustrine matrix and that ancient Lake invasion favoured weathering processes of the Tertiary sedimentary bedrock rich in limestone. Moreover, groundwater is undersaturated with respect to gypsum suggesting that it haven't had enough time to equilibrate with respect to gypsum.

In regards with Figure S1 (SM), the presence of evaporite minerals is evidenced with the molar ratios of  $Ca^{2+}/Na^{+} \sim 0.1 - 0.3$  and  $HCO_3^{-}/Na^{+} \sim 0.15 - 0.4$ . In fact, evaporation processes occurring during those paleoclimatic -warm and dry conditions of regional glacial retreat (Fritz et al., 2007) may be responsible for the presence of evaporites in lacustrine layers. However, we believe that the impact of those evaporation processes that led to Lake paleo-salinity of 60-90g/L and influenced aquifers in the Central Altiplano (Coudrain et al., 1995) were not that higher as in the Northern Altiplano (Coudrain et al., 1995) because of presence of the Ulloma Formation (Qull), a clayey deposit resulting of Paleolake Ballivian invasion (Lavenu, 1992; Zeballos et al., 2017; Flores-Avilés et al., 2019).

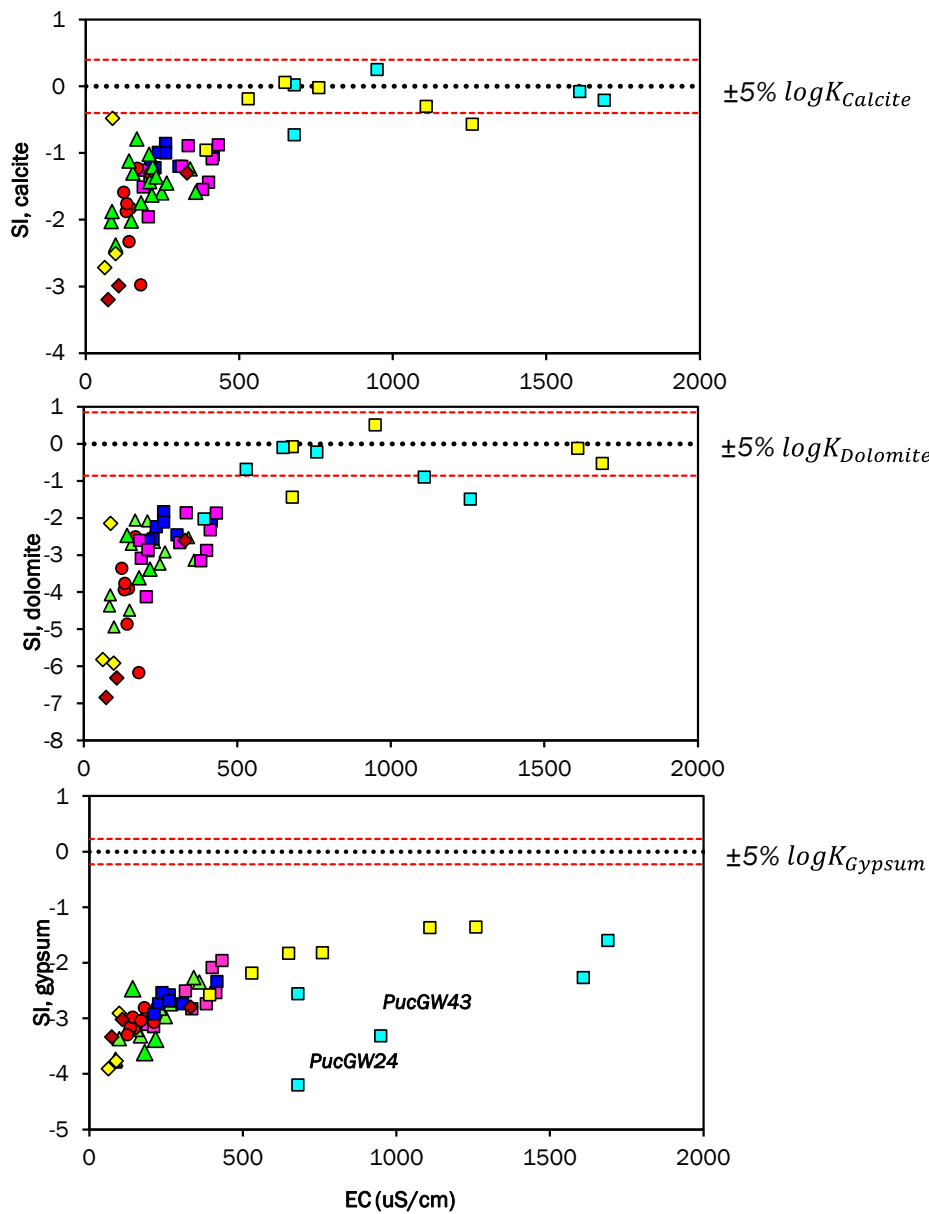


Figure 5. Plots of Saturation indexes vs electrical conductivity a) Saturation index for Calcite versus EC, b) Saturation index for Dolomite versus EC and c) Saturation index for Gypsum versus EC, in groundwater of Lake Titicaca Aquifer System. Each symbol represents samples located on the Piedmont subsystem or in the Lacustrine plain.

### *4.3 Nitrate Contamination along the groundwater flow system*

In order to investigate the behaviour of nitrate in groundwater of Lake Titicaca aquifer system, nitrate and chloride concentrations, along the groundwater flow systems of the Piedmont and Lacustrine plain (Fig.1, 6, 7, 8 and 9), were obtained by plotting their concentration with altitude depth of wells (m a.s.l – meters above sea level) and distance (m-meters) from the maximum high boundary of the aquifer (Flores-Avilés et al., 2019). In addition, the regional geophysical characterization allowed to plot the approximate thickness of Piedmont layers and Lacustrine layers displayed in Figures 7, 8 and 9.

Generally, groundwater in the Katari and Lago Menor Basin aquifer present nitrate concentrations that do not exceed the drinking water limit recommended by the World Health Organization (WHO) 50 mg/L (Table S1, SM). For instance, Figure 6 compares nitrate and chloride concentrations from the Piedmont subsystem to the Lacustrine plain. Groundwater in the Piedmont subsystem influenced by nitrate contaminated sites show also an increase in chloride concentrations, while groundwater in the Lacustrine plain present a decrease in nitrate concentrations.

In the upper part of the Piedmont subsystem, groundwater circulating through the Piedmont layers presents very low concentrations of chloride and nitrate (Fig.7 and 8). In fact,  $[Cl^-]$  range from 0.2 to 1.5 mg/L and  $[NO_3^-]$  from 1.2 to 2.9 mg/L. These concentrations can be considered as the initial compositions of groundwater regarding that very low mineralization rates suggested natural backgrounds of groundwater. However, an increase of both concentrations could be evidenced in the lower sectors of the Piedmont suggesting a direct influence from the urbanization and other anthropogenic activities (Fig.1).

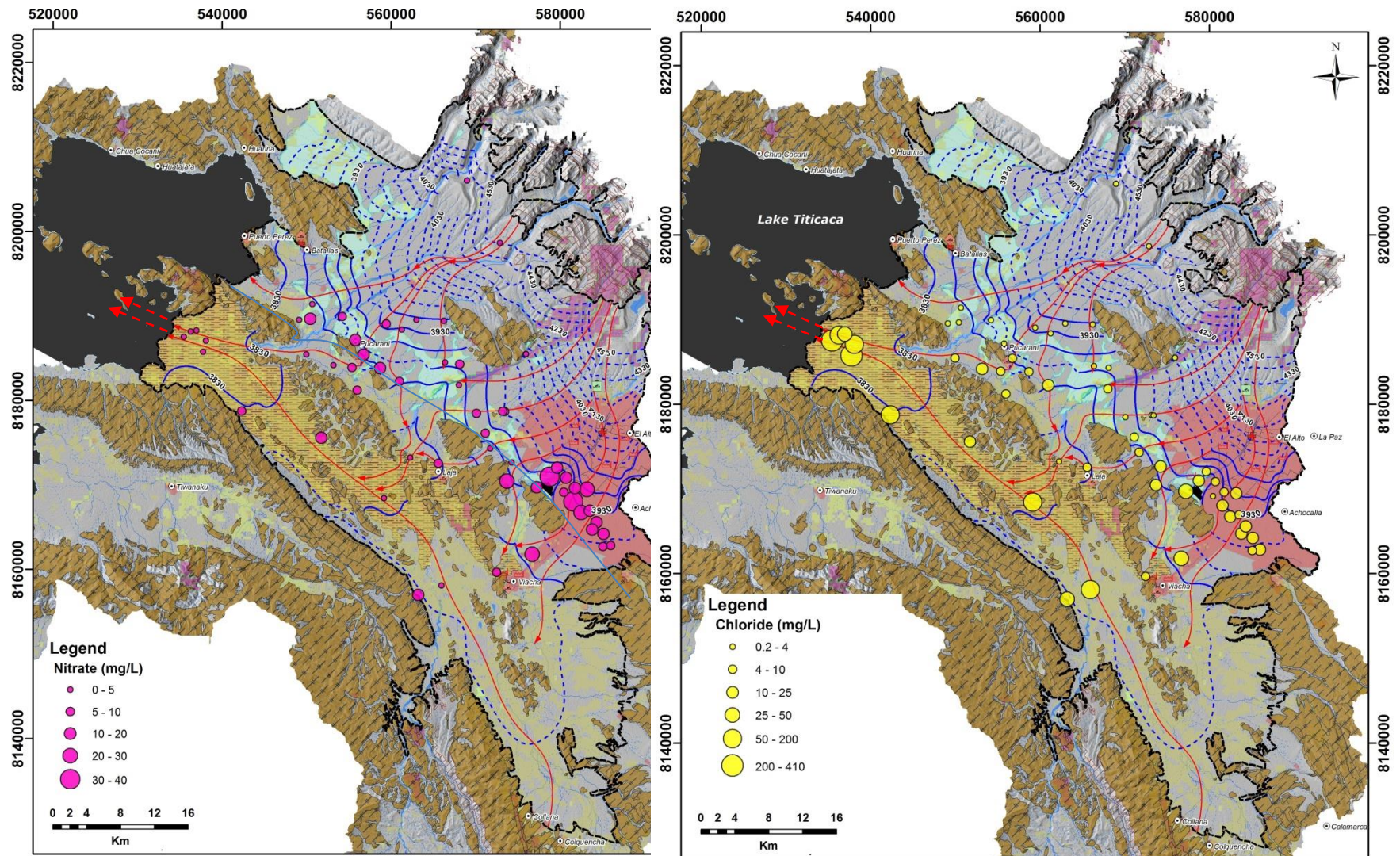


Figure 6. Maps showing spatial concentrations of nitrate and chloride from the Piedmont subsystem to the Lacustrine plain.

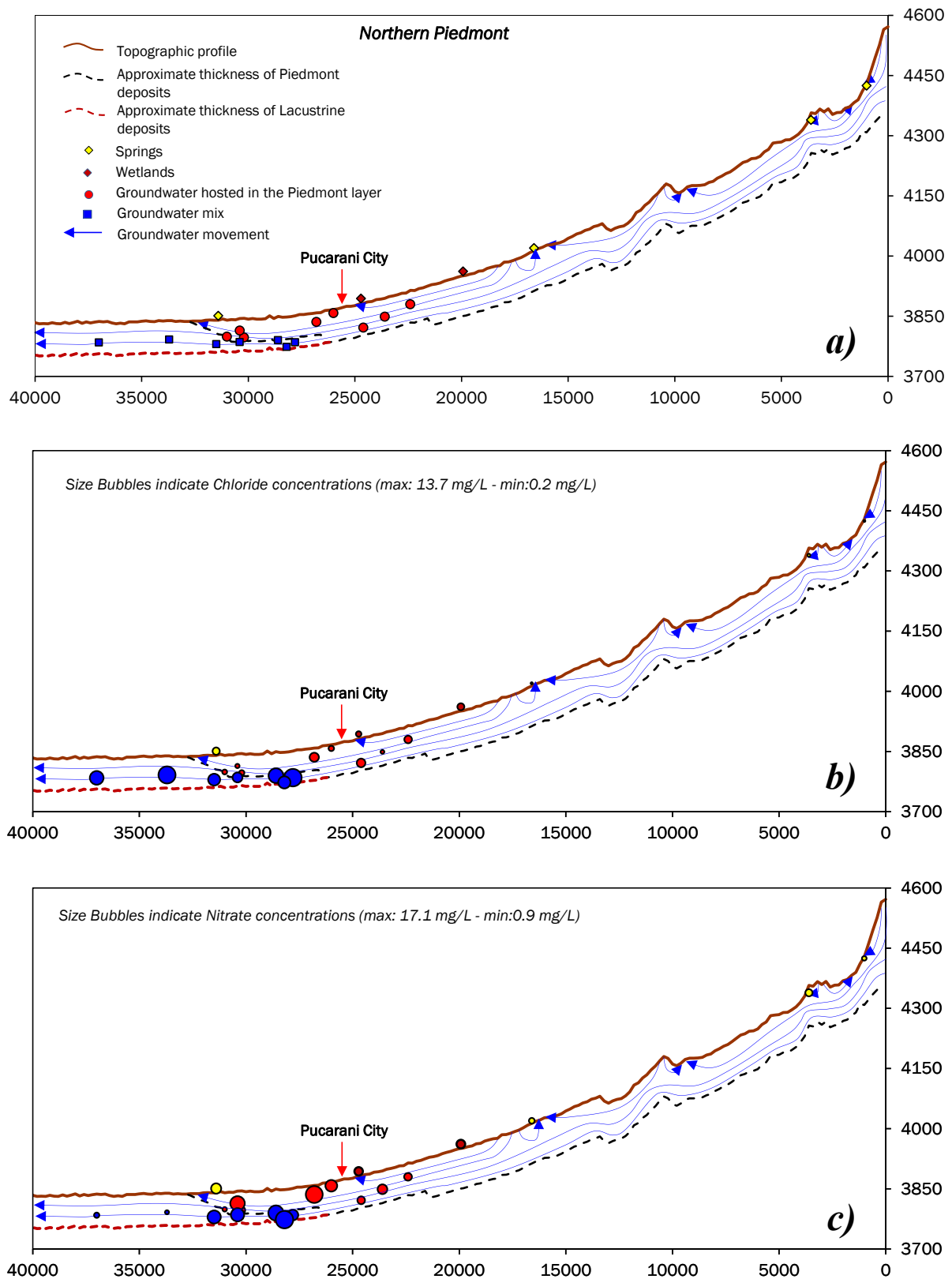


Figure 7. Plots of altitude (masl) versus distance (km) along groundwater flow systems in Piedmont Subsystem (Northern Piedmont). The different sizes of the bubbles represent the concentrations of a) location symbols to identify in Fig.1, b)  $\text{NO}_3$  and c) Cl. Plots also depicts the topographic altitude, depth of wells and approximate thickness of Piedmont and Lacustrine layers.

Towards the northern zone, the increase of  $[\text{Cl}^-]$  oscillates between 0.7 to 3.7 mg/L (Fig.5b) and that of  $[\text{NO}_3^-]$  from 1.0 to 15.6 mg/L (Fig.7c). Moreover, when groundwater mixes with the reservoir of Lacustrine origin (blue squares, Fig.7a), an increase of chloride concentrations is evidenced (4.5 to 13.7 mg/L) whereas nitrate concentrations decrease from 12.9 to 1.6 mg/L (Fig.7c). Although the higher concentrations of chloride in this zone are mostly attributed to the matrix of the Paleolacustrine layers, the influence of contaminated groundwater might also have influenced in the final composition of groundwater.

In the case of the southern zone, the increase of  $[\text{Cl}^-]$  oscillates between 5.8 to 49.2 mg/L (Fig.6b) and that of  $[\text{NO}_3^-]$  from 3.5 to 35.6 mg/L (Fig.8c). Initial compositions of groundwater could still be evidenced in some intermediary flow systems (Fig.8b and 8c). The final compositions of chloride and nitrate concentrations in these downgradient wells, evidence the high influence of El Alto urbanization. Then, when groundwater mixes with the reservoir of Lacustrine origin (pink squares, Fig. 8a), chloride concentrations range between 6.1 to 24.8 mg/L while  $[\text{NO}_3^-]$  tend to decrease from 31.3 to 6.9 mg/L (Fig.7c). Similarly to the northern zone, besides that higher concentrations of chloride are mostly attributed to the matrix of the Paleolacustrine layers, the influence of contaminated groundwater also may influence in the final composition of groundwater.

Hydrochemical evolution of groundwater circulating in the Piedmont subsystem reflects that anthropogenic activities from the southern zone influence in the final compositions of groundwater in the lower sector of the Piedmont, in a higher magnitude than in the northern zone.

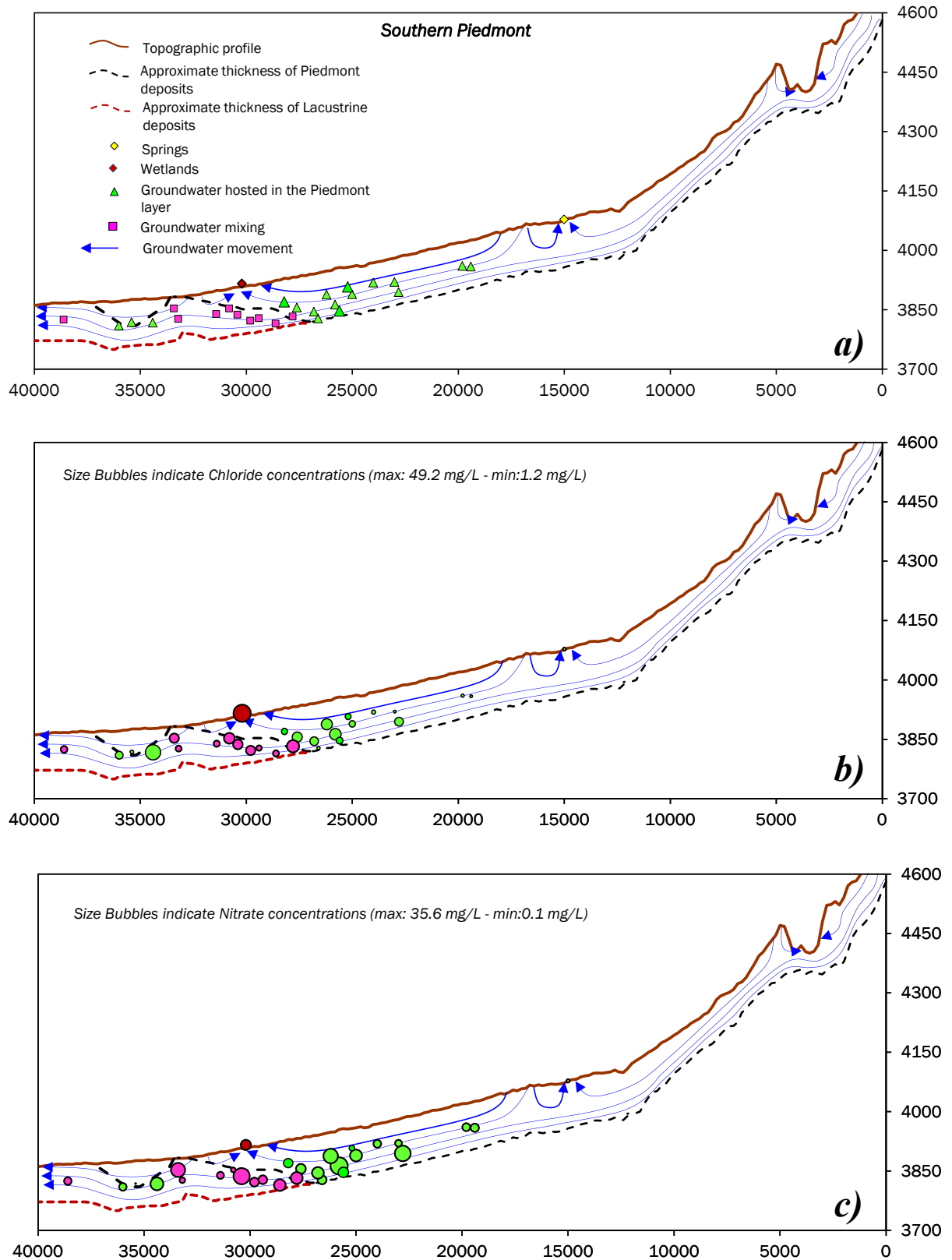


Figure 8. Plots of altitude (masl) versus distance (km) along groundwater flow systems in Piedmont Subsystem (Southern Piedmont). The different sizes of the bubbles represent the concentrations of a) location symbols to identify in Fig.1, b)  $\text{NO}_3$  and c)  $\text{Cl}$ . Plots also depicts the topographic altitude, depth of wells and approximate thickness of Piedmont and Lacustrine layers.

Finally, in the Lacustrine plain  $[Cl^-]$  oscillates between 18.7 to 409 mg/L (Fig. 9b). Lower values of chloride are evidenced in places where the clay layer is absent or in places where subterranean channels are evidenced, allowing groundwater mixing from the Piedmont subsystem (Fig.1). In addition, lower concentrations of chloride relate higher concentrations of sulphate suggesting other type of hydrochemical processes that might be influencing the solubility of gypsum evaporites (yellow squares). In addition  $[NO_3^-]$  oscillating between 0.8 to 17.8 mg/L show a decrease pattern when the clay layer is absent (Fig.9c). Moreover, punctual increases and decreases relate the connection with the Piedmont subsystem.

#### *4.4 Identification of potential nitrate sources and processes*

The objective of this section is to integrate geochemistry and nitrogen isotopes in order to identify the potential nitrate sources and processes occurring in Lake Titicaca aquifer system. Figures 10 displays dual isotope plots ( $\delta^{15}N_{NO_3}$  versus  $\delta^{18}O_{NO_3}$ ) for identifying the main sources of nitrate contamination in the aquifer system and the possible processes such as nitrification and denitrification that could modify groundwater nitrate concentrations.

Ranges of nitrification displayed in Fig.10 were controlled on stable isotopic compositions of oxygen 18. In fact,  $\delta^{18}O_{H_2O}$  compositions of groundwater from the lower sector of the southern Piedmont (MMAyA, 2016) range between (ca.  $-13.5\text{‰}$  to  $-17.3\text{‰}$ , Fig. S2-SM). The  $\delta^{18}O_{NO_3}$  value of the newly formed  $NO_3^-$  can be calculated from the experimental expression (Kendall et al., 2007):

$$\delta^{18}O_{NO_3} = \frac{2}{3}(\delta^{18}O_{H_2O}) + \frac{1}{3}(\delta^{18}O_{O_2})$$

Where  $\delta^{18}O_{H_2O}$  was assumed to be that of the Southern Piedmont groundwater (ca.  $-13.5\text{‰}$  to  $-17.3\text{‰}$ ) and  $\delta^{18}O_{O_2}$  was assumed to be that of atmospheric  $O_2$  (ca.  $+23.5\text{‰}$ ).

Therefore, the expected  $\delta^{18}O_{NO_3}$  values in local groundwater typical for nitrate derived for nitrification would be around  $-1.2\text{‰}$  to  $-3.7\text{‰}$ . These values were observed in many samples of the lower sector of the southern Piedmont (Table S1-SM), indicating

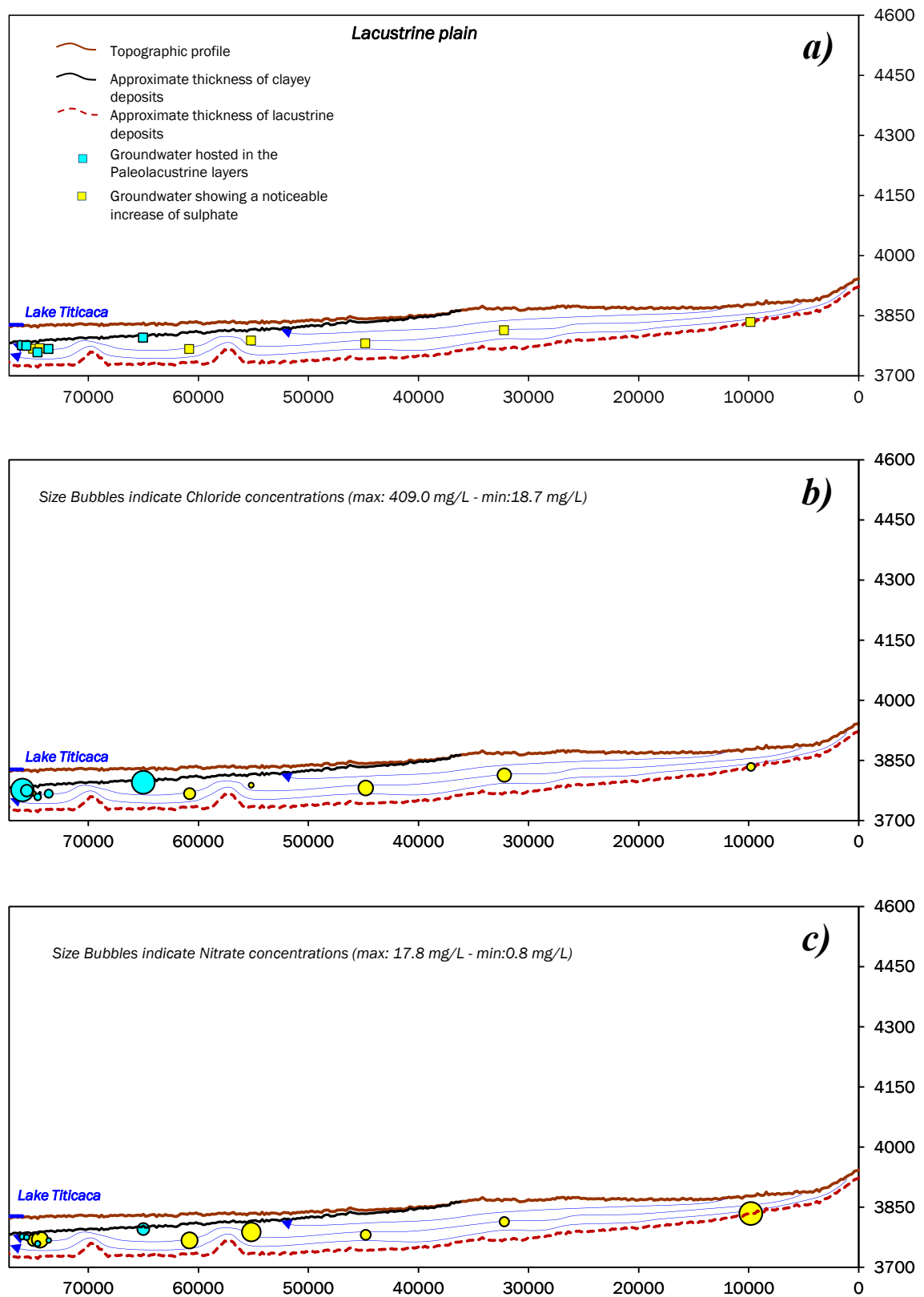


Figure 9. Plots of altitude (masl) versus distance (km) along groundwater flow systems in the Lacustrine plain. The different sizes of the bubbles represent the concentrations of a) location symbols to identify in Fig.1, b)  $\text{NO}_3$  and c) Cl. Plots also depicts the topographic altitude, depth of wells and approximate thickness of Lacustrine layers.

that groundwater nitrate was derived from nitrification of organic soil, manure and denitrification was not possible due to aerobic conditions.

In the Piedmont subsystem, towards the northern zone, groundwater present  $\delta^{15}N_{NO_3}$  values ranging between 0.4 ‰ and 28.6 ‰ while  $\delta^{18}O_{NO_3}$  isotopic compositions range between -6.9 ‰ and 15.5 ‰ (Table S1-SM; Fig.10 a, d; Fig.11). The main sources of nitrate contamination could be attributed to agriculture activities such as the use of manure and sometimes of mineralised and synthetic fertilizers (FAO, 1999).

The use of synthetic fertilizers could be evidenced in Fig. 10d; Fig.11, showing in some cases groundwater with an evolution pattern of nitrification. Indeed,  $\delta^{15}N_{NO_3}$  values ranging between +2 and +8.5 ‰ suggest a mixture of manure and fertilizers. Additional point sources of contamination could be due to the lack of sanitary sewage systems (use of latrines) and open landfills as evidenced close to the City of Pucarani (Fig.1).

In addition, Figure 12a displays the isotopic compositions of  $\delta^{15}O_{NO_3}$  along groundwater flow systems as a function of the depth well altitude (m a.s.l) and distance (meters). In fact, groundwater circulating through the northern Piedmont layers, that appears to be not influenced by any nitrate source, present isotopic compositions around 4.1 to 4.7 ‰. Moreover, groundwater flowing immediately after the City of Pucarani present high concentrations of nitrate (Fig. 7c) but this concentrations are reduced at a distance of 33km suggesting denitrification processes. This process is verified with the dual isotopes of nitrogen, showing enriched values of  $\delta^{15}N_{NO_3}$  from +7 to +28‰ (Fig.12a). Besides, the coupled analysis of  $\delta^{15}N_{NO_3}$  and  $\delta^{18}O_{NO_3}$  along a groundwater representative flow system in the northern lower Piedmont areas, evidenced denitrification processes with a slope of 0.9 (1.1 : 1). Denitrification processes in this area might be originated from the use of manure for agriculture activities and septic waste coming from the city of Pucarani.

Indeed, prior research around the world generally confirms that low concentrations of nitrate in groundwater is associated with high  $\delta^{18}O_{NO_3}$  and  $\delta^{15}O_{NO_3}$  with denitrification slopes ranging from 0.5 to ca. 0.7 (Kendall et al., 2007; Pauwels et al., 2010).

Moreover, deviations from a coupled 1:1 pattern of  $\delta^{15}O_{NO_3}$  and  $\delta^{18}O_{NO_3}$  suggest the influence of additional processes such as nitrification or mixing (Sacchi et al., 2013).

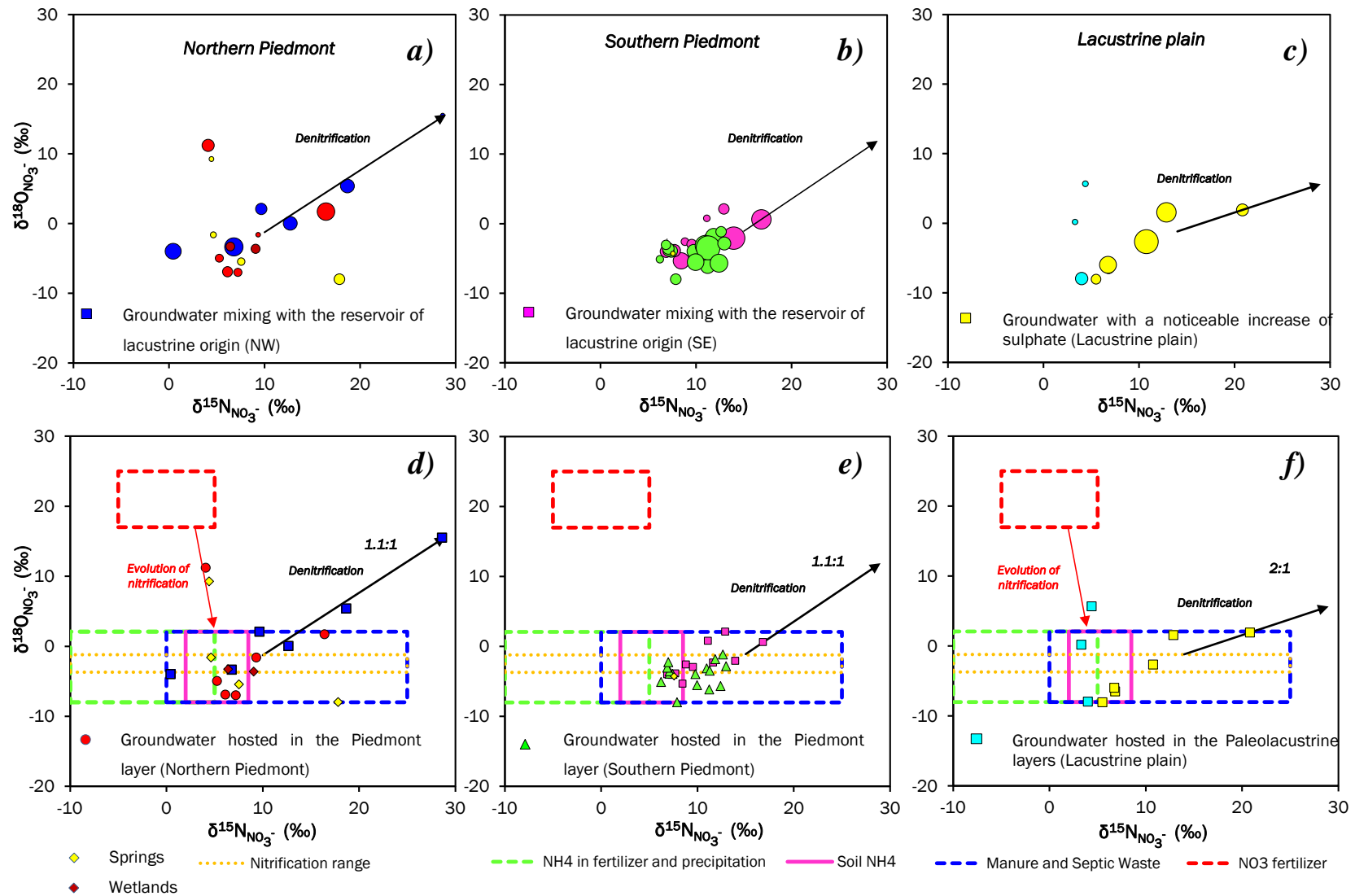


Figure 10. Biplots of  $\delta^{15}\text{N}_{\text{NO}_3^-}$  and  $\delta^{18}\text{O}_{\text{NO}_3^-}$  isotopic compositions (modified after Kendall et al., 2007) in the a), d) Northern Piedmont, b), e) Southern Piedmont and c), f) Lacustrine plain. Bubbles in plots a, b and c represent the  $\text{NO}_3^-$  concentrations

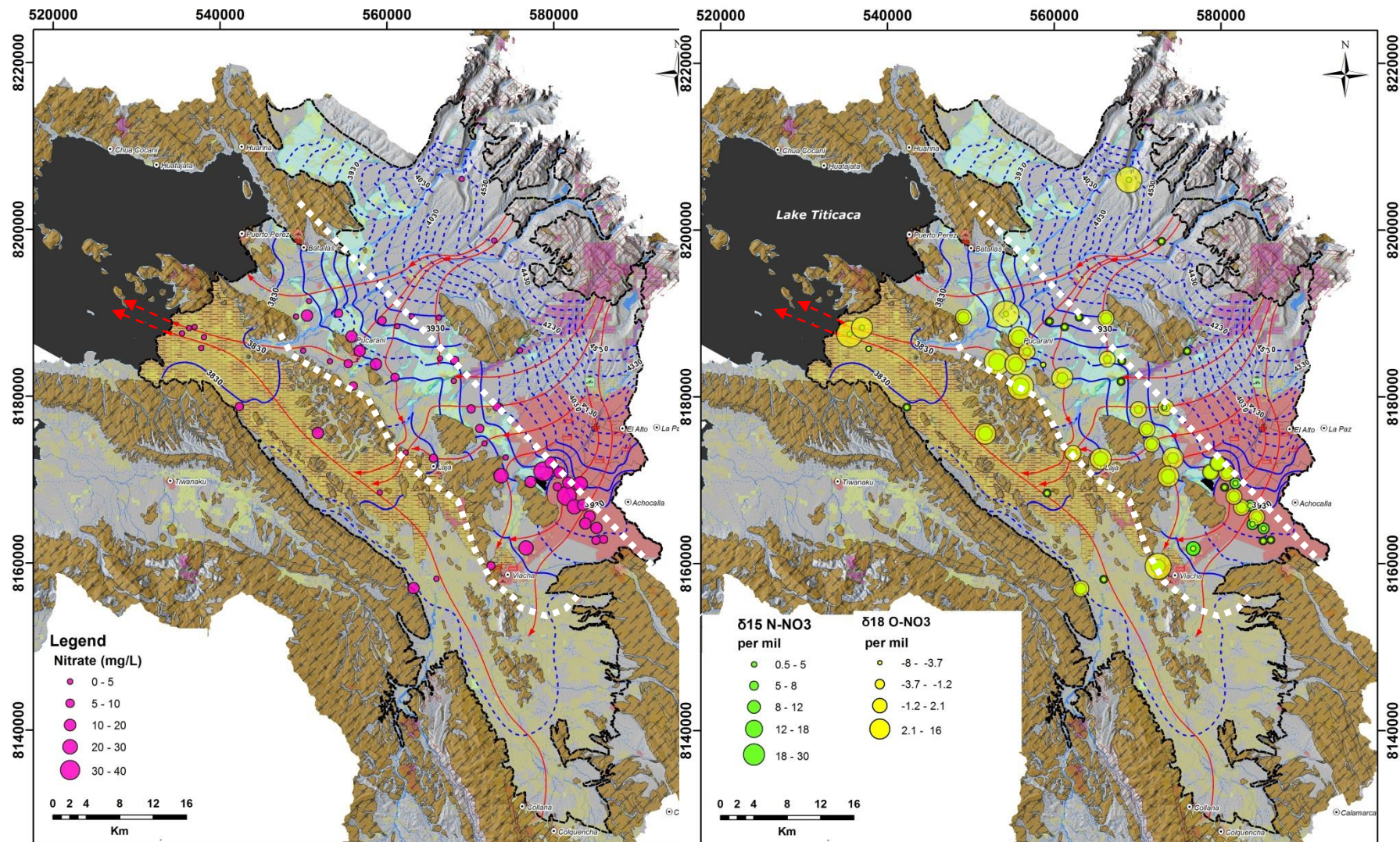


Figure 11. Maps showing spatial concentrations of nitrate and dual isotopes of nitrogen 15 and oxygen 18. Zones delimited by the white lines show areas of natural attenuation processes.

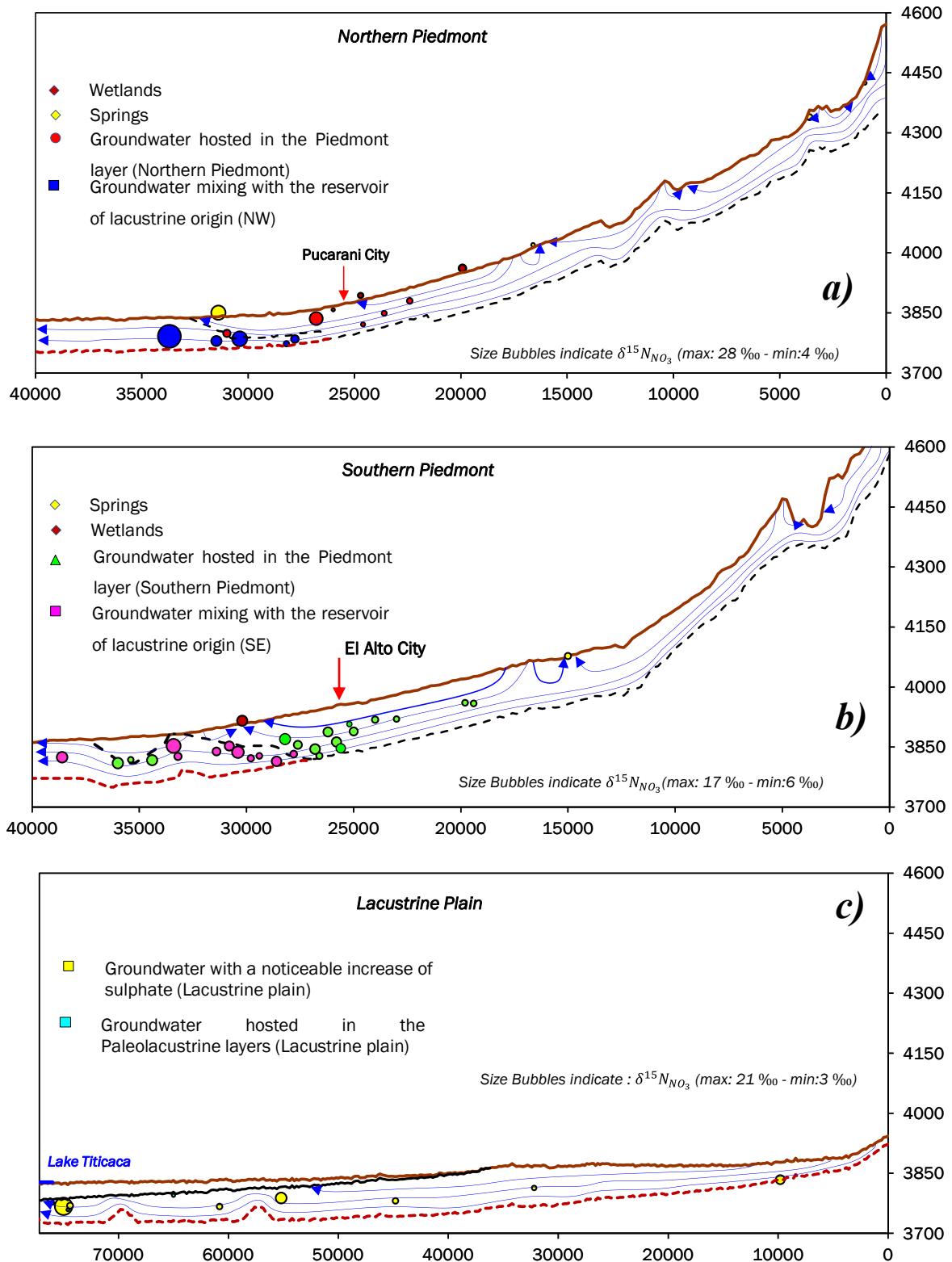


Figure 12. Plots of altitude (m a.s.l) versus distance (km) along groundwater flow systems in the a) Southern Piedmont, b) Northern Piedmont and c) Lacustrine plain. The bubbles represent the isotopic compositions of  $\delta^{15}N_{NO_3}$ . Plots also depicts the topographic altitude and depth of wells.

On the other hand, groundwater circulating through the southern Piedmont layers, present isotopic compositions of  $\delta^{15}N_{NO_3}$  ranging from +6 ‰ and +17 ‰ while the  $\delta^{18}O_{NO_3}$  oscillates between -7.9 ‰ and +16.8 ‰ (Table S1-SM; Fig.10 b, e). Figure 10e suggests that septic waste water and manure could be a dominant source of contamination in this area. This is coherent due to its proximity to the City of El Alto. In fact, many problems related to urban contamination had been reported in the City of El Alto, the second largest city of Bolivia (Archundia et al., 2017).

Similarly to the northern Piedmont, groundwater  $\delta^{15}N_{NO_3}$  isotopic compositions were plotted as a function of well depth altitude (m a.s.l) and distance (meters) along groundwater flow systems (Fig.12b). In fact, groundwater circulating through the southern Piedmont layers present a slight enrichment from -6 ‰ to +13 ‰. However, when groundwater mixes with the reservoir of lacustrine origin, a clear enrichment pattern from -8 ‰ to 18 ‰ is evidenced in the lower sector of the southern Piedmont (Fig.9b). This higher  $\delta^{15}N_{NO_3}$  isotopic compositions associated with the low concentrations of nitrate presented in Fig. 6c, reflect denitrification process.

The dual isotopes of  $\delta^{18}O_{NO_3}$  versus  $\delta^{15}O_{NO_3}$  were also analyzed along different flow systems (local, intermediate or regional) identified in the southern Piedmont. In fact denitrification process with a coupled 1.1:1 (slope=0.9) was evidenced along a representative flow system. Denitrification process in this area might be originated mainly from sewage septic inputs as shown in Fig. 10e.

In summary, groundwater circulating through the Piedmont layers, present natural backgrounds of nitrate in the topographic highs. Whereas downgradient groundwater is clearly influenced by nitrogen sources. This is evidenced especially after groundwater flows below the urbanization areas and farmlands (Pucarani and El Alto Cities). Afterwards, when groundwater mixes with the reservoir of lacustrine origin, nitrate concentrations are reduced. This could be attributed to the topographic lows of the Piedmont subsystem, where groundwater discharges to wetlands. Water in this areas might present high concentrations of dissolved mineral and organic matter which could enhance biogeochemical processes that controls nitrate attenuation (Rivett et al., 2008).

Finally, groundwater flowing through the Paleolacustrine layers (lacustrine plain) show  $\delta^{15}N_{NO_3}$  values between 4.0 ‰ and 20.8 ‰ while the  $\delta^{18}O_{NO_3}$  values are between

-8.0 ‰ and 5.6 ‰ (Table S1-SM; Fig.10c, f). Mainly agriculture activities (farmlands) are carried out in this area (Fig.1), so it is possible to expect the use of manure and also mineralised and/or synthetic fertilizers for agriculture activities.

In some cases, groundwater present a nitrification pattern of synthetic fertilizers (10f). Indeed, isotopic compositions of  $\delta^{15}N_{NO_3}$  ranging between +2 and +8.5 ‰ suggests a mixture of manure and fertilizers in groundwater, relating a seepage from Lake Titicaca to the groundwater system (cyan squares). And in another cases, the coupled  $\delta^{18}O_{NO_3}$  and  $\delta^{15}N_{NO_3}$  evidence that groundwater is prone to contamination (Fig.10f), especially when the clay layer is absent and in places where a connection to the Piedmont subsystem is evident (subterranean channels).

#### *4.6 Identification of possible mixing patterns*

Mixing process between  $NO_3^-$  -rich and poor- waters bring about a hyperbolic relation between  $\delta^{15}N_{NO_3}$  and nitrate concentrations, provided that the low concentration end-member is isotopically enriched (Pauwels et al., 2000). Distinguishing between mixing and denitrification processes is of vital importance, as denitrification processes can sometimes be confused with mixing of  $NO_3^-$  sources (Kendall et al., 2007). For this reason, Fig. 13 (a, b and c) display  $\delta^{15}N_{NO_3}$  versus  $1/[NO_3^-]$  plots, in order to identify possible mixing patterns in the aquifer system.

In the Piedmont subsystem, towards the northern zone, denitrification fractionation in groundwater is confirmed yielding a curve showing an enrichment factor of  $\epsilon$  ca. 6‰ (Fig.13a). This factor is within the range of the proposed values by Robertson and Aravena et al. (1998). Besides, mixing patterns (straight lines) along regional flow systems are evidenced in Fig. 10a. The blue straight line suggest that groundwater flowing from the upper part presenting an isotopic composition of  $\delta^{15}N_{NO_3}$  (+7.54‰) is depleted to (+0.44‰). This mixing pattern could suggest the nitrogen inputs of ammonium fertilizers.

In fact this mixing pattern in the northern Piedmont, where there are two main sources: natural nitrate in groundwater and nitrate derived from nitrogen fertilizers, could be quantified by the following equation (Delconte et al., 2014; Vadillo et al., 2015):

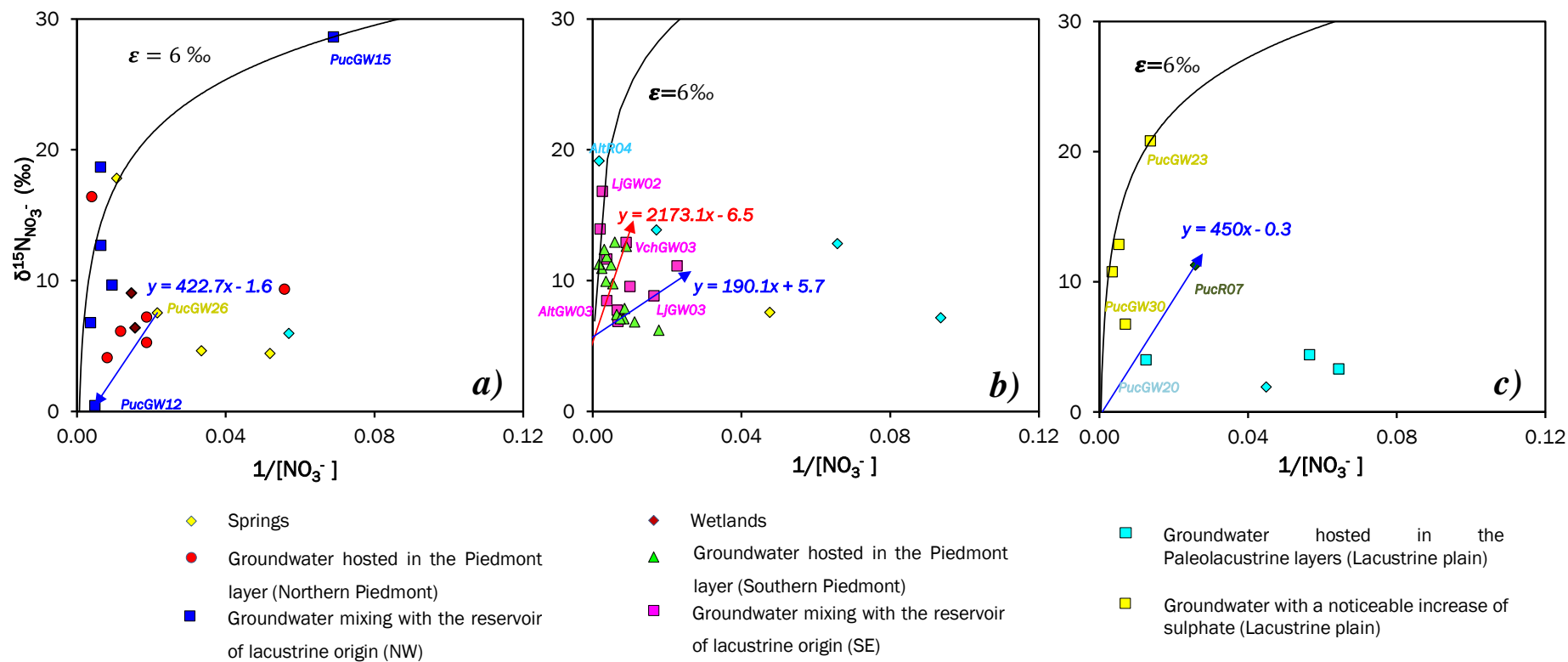


Figure 13. Plots of  $\delta^{15}N_{NO_3^-}$  versus  $1/[NO_3^-]$  (nitrate concentrations are given in  $\mu M$ ) in the a) the Northern Piedmont, b), Southern Piedmont and c) Lacustrine plain. The different denitrification fractionation yield curves whereas mixing yields straight lines

$$C_T \cdot \delta^{15}(N_{NO_3})_T = C_N \cdot \delta^{15}(N_{NO_3})_N + C_A \cdot \delta^{15}(N_{NO_3})_A$$

Where,  $C = [NO_3^-]$  groundwater nitrate concentration in  $\mu\text{M}$  and  $\delta^{15}N_{NO_3}$  = nitrate isotope composition;  $C_T$  = total groundwater nitrate;  $N$  = natural nitrate component and  $A$  = antropogenic nitrate component.

$$\therefore \delta^{15}N_{NO_3} = 422.7 \frac{1}{[NO_3^-]} - 1.6$$

In the Southern Piedmont, the enrichment factor yielding denitrification fractionation is  $\varepsilon$  ca. 6‰ (Fig. 13b). As for the Northern Piedmont, straight lines evidence mixing patterns along flow systems. Both straight lines (blue and red) suggest nitrogen inputs with  $\delta^{15}N_{NO_3}$  of +5‰ relating most likely soil organic matter and human waste. In fact, nitrate concentrations of groundwater that mixes with a (+5‰) nitrogen source is attenuated by dilution downgradient.

Finally, in the lacustrine plain, the enrichment factor yielding denitrification fractionation is also  $\varepsilon$  ca. 6‰ (Fig. 13c). Besides, groundwater mixing patterns are evidenced with the blue straight line. This mixing pattern, as for the Northern Piedmont, evidence nitrogen inputs of amonium fertilizers ( $\delta^{15}N_{NO_3}=0$  ‰). Indeed, the mixing pattern suggest that nitrate concentrations of groundwater are diluted when entering Lake Titicaca. Furthermore, the contribution of groundwater to the current Lake Titicaca (Cohana Bay) appears to be retarded due to the presence of the clay layer.

Generally, denitrification fractionation processes in groundwater from Lake Titicaca Aquifer System yields an enrichment factor of  $\varepsilon$  ca. 6‰. The main sources of nitrogen pollution, relate nitrogen fertilizers (northern Piedmont) and human waste (southern Piedmont) on the Piedmont, and nitrogen fertilizers in the Lacustrine plain.

## 6. Conclusions

The analysis of hydrochemical data and nitrogen-oxygen isotopes of nitrate resulted in an excellent technique for understanding the natural background levels of groundwater quality and the behaviour of nitrate along the groundwater flow system. The application of these tools in such particular hydrogeologic environment ( gravity-driven siliciclastic

aquifer), allowed identifying the locations where nitrate attenuation takes place and fingerprinting nitrate sources.

Generally, groundwater circulating through the Piedmont layers present Ca (Mg)-HCO<sub>3</sub> facies with low mineralization, low nitrate and chloride concentrations in the high recharge areas, which can be considered as natural background limits of groundwater quality. Whereas, downgradient a noticeable enrichment trend of chloride, sulphate, nitrate and a higher mineralization, relates anthropogenic urban and mining contamination. Afterwards, groundwater mix with the reservoir of Lacustrine origin transforming the dominant Ca(Mg)-HCO<sub>3</sub> facies to Na(K)- HCO<sub>3</sub> facies. Although chloride concentrations in this sector increase due to the presence of evaporites in the lacustrine matrix, nitrate concentrations are reduced. Finally, in the Lacustrine plain, groundwater present primarily Na(K)-Cl facies relating the presence of evaporites. In this area groundwater is prone to contamination, especially when the clay layer is absent and in places where a connection to the Piedmont subsystem is evident, through the subterranean channels.

The  $\delta^{15}N_{NO_3}$  and  $\delta^{18}O_{NO_3}$  confirmed that human/animal waste, especially in the southern zone of the Piedmont and nitrogen fertilizers, in the northern zone of the Piedmont and Lacustrine plain, are the main sources of  $NO_3^-$  contamination in the aquifer. Groundwater circulating through the Piedmont layers is naturally attenuated when mixing with the reservoir of Lacustrine origin, we attribute this to the slow groundwater flow occurring in this zone as it behaves as a topographical low where groundwater is naturally discharging to wetlands. Indeed, denitrification fractionation processes in groundwater from Lake Titicaca Aquifer System yields an enrichment factor of  $\epsilon$  ca. 6‰.

The particular hydrogeological environment of the siliciclastic Lake Titicaca aquifer system (Piedmont and Lacustrine plain), represent a source of high quality especially in the upper Piedmont, where besides the high hydraulic heads, till glacial deposits (low hydraulic conductivities) overlying fluvio-glacial deposits may protect groundwater resources. Moreover, the absence of this till layer in the lower Piedmont and the shallower water tables of the alluvial-fluvio-glacial—lacustrine sequence, make this area more vulnerable to contamination. Furthermore, groundwater flowing from the Piedmont layers through the subterranean channels and reaching the Lacustrine plain,

influence groundwater chemistry in the Lacustrine Plain locally. Also, contamination is evidenced in areas where the clay aquitard is absent.

#### *Acknowledgments*

*The present study was undertaken with the financial support of the Government of the Plurinational State of Bolivia through the Program “100 Scholarships for Postgraduate Education within the Framework of Technological and Scientific Sovereignty”, administered by the Ministry of Education (MINEDU) and partly funded by LABEX OSUG@2020, ANR grant no.ANR-10-LABX-56 (financed by the Future Investments programme launched by the French government and implemented by the ANR). Special thanks to the Ministry of Environment and Water (M.M.A.Y.A, La Paz) and the University of San Andres (UMSA, La Paz) for the logistical and technical support.*

## References

- Abbott MB, Wolfe BB, Wolfe AP, Seltzer GO, Aravena R, Mark BG, Polissar PJ, Rodbell DT, Rowe HD, Vuille M (2003) Holocene paleohydrology and glacial history of the central Andes using multiproxy lake sediment studies. *Palaeogeography, Palaeoclimatology, Palaeoecology* 194 (2003) 123-138.
- Archundia D, Duwig C, Spadini L, Uzu G, Guedron S, Morel MC (2017a) How Uncontrolled Urban Expansion Increases the Contamination of the Titicaca Lake Basin (El Alto, La Paz, Bolivia). *Water Air And Soil Pollution*, 228(1).
- Archundia D., Duwig C., Lehembre F., Chiron S., Morel M-C., Prado B., Bourdat-Deschamps M., Vince E., Flores Aviles G., Martins J.M.F., 2017b. Antibiotic pollution in the Katari subcatchment of the Titicaca Lake: major transformation products and occurrence of resistance genes. *Science of the Total Environment*, 576, 671–682.
- B.I.D (2016) Programa de Saneamiento del Lago Titicaca (Cuenca Katari, Bahía Cohana) BO-L1118. Marco de Gestión Ambiental y Social (MGAS), 87 pages.
- Bourgeois I, Savarino J, Némery J, Caillon N, Albertin S, Delbart F, Voisin D, Clément JC (2018) Atmospheric nitrate export in streams along amontane to urban gradient. *Science of the Total Environment* 633 (2018) 329–340
- Coudrain-Ribstein A, Olive P, Quintanilla J, Sondag F, Cahuaya D (1995) Salinity and isotopic dynamics of the groundwater resources on the Bolivian Altiplano. *Application of Tracers in Arid Zone Hydrology (Proceedings of the Vienna Symposium, August 1994)*. IAHS Publ. No. 232, 1995.
- Clark I (2015) *Groundwater Geochemistry and Isotopes*. CRC Press is an imprint of Taylor & Francis Group, an Informa business. International Standard Book Number-13: 978-1-4665-9174-5 (eBook - PDF).
- Cross S, Baker P, Seltzer G, Fritz S, Dunbar R (2001) Late Quaternary Climate and Hydrology of Tropical South America Inferred from an Isotopic and Chemical Model of Lake Titicaca, Bolivia and Perú. *Quaternary Research* 56:1, pp. 1-9; doi 10.1006/qres.2001.2244.

- Delconte CA, Sacchi E, Racchetti E, Bartoli M, Mas-Pla J, Re V (2014) Nitrogen inputs to a river course in a heavily impacted watershed: A combined hydrochemical and isotopic evaluation (Oglio River Basin, N Italy). *Science of the Total Environment* 466–467 (2014) 924–938.
- Delclaux F, Coudrain A, Condom T (2007) Evaporation estimation on Lake Titicaca: a synthesis review and modelling. *Hydrol. Process.* 21, 1664–1677 (2007). DOI: 10.1002/hyp.6360
- FAO-Organización de las Naciones Unidas para la Agricultura y la Alimentación (1999) Bolivia hacia una estrategia de Fertilizantes. Informe preparado para el Gobierno de Bolivia por el Proyecto Manejo de Suelos y Nutrición Vegetal en Sistemas de Cultivos GCPF/BOL/018/NET – “Fertisuelos”.
- Flores-Avilés GP, Descloitres M, Duwig C, Rossier Y, Spadini L, Legtchenko A, Soruco A, Argollo J, Perez M, Medinaceli W (2019) Insight into the Bolivian Lake Titicaca aquifer system, inferred from geophysical (TDEM) and hydrogeological data (*Submitted*)
- Fritz SC; Baker PA; Seltzer GO; Ballantyne A; Tapia P; Cheng H, Edwards, RL (2007) Quaternary glaciation and hydrologic variation in the South American tropics as reconstructed from the Lake Titicaca drilling project. *Quaternary Research* 68:3, pp. 410-420; doi:10.1016/j.yqres.2007.07.008.
- Garcia ME, Bengtsson L, Persson KM (2010) On the distribution of saline groundwater in the Poopó basin, Central Bolivian Highland. *Vatten* 66:199-203. Lund 2010.
- G.E.O.S.I.R.H. (2017) Infraestructura de Datos Espaciales. Plan Director de la Cuenca Katari y Lago Menor del Titicaca available at <http://geosirh.riegobolivia.org/layers/geosirh>. Ministerio de Medio Ambiente y Agua. Viceministerio de Recursos Hídricos y Riego.
- Guédron S, Point D, Acha D, Bouchet S, Baya PA, Tessier E, Monperrus M, Molina CI, Groleau A, Chauvaud L, Thebault J, Amice E, Alanoca L, Duwig C, Uzu G, Lazarro X, Bertrand A, Bertrand S, Barbraud C, Delord K, Gibon FM, Ibanez C, Flores M, Fernandez Saavedra P, Ezpinoza ME, Heredia C, Rocha F, Zepita C, Amouroux D (2017) Mercury contamination level and speciation inventory in Lakes Titicaca &

- Uru-Uru (Bolivia): Current status and future trends. *Environmental Pollution* 231 (2017) 262-270.
- Griffiths N, Jackson C, McDonnell JJ, Klaus J, Du E, Bitew M (2016) Dual nitrate isotopes clarify the role of biological processing and hydrologic flow paths on nitrogen cycling in subtropical low-gradient watersheds. *J. Geophys. Res. Biogeosci.*, 121, 422–437, doi:10.1002/2015JG003189.
- Hardy S, Valton C, Guislain S, Larrazabal Cardova N (2015). Atlas de la vulnerabilidad de la aglomeracion de La Paz. IRD. Plural editores.
- INE-National Institute of Statistics of the Bolivian Plurinational State (2015) Censo de Población y Vivienda 2012 Bolivia (available at [www.ine.gob.bo](http://www.ine.gob.bo))
- Kaiser J, Hastings MG, Houlton BZ, Röckmann T, Sigman D (2007) Triple Oxygen Isotope Analysis of Nitrate Using the Denitrifier Method and Thermal Decomposition of N<sub>2</sub>O. *Anal. Chem.* 2007, 79, 599-607.
- Kendall C, Elliott EM, Wankel SD (2007) Tracing anthropogenic inputs of nitrogen to ecosystems, Chapter 12, In: R.H. Michener and K. Lajtha (Eds.), *Stable Isotopes in Ecology and Environmental Science*, 2nd edition, Blackwell Publishing, p. 375- 449.
- Kinouchi T, Liu T, Mendoza J, Asaoka Y (2013) Modeling glacier melt and runoff in a high-altitude headwater catchment in the Cordillera Real, Andes. *Hydrol. Earth Syst. Sci. Discuss.*, 10, 13093–13144, 2013. DOI:10.5194/hessd-10-13093-2013.
- Lavenu A (1992) Origins: Formation and geological evolution. C. Dejoux and A. Iltis (Eds.). *Lake Titicaca*, 3-15. 589 Pages.
- Mahlknecht J, Gárfias-Solis J, Aravena R, Tesh R (2005) Geochemical and isotopic investigations on groundwater residence time and flow in the Independence Basin, Mexico. *Journal of Hydrology* 324 (2006) 283–300
- Martinelli G, Dadomo A, De Luca DA, Mazzola M, Lasagna M, Pennissi M, Pilla G, Sacchi E, Saccon P (2018) Nitrate sources, accumulation and reduction in groundwater from Northern Italy: Insights provided by a nitrate and boron isotopic database. *Applied Geochemistry* 91 (2018) 23–35.

- Murray BP, Horton BK, Matos R, Heizler MT (2010) Oligocene–Miocene basin evolution in the northern Altiplano, Bolivia: Implications for evolution of the central Andean backthrust belt and high plateau. *GSA Bulletin*; September/October 2010; v. 122; no. 9/10; p. 1443–1462; doi: 10.1130/B30129.1
- M.M.A.y.A – Environmental Audit (2014) Informe de Auditoría sobre el Desempeño Ambiental respecto de la Contaminación Hídrica en la Cuenca del Río Katari y la Bahía de Cohana K2/AP05/J13 (available at <https://www.contraloria.gob.bo/portal>)
- M.M.A.y.A (2016) Plan de Manejo Preliminar de los Acuíferos de Purapurani y Viacha. Ministerio de Medio Ambiente y Agua/Viceministerio de Recursos Hídricos y Riego, La Paz, Bolivia, 184 pages.
- Oyarzún R, Barrera F, Salazar P, Maturana H, Oyarzún J, Aguirre E, Alvarez P, Jourde Hervé, Kretschmer N (2014) Multi-method assessment of connectivity between surface water and shallow groundwater: the case of Limarí River basin, north-central Chile. *Hydrogeology Journal* (2014) 22: 1857–1873. DOI 10.1007/s10040-014-1170-9.
- Özen A, Karapınar B, Kucuk I, Jeppesen E, Beklioglu M (2010) Drought-induced changes in nutrient concentrations and retention in two shallow Mediterranean lakes subjected to different degrees of management. *Hydrobiologia*, 646:61–72
- Pilla Giorgio, Sacchi Elisa, Zuppi Gianmaria, Braga Giovanni, Ciancetti Gianfranco (2005) Hydrochemistry and isotope geochemistry as tools for groundwater hydrodynamic investigation in multilayer aquifers: a case study from Lomellina, Po plain, South-Western Lombardy, Italy. *Hydrogeology Journal* (2006) 14: 795–808
- Pauwels H, Foucher JC, Kloppmann W (2000) Denitrification and mixing in a schist aquifer: influence on water chemistry and isotopes. *Chemical Geology* 168 (2000) 307–324.
- Quino Lima I, Ormachea Muñoz M, Ramos Ramos OE, Bhattacharya P, Quispe Choque R, Quintanilla Aguirre J, Sracek O (2019) Hydrochemical assessment with respect to arsenic and other trace elements in the Lower Katari Basin, Bolivian Altiplano. *Groundwater for Sustainable Development* 8 (2019) 281–293.

- Rabatel A, Machaca A, Francou B, Jomelli V (2006) Glacier recession on Cerro Charquini (16°S), Bolivia, since maximum of the Little Ice Age (17th century) . Journal of Glaciology, Vol.52, N°176,2006.
- Ramos Ramos OE (2014) Geochemistry of trace elements in the Bolivian Altiplano – Effects of natural processes and anthropogenic activities. TRITA-LWR PHD-2014:04 ISSN 1650-8602; ISBN 978-91-7595-177-5.
- Re V, Sacchi E, Kammoun S, Triangli C, Trabelsi R, Zouari K, Daniele S (2017) Integrated socio-hydrogeological approach to tackle nitrate contamination in groundwater resources. The case of Grombalia Basin (Tunisia). Science of the Total Environment 593–594 (2017) 664–676.
- Rivett MO, Buss SR, Morgan P, Smith JWN, Bemment CD (2008) Nitrate attenuation in groundwater: A review of biogeochemical controlling processes. Water Research 42 (2008) 4215 – 4232.
- Robertson DM, Rose WJ, Saad DA (2005) Water quality, hydrology, and phosphorus loading to Little St. Germain Lake, Wisconsin, with special emphasis on the effects of winter aeration and groundwater inputs. US Geol Surv Sci Invest Rep 2005-5071.
- Sacchi E, Acutis M, Bartoli M, Brenna S, Delconte CA, Laini A, Pennisi M (2013) Origin and fate of nitrates in groundwater from the central Po plain: Insights from isotopic investigations. Applied Geochemistry 34 (2013) 164–180.
- Salvaderry - Aranguren MM, Probst A, Roulet M, Isaure MP (2008) Contamination of surface waters by mining wastes in the Milluni Valley (Cordillera Real, Bolivia): Mineralogical and hydrological influences. 2008 Elsevier Ltd. All rights reserved.
- Shaw RD, Shaw JFH, Fricker H, Prepas EE (1990) An integrated approach to quantify groundwater transport of phosphorus to Narrow Lake, Alberta. Limnol. Oceanogr.,35 (4),870–886
- Sigman DM, Caciotti KL, Andreani M, Barford C, Galanter M, Böhkke (2001) A Bacterial Method for the Nitrogen Isotopic Analysis of Nitrate in Seawater and Freshwater. Anal. Chem. 2001, 73, 4145-4153

- Spalding RF, Hirsh, Exner ME, Little NA, Kloppenborg KL (2019) Applicability of the dual isotopes  $\delta^{15}\text{N}$  and  $\delta^{18}\text{O}$  to identify nitrate in groundwater beneath irrigated cropland. *Journal of Contaminant Hydrology* 220 (2019) 128–135.
- Sugaki A, Kitakaze A (1988) Tin-bearing Minerals from Bolivian Polymetallic Deposits and their Mineralization Stages. *Mining Geology*, 38(5) 419-435, 1988.
- Tang C, Azuma K, Yoshifumi I, Baku O, Sakura Y (2004) Nitrate behaviour in the groundwater of a headwater wetlands, Chiba, Japan. *Hydrol. Process.* 18, 3159–3168 (2004).
- Tóth J (1962) A theory of Groundwater Motion in Small Drainage Basins in Central Alberta, Canadá. *Journal of Geophysical Research*, Vol.67, N°11
- Tóth J (1963) A theoretical Analysis of Groundwater Flow in Small Drainage Basins. *Journal of Geophysical Research*, Vol.68, N°16
- Tóth J (1995) Hydraulic Continuity in large Sedimentary Basins. *Hydrogeology Journal*, v.3, no 4, 1995
- Tóth J (1999) Groundwater as a geologic agent: An overview of the causes, processes, and manifestations. *Hydrogeology Journal* (1999) 7:1–14
- Tóth J (2010) The theory of basinal gravity flow of groundwater and its impacts on hydrology Japan. *Special Issue Review* 335-354 (2010)
- Uribe J, Muñoz JF, Gironás J, Oyarzún R, Aguirre E, Aravena R (2015) Assessing groundwater recharge in an Andean closed basin using isotopic characterization and a rainfall-runoff model: Salar del Huasco basin, Chile. *Hydrogeology Journal* (2015) 23: 1535–1551. DOI 10.1007/s10040-015-1300-z.
- US Army Corps of Engineers (2014) Water Resources Assessment of Bolivia (available at <http://www.sam.usace.army.mil/en/wra/wra.html>).
- Widory D, Petelet-Giraud E, Négrel P, Ladouche B (2005) Tracking the Sources of Nitrate in Groundwater Using Coupled Nitrogen and Boron Isotopes: A Synthesis. *Environ. Sci. Technol.* 2005, 39, 539-548.

Veettil BK, Wang S, Simões JC, Ruiz Pereira SF (2018) Glacier monitoring in the eastern mountain ranges of Bolivia from 1975 to 2016 using Landsat and Sentinel-2 data. *Environmental Earth Sciences* (2018) 77:452. <https://doi.org/10.1007/s12665-018-7640-y>

Zhai Yuanzheng, Wang Jinsheng, Teng Yanguo, Zuo Rui (2012) Hydrogeochemical and isotopic evidence of groundwater evolution and recharge in aquifers in Beijing Plain, China. *Environ Earth Sci* (2013) 69:2167–2177. DOI 10.1007/s12665-012-2045-9

Zeballos A, Weihd P, Blanco M, Machaca V (2016) Geological, mineralogical and chemical characterization of Devonian kaolinite-bearing sediments for further applications in the ceramic (tiles) industry in La Paz, Bolivia. *Environ Earth Sci* (2016) 75:546. DOI 10.1007/s12665-015-5212-y.

---

## **Supplementary Material (SM)**

Table S1. Major ions concentrations and nitrogen isotopic compositions of groundwater hosted in Lake Titicaca Aquifer System.

Code	Type	Depth (m) b.g.l	T (°C)	pH	EC (µS/cm)	DO (mg/L)	Eh (mV)	Alkalinity (mg/L CaCO <sub>3</sub> <sup>2-</sup> )	Ca <sup>2+</sup> (mg/L)	Mg <sup>2+</sup> (mg/L)	Na <sup>+</sup> (mg/L)	K <sup>+</sup> (mg/L)	NH <sub>4</sub> <sup>+</sup> (mg/L)	HCO <sub>3</sub> <sup>-</sup> (mg/L)	SO <sub>4</sub> <sup>2-</sup> (mg/L)	Cl <sup>-</sup> (mg/L)	NO <sub>3</sub> <sup>-</sup> (mg/L)	NO <sub>2</sub> <sup>-</sup> (mg/L)	H <sub>3</sub> PO <sub>4</sub> <sup>-</sup> (mg/L)	δ <sup>18</sup> O <sub>NO3</sub> (‰)	δ <sup>15</sup> N <sub>NO3</sub> (‰)	
<b>Piedmont Subsystem</b>																						
<i>Northern Piedmont</i>																						
1	PucGW01	Well	40	12.7	7.3	146.0	2.6	80	23	8.0	3.1	7.8	0.8	10.4	28.0	11.3	1.0	1.1	0.0	0.0	-1.6	9.3
2	PucGW38	Well	30	14.3	7.3	133.0	1.62	327	21	8.0	3.3	6.3	0.8	0.0	25.6	10.7	0.8	11.7	0.0	0.0	--	--
3	PucGW40	Well	50	13.5	7.3	135.0	1.84	303	28	9.3	3.4	8.3	1.2	0.7	34.1	10.8	1.2	2.7	0.0	0.0	--	--
4	PucGW05	Well	3	13.2	6.8	142.0	1.02	43	24	9.2	3.8	4.7	1.1	0.4	29.3	16.0	1.3	7.6	0.0	0.0	11.2	4.1
5	PucGW04	Well	18	13.4	7.6	211.0	2.94	267	36	10.2	5.6	10.3	1.0	0.1	43.8	12.0	3.7	15.6	0.0	0.0	1.7	16.4
6	PucGW06	Well	47	15.7	7.7	169.0	4.08	226	34	8.9	4.8	8.6	1.1	0.0	41.3	14.7	0.7	5.3	0.0	0.0	-6.9	6.1
7	PucGW08	Well	60	12.8	6.0	180.0	3.09	289	26	10.4	4.3	5.3	2.4	0.0	32.0	21.1	2.6	3.3	0.0	0.0	-7.0	7.2
8	PucGW09	Well	80	15.9	7.5	125.0	3.38	267	25	7.3	2.8	7.6	0.7	0.0	30.3	9.5	3.3	3.3	0.0	0.1	-5.0	5.3
9	PucGW16	Well	62	15.4	7.3	226.0	2.61	228	53	14.0	6.3	13.5	2.0	0.0	64.3	20.0	6.3	9.7	0.0	0.1	0.0	12.7
10	PucGW14	Well	55	13.0	7.6	261.0	4.5	213	72	15.4	8.2	18.8	2.7	0.0	88.0	27.5	4.5	9.8	0.0	0.1	5.4	18.7
11	PucGW41	Well	50	13.7	7.6	237.0	0.4	30	55	14.8	5.4	19.1	2.1	0.0	66.7	30.3	8.3	1.6	0.0	0.3	--	--
12	PucGW15	Well	45	13.8	7.6	261.0	0.71	95	54	11.8	6.1	22.1	1.7	0.0	66.1	27.1	13.0	0.9	0.0	0.5	15.5	28.6
13	PucGW11	Well	76	12.9	7.6	212.0	2.7	229	41	10.8	4.3	15.0	2.3	0.2	49.8	16.7	6.6	17.1	0.0	0.0	-3.4	6.8
14	PucGW12	Well	60	15.8	7.4	305.0	2.28	236	64	10.9	5.7	25.9	1.7	0.0	77.9	26.0	9.8	12.9	0.0	0.0	-4.0	0.4
15	PucGW13	Well	70	13.3	7.1	416.0	1.33	207	113	18.8	12.1	35.4	2.3	0.0	137.7	42.2	13.7	6.6	0.0	0.1	2.1	9.7
16	PucGW10	Spring	--	13.5	8.5	88.0	6.88	202	27	11.3	0.5	1.7	1.2	0.0	31.4	2.0	0.2	1.9	0.0	0.0	-1.6	4.6
17	PucGW26	Spring	--	8.8	6.8	63.0	4.52	277	17	5.1	1.7	3.9	0.9	0.2	20.7	3.0	0.4	2.9	0.0	0.1	-5.5	7.5
18	PucGW07	Spring	--	8.8	7.1	98.0	5.8	282	9	9.3	0.9	1.7	0.7	--	11.0	17.4	0.2	1.2	0.0	0.0	9.3	4.4
19	PucGW03	Spring	--	15.3	7.1	265.0	2.84	330	60	16.9	9.1	20.9	4.2	0.4	73.1	17.6	2.4	5.8	0.0	0.0	-8.0	17.8
20	PucGW28	Wetland	--	14.0	6.6	74.0	1.22	268	7	5.6	1.3	3.6	0.9	0.0	8.5	10.4	1.4	4.0	0.0	0.1	-3.3	6.4
21	PucGW27	Wetland	--	14.0	6.4	108.0	1.09	258	12	8.9	2.7	4.0	1.4	0.0	14.6	14.5	2.1	4.2	0.0	0.0	-3.6	9.1
22	PpR01	Lake	--	13.7	7.8	790.0	3.41	--	79	33.6	14.8	76.6	8.6	0.0	95.8	119.4	114.4	0.03	0.0	0.0	--	--
23	PpR02	Lake	--	13.8	8.2	942.0	4.35	--	68	29.1	26.0	122.0	11.8	0.0	81.7	180.0	177.5	0.03	0.0	0.0	2.8	10.1
24	BtR02	River	--	--	7.1	144.0	--	--	14	7.2	1.8	3.1	1.2	0.7	17.4	11.2	0.5	1.1	0.0	0.0	-1.4	6.0

-- Not measured

Table S1 continued

Code	Type	Depth (m) b.g.l	T (°C)	pH	EC (µS/cm)	DO (mg/L)	Eh (mV)	Alkalinity (mg/L CaCO <sub>3</sub> <sup>2-</sup> )	Ca <sup>2+</sup> (mg/L)	Mg <sup>2+</sup> (mg/L)	Na <sup>+</sup> (mg/L)	K <sup>+</sup> (mg/L)	NH <sub>4</sub> <sup>+</sup> (mg/L)	HCO <sub>3</sub> <sup>-</sup> (mg/L)	SO <sub>4</sub> <sup>2-</sup> (mg/L)	Cl <sup>-</sup> (mg/L)	NO <sub>3</sub> <sup>-</sup> (mg/L)	NO <sub>2</sub> <sup>-</sup> (mg/L)	H <sub>3</sub> PO <sub>4</sub> <sup>-</sup> (mg/L)	δ <sup>18</sup> O <sub>NO3</sub> (‰)	δ <sup>15</sup> N <sub>NO3</sub> (‰)	
25	PucR03	Lagoon	--	11.9	7.5	181.0	3.29	224	13	15.7	2.9	1.6	0.6	0.0	15.7	39.0	0.1	0.9	0.0	0.0	--	--
26	PucR04	Lagoon	--	12.4	9.2	131.0	3.99	176	15	11.6	2.8	1.8	0.6	5.0	15.3	21.5	0.2	0.7	0.0	0.0	--	--
<i>Southern Piedmont</i>																						
27	PucGW21	Well	50	13	7.2	216	3.74	144	39	10.5	5.4	17.2	1.8	0.2	47.5	27.7	5.8	3.5	0.0	0.1	-5.10	6.22
28	LjGW04	Well	60	13	6.9	205	1.25	118	42	9.9	4.1	17.5	2.9	0.0	51.2	17.9	6.3	6.2	0.0	0.1	-2.95	9.55
29	LjGW03	Well	55	15	6.9	401	1.39	106	74	18.1	11.1	31.5	5.1	0.0	90.2	78.4	6.0	3.8	0.0	0.2	-2.60	8.83
30	LjGW01	Well	50	15	6.8	382	1.4	116	113	11.1	6.2	55.6	4.3	0.2	137.8	27.5	19.4	2.7	0.0	0.3	0.78	11.11
31	LjGW02	Well	30	13	7.5	433	1.66	121	60	21.9	11.5	30.9	6.0	0.2	73.0	88.8	14.4	23.8	0.0	0.0	0.60	16.83
32	AltGW10	Well	70	12	7.5	314	2.04	207	41	14.8	5.6	24.3	5.2	26.4	49.9	34.6	15.7	31.3	0.0	0.1	-2.08	13.94
33	AltGW11	Well	60	13	7.3	181	3.39	221	27	8.8	4.5	12.1	2.5	14.9	32.9	22.6	6.3	10.5	0.0	0.2	-2.84	12.96
34	AltGW12	Well	110	15	7.3	188	1.95	176	42	9.1	4.7	13.0	3.0	0.0	51.1	17.8	6.1	16.3	0.0	0.5	-2.30	11.65
35	AltGW01	Well	110	14	7.9	142	1.25	156	36	6.6	2.6	11.3	2.3	0.0	43.6	6.1	7.3	12.5	0.0	0.3	-6.15	11.21
36	AltGW03	Well	100	14	7.1	413	3.14	185	118	16.6	7.6	44.3	3.5	0.1	143.8	29.6	24.8	16.6	0.0	0.2	-5.34	8.46
37	AltGW04	Well	90	14	7.7	335	2.87	186	74	9.1	5.0	39.1	2.5	0.0	89.8	25.6	14.7	9.4	0.0	0.1	-3.88	7.73
38	AltGW05	Well	87	14	7.6	183	2.87	176	44	8.2	4.3	14.5	2.0	0.0	53.5	13.5	5.1	9.2	0.0	0.1	-4.00	6.87
39	VchGW03	Well	43	14	7.6	210	3.49	236	45	6.9	3.7	21.0	3.2	0.0	54.7	15.1	7.5	6.9	0.0	0.2	2.12	12.90
40	VchGW06	Well	60	16	6.9	359	2.12	202	41	21.4	14.3	13.2	3.2	0.1	50.0	35.5	37.9	20.0	0.0	0.0	-5.68	12.39
41	AltGW06	Well	77	13	7.5	209	2.07	192	31	10.4	6.3	12.4	2.1	0.2	37.7	18.7	16.6	11.5	0.0	0.0	-3.97	9.77
42	AltGW02	Well	95	13	7.6	219	1.93	154	40	11.0	6.4	14.4	2.5	0.1	48.6	15.7	12.4	16.4	0.0	0.1	-1.84	11.84
43	AltGW07	Well	90	13	7.2	248	2.07	132	39	12.1	6.9	15.8	2.9	17.8	47.5	13.9	20.2	25.5	0.0	0.0	-3.16	10.95
44	AltGW08	Well	92	13	7.4	265	2.82	142	30	14.7	9.4	11.1	2.9	13.4	36.5	19.7	21.8	35.6	0.0	0.0	-3.48	11.26
45	AltGW09	Well	115	14	8.2	167	2.23	132	36	8.2	1.7	8.2	2.4	0.0	43.3	8.1	2.0	9.6	0.0	0.0	-3.93	7.42
46	AltGW13	Well	70	14	7.6	155	2.11	185	31	9.8	4.9	7.0	1.5	0.0	37.7	9.2	6.5	17.3	0.0	0.1	-5.54	9.95
47	AltGW14	Well	90	14	7.6	230	1.61	195	27	12.5	9.2	8.5	1.4	0.0	32.8	18.5	12.6	29.7	0.0	0.1	--	--
48	LjGW22	Well	50	13	7	149	5.77	175	19	13.2	3.2	5.6	1.7	0.0	23.2	9.3	2.8	7.2	0.0	0.1	-7.99	7.87
49	LjGW05	Well	60	13	7.4	84	5.61	282	18	5.6	1.8	5.8	1.1	0.1	21.9	3.9	1.6	7.4	0.0	0.1	-3.89	7.10

-- Not measured

Table S1 continued

Code	Type	Depth (m) b.g.l	T (°C)	pH	EC (µS/cm)	DO (mg/L)	Eh (mV)	Alkalinity (mg/L CaCO <sub>3</sub> <sup>2-</sup> )	Ca <sup>2+</sup> (mg/L)	Mg <sup>2+</sup> (mg/L)	Na <sup>+</sup> (mg/L)	K <sup>+</sup> (mg/L)	NH <sub>4</sub> <sup>+</sup> (mg/L)	HCO <sub>3</sub> <sup>-</sup> (mg/L)	SO <sub>4</sub> <sup>2-</sup> (mg/L)	Cl <sup>-</sup> (mg/L)	NO <sub>3</sub> <sup>-</sup> (mg/L)	NO <sub>2</sub> <sup>-</sup> (mg/L)	H <sub>3</sub> PO <sub>4</sub> <sup>-</sup> (mg/L)	δ <sup>18</sup> O <sub>NO3</sub> (‰)	δ <sup>15</sup> N <sub>NO3</sub> (‰)	
50	LjGW06	Well	67	13	7.5	86	5.47	280	21	5.6	1.8	5.2	1.2	0.0	25.5	4.3	1.2	8.4	0.0	0.1	-3.57	7.09
51	LjGW07	Well	60	14	6.9	98	4.05	270	20	6.2	2.7	5.5	1.2	0.0	24.4	9.2	1.3	5.5	0.0	0.1	-3.04	6.85
52	PucGW33	Well	61	15	6.9	341	1.42	85	89	20.7	11.4	18.4	4.3	0.2	108.5	44.1	9.7	6.9	0.0	0.1	-1.18	12.62
53	PucGW34	Well	58	16	7.7	207	1.5	54	44	11.5	6.2	14.4	2.1	0.4	53.4	18.4	2.2	0.01	0.0	0.5	-2.26	6.95
54	PucGW29	Spring	--	12	6.7	221	1.98	78	--	11.5	10.8	6.9	1.7	0.0	--	57.8	1.5	1.3	0.0	0.0	-4.28	7.58
55	VchGW07	Wetland																				
56	AltR04	River	--	17	8.2	1230	3.66	154	195	45.2	15.8	114.2	23.4	36.0	234.3	163.1	121.3	36.5	0.7	2.6	0.68	19.15
57	AltR05	River	--	16	8.2	1340	3.42	209	219	40.4	16.0	109.6	30.8	42.5	262.7	175.7	148.3	3.6	0.0	2.7	13.27	13.88
58	AltR03	River	--	8	3.6	344	36	501	--	16.0	6.3	4.4	1.5	0.2	--	107.6	0.9	0.9	0.0	0.0	1.32	12.84
59	AltR02	River	--	7.2	3.3	720	6.05	537	--	24.4	16.1	8.3	2.4	0.3	--	278.3	2.1	0.7	0.0	0.0	0.07	7.17
60	AltR01	Lagoon	--	3.3	8.5	97	8.43	190	15	13.3	0.7	3.4	1.0	0.4	17.8	15.8	0.2	0.6	0.0	0.0	0.34	-0.98
<b>Lacustrine Plain</b>																						
61	PucGW25	Well	51	13	7.6	1610	1.86	94	195	48.5	34.7	154.8	14.8	10.8	237.1	27.1	404.2	1.1	0.0	0.0	5.67	4.38
62	PucGW43	Well	51	14	7.8	950	2.3	79	343	31.8	20.4	97.0	13.8	8.7	416.0	3.2	107.5	1.1	0.2	0.9	--	--
63	PucGW24	Well	70	15	7.9	680	2.17	91	31	23.5	15.8	91.5	6.0	5.2	37.4	0.5	34.3	1.0	0.1	2.1	0.19	3.31
64	PucGW42	Well	60	17	7.8	680	2.87	23	231	22.9	10.2	89.2	6.6	1.0	280.2	23.2	50.3	0.8	0.0	1.0	--	--
65	PucGW20	Well	30	15	7.5	1690	1.8	229	140	52.0	25.0	169.9	14.4	4.0	170.2	118.0	409.0	4.9	1.9	0.0	-7.95	4.00
66	PucGW32	Well	65	13	7.7	1260	0.57	106	47	44.5	13.2	137.1	4.0	0.0	57.1	221.1	171.6	3.4	0.0	0.0	-6.50	6.82
67	VchGW05	Well	50	14	7.5	1110	0.7	161	114	48.2	15.3	101.5	3.9	0.0	138.6	195.9	143.1	3.0	0.0	0.0	-8.05	5.50
68	PucGW23	Well	60	15	7	393	3.3	71	131	22.4	10.7	34.0	3.6	0.3	159.6	20.2	18.9	4.5	0.0	0.4	1.92	20.82
69	PucGW30	Well	64	14	7.7	760	3.16	121	168	39.9	16.5	59.6	4.2	0.2	204.0	76.6	99.4	8.8	0.0	0.0	-5.98	6.74
70	PucGW17	Well	47	14	7.6	530	4.49	209	150	30.1	9.6	34.9	8.1	0.7	182.2	38.6	18.7	11.8	0.0	0.7	1.56	12.86
71	VchGW04	Well	36	13	7.9	650	0.72	--	135	34.5	13.7	54.8	6.9	0.0	163.3	82.2	48.8	17.8	0.0	0.0	-2.65	10.77
72	PucR06	River	--	15	7.5	610	3.37	136	119	44.0	10.4	55.5	10.1	0.0	144.7	76.6	47.5	1.4	0.0	0.6	-6.25	1.92
73	PucR05	River	--	12	8.4	108	7.19	238	22	10.2	3.2	3.0	1.2	0.0	26.1	17.2	0.4	0.2	0.0	0.0	--	--
74	VchR01	River	--	9.2	8.5	1300	4.75	255	144	57.8	19.3	130.5	5.6	0.0	170.5	270.6	162.0	0.03	0.0	0.0	--	--
75	VchR02	River	--	15	8.4	1700	0.05	161	536	48.0	13.6	152.3	34.0	129.9	637.5	41.2	155.9	0.3	0.0	20.9	--	--
76	PucR07	Lake	--	20	###	550	6.31	197	92	48.0	9.6	51.4	9.7	0.0	37.4	93.0	55.3	2.4	0.3	0.0	-10.87	11.29
77	PucR08	Lake	--	17	8.2	1050	3.31	121	185	41.8	16.2	85.2	17.8	16.8	222.5	122.9	105.90	2.40	0.00	0.00	--	--

Carbonates

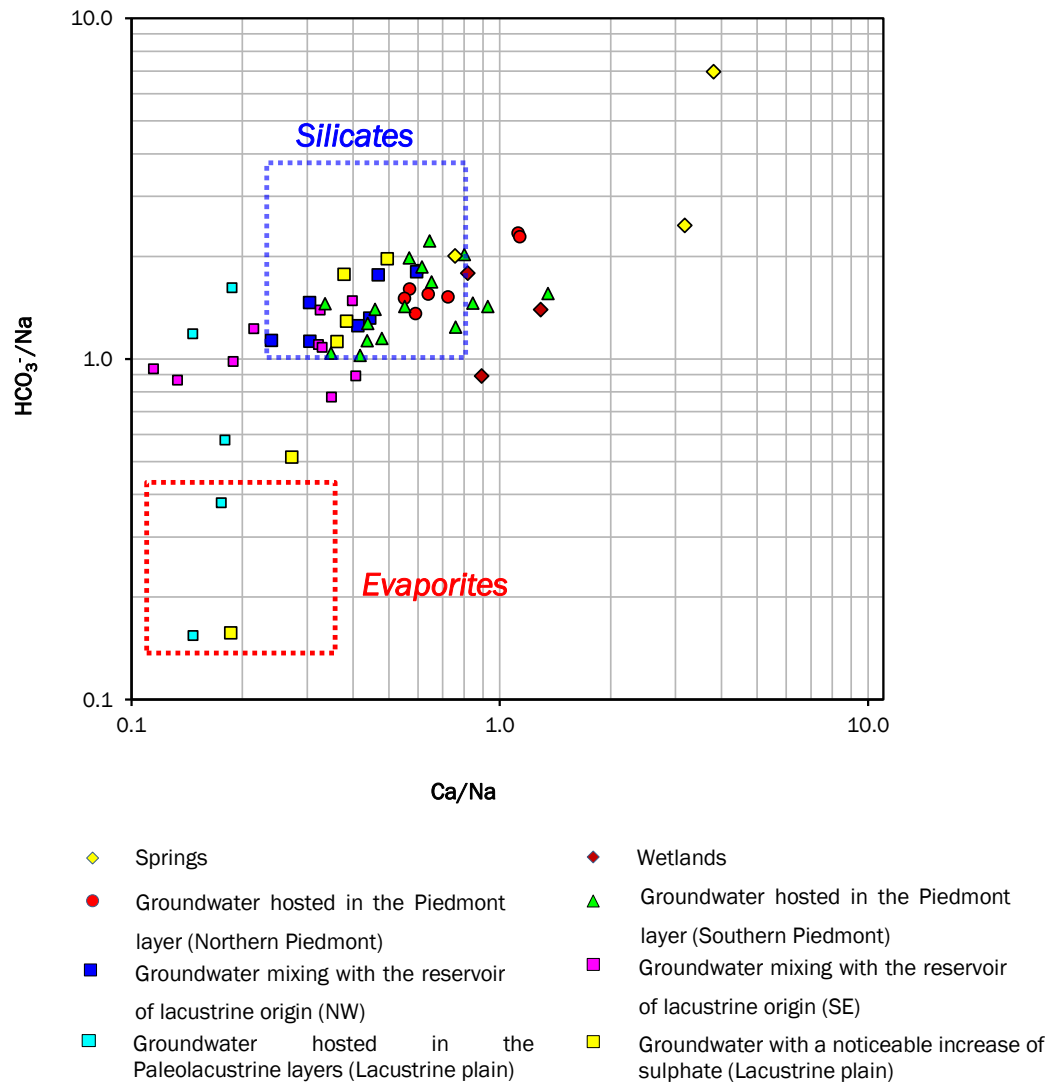


**Figure S1.** Plot showing molar ratios of  $\text{HCO}_3^-/\text{Na}$  and  $\text{Ca}/\text{Na}$  in groundwater of Lake Titicaca Aquifer System as indicators of silicate versus carbonate weathering (Modified after Clark, 2015). Each symbol represents samples located in the Piedmont subsystem or Lacustrine plain.

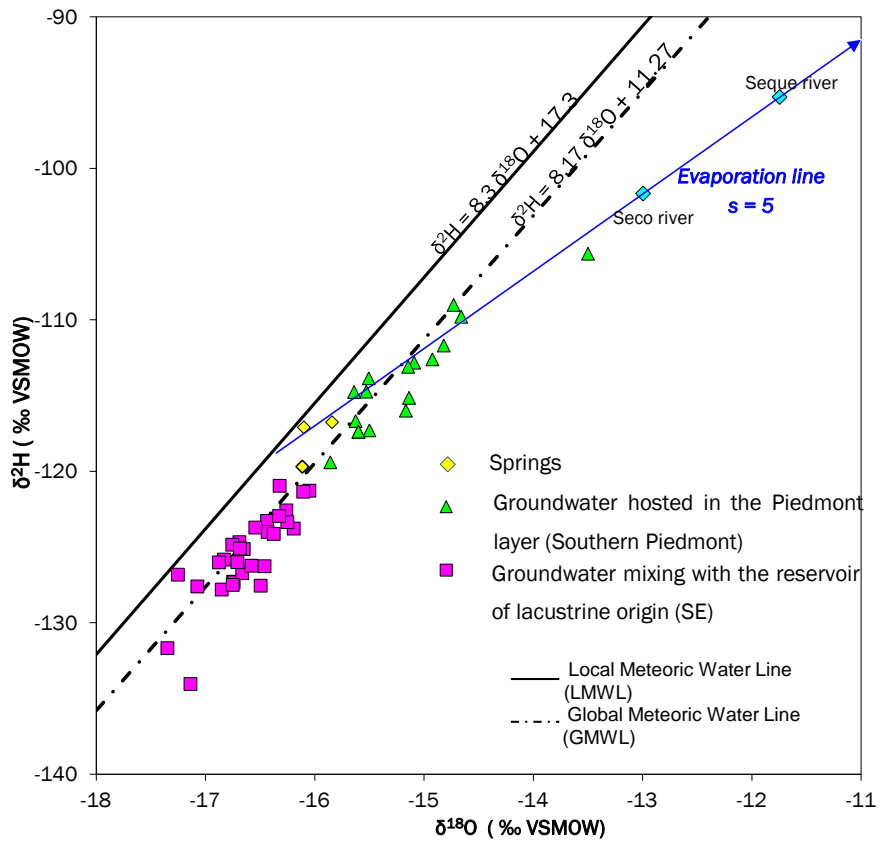


**Figure S2.** Stable hydrogen and oxygen isotopic composition of surface water and groundwater at the Bolivian Lake Titicaca aquifer system (Purapurani Zone), modified after MMAyA (2016).

### 6.3 Conclusions

The use of hydrogeochemistry and dual isotopes of  $\delta^{15}N_{NO_3}$  and  $\delta^{18}O_{NO_3}$  allowed to characterize the natural background levels of groundwater, to determine nitrate pollution sources and natural attenuation processes in the groundwater system.

In fact, the lower mineralization, the chemical and isotopic compositions of groundwater in the upper Piedmont, suggest that this water could be considered as the natural background levels of the Piedmont subsystem. Moreover, in the lower Piedmont, the isotopic composition of the dissolved  $NO_3^-$  revealed that the main origin of this anion is related to nitrogen fertilizers towards the NW and human/animal waste towards the SE of the Piedmont. The principal mechanism for the depletion of nitrate concentrations is denitrification that occurs mainly in the lower sector of the Piedmont, where groundwater mixes with the reservoir of lacustrine origin.

Furthermore, in the Lacustrine Plain the main origin of nitrate is related to nitrogen fertilizers. Suggesting that the groundwater contribution of nitrate to the current Lake Titicaca is retarded due to the thick clay layer, deposited during the ancient Paleolake expansions.

# Conclusions and perspectives

## 7.1 Conclusions

The objective of this investigation was to apply a multidisciplinary approach (geology, geophysics, hydrogeochemistry, GIS, isotopy and groundwater level data) in order to conceptualize subsurface flow and trace nitrate contamination sources and fate within the Katari and Lago menor region (6,350  $Km^2$ ).

Therefore, a multidisciplinary approach was conducted to build up a conceptualized subsurface flow model within the semi-arid Katari and Lago Menor region. For this purpose, a regional field campaign was carried out from April to August of 2017. A total of 187 TDEM (Time Domain ElectroMagnetic) soundings were performed within the region, a total of 97 groundwater source (19 artesian wells, 36 deep wells, 32 dug wells, 8 springs and 2 wetlands) were inventoried and five new piezometers were designed and installed to characterize: i) the regional continuity and geometry of the Quaternary porous geologic media, ii) the bottom boundaries (depth to the top of the Tertiary/Devonian sedimentary bedrock) and eventually iii) propose a basin-scale conceptual groundwater flow model, named Lake Titicaca aquifer system. This is the first study at the scale of the Katari and Lago Menor basin to provide an integrated

understanding of the aquifer functioning and of nitrate sources and fate. This represents an element of novelty to the international audience and to decision makers.

In addition, groundwater samples from 52 deep wells (30–110 m b.g.l), 5 springs, 2 wetlands, and surface water from rivers (8), lagoons (3) in the upper part of the glaciated peaks and from the shore of Lake Titicaca (5), were collected for the analysis of major ion chemistry and dual isotopes of  $\delta^{15}N_{NO_3}$  and  $\delta^{18}O_{NO_3}$ , in order to trace the natural background levels of groundwater and if groundwater resource is threatened by agricultural leaching, livestock production and/or by domestic wastewater.

Results from the regional geophysical characterization confirmed that the Quaternary porous geologic media that fills up the Katari and Lago Menor Basin behaves as one single complex entity, hydraulically connected and that groundwater is moving in gravity-driven flow systems (Article I).

The findings of the basin-scale conceptual groundwater flow and the first numerical 2D modeling approach provided an advanced understanding of the groundwater flow dynamics under natural conditions and a guide to future data collection in order to improve the robustness of 3D future groundwater flow numerical modeling (Article II).

The use of hydrogeochemistry and dual isotopes of  $\delta^{15}N_{NO_3}$  and  $\delta^{18}O_{NO_3}$  allowed to characterize the groundwater hydrochemical patterns and their evolution, to determine nitrate pollution sources, fate and natural attenuation processes in the groundwater system (Article III).

The groundwater flow concept and nitrate fate are displayed in Figure 7.1. It corresponds to a classical gravity-driven regional groundwater flow (GDRGF). Six Subdomains (regions possessing different hydraulic properties) were identified. A large portion of the aquifer presents an unconfined behaviour, mainly on the Piedmont, whereas it remains confined in the plain areas. The thickness of the unconfined portion varies from 50 to 150 meters. Values of hydraulic conductivity for the unconfined portion range from  $1.1 \times 10^{-4}$  to  $5.9 \times 10^{-8} m/sec$ , specific yield ranges from 0.16 to 0.20 and recharge values range from 118 to 382 *mm/year*, while for the confined part

the transmissivity values range around  $6.0 \times 10^{-6} \text{ m}^2/\text{sec}$  with a storativity value of  $1.2 \times 10^{-2}$  to  $6.0 \times 10^{-3}$ .

Initially, water from relict rock glaciers and meteoric water enter the aquifer through the Eastern boundary and flows NE-SW. During this travel, an amount of water leaves the aquifer through a portion of the Southern and Northern boundaries. And another amount travels to the plain area, through subterranean channels, to finally leave the aquifer by seepage into the effluent Lake Titicaca. Subsequently, meteoric water enters into the aquifer over Subdomain 1 (glacial deposits), Subdomain 2 (fluvio-glacial deposits), Subdomain 3 (alluvial fan deposits), Subdomain 4 (fluvio-lacustrine deposits) and Subdomain 5 (Paleo-lacustrine deposits) (Figure 7.1). Besides, seepage from deep buried valleys allowing melt-water drainage also enters into the aquifer (Seque, Huayna Potosí and Jachallani rivers). Conversely, groundwater is lost inside the domain by evapotranspiration occurring due to shallow water tables (wetlands) over a portion of fluvio-glacial deposits, alluvial fan deposits and paleolacustrine deposits (Fig.7.1), by seepage into the effluents (Seco, Pampasi, Sorechata, Vilaque, Huayna Potosí and Khullukhachi rivers), and by leakage out into the overlying clay aquitard.

Notably, the high hydraulic heads, the lower mineralization, chemical and isotopic compositions represent a groundwater source of good quality in the high Piedmont areas. In contrast, the shallower water tables of the alluvial-fluvioglacial-lacustrine sequence in the lower sector of the Piedmont, make this area more vulnerable to contamination. In fact, chemical facies and the isotopic composition of the dissolved  $\text{NO}_3^-$  revealed that the main origin of this anion is related to nitrogen fertilizers towards the NW of the Piedmont and human/animal waste towards the SE. Moreover, natural nitrate attenuation processes occur mainly in the lower sector of the Piedmont, when groundwater mixes with the reservoir of lacustrine origin

On the other hand, groundwater flowing in the plain areas present primarily Na(K)-Cl facies relating the presence of evaporites. In this area groundwater is prone to contamination, especially when the clay layer is absent and in places where a connection to the Piedmont is evidenced (subterranean channels). The contribution of groundwater to the current Lake Titicaca (Cohana Bay) appears to be retarded due to the presence of the clay layer (Subdomain 6).

Finally, all the science-based information generated from this research was arranged into a GIS spatial database to support decision makers in the management and protection of groundwater resources within the Katari and Lago Menor region. This conceptual model also provides input datasets for future groundwater numerical modeling and a guide to future data collection, particularly in those areas where data are required to improve the robustness of a 3D groundwater flow numerical modeling. This information will also contribute to the environmental remediation of Lake Titicaca, a national priority for the Plurinational State of Bolivia.

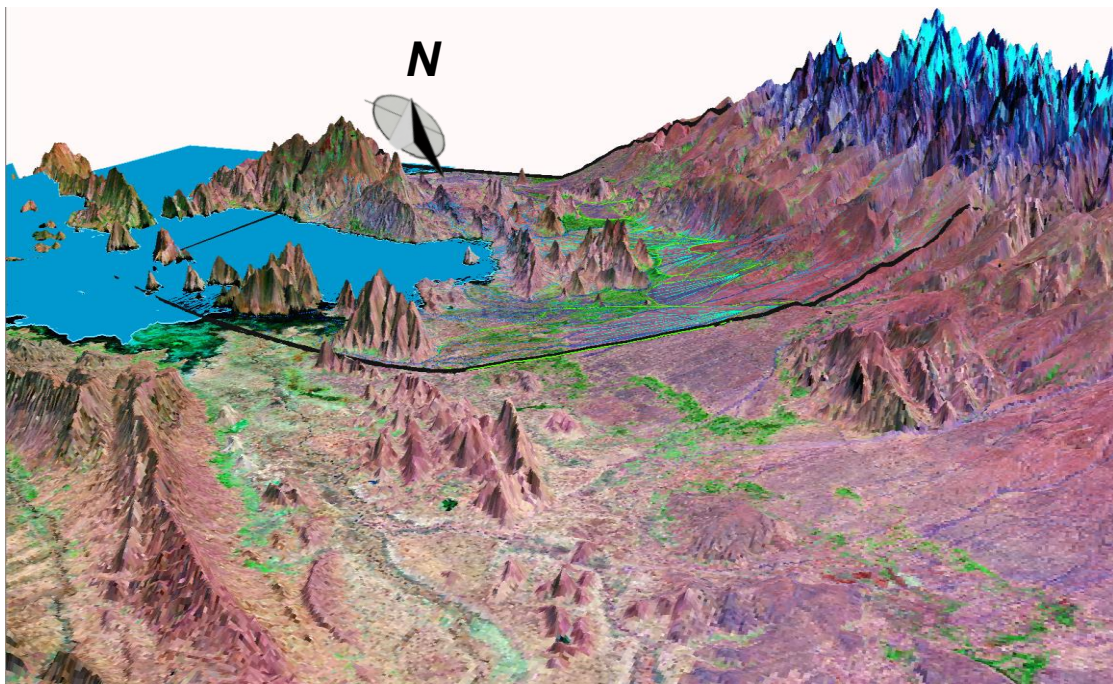


*Figure 7. 1. Location of the profile for the 3D cut.*

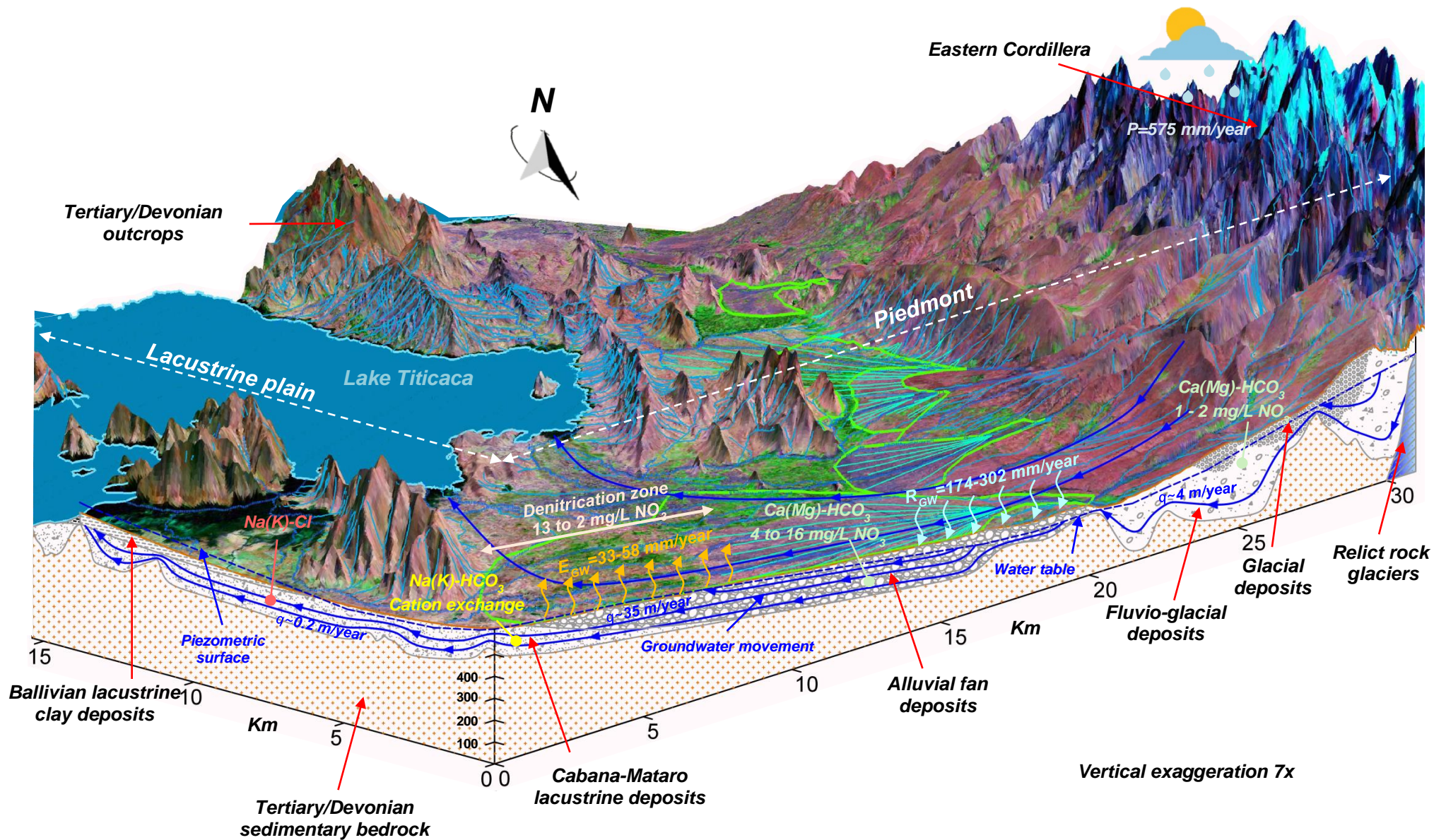


Figure 7. 2. Conceptual groundwater flow model incorporating the results of the different investigation techniques.

## 7.2 Perspectives

The present gravity-driven groundwater flow concept allowed the correct interpretation of natural flow processes and phenomena within the Katari and Lago Menor region. However, there is still more research needed in order to refine and improve the robustness of 3D groundwater flow numerical modeling. Thus, the future work following this study might be directed:

- To investigate the geometry and thickness of: i) glacial and fluvioglacial layers towards the NE sector of the Piedmont (Achacachi zone, yellow area of Fig.7.3), ii) the actual extent and thickness of the paleo-lacustrine clay layer (Ulloma formation), and iii) the extent and thickness of the paleo-lacustrine Cabana and Mataro formation (Qcb-mt) towards the south of Viacha (red area of Fig.7.3).
- To increase and improve the actual monitoring network considering the defined extension of the Domain and its Subdomains. These monitoring points should be instrumented anywhere possible considering at least a daily time step. A regional groundwater level monitoring network is essential to provide time series of groundwater levels for the flow system analysis, calibration of groundwater numerical models and as a basis to forecast the effects of some future action or hydrologic conditions.
- To conduct at least one multi-well pumping test in each defined Subdomain, considering that longer periods than 52 hours are required for displaying late-time response of the aquifer in the case of the Subdomains presenting unconfined behaviour.
- To investigate and quantify the discharge behavior of the alpine landforms in the Eastern boundary (Relict rock glaciers).
- To measure the exchange of water between surface water and groundwater inside the domain (seepage from influent rivers or seepage into effluent rivers).



- To investigate and quantify groundwater discharge by evapotranspiration in relation to water table depth (Wetlands). It is required to instrument the outflowing sites, located over a portion of Subdomain 2, Subdomain 3 and Subdomain 5, considering a daily time step as longer periods tends to disregard extrem events.
- To perform measurements of spring discharges along a portion of the Southern boundary. Time series information would allow the development of a transient numerical model which could also be used to investigate future modeling scenarios.
- To investigate the extent and thickness of paleo-lacustrine deposits (from Lake Mataro, Cabana and Ballivian) in the Tiwanacu region which appears to be an isolated aquifer if presenting the same behaviour as in the Lacustrine plain of the Katari and Lago Menor Basin aquifer.
- To investigate the chemical and isotopic compositions: i) of groundwater-lake interactions at the Puerto Pérez bays, ii) in the south of Viacha, iii) in the north of El Alto, and iv) in the north of Batallas (Figure 7.4).

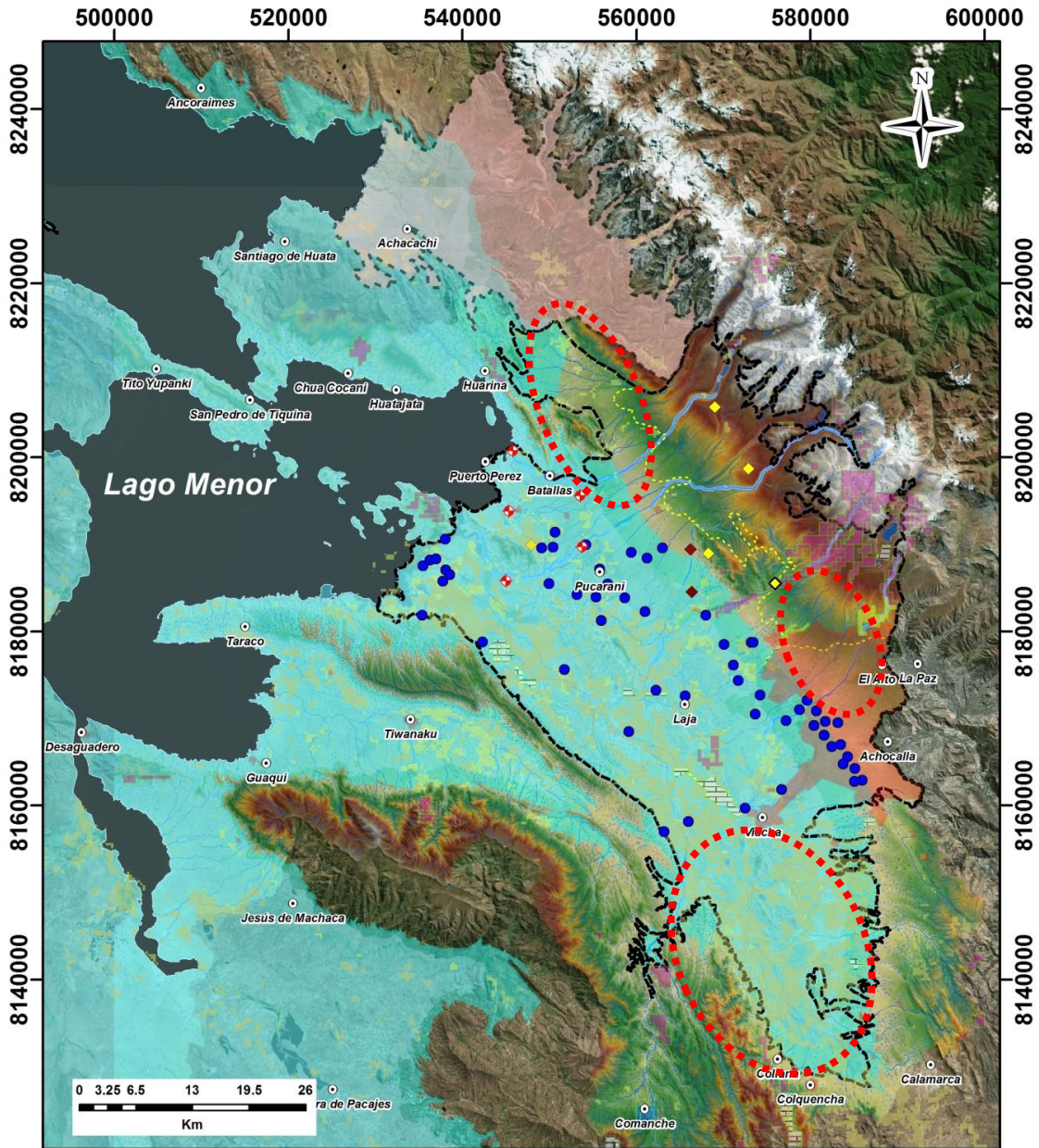


*Figure 7. 4. Map showing the current available groundwater sampling points for measuring hydrogeochemical and isotopic information within the Katari and Lago Menor Basin aquifer after the present investigation. The red areas indicate the future work that might be performed following this study.*

## References

- Abbott, M.B., Wolfe BB, Wolfe AP, Seltzer GO, Aravena R, Mark BG, Polissar PJ, Rodbell DT, Rowe HD, Vuille M (2003) Holocene paleohydrology and glacial history of the central Andes using multiproxy lake sediment studies. *Palaeogeography, Palaeoclimatology, Palaeoecology* 194 (2003) 123-138.
- A.E.M.R (2012) Applied ElectroMagnetic Research. TEM RESEARCHER version 8 Manual. Pages 1-63
- Autodesk (2019) AUTOCAD Student Version
- Agramont A, Craps M, Balderrama M, Huysmans M (2019) Transdisciplinary Learning Communities to Involve Vulnerable Social Groups in Solving Complex Water-Related Problems in Bolivia. *Water* 2019, 11, 385; doi:10.3390/w11020385
- Archundia D, Duwig C, Spadini L, Uzu G, Guedron S, Morel MC (2017a) How Uncontrolled Urban Expansion Increases the Contamination of the Titicaca Lake Basin (El Alto, La Paz, Bolivia). *Water Air And Soil Pollution*, 228(1)
- Archundia D, Duwig C, Lehembre F, Chiron S, Morel M-C, Prado B, Bourdat-Deschamps M, Vince E, **Flores Aviles G**, Martins JMF (2017b) Antibiotic pollution in the Katari subcatchment of the Titicaca Lake: major transformation products and occurrence of resistance genes. *Science of the Total Environment*, 576, 671–682.
- Archundia D, Boithias L, Duwig C, Morel, MC, **Flores Aviles G**, Martins J, 2018 Environmental fate and ecotoxicological risk of the Sulfamethoxazole antibiotic across the Katari catchment (Bolivian Altiplano): Application of the GREAT-ER model. *Science of the Total Environment* 622–623, 1046–1055.
- Argollo J, Murguiart P (1995) Los Climas Cuaternarios de Bolivia. *Cambios Cuaternarios en América del Sur*. J.Argollo & Ph. Murguiart (eds.) 1995, 135-155
- Argollo J, Murguiart P (2000) Late Quaternary climate history of the Bolivian Altiplano. *Quaternary International* 72, 37-51

- Argollo J, Iriondo M (2008) El Cuaternario de Bolivia y Regiones vecinas. ed.: Moglia (ISBN 9872463700), 280 pages
- Araújo LM, França AB, Potter PE (1999) Hydrogeology of the Mercosul aquifer system in the Paraná and Chaco-Paraná Basins, South America, and comparison with the Navajo-Nugget aquifer system, USA. *Hydrogeology Journal* (1999) 7:317–336
- ASTM D 4448-85a (1994) Standard Guide for Sampling Groundwater Monitoring Wells. American Society for Testing and Materials. Appendix C. pages 193-206
- Ballivian O, Bles JE, Servant M (1978) El Plio-Cuaternario de la Región de La Paz (Andes Orientales, Bolivia). *Cah. O.R.S.T.O.M., sér. Géol., vol. X, n°1, 1978, 101–113.*
- Barroso Chulve A, Garfias Soliz J (2010) Delimitación de la contaminación del agua subterránea por lixiviados en un till glacial del relleno sanitario “Villa Ingenio”: El Alto-Bolivia. Universidad Mayor Real Pontificia de San Francisco Xavier de Chuquisaca. Tesis de Posgrado. Maestría en Hidrogeología y Recursos Hídricos
- Bayanzul B, Nakamura K, Machida I, Watanabe N, Komai T (2018) Construction of a conceptual model for confined groundwater flow in the Gunii Khooloi Basin, Southern Gobi Region, Mongolia. *Hydrogeology Journal*. <https://doi.org/10.1007/s10040-019-01955-8>
- B.I.D (2016) Programa de Saneamiento del Lago Titicaca (Cuenca Katari, Bahía Cohana) BO-L1118. Marco de Gestión Ambiental y Social (MGAS), 87 pages.
- Bolivian Water Law of 1906, in force at the present, available at <https://bolivia.infoleyes.com/norma/2442/reglamento-de-aguas-s-n-de-08-09-1879>
- Bush MB, Hanselman JA, Gosling WD (2010) Nonlinear climate change and Andean feedbacks: an imminent turning point? *Global Change Biology* (2010), doi: 10.1111/j.1365-2486.2010.02203.x.
- Bredehoeft J (2004) The conceptualization model problem—surprise. *Hydrogeol J* (2005) 13:37–46

- Calderón H, Bentley L (2007) A regional-scale groundwater flow model for the Leon-Chinandega aquifer, Nicaragua. *Hydrogeology Journal* (2007) 15: 1457–1472
- Canedo C, Pillco Zolá R, Berndtsson R (2016) Role of Hydrological Studies for the Development of the TDPS System. *Water* 2016, 8, 144; doi:10.3390/w8040144
- Condom T, Coudrain A, Dezetter A, Brunstein D, Delclaux F, Jean-Emmanuel Sicart (2004) Transient modelling of lacustrine regressions: two case studies from the Andean Altiplano. *HYDROLOGICAL PROCESSES Hydrol. Process.* 18, 2395–2408 (2004)
- Corbet T (2000) A groundwater-basin approach to conceptualize and simulate post-Pleistocene subsurface flow in a semi-arid region, southeastern New Mexico and western Texas, USA. *Hydrogeology Journal* (2000) 8: 310-327
- Cross S, Baker P, Seltzer G, Fritz S, Dunbar R (2001) Late Quaternary Climate and Hydrology of Tropical South America Inferred from an Isotopic and Chemical Model of Lake Titicaca, Bolivia and Perú. *Quaternary Research* 56:1, pp. 1-9; doi 10.1006/qres.2001.2244.
- D'Agostino K, Geoffrey S, Paul B, Fritz S, Dunbar R (2002) Late-Quaternary lowstands of Lake Titicaca: Evidence from high-resolution seismic data. *Palaeogeography, Palaeoclimatology, Palaeoecology* 179:1-2, pp. 97-111; doi:10.1016/S0031-0182(01)00411-4.
- Delclaux F, Coudrain A, Condom T (2007) Evaporation estimation on Lake Titicaca: a synthesis review and modelling. *Hydrol. Process.* 21, 1664–1677 (2007). DOI: 10.1002/hyp.6360
- Diersch HJ (2014) *FEFLOW Finite Element Modeling of Flow, Mass and Heat Transport in Porous and Fractured Media*. Springer Heidelberg New York Dordrecht London
- Doble RC, Crosbie RS (2017) Review: Current and emerging methods for catchment-scale modelling of recharge and evapotranspiration from shallow groundwater. *Hydrogeol J* (2017) 25:3–23. DOI 10.1007/s10040-016-1470-3

- Ebrahim GY, Villholth KG, Bolous M (2019) Integrated hydrogeological modelling of hard-rock semi-arid terrain: supporting sustainable agricultural groundwater use in Hout catchment, Limpopo Province, South Africa. *Hydrogeology Journal*. <https://doi.org/10.1007/s10040-019-01957-6>
- ESRI (2018) ArcGIS Desktop: Release 10. Redlands, CA: Environmental Systems Research Institute
- F.A.O. (1999) Organización de las Naciones Unidas para la Agricultura y la Alimentación Bolivia hacia una estrategia de Fertilizantes. Informe preparado para el Gobierno de Bolivia por el Proyecto Manejo de Suelos y Nutrición Vegetal en Sistemas de Cultivos GCPF/BOL/018/NET – “Fertisuelos”
- Fernandes AJ, Maldaner CH, Negri F, Rouleau A, Wahnfried ID (2016) Aspects of a conceptual groundwater flow model of the Serra Geral basalt aquifer (Sao Paulo, Brazil) from physical and structural geology data. *Hydrogeol J* (2016) 24:1199–1212. DOI 10.1007/s10040-016-1370-6
- Foster S, Koundouri P, Tuinhof A, Kemper K, Nanni M, Garduno H (2006) Groundwater dependent ecosystems: the challenge of balanced assessment and adequate conservation. GW Mate briefing note series; no. 15. Washington, DC: World Bank. <http://documents.worldbank.org/curated/en/407851468138596688>
- Fonturbel F (2005) Physico-chemical and biological indicators of the eutrophication process at Titicaca Lake (Bolivia). *Ecología Aplicada*, 2005, 135–141
- Freeze and Cherry (1979) *Environmental Isotopes in Hydrogeology*. p. 149, p.150, p.151, available at <http://hydrogeologistswithoutborders.org/wordpress/1979-toc/>
- Fritz SC, Baker PA, Lowenstein TK, Seltzer GO, Rigsby CA, Dwyer GS, Tapia PM, Arnold KK, Ku TL, Luo S (2004) Hydrologic variation during the last 170,000 years in the southern hemisphere tropics of South America. *Quaternary Research* 61 (2004) 95– 104. doi:10.1016/j.yqres.2003.08.007
- Fritz SC, Baker PA, Tapia P, Garland J (2006) Spatial and temporal variation in cores from Lake Titicaca, Bolivia/Peru during the last 13,000 years. *Quaternary*

- International 158:1 (December 2006), pp. 23-29, in a special issue “Holocene environmental catastrophes in South America: from the lowlands to the Andes”; doi:10.1016/j.quaint.2006.05.014
- Fritz SC; Baker PA; Seltzer GO; Ballantyne A; Tapia P; Cheng H, Edwards, RL (2007) Quaternary glaciation and hydrologic variation in the South American tropics as reconstructed from the Lake Titicaca drilling project. *Quaternary Research* 68:3, pp. 410-420; doi:10.1016/j.yqres.2007.07.008
- Fritz SC, Baker PA, Tapia, Ballantyne A, Tapia P, Spanbauer T, Westover K (2012) Evolution of the Lake Titicaca basin and its diatom flora over the last ~370,000 years. *Palaeogeography, Palaeoclimatology, Palaeoecology* 317–318 (2012) 93–103.
- G.E.O.S.I.R.H. (2017) Infraestructura de Datos Espaciales. Plan Director de la Cuenca Katari y Lago Menor del Titicaca. Available at <http://geosirh.riegobolivia.org/layers/geosirh>. Ministerio de Medio Ambiente y Agua. Viceministerio de Recursos Hídricos y Riego.
- G.E.O.B.O.L & Swedish Geological AB Suecia (1995) Calamarca 5943, Jesús Macha 5843, Tiahuanacu 5844, La Paz 5944, Achacachi 5845 and Milluni 5945 Geological sheets. Servicio Geológico de Bolivia.
- Gómez-López E (2012) Caracterización hidrogeoquímica del sistema acuífero Purapurani. Universidad Mayor Real Pontificia de San Francisco Xavier de Chuquisaca. Tesis de Posgrado. Maestría en Hidrogeología y Recursos Hídricos
- Gómez E, Larsson M, Dahlin T, Barmen G, Rosberg JE (2019) Alluvial aquifer thickness and bedrock structure delineation by electromagnetic methods in the highlands of Bolivia. *Environmental Earth Sciences* (2019) 78:84 <https://doi.org/10.1007/s12665-019-8074-x>
- Gonzales-Amaya A, Mardh J, Dahlin T (2018) Delimiting a saline water zone in Quaternary fluvial–alluvial deposits using transient electromagnetic: a case study in Punata, Bolivia. *Environmental Earth Sciences* (2018) 77:46. <https://doi.org/10.1007/s12665-017-7213-5>

- Gonzales Amaya A, Ortiz J, Durán A, Villazón M (2018) Hydrogeophysical methods and hydrogeological models: basis for groundwater sustainable management in Valle Alto (Bolivia). *Sustainable Water Resources Management* <https://doi.org/10.1007/s40899-018-0293-x>
- Grenier C, Régnier D, Mouche E, Benabderrahmane H, Costard F, Davy P (2013) Impact of permafrost development on groundwater flow patterns: a numerical study considering freezing cycles on a two-dimensional vertical cut through a generic river-plain system. *Hydrogeology Journal* (2013) 21: 257–270. DOI 10.1007/s10040-012-0909-4
- Grizard P, Schmitt JM, Goblet P (2018) Hydrogeology of an arid endorheic basin (Tsagaan Els, Dornogobi, Mongolia): field data and conceptualization, three-dimensional groundwater modeling, and water budget. *Hydrogeology Journal* <https://doi.org/10.1007/s10040-018-1868-1>
- Guédron S, Point D, Acha D, Bouchet S, Baya PA, Tessier E, Monperrus M, Molina CI, Groleau A, Chauvaud L, Thebault J, Amice E, Alanoca L, Duwig C, Uzu G, Lazarro X, Bertrand A, Bertrand S, Barbraud C, Delord K, Gibon FM, Ibanez C, Flores M, Fernandez Saavedra P, Ezpinoza ME, Heredia C, Rocha F, Zepita C, Amouroux D (2017) Mercury contamination level and speciation inventory in Lakes Titicaca & Uru-Uru (Bolivia): Current status and future trends. *Environmental Pollution* 231 (2017) 262-270
- Guérin R, Descloitres M, Coudrain A, Talbi A, Gallaire R (2001) Geophysical surveys for identifying saline groundwater in the semi-arid region of the central Altiplano, Bolivia. *Hydrol. Process.* 15, 3287–3301 (2001), DOI: 10.1002/hyp.284
- Heine K (2004) Late Quaternary Glaciations of Bolivia. *Quaternary Glaciations-Extent and Chronology, Part III*, Elsevier B.V, 83–87
- Hu L, Jiao JJ (2015) Calibration of a large-scale groundwater flow model using GRACE data: a case study in the Qaidam Basin, China. *Hydrogeology Journal*. DOI 10.1007/s10040-015-1278-6

- Izady A, Davary K, Alizadeh A, Ziaei AN, Akhavan S, Alipoor A, Joodavi A, Brusseau ML (2015) Groundwater conceptualization and modeling using distributed SWAT based recharge for the semi-arid agricultural Neishaboor plain, Iran 2015. *Hydrogeology Journal* (2015) 23: 47–68. DOI 10.1007/s10040-014-1219-9
- Jayne RS, Pollyea RM, Dodd JP, Olson EJ, Swanson SK (2016) Spatial and temporal constraints on regional-scale groundwater flow in the Pampa del Tamarugal Basin, Atacama Desert, Chile. *Hydrogeol J*. DOI 10.1007/s10040-016-1454-3
- Jiráková H, Huneau F, Celle-Jeanton H, Hrkal Z, Le Coustumer P (2010) Insights into palaeorecharge conditions for European deep aquifers. *Hydrogeology Journal* (2011) 19: 1545–1562. DOI 10.1007/s10040-011-0765-7
- Kaiser J, Hastings MG, Houlton BZ, Röckmann T, Sigman D (2007) Triple Oxygen Isotope Analysis of Nitrate Using the Denitrifier Method and Thermal Decomposition of N<sub>2</sub>O. *Anal. Chem.* 2007, 79, 599-607
- Kane DL, Yoshikawa K, McNamara JP (2012) Regional groundwater flow in an area mapped as continuous permafrost, NE Alaska (USA). *Hydrogeology Journal* (2013) 21: 41–52. DOI 10.1007/s10040-012-0937-0
- Kendall C, Elliott EM, Wankel SD (2007) Tracing anthropogenic inputs of nitrogen to ecosystems, Chapter 12, In: R.H. Michener and K. Lajtha (Eds.), *Stable Isotopes in Ecology and Environmental Science*, 2nd edition, Blackwell Publishing, p. 375- 449
- Kinouchi T, Liu T, Mendoza J, Asaoka Y (2013) Modeling glacier melt and runoff in a high-altitude headwater catchment in the Cordillera Real, Andes. *Hydrol. Earth Syst. Sci. Discuss.*, 10, 13093–13144, 2013. DOI:10.5194/hessd-10-13093-2013
- Kinouchi T, Nakajima T, Mendoza J, Fuchs P, Asaoka Y (2019) Water security in high mountain cities of the Andes under a growing population and climate change: A case study of La Paz and El Alto, Bolivia. *Water Security* 6 (2019) 100025. <https://doi.org/10.1016/j.wasec.2019.100025>
- Lachaal F, Mlayah A, Anane M, Bédir M, Tarhouni J, Leduc C (2011) Comprehension and hydrogeological conceptualization of aquifer in arid and semi-arid regions using

- integrated hydrogeological information system: case of the deep aquifer of Zéramdine-Béni Hassen (east-central Tunisia). *Arab J Geosci*. DOI 10.1007/s12517-011-0498-x
- Lamb S, Hoke L (1997) Origin of the high plateau in the Central Andes, Bolivia, South America. *Tectonics*, Vol.16, N°4, Pages 623-649, August 1997.
- Lavenu A (1981) Origin et évolution néotectonique du lac Titicaca. *Rev. Hydrobiol. trop.* 14 (4): 289-297 (1981).
- Lavenu A (1992) Origins: Formation and geological evolution. C. Dejoux and A. Iltis (Eds.). *Lake Titicaca*, 3-15. 589 Pages
- Lazzaro X, Rybarczyk H, Meziane T, Hubas C, Lamy D, Point D, Martinez JM, Guédron S, Duwig C, Groleau A, Rocha S, Alcoreza MP, Lanza WG, Flores AJ, Loyza EZ, Ibañez L, Nuñez J, Gamarra C, Villanueva C, La Cruz L, Villafañe V, Helbling W, Lebourges A (2016) Accelerated eutrophication in Lake Titicaca: historical evolution, mechanisms, monitoring, and observatory approach. In : Guédron Stéphane (ed.), Acha Cordero D. (ed.), Vella M.A. (ed.), Ramos Ramos O.E. (ed.) *International colloquium on current and ancient contamination in Andes aquatic ecosystems proceedings*
- Lemke LD, Cypher JA (2009) Postaudit evaluation of conceptual model uncertainty for a glacial aquifer groundwater flow and contaminant transport model. *Hydrogeology Journal* (2010) 18: 945–958. DOI 10.1007/s10040-009-0554-8
- Limpias-Camacho MF, Bethune D (2010) Impacto de la ciudad de El Alto en el Campo de Pozos Tilata. Universidad Mayor Real Pontificia de San Francisco Xavier de Chuquisaca. Tesis de Posgrado. Maestría en Hidrogeología y Recursos Hídricos
- Mazor E (2004) *Chemical and Isotopic Groundwater Hydrology*. Third Edition, Marcel Dekker, Inc. Pages 392-409
- Maldonado L, Bécher F, Cabrera A, Blarasina M, Lutria V, Matteoda E, Giuliano J (2018) Hydrogeochemical features and groundwater renewal rate estimates from

- deep aquifers in the Pampean plain, Córdoba province, Argentina. *Journal of South American Earth Sciences* 85 (2018) 126–134
- Mádl-Szönyl J, Tóth Á (2015) Basin-scale conceptual groundwater flow model for an unconfined and confined thick carbonate region. *Hydrogeology Journal* (2015) 23: 1359–1380. DOI 10.1007/s10040-015-1274-x
- Melly BL, Schael DM, Gama PT (2017) Perched wetlands: An explanation to wetland formation in semi-arid areas. *Journal of Arid Environments* 141 (2017) 34e39
- Michael HA, Voss CI (2009) Estimation of regional-scale groundwater flow properties in the Bengal Basin of India and Bangladesh. *Hydrogeology Journal* (2009) 17: 1329–1346
- M.M.A.y.A (2010) Implementación de la Cuenca Pedagógica del Río Katari “Fase 0” Ministerio de Medio Ambiente y Agua/Viceministerio de Recursos Hídricos y Riego, La Paz, Bolivia, p.6, p.7, p.8. [www.mmaya.gob.bo](http://www.mmaya.gob.bo)
- M.M.A.y.A – Environmental Audit (2014) Informe de Auditoría sobre el Desempeño Ambiental respecto de la Contaminación Hídrica en la Cuenca del Río Katari y la Bahía de Cohana K2/AP05/J13 (available at <https://www.contraloria.gob.bo/portal>)
- M.M.A.y.A (2014) Plan Maestro Metropolitano de Agua Potable y Saneamiento La Paz-El Alto Bolivia. Ministerio de Medio Ambiente y Agua/Viceministerio de Recursos Hídricos y Riego, La Paz, Bolivia, p.106-172. [www.mmaya.gob.bo](http://www.mmaya.gob.bo)
- M.M.A.y.A (2016) Plan de Manejo Preliminar de los Acuíferos de Purapurani y Viacha. Ministerio de Medio Ambiente y Agua/Viceministerio de Recursos Hídricos y Riego, La Paz, Bolivia, 184 pages.
- M.M.A.y.A (2019) El Alto avanza en cobertura de agua y alcantarillado. Ministerio de Medio Ambiente y Agua/Viceministerio de Recursos Hídricos y Riego, La Paz, Bolivia. Año 3, Separata N°22, p.1-4. [www.mmaya.gob.bo](http://www.mmaya.gob.bo)

- Mira A, Veroslavsky G, Rossello E, Vives L (2015) Subsurface geological modeling of Corrientes province (NE Argentina) and its relationships with the Guaraní Aquifer system function. *Journal of South American Earth Sciences* 62 (2015) 148-163.
- Murray BP, Horton BK, Matos R, Heizler MT (2010) Oligocene–Miocene basin evolution in the northern Altiplano, Bolivia: Implications for evolution of the central Andean backthrust belt and high plateau. *GSA Bulletin*; September/October 2010; v. 122; no. 9/10; p. 1443–1462; doi: 10.1130/B30129.1
- Navarro de León I, Gárfias-Soliz J, Mahlknecht J (2005) Groundwater flow regime under natural conditions as inferred from past evidence and contemporary field observations in a semi-arid basin: Cuenca de la Independencia, Guanajuato, México. *Journal of Arid Environments* 63 (2005) 756–771
- N.A.S.A (2000) Shuttle Radar Topography Mission (SRTM) 1 Arc-Second Global, project from the National Aeronautics and Space Administration. Available at <http://dds.cr.usgs.gov/ee-data/coveragemaps/shp/ee/srtm/srtm.zip>
- Nickson A, Vargas C (2002) The limitations of water regulation: The failure of the Cochabamba concession in Bolivia. *Bulletin of Latin America Research*, Vol.21, N°1, pp- 99-120, 2002
- Nielsen (2006) *Practical Handbook of Environmental Characterization and Ground-Water Monitoring*. Second Edition. CRC Press by Taylor & Francis. Pages 639-806; 1113-1134
- Oyarzún R, Barrera F, Salazar P, Maturama H, Oyarzún J, Aguirre E, Alvarez P, Jourde H, Kretschmer N (2014) Multi-method assessment of connectivity between surface water and shallow groundwater: the case of Limarí River basin, north-central Chile. *Hydrogeology Journal* (2014) 22: 1857–1873. DOI 10.1007/s10040-014-1170-9
- Özen A, Karapinar B, Kucuk I, Jeppesen E, Beklioglu M (2010) Drought-induced changes in nutrient concentrations and retention in two shallow Mediterranean lakes subjected to different degrees of management. *Hydrobiologia*, 646:61–72

- Passadore G, Monego M, Altissimo L, Sottani A, Putti , Rinaldo A (2012) Alternative conceptual models and the robustness of groundwater management scenarios in the multi-aquifer system of the Central Veneto Basin, Italy. *Hydrogeology Journal* (2012) 20: 419–433
- Pauritsh M, Wagner T, Winkler G, Birk S (2017) Investigating groundwater flow components in an Alpine relict rock glacier (Austria) using a numerical model. *Hydrogeol J* (2017) 25:371–383. DOI 10.1007/s10040-016-1484-x
- Pilla G, Sacchi E, Zuppi G, Braga G, Ciancetti G (2006) Hydrochemistry and isotope geochemistry as tools for groundwater hydrodynamic investigation in multilayer aquifers: a case study from Lomellina, Po plain, South-Western Lombardy, Italy. *Hydrogeology Journal* (2006) 14: 795–808, DOI 10.1007/s10040-005-0465-2
- Pillco-Zolá R, Bengtsson L, Berndtsson R, Martí-Cardona B, Satgé F, Timouk F, Bonnet MP, Mollericon L, Gamarra C, Pasarepa J (2019) Modelling Lake Titicaca's daily and monthly evaporation. *Hydrol. Earth Syst. Sci.*, 23, 657–668, 2019 <https://doi.org/10.5194/hess-23-657-2019>
- Placzek CJ, Quade J, Patchett PJ (2011) Isotopic tracers of paleohydrologic change in large lakes of the Bolivian Altiplano. *Quaternary Research* 75 (2011) 231–244.
- Quesada B, Sylvestre F, Vimeux F, Black J, Christine P, Sonzogni C, Alexandre A, Blard P, Tonetto A, Mazur JC, Bruneton H (2015) Impact of Bolivian paleolake evaporation on the d18O of the Andean glaciers during the last deglaciation (18.5e11.7 ka): diatom-inferred d18O values and hydro-isotopic modeling. *Quaternary Science Reviews* 120 (2015) 93e106. <https://hal.archives-ouvertes.fr/hal-01909526>
- Quino Lima I, Ormachea Muñoz M, Ramos Ramos OE, Bhattacharya P, Quispe Choque R, Quintanilla Aguirre J, Sracek O (2019) Hydrochemical assessment with respect to arsenic and other trace elements in the Lower Katari Basin, Bolivian Altiplano. *Groundwater for Sustainable Development* 8 (2019) 281–293

- Rabatel A, Machaca A, Francou B, Jomelli V (2006) Glacier recession on Cerro Charquini (16°S), Bolivia, since maximum of the Little Ice Age (17th century) . Journal of Glaciology, Vol.52, N°176, 2006
- Rangecroft S, Harrison S, Anderson K (2014) Rock glaciers, water security and climate change in the Bolivian Andes. University of Exeter as a thesis for the degree of Doctor of Philosophy in Physical Geography, Oct 2014
- Rangecroft S, Suggitt AJ, Anderson K, Harrison S (2016) Future climate warming and changes to mountain permafrost in the Bolivian Andes. Climatic Change. DOI 10.1007/s10584-016-1655-8
- Robertson DM, Rose WJ, Saad DA (2005) Water quality, hydrology, and phosphorus loading to Little St. Germain Lake, Wisconsin, with special emphasis on the effects of winter aeration and groundwater inputs. US Geol Surv Sci Invest Rep 2005-5071.
- Roeder D (1988) Andean-Age structure of Eastern Cordillera (Province of La Paz, Bolivia). Tectonics, Vol.7, N°1, Pages 23-39, February 1988.
- Sahoo S, Jha MK (2017) Numerical groundwater-flow modeling to evaluate potential effects of pumping and recharge: implications for sustainable groundwater management in the Mahanadi delta region, India. Hydrogeol J (2017) 25:2489–2511. DOI 10.1007/s10040-017-1610-4
- Saltel M, Rebeix R, Thomas B, Franceschi M, Lavielle B, Bertran P (2019) Paleoclimate variations and impact on groundwater recharge in multi-layer aquifer systems using a multi-tracer approach (northern Aquitaine basin, France). Hydrogeology Journal. <https://doi.org/10.1007/s10040-019-01944-x>
- Salvaderry - Aranguren MM, Probst A, Roulet M, Isaure MP (2008) Contamination of surface waters by mining wastes in the Milluni Valley (Cordillera Real, Bolivia): Mineralogical and hydrological influences.
- Sapina Juan Nuria, 2018. Groundwater modelling of the Katari watershed aquifer with Feflow model. Grenoble INP -ENS3. Internship supervised by Gabriela Flores Avilés and Yvan Rossier.

- Sánchez-Saldías A, Fariña RA (2014) Palaeogeographic reconstruction of Minchin palaeolake system, South America: The influence of astronomical forcing. *Geoscience Frontiers* 5 (2014) 249e259. <http://dx.doi.org/10.1016/j.gsf.2013.06.004>
- Sanders L (1998) A manual of Field Hydrogeology. Prentice-Hall, Inc. Pages 233-261, 263-301
- Saroli M, Lancia M, Albano M, Casale A, Giovinco G, Petitta M, Zarlenga F, dell'Isola M (2017) A hydrogeological conceptual model of the Suio hydrothermal area (central Italy). *Hydrogeol J* (2017) 25:1811–1832. DOI 10.1007/s10040-017-1549-5
- Sauriol J (2016) Provenance of buried esker groundwater: the case of Vars-Winchester esker aquifer, Eastern Ontario, Canada. *Hydrogeol J* (2016) 24:123–139. DOI 10.1007/s10040-015-1327-1
- Schwartz F, Zhang H (2003) *Fundamentals of Ground Water*. Press by Jhon Wiley & Sons, Inc. Pages 369-395
- Shaw RD, Shaw JFH, Fricker H, Prepas EE (1990) An integrated approach to quantify groundwater transport of phosphorus to Narrow Lake, Alberta. *Limnol. Oceanogr.*,35 (4),870–886
- Sigman DM, Caciotti KL, Andreani M, Barford C, Galanter M, Böhkke (2001) A Bacterial Method for the Nitrogen Isotopic Analysis of Nitrate in Seawater and Freshwater. *Anal. Chem.* 2001, 73, 4145-4153
- Simler R (2014) Manuel d'utilisation DIAGRAMMES. Pages 1-42
- Soruco A, Vincent C, Rabatel A, Francou B, Thibert E, Sicart JM, Condom T (2015) Contribution of glacier runoff to water resources of La Paz city, Bolivia (16° S). *Annals of Glaciology* 56(70) 2015 doi: 10.3189/2015AoG70A001
- Solinst (2018) *Levelogger Series User Guide*. 2018 Solinst Canada Ltd. All rights reserved.
- Spadini (2013) Analyse des anions d'eaux usées (et potables): Chromatographie ionique. IGE (Institut des Géosciences de l'Environnement). Pages 1-15

- Sterckx A, Lemieux JM, Vaikmäe R (2018) Assessment of paleo-recharge under the Fennoscandian Ice Sheet and its impact on regional groundwater flow in the northern Baltic Artesian Basin using a numerical model. *Hydrogeology Journal* (2018) 26:2793–2810. <https://doi.org/10.1007/s10040-018-1838-7>
- Sugaki A, Kitakaze A (1988) Tin-bearing Minerals from Bolivian Polymetallic Deposits and their Mineralization Stages. *Mining Geology*, 38(5) 419-435, 1988
- Tóth J (1962) A theory of Groundwater Motion in Small Drainage Basins in Central Alberta, Canadá. *Journal of Geophysical Research*, Vol.67, N°11
- Tóth J (1963) A theoretical Analysis of Groundwater Flow in Small Drainage Basins. *Journal of Geophysical Research*, Vol.68, N°16
- Tóth J (1995) Hydraulic Continuity in large Sedimentary Basins. *Hydrogeology Journal*, v.3, no 4, 1995
- Tóth J (1999) Groundwater as a geologic agent: An overview of the causes, processes, and manifestations. *Hydrogeology Journal* (1999) 7:1–14
- Tóth J (2010) The theory of basinal gravity flow of groundwater and its impacts on hydrology Japan. *Special Issue Review* 335-354 (2010)
- Turner RJ, Mansour MM, Dearden R, Dochartaigh BEO, Hughes AG (2015) Improved understanding of groundwater flow in complex superficial deposits using three-dimensional geological-framework and groundwater models: an example from Glasgow, Scotland (UK). *Hydrogeology Journal* (2015) 23: 493–506. DOI 10.1007/s10040-014-1207-0
- Uribe J, Muñoz JF, Gironás J, Oyarzún R, Aguirre E, Aravena R (2015) Assessing groundwater recharge in an Andean closed basin using isotopic characterization and a rainfall-runoff model: Salar del Huasco basin, Chile. *Hydrogeology Journal* (2015) 23: 1535–1551, DOI 10.1007/s10040-015-1300-z

- Van der Kamp G, Hayashi M (2009) Groundwater-wetland ecosystem interaction in the semiarid glaciated plains of North America. *Hydrogeology Journal* (2009) 17: 203–214
- Varni MR, Usunoff EJ (1999) Simulation of regional-scale groundwater flow in the Azul River basin, Buenos Aires Province, Argentina. *Hydrogeology Journal* (1999) 7:180–187
- Veettil BK, Wang S, Simões JC, Ruiz Pereira SF (2018) Glacier monitoring in the eastern mountain ranges of Bolivia from 1975 to 2016 using Landsat and Sentinel-2 data. *Environmental Earth Sciences* (2018) 77:452. <https://doi.org/10.1007/s12665-018-7640-y>
- Viguiier B, Jourde H, Yáñez G, Lirab E, Leonardia V, Moya C, García-Pérez T, Maringue J, Lictevoute E (2018) Multidisciplinary study for the assessment of the geometry, boundaries and preferential recharge zones of an overexploited aquifer in the Atacama Desert (Pampa del Tamarugal, Northern Chile). *Journal of South American Earth Sciences* 86 (2018) 366–383.
- Wei G, Chen F, Ma J, Dong Y, Zhu G, Edmunds WM (2014) Groundwater recharge and evolution of water quality in China's Jilantai Basin based on hydrogeochemical and isotopic evidence. *Environ Earth Sci* DOI 10.1007/s12665-014-3257-y
- Winkler G, Wagner T, Pauritsch M, Birk S, Kellerer-Pirklbauer A, Benischke R, Leis A, Morawetz R, Schreilechner MG, Hergarten S (2016) Identification and assessment of groundwater flow and storage components of the relict Schöneben Rock Glacier, Niedere Tauern Range, Eastern Alps (Austria). *Hydrogeol J* (2016) 24:937–953. DOI 10.1007/s10040-015-1348-9
- Woods S, MacDonald LH, Westbrook CJ (2006) Hydrologic interactions between an alluvial fan and a slope wetland in the Central Rocky Mountains, USA. *WETLANDS*, Vol. 26, No. 1, March 2006, pp. 230–243
- Yousif M, van Geldern R, Bubenzer O (2016) Hydrogeological investigation of shallow aquifers in an arid data-scarce coastal region (El Dab'a, northwestern Egypt) *Hydrogeol J* (2016) 24:159–179, DOI 10.1007/s10040-015-1308-4

Zeballos A, Weihd P, Blanco M, Machaca V (2016) Geological, mineralogical and chemical characterization of Devonian kaolinite-bearing sediments for further applications in the ceramic (tiles) industry in La Paz, Bolivia. *Environ Earth Sci* (2016) 75:546. DOI 10.1007/s12665-015-5212-y.

Zeballos A, Weihd P, Blanco M, Machaca V (2017) Characterization of some nonmetallic resources in Bolivia: an overview of their potentiality and their application in specialized formulations. *Environ Earth Sci* (2017) 76:754 DOI 10.1007/s12665-017-7094-7

Zech R, Kull Ch, Kubik PW, Veit H (2007) LGM and Late Glacial glacier advances in the Cordillera Real and Cochabamba (Bolivia) deduced from <sup>10</sup>Be surface exposure dating. *Clim. Past*, 3, 623–635, 2007.

Zhou Y, Li W (2011) A review of regional groundwater flow modeling. *GEOSCIENCE FRONTIERS* 2(2) (2011) 205e214 available at [www.sciencedirect.com](http://www.sciencedirect.com)

Zhou Y, Heralth HMPSD (2017) Evaluation of alternative conceptual models for groundwater modelling. *Geoscience Frontiers* 8 (2017) 437e443

# **APPENDIX**

---

## **APPENDIX A:**

### *Pumping test performed at Subdomain 2(fluvioglacial deposits)*

A pumping test was performed during March 2013 (raw field data available at MMAyA geodatabase). The monitoring well P-180 was pumped at a pumping rate of 10.4 L/sec. The duration of the pumping test was 51.7 hours, then the pump was turned off and it reached the steady state after 29.2 hours. The drawdowns, measured in the pumping well and in two observation wells, (OW-1) at 4.7 m away and (OW-2) at 4.1 m, are shown in Fig. A1.

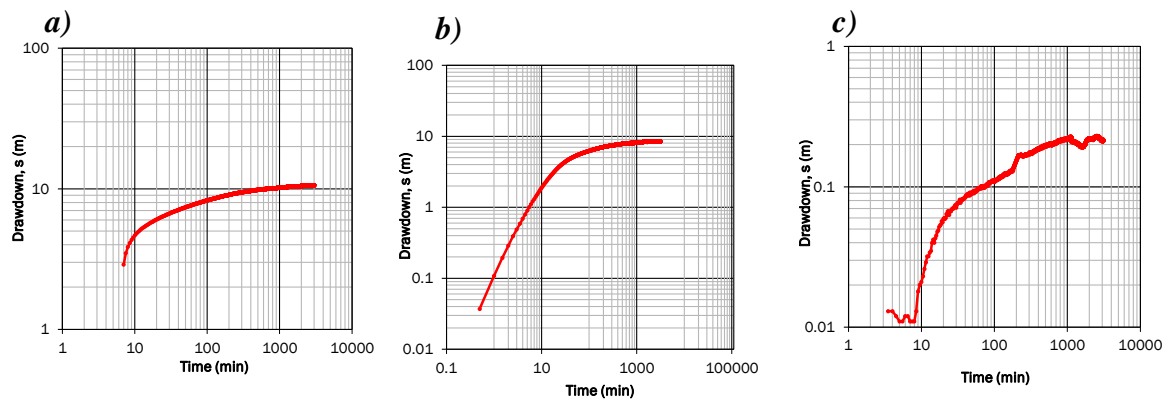


*Figure A1. Field data plot on logarithmic scale for Neuman curve matching technique, a) field data for the pumping well P-180, b) for OW-1 and c) for OW-2 (raw field data is available at MMAyA geodatabase).*

Apparently, the logarithmic plots show the response for an unconfined aquifer at early and medium pumping times. It shows a flat segment at medium pumping times ~600 min (Fig. 1b) reflecting a recharge from an overlying layer which may stabilize the drawdown. The duration of the pumping test didn't allow recording the response at late-times. According to Kruseman & De Ridder (1990) the duration of pumping tests in unconfined aquifers requires a longer period for reaching equilibrium conditions, around 3 days.

From geophysics results, the monitoring well P-180 (A-9) drilled at a depth of 123 m, may traverse layer 2 (Table 1, fluviglacial deposits) and layer 5 (Table 2, paleo-lacustrine deposits).

Considering the solution of Neuman (1975) for unconfined aquifers, from the theoretical curves of  $W(u_A, u_B, \beta)$  versus  $(1/u_A), (1/u_B)$  reported in Freeze and Cherry (1979), we will have the following parameters.

The early time segment of the plot gives the best match with the Neuman type A curve for  $\beta = 0.03$ . The match point A has the coordinates:

$$W(u_A, \beta) = 1, \quad 1/u_A = 10, \quad t = 53 \text{ min}, \quad s = 2.911 \text{ m}$$

$$Q = 10.4 \text{ L/sec} = 0.624 \text{ m}^3/\text{min}$$

$$T = \frac{Q}{4 \cdot \pi} \cdot \frac{W(u_A, \beta)}{s} = \frac{0.624 \frac{\text{m}^3}{\text{min}} \cdot 1}{4 \cdot \pi \cdot 2.911 \text{ m}} = 0.017 \frac{\text{m}^2}{\text{min}} = 2.8 \cdot 10^{-4} \frac{\text{m}^2}{\text{sec}}$$

Assuming a fully penetrating well, then  $B = 122.4 \text{ m}$  and the hydraulic conductivity for horizontal flow in m/sec, is:

$$\therefore K_h = \frac{T}{b} = 2.3 \cdot 10^{-6} \text{ m/sec}$$

The elastic early-time storativity is:

$$S_A = \frac{4 \cdot T \cdot t}{r^2} \cdot u_A = \frac{4 \cdot 0.017 \frac{\text{m}^2}{\text{min}} \cdot 53 \text{ min}}{(4.7 \text{ m})^2} \cdot 0.1$$

$$S_A = 0.016$$

The effects of elasticity of the aquifer matrix are generally very low in unconfined aquifers.

The coordinates for match point B, by matching the medium-time data with type B curves, are:  $W(u_B, \beta) = 1, 1/u_B = 1, t = 359 \text{ min}, s = 2.619 \text{ m}$

Calculating the values of T and  $S_y$ , we obtain:

$$T = \frac{Q}{4 \cdot \pi} \cdot \frac{W(u_B, \beta)}{s} = \frac{0.624 \frac{m^3}{min} \cdot 1}{4 \cdot \pi \cdot 2.619 m} = 0.019 \frac{m^2}{min} = 3.2 \cdot 10^{-4} \frac{m^2}{sec}$$

$$\therefore K_h = \frac{T}{b} = 2.6 \cdot 10^{-6} m/sec$$

$$S_y = \frac{4 \cdot T \cdot t}{r^2} \cdot u_B = \frac{4 \cdot 0.019 \frac{m^2}{min} \cdot 359 min}{(4.7 m)^2} \cdot 1$$

$$S_y = 1.23 ???$$

A specific yield value of  $S_y = 1.23$  is not reasonable. It is quite difficult to estimate the specific yield with the data recorded in the observation wells. For this reason, the solution of Neuman (Neuman, 1975) could not be applied for estimating the specific yield because the duration of the pumping test was not enough longer to display the late-time response of the aquifer.

According to Kruseman & De Ridder (1990) the following condition should also be fulfilled:

$$\frac{S_y}{S_A} > 10$$

Lohman (1972) indicated that storativity values for unconfined aquifers typically range from 0.1 to 0.3. In addition, Kruseman & De Ridder (1990) reported specific yield values around 0.16 for till predominantly sand or gravel materials. Moreover, Healey and Cook (2002) reported specific yield values of 0.07 for sandy clay materials, 0.27 for coarse sand materials and 0.35 for gravelly sand materials. Lithological descriptions of boreholes drilled at a depth of 60 meters, (G.E.O.S.I.R.H, 2016) located at Subdomain 2, show layers that comprises: medium gravel granular materials varying from 60 to 80%, clay materials varying from 30% to 10% and fine sand materials (10%). Deposits located at subdomain 2, has mainly a glacial origin with predominantly gravel materials. For this reason, a specific yield of 0.16 could be appropriate for the type of materials comprised at subdomain 3.

If we assume a specific yield value of 0.16, we will have:

$$S = S_A + S_y$$

$$S = 0.016 + 0.16$$

$$S = 0.144$$

Indeed, a specific yield value of 0.16, fulfill the condition of  $S_y/S_A > 10$ . This value is attributed to the presence of clay or silt sediments in the matrix related to the glacial origin of those deposits.

From the above calculations, the mean horizontal hydraulic conductivity will be:

$$\therefore K_h = (2.3 \cdot 10^{-6} \text{ m/sec} + 2.6 \cdot 10^{-6} \text{ m/sec})/2$$

$$\therefore K_h = 2.5 \cdot 10^{-6} \text{ m/sec}$$

Constructive details for the pumping well reported in MMAyA (2014), suggest that the screens for this well were installed in both layers (layer 2 and layer 4). This means that the value of  $K_h = 2.5 \cdot 10^{-6} \text{ m/sec}$  is an equivalent hydraulic conductivity for both layers.

From the Neuman method, hydraulic conductivity for vertical flow can also be calculated:

$$K_v = \frac{\beta \cdot K_h \cdot B^2}{r^2} = \frac{0.03 \cdot 2.5 \cdot 10^{-6} \text{ m/sec} \cdot (122.4 \text{ m})^2}{(4.7 \text{ m})^2}$$

$$K_v = 5.09 \cdot 10^{-5} \text{ m/sec}$$

Other way for estimating aquifer properties in the aquifer is by using the recovery data. The application of the straight-line method using the residual drawdowns from observation well OW-1 can help in estimating T and S.

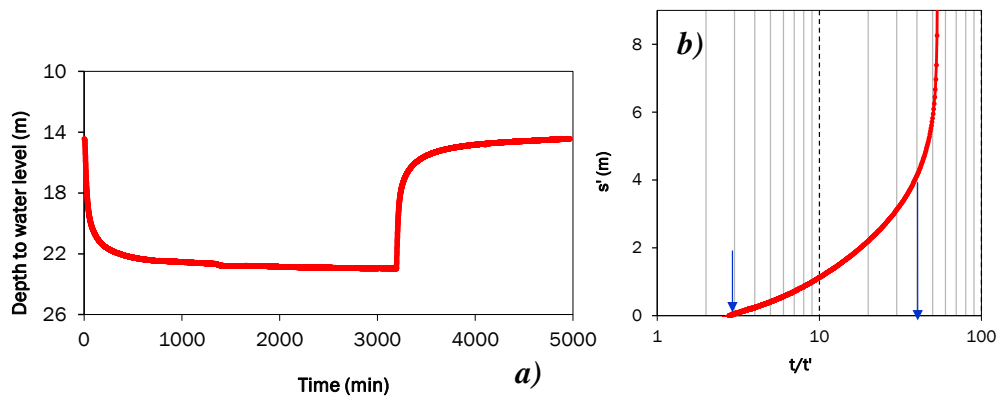


Figure A2. a) Depth to water level (m) versus time (min) measured in OW-1 and b) Field data of OW-1 for the residual drawdown ( $s'$ ) plot on semi-logarithmic scale (raw field data is available at MMAyA geodatabase).

The change in residual drawdown over one log cycle ( $t/t'$ ) is,  $\Delta s' = 4.079 \text{ m}$

$$T = \frac{2.3 \cdot Q}{4 \cdot \pi \cdot \Delta s'} = \frac{2.3 \cdot 0.624 \frac{\text{m}^3}{\text{min}}}{4 \cdot \pi \cdot 4.079 \text{ m}} = 0.028 \frac{\text{m}^2}{\text{min}}$$

$$K = 3.8 \cdot 10^{-6} \text{ m/sec}$$

The drawdown  $s_p = 10.606 \text{ m}$  when the pump is turned off at time  $t_p = 3140.5 \text{ min}$  is expressed as:

$$s_p = \frac{2.3 \cdot Q}{4 \cdot \pi \cdot T} \cdot \log \frac{2.25 \cdot T \cdot t_p}{r^2 \cdot S}$$

Then the storativity can be obtained by

$$S = \frac{2.25 \cdot T \cdot t_p}{r^2} \cdot 10^{-\frac{4 \cdot \pi \cdot T \cdot s_p}{2.3 \cdot Q}}$$

$$S = 0.023$$

Both values of hydraulic conductivity  $K = 3.8 \cdot 10^{-6} \text{ m/sec}$  and elastic storativity  $S = 0.023$  are coherent with the values estimated with the Neuman solution.

However, we will consider  $K_h, K_v, S$  and  $S_y$  values from the Neuman solution as this solution was developed for unconfined aquifers.

***Pumping test performed over at Subdomain 3 (old alluvial fan deposits close to El Alto)***

A pumping test was performed during March 2013 (raw field data available at MMAyA geodatabase). The monitoring well P-525 was pumped at a pumping rate of  $0.46 \text{ L/sec}$ . The duration of the pumping test was 23.9 hours, then the pump was turned off and it reached the steady state after 2.6 hours. The drawdowns, measured in the pumping well and in one observation well, (P-524) at 25 m away, are shown in Fig. 3.

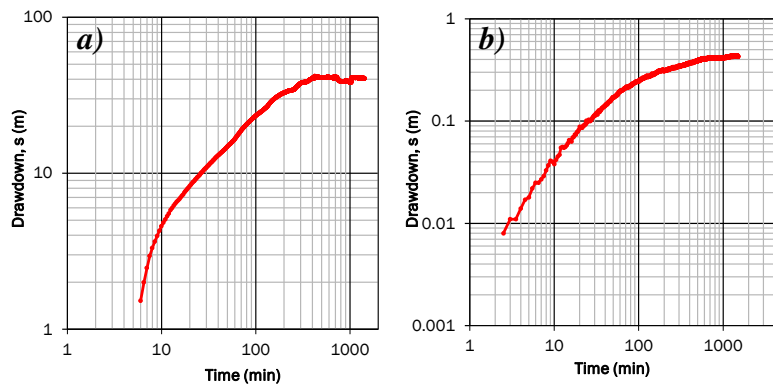


*Figure A3. Field data plot on logarithmic scale for the Neuman curve matching technique, a) field data for the pumping well P-525, b) for observation well P-524 (raw field data is available at MMAyA geodatabase).*

From the Neuman's curve fitting method (Neuman, 1975), the early time segment of the plot gives the best match with the Neuman type A curve for  $\beta = 0.03$ . The match point A has the coordinates:

$$W(u_A, \beta) = 1, \quad 1/u_A = 10, \quad t = 89.5 \text{ min}, \quad s = 0.152 \text{ m}$$

$$Q = 0.46 \text{ L/sec} = 0.028 \text{ m}^3/\text{min}$$

$$T = \frac{Q}{4 \cdot \pi} \cdot \frac{W(u_A, \beta)}{s} = \frac{0.028 \cdot 1}{4 \cdot \pi \cdot 0.152 \text{ m}} = 0.014 \frac{\text{m}^2}{\text{min}} = 2.4 \cdot 10^{-4} \frac{\text{m}^2}{\text{min}}$$

Assuming a fully penetrating well, then  $B = 70 \text{ m}$  and the hydraulic conductivity for horizontal flow in m/sec, is:

$$\therefore K_h = \frac{T}{b} = 3.5 \cdot 10^{-6} \text{ m/sec}$$

The elastic early-time storativity is:

$$S_A = \frac{4 \cdot T \cdot t}{r^2} \cdot u_A = \frac{4 \cdot 0.014 \frac{\text{m}^2}{\text{min}} \cdot 89.5 \text{ min}}{(25 \text{ m})^2} \cdot 10$$

$$S_A = 0.008$$

The coordinates for match point B couldn't be determined as the pumping test duration was very short. Again it was not possible to estimate the specific yield because the late-time response was not recorded.

From the above calculations, the mean horizontal hydraulic conductivity will be:

$$\therefore K_h = 3.5 \cdot 10^{-6} \text{ m/sec}$$

Even though that the monitoring wells (P-524 and P-525) appear to be located at subdomain 3 (alluvial fan deposits), it seems that in this zone alluvial deposits might be thinner or that screens are installed along the fluvio-glacial deposits. Geophysics results close to this zone (Flores G et al., 2019) show fluvio-glacial deposits overlaying paleolacustrine deposits, the same as for monitoring well P-180. However, the location of the well and the elevation depth (3910 masl) suggest that this well could not reach the paleolacustrine layer (layer 5). Indeed, constructive details for the pumping well reported in MMAyA (2014), suggest that the screens were installed along layer 2

(fluvioglacial deposits). This means that the value of  $K_h = 3.5 \cdot 10^{-6} \text{ m/sec}$  would correspond to layer 2.

From the Neuman method, hydraulic conductivity for vertical flow is estimated as follows:

$$K_v = \frac{\beta \cdot K_h \cdot B^2}{r^2} = \frac{0.03 \cdot 5.5 \cdot 10^{-6} \text{ m/sec} \cdot (70 \text{ m})^2}{(25 \text{ m})^2}$$

$$K_v = 1.3 \cdot 10^{-6} \text{ m/sec}$$

Applying the straight-line method using the residual drawdowns from observation well P-524, in order to verify values obtained with the Neuman method.

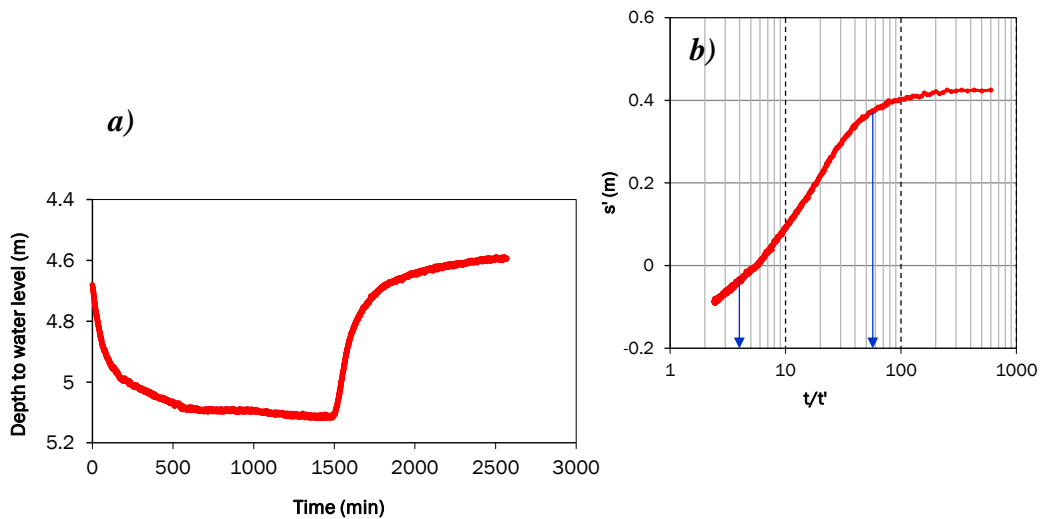


Figure A4.a) Depth to water level (m) versus time (min) measured in P-524 and b) Field data of OW-1 (P-524) for the residual drawdown ( $s'$ ) plot on semi-logarithmic scale (raw field data is available at MMAyA geodatabase).

The change in the residual drawdown over one log cycle ( $t/t'$ ) is,  $\Delta s' = 0.396 \text{ m}$

$$T = \frac{2.3 \cdot Q}{4 \cdot \pi \cdot \Delta s'} = \frac{2.3 \cdot 0.028 \frac{m^3}{min}}{4 \cdot \pi \cdot 0.396 m} = 0.013 \frac{m^2}{min}$$

$$K = 3.03 \cdot 10^{-6} m/sec$$

The drawdown  $s_p = 0.422 m$  when the pump is turned off at time  $t_p = 1501.5 min$  is expressed as:

$$s_p = \frac{2.3 \cdot Q}{4 \cdot \pi \cdot T} \cdot \log \frac{2.25 \cdot T \cdot t_p}{r^2 \cdot S}$$

The storativity is obtained by

$$S = \frac{2.25 \cdot T \cdot t_p}{r^2} \cdot 10^{-\frac{4 \cdot \pi \cdot T \cdot s_p}{2.3 \cdot Q}}$$

$$\therefore S = 0.006$$

The estimated values for hydraulic conductivity and storativity with this method compared to the Neuman method are consistent.

To summarize:

*Table A 1. Summary of aquifer properties obtained from the analysis of Multi-well pumping tests performed during March of 2013 at monitoring wells P-180, OW-1, OW-2 and P-525, P-524 (raw field data is available at MMAyA geodatabase).*

Layer	Horizontal Hydraulic conductivity, $K_h$ (m/sec)	Vertical Horizontal Hydraulic conductivity, $K_v$ (m/sec)	Elastic storativity, $S_A$ (**)	Specific yield, $S_y$ (**)	Storativity, $S$ (**)
Layer 2 + Layer 5 (P-180)	$2.5 \cdot 10^{-6}$	$5.09 \cdot 10^{-5}$	0.016	~0.16*	0.144
Layer 3 + Layer 2 (P-525)	$3.5 \cdot 10^{-6}$	$1.3 \cdot 10^{-6}$	0.008	–	–

\* Assumed from literature considering its glacial origin and predominantly gravel composition (Kruseman & De Ridder, 1990)

\*\* Dimensionless

-- Not able to estimate because the duration of the pumping test was not enough longer to display the late-time response of the aquifer

In the first case, the depth elevation of P-180 (~3831 masl) compared with the approximate altitude of Paleolake invasion (~3853 masl) estimated with geophysics (Flores G et al., 2019), suggest that layer 2 has a thickness of ~100 m and layer 5, a thickness of ~22 m. In the second case, low hydraulic conductivities suggest that layer 3 (alluvial fan deposits) is thin or that the screen of the well was installed along layer 2. Thus, the aquifer properties obtained from both pumping tests are representative values for layer 2 (fluvioglacial deposits). This value will be considered for estimating recharge by the WTF (Water fluctuation method).

#### ***Automatic water level measurements recorded from 2010 to 2015***

Automatic water level measurements were recorded by the Ministry of Water and Environment (MMAyA) between December of 2010 and February of 2015.

There were installed ten Mini-Divers (DI501- [www.swstechnology.com](http://www.swstechnology.com)) for measuring water pressure in the monitoring wells: P-233, P-524, P-514, P-085, P-084, P-100, P-509, P-667, P-092 and P-192. And a Baro-Diver (DI500- [www.swstechnology.com](http://www.swstechnology.com)) for measuring barometric fluctuations was also installed in the monitoring well P-084. All divers establish the height of a water column by measuring the water pressure. Measurements of water pressure at each monitoring location were compensated by the barometric pressure fluctuations in order to get the true height of water column measurements.

Besides the compensation of barometric pressure fluctuations, additional information of monthly manual measurements recorded from each monitoring point, helped in calculating the depth to water table. Figures 5, 6 and 7 show the depth to water table versus date at each monitoring point after the compensation.

#### ***Monitoring wells located at Subdomain 2 (fluvioglacial deposits)***

Daily automatic depth to water level results and precipitation, recorded from 04/11/2011 to 07/02/2015, are depicted in Fig.5a. The monitoring well P-233 is located at subdomain 2, ~1100 meters NW away from the Seco river and ~3200 meters from subdomain 1 (moraines). It displays a sharp rise of the water table during the rainy event of 01/10/2012 to 31/03/2013 and decline and rises during the dry season

(01/04/2013 to 30/09/2013). However, during the next rainy events “10/2013-03/2014” and “10/2014-03/2015”, there are punctual rises of water table but generally the tendency of the water level fluctuations is horizontal. This monitoring well belongs to the CBN-Pepsi enterprise. This enterprise use groundwater for economic purposes. The high depth of water table registered in this monitoring well is attributed to well interference, as much of the groundwater for the enterprise’s consumption is pumped from wells located very close (no more than 100 meters). Indeed, Fig. 5a displays a section with a constant horizontal tendency during 23/01/2014 to 15/02/2014. This reflects that even though the diver was placed at the same depth, the height of water column measured at this time was nearly 0. This can prove well interference. As a matter of fact, the depth of the water table (WL) measured at the end of each year (WL=49.96m, 31/12/2011; WL=45.67 m, 31/12/2012; WL=45.19m, 31/12/2013; WL=46.30, 31/12/2014) as depicted in Fig. 5a), evidence a rise of 4.3 m from 2011 to 2012, a rise of 0.5 m from 2012 to 2013 and a decline of 1.1 m from 2013 to 2014. The analysis of water level fluctuations (WTF) was not considered for this well due to well interference.

In the monitoring well (P-524), where the multi-well pumping test was performed, daily automatic depth to water level results and precipitation, recorded from 10/07/2013 to 22/02/2015, are illustrated in Fig. 5b. It evidences a sharp rise of water table during the “rainy season” of 01/10/2013 to 31/03/2014 and a clear decline during the “dry season” of 01/04/2014 to 30/09/2014. Punctual rises of water table could be attributed to the response of the aquifer to short storm events. Moreover, small water level fluctuations, the same as the one observed in well P-233, are observed during the period of 03/01/2014 to 21/03/2014. The response to precipitation in this period is different compared to the next “rainy season” 01/10/2014 to 31/03/2015. The WTF method was applied for estimating the net recharge over the period of 08/10/2013 to 06/11/2013 and 05/12/2013 to 06/01/2014 as showed in Fig.5b and Table 2. The specific yield was assumed to be 0.16. As previously explained, data of the pumping test didn’t allow estimating the specific yield because the aquifer test was not enough longer to display the late-time response of the aquifer. Therefore, a net recharge of 77 mm was estimated for the 30-day period of 08/10/2013 to 06/11/2013 and 224 mm for the 33-day period of 05/12/2013 to 24/01/2014 (Table 2). If we compare these values with the total precipitation of 80 mm and 228 mm, for the same periods, results suggest that near 98%

of the total precipitation could have reached the water table. These results could be truth regarding the shallow water table at this monitoring point, showing a maximum peak level on January (4.6 m) and a minimum peak level on October (6.2 m). Moreover, additional information of reference evapotranspiration for both periods gives an idea of how much water is loss to the atmosphere, considering a standard grassy surface covering the soil, with no humidity restriction (MacMahon et al.,2013; Ebrahim et al., 2019). The values determined for the first and second periods were 108 mm and 109 mm, respectively. However, after analyzing the results of net recharge estimations, precipitation and reference evapotranspiration, at each monitoring well, we will arrive to a conclusion at the end of this section.

In the monitoring well P-514, located at 214 m SE away from the Seque river, daily automatic depth to water levels results and precipitation, recorded from 04/10/2013 to 15/02/2015, are displayed in Fig. 5c. It shows a sharp rise of the water table of ~1.1 m during the “rainy period” of 01/10/2013 to 31/03/2014 and a decline from 9.7 m to 10.2 m (~0.5 m) during the “dry period” of 01/04/2014 to 30/09/2014. Punctual rises of water table could be attributed to the response of the aquifer to short storm events. Moreover, during the “dry period” rises of water table suggest the influence of the Seque river as no precipitation events were registered. The WTF method was applied for estimating the net recharge over the “rainy period” of 01/10/2013 to 31/03/2014. The specific yield was assumed to be 0.16. Therefore, from table 2, a net recharge of ~36 mm was estimated for the period of 21/10/2013 to 04/11/2013, ~155 mm for the period of 06/12/2013 to 11/02/2014 and ~40 mm for the period of 08/03/2014 to 27/03/2014. Total precipitations during those periods were 59 mm, 282 mm and 52 mm, respectively. And the total reference evapotranspiration for the same periods: 50 mm, 219 mm, 65 mm. Results show that 60% of the total precipitation measured for 15-day first period, 55% for the 68-day second period and 76% for the 20-day period arrived to the water table.

Figure 5d displays results from daily depth to water level measurements and precipitation, recorded from 26/01/2013 to 29/03/2014, in the monitoring well P-085. This well is located 580 m NW away the Seco river. The WTF method was not applied for calculating recharge as this well do not show any tendency of rise during year 2013. According to MMAyA (2014), this well belongs to the Tilata Pumping System, which

accounts with 30 pumping wells. These wells provide water supply for approximate 20% of inhabitants from El Alto city. Even though that this well was not pumped. Field observations from MMAyA (2016) reported a pumping well at less than 5m from well P-085 that began to function after March 2014. If we compare the heights of water columns in the periods of 01/2013 (~52.8 m) and of 01/2014 (~52.8 m) this results evidence that there was no significant change over this period. The shallow water table (5.6 m) and the insignificant fluctuation behavior could be attributed to its location, a discharge zone, evidenced in the field by wetlands ecosystems. Moreover, manual monthly water level measurements reported by MMAyA (2016), reflects a decline of the water table after the pumping began.

The monitoring well P-084 also belongs to the Tilata Pumping System. This well is located 150 m SE away the Seco river. As for the monitoring well P-085, depth to water table measurements show no significant rise or decline during the period of 10/07/2013 to 07/02/014. MMAyA (2004) also reported a well located at less than 5 meters being pumped at a mean rate of  $25 \text{ m}^3/\text{h}$ . Indeed, monthly manual water level measurements reported by MMAyA (2016) show a decline of the water table after 07/02/2014, when pumping began. If we compare the height of water columns at the end of the “dry season” of 30/09/2013 (39 m) and of 30/09/2014 (11 m), results evidence decline of 28 meters. This decline not necessarily reflects that the aquifer is being over exploited; instead it shows the behaviour of a long term pumping test that could reach the steady state or equilibrium conditions after 28/08/2014.

Figure 6b show observed results of water table measurements and precipitation, recorded from the monitoring well P-100. These data was recorded during the period of 10/07/2013 to 23/02/2015. The monitoring well P-100 also belongs to the Tilata Pumping System and is located 871 m NW away the Seco river. Field observations corroborate that the configuration at each pumping house always show a pumping and a monitoring well, being this last where water level measurements are recorded. MMAyA (2014) reported a height of water column of ~83.3 m for year 1989. Then when pumping began, at a mean rate of  $47.5 \text{ m}^3/\text{h}$  (year 1990), the

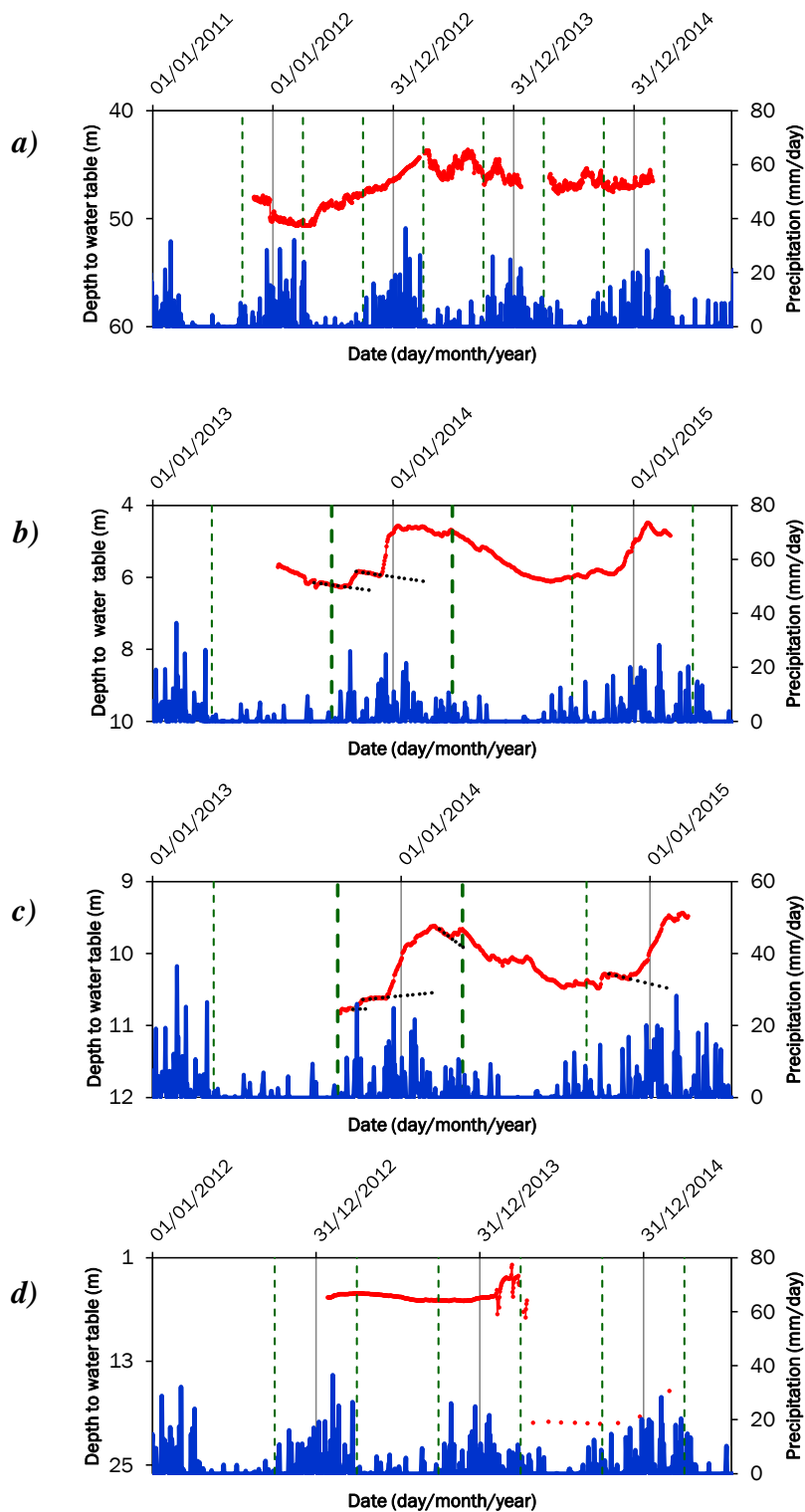


Figure A5. Hydrographs of water level fluctuations (red line) in wells located at subdomain 2 (fluvioglacial deposits) and bar graphs of daily average precipitation (blue line), for monitoring wells a) P-233, b) P-524, c) P-514 and d) P-085 (raw field data is available at MMAYa geodatabase). Gray lines represent the end of a hydrological year. Green dashed lines represent seasonal limits (01/04 to 30/09 – “Dry season”) and (01/10 to 31/03 “Wet season”). Black dotted lines represent hypothetical extrapolated recession curves for WTF analysis.

water table arose to decline. For instance, in 2010 the height of water column registered a value of ~72.7 m evidencing a decline in 10.6 m from 1990. Figure 6b, show water table levels of 15.9 m and 16.9 at the end of years 2013 and 2014, respectively. These measurements register a decline of 1 meter from 2013 to 2014. Even though, this well was influenced by pumping, data displays a clear response to precipitation events. For this reason, the WTF method was applied for the “rainy period” of 01/10/2013 to 18/04/2014.

A net recharge of 52 mm was calculated for the 31-day period of 01/10/2013 to 31/01/2013, 68 mm for the 28-day period of 12/01/2014 to 08/02/2014 and 53 mm for the 43-day period of 07/03/2014 to 18/04/2014, as displayed in Fig. 6b. Total precipitations of 70 mm, 114 mm and 76 mm were measured for the 31-day period, 28-day period and 43-day period, respectively. Results suggest that 75% of the total precipitation for the 31-day period, 60% for the 28 day-period and 71% for the 43-day period could have reached the water table.

Figure 6c displays depth to water table measurements and precipitation, for the monitoring well P-509. Data in this well was recorded from 14/08/2013 to 23/02/2015. In addition, water column heights show a maximum value of 76.3 m on 12/02/2014 and a minimum of 74.9 m on 20/11/2014. Rises of groundwater level are evidenced during the “rainy season of 2013-2014” for the periods of 14/10/2013 to 30/10/2013 and 06/12/2013 to 15/02/2014 (Fig. 6c). Water levels prior to rises were extrapolated to their expected positions if there was no precipitation. Then a clear decline is observed during the “dry season” of 2014. Calculations of net recharge by the WTF method accounted for 37 mm for the 17-day period of 14/10/2013 to 30/10/2013 and 209 mm for the 72-day period of 06/12/2013 to 15/02/2014. Total precipitation measurements account for 55 mm during the 17-day period, 288 mm for the 72-day period. Results of net recharge estimations suggest that 68 % of the precipitation for the 17-day period and 72 % for the 72-day period could have reached water table.

Depths to water table results and precipitation, from 05/10/2013 to 16/02/2015, are displayed for the monitoring point P-667 (Figure 6d). The maximum water column height (87.9 m) was recorded on 12/02/2014 and the minimum (86.6 m) on 20/11/2014. Results for P-667 show almost the same tendency of water level fluctuation as for P-

509. The monitoring well P-667 is located 600 m SE away from the monitoring well P-509. Groundwater level rises were registered for the 16-day period of 14/10/2013 to 29/10/2013 and for the 76-day period of 02/12/2013 to 15/02/2014. Results of recharge calculations (Table 2) show a net recharge of 38 mm for the 16-day period and 208 mm for the 76-day period. Total precipitation values accounts for 53 mm during the 16-day period and 290 mm during the 76-day period, suggesting that over 72% of the total precipitation for both periods could have reached the water table.

Figure 7a shows groundwater level fluctuations and precipitation for the monitoring point P-092 during the period of 03/12/2010 to 12/07/2013. Minimum values, of depth to water table, were registered at the end of the “rainy season”, accounting for 7.8 meters on 31/03/2011, 7.45 meters on 31/03/2012 and 7.8 meters on 31/03/2013. In contrast, the maximum values were registered during the month of December, showing 8.5 m on 15/12/2011, 8.9 m on 04/12/2012 and 8.9 m on 07/12/2013. The WTF method was applied for the “rainy season of 2011-2012” for the period of 01/12/2011 to 20/03/2012. A total recharge of 382 mm was calculated for this 111-day period. The amount of total precipitation registered for this period (Table 2) suggests that over 76 % of the precipitation could have arrived at the water table. In addition, Fig.7a clearly illustrates that water table, prior to begin rising gradually, recedes during April to December accounting for at least 91 days at the beginning of the “rainy season” (01/10 to 31/12). This could account to the slow drainage of the aquifer in response to precipitation events. However, the WTF method is incapable to estimate recharge occurring during the hydrograph recession (Healy R and Cook P, 2002).

Finally, figure 7b displays results of depth to water table and precipitation for the monitoring point P-192. Groundwater level fluctuates from a maximum of 30.9 meters (31/03/2011) and

29.7 meters (12/04/2012), and a maximum of 34.3 meters registered on 11/12/2010 and 36.1 registered on 12/12/2011. Even though, that this monitoring point has a deep groundwater level, clear rises of water level accounting for 1.6 meters for the 31-day period of 08/12/2010 to 07/01/2011 and of 3.1 meters for the 53-day period of 03/02/2011 to 27/03/2011, are evidenced in Fig.7b. Moreover, daily measurements of precipitation recorded from El Alto station show a total precipitation of 133 mm for the

31-day period and of 207 mm for the 53-day period. In addition, a net recharge of 254 mm was calculated for the 31-day period and of 490 mm for the 53-day period. Unless, that during the receding times “April to December” recharge from precipitation was still occurring due to the slow drainage of the aquifer. Another source than precipitation attempting to arrive at the water table should be considered.

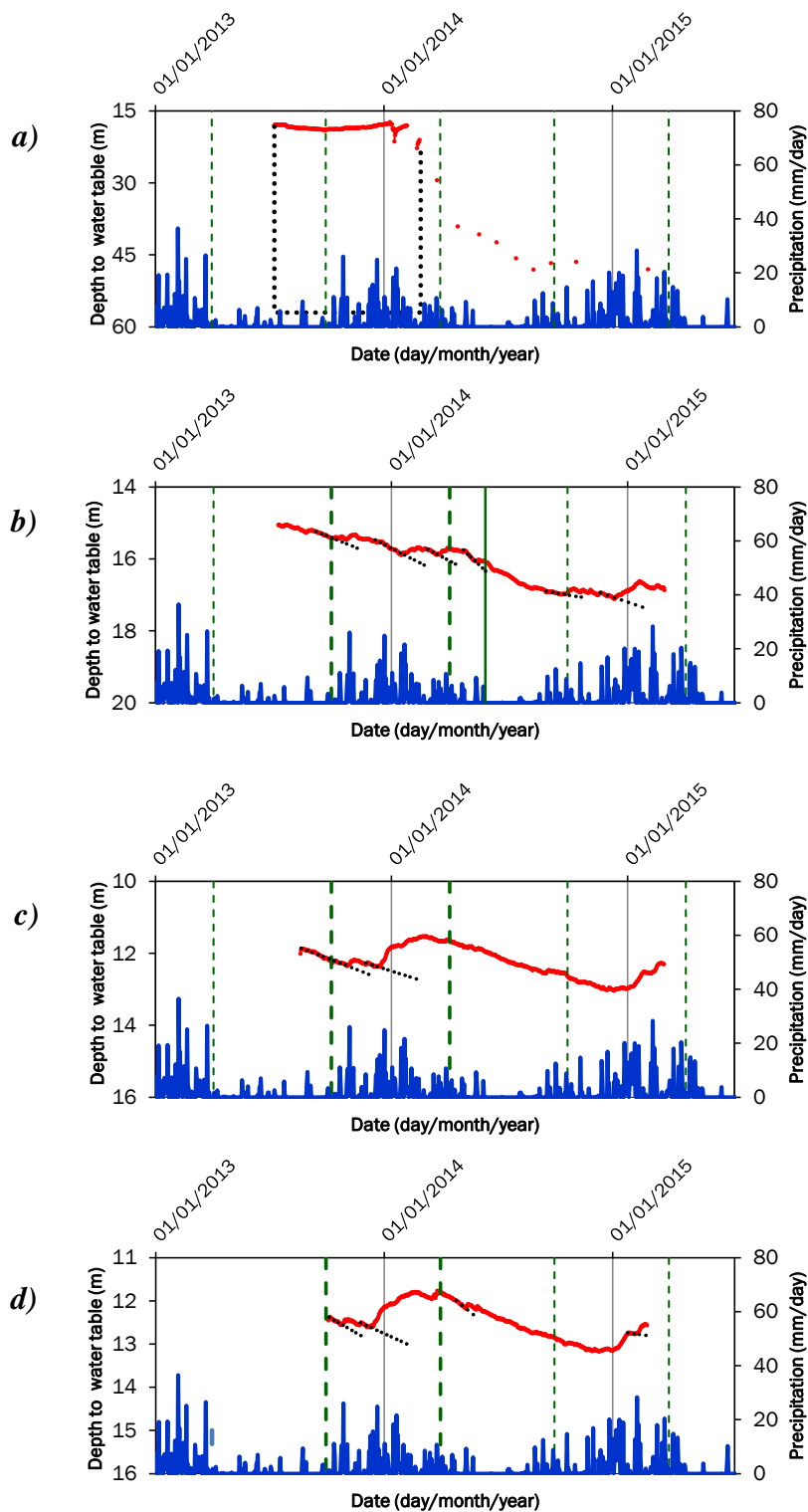


Figure A6. Hydrographs of water level fluctuations (red line) in wells located at subdomain 3 (fluvioglacial deposits) and bar graphs of daily average precipitation (blue line), for monitoring wells a) P-084, b) P-100, c) P-509 and d) P-667 (raw field data is available at MMAyA geodatabase). Gray lines represent the end of a hydrological year. Green dashed lines represent seasonal limits (01/04 to 30/09 – “Dry season”) and (01/10 to 31/03 “Wet season”). Black dotted lines represent hypothetical extrapolated recession curves for WTF (Water table fluctuation) analysis.

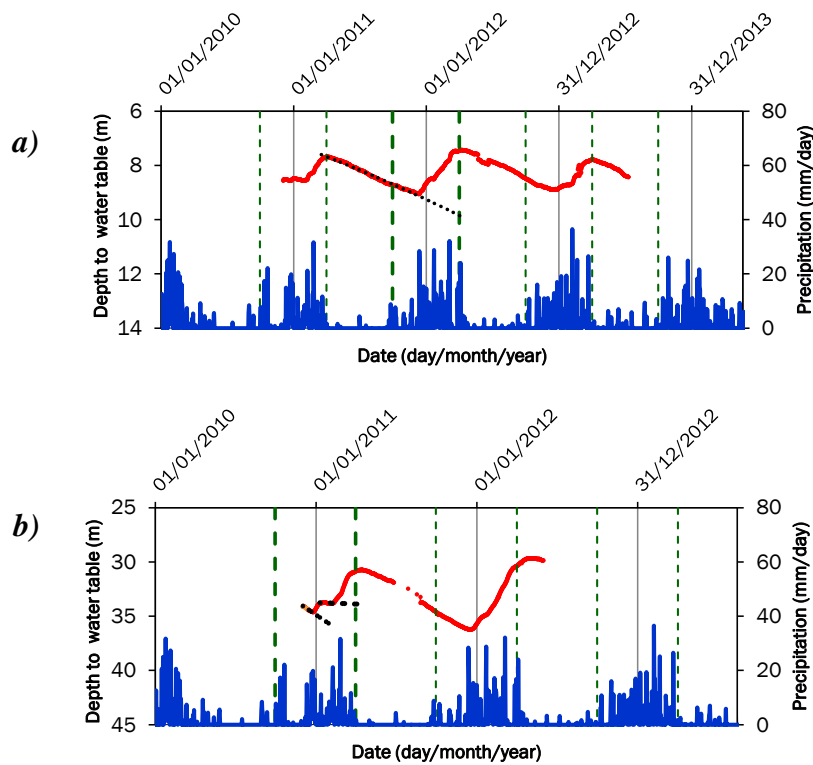


Figure A7. Hydrographs of water level fluctuations (red line) in wells located at subdomain 2 (fluvioglacial deposits) and bar graphs of daily average precipitation (blue line), for monitoring wells a) P-092 and b) P-192. Gray lines represent the end of a hydrological year. Green dashed lines represent seasonal limits (01/04 to 30/09 – “Dry season”) and (01/10 to 31/03 “Wet season”). Black dotted lines represent the hypothetical extrapolated recession curves for WTF (Water table fluctuation) analysis.

Generally, three situations could be derived from the above results:

- Groundwater levels recede during April to December. From October to December, the aquifer response to precipitation is slow. Then water level begins rising gradually from January to March, reaching its maximum peak level by the middle of February (P-509; P-667; P-092). Water level rises of 1.5 meters were estimated from 10/2013 to 02/2014, accounting for a total recharge of 246 mm, representing 71 % of the total precipitation. And rises of 2.4 meters were estimated from 12/2011 to 03/2012 accounting for a total recharge of 382 mm, representing 76 % of the total precipitation.

- Monitoring points, located in the discharge zone (evidenced by wetland ecosystems) and close to the Seco river (P-084; P-085; P-100), but influenced by a near pumping well, show different fluctuations of groundwater levels. However, considering a constant pumping rate (MMAyA, 2014), water levels rise in response to precipitation. Indeed, water levels rise was estimated to be 1.09 meters from 10/2013 to 04/2014 accounting for a total recharge of 174 mm, representing 69 % of the total precipitation.
- Monitoring points, located near the Seque river (P-514; P524) show small rises of water level, from October to December, in response to precipitation. Then, water table gradually rises reaching its maximum peak level by the middle of February. After, water table begins to decline from April to September. During this period, punctual water table rises could be attributed to the Seque river influence. Indeed, at monitoring point P-514, a total water level rise of 1.4 meters was estimated from 10/2013 to 03/2014, accounting for a total recharge of 230 mm, representing around 64 % of the total precipitation for that period. Moreover, at shallower water tables (P-524), total water level rise was estimated to be (1.9 m) from 10/2013 to 01/2014, accounting for a total recharge of 302 mm, representing over 98% of the total precipitation.
- Level rises at deep water tables (29.7-34.3 m) as in monitoring point P-192. Show the same behavior of level fluctuations: A decline a water table from April to December, then it gradually rises from January to March showing its maximum peak level by the end of March. Estimations of water level rise from 12/10 to 03/2011, accounts for a total rise of 4.7 meters, meaning a total of 744 mm of recharge. This value surpasses the total precipitation of 340 mm, suggesting that in addition to the natural replenishment, there is another source of recharge.
- An estimation of the actual evapotranspiration could help in adjusting the specific yield value.

### ***Automatic water level measurements recorded from 2018-2019***

Automatic water level measurements were recorded between August of 2018 and March of 2019, in coordination with the Ministry of Water and Environment (MMAyA).

There were installed four levelloggers (Solinst) for measuring water pressure and electrical conductivity, in the monitoring wells: P-1, P-2, P-3, P-5. In addition, a Barologger (Solinst) was installed in the monitoring well P-2, for measuring barometric fluctuations. All levelloggers establish the height of a water column by measuring the water pressure. Measurements of water pressure at each monitoring location were compensated by the barometric pressure fluctuations in order to get the true height of water column measurements. Besides the compensation of barometric pressure fluctuations, additional information of the initial manual water level measurement recorded at each monitoring point, were used for calculating the depth to water table. Figure 8, show the depth to water table and precipitation versus the date, at each monitoring point after the compensations.

### ***Monitoring wells located at Subdomain 4 (fluvio-lacustrine deposits)***

Figure 8a, displays results of hourly automatic water level measurements versus date, recorded from 30/08/2018 to 21/03/2019, at monitoring point P-1. This monitoring well is located at subdomain 4, at the northwest of Batallas City, 400 m SE away Lake Titicaca (Puerto Pérez Bay 1). Even though that no clay layer was identified by geophysics, due to the vertical resolution of the method (Flores G et al., 2019), borehole lithological information (50 meters depth) show a first clay layer of 4 meters. Then 47 meters of thin layered sequences that comprises medium to coarse sand materials with clay content. These deposits were interpreted to be the result of Holocene Lake invasion (Flores G. et al, 2019). Daily precipitations plotted in Fig. 8a corresponds to data recorded in El Alto airport station, as no other source of daily measurements were available in the zone. Groundwater level measurements show a maximum peak level (0.04 m) on February (22/02/2019) and a minimum level (0.5 m) on December (24/12/2018). The WTF method is only valid for unconfined aquifers. However, based on the premise of the WTF method, water levels prior to rises were extrapolated to their expected position as if there were not any source of recharge. Then, water level rises

were estimated as the difference between the peak level and the extrapolated antecedent level. A total water level rise of 18 cm was estimated for the 29-day period of 12/10/2018 to 09/11/2018, 13 cm for the 18-day period of 02/01/2019 to 19/01/2019 and 41 cm for the 27-day period of 29/01/2019 to 24/02/2019. Recharge to the aquifer in this area might be by seepage from the influent Lake Titicaca. This will be verified by the electrical conductivity records.

Automatic electrical conductivity records registered during 30/08/2018 to 21/03/2019 are displayed in Fig. 8b. Electrical conductivity fluctuations, showed a maximum peak (632  $\mu\text{S}/\text{cm}$ ) on December (24/12/2018) and a minimum peak (563  $\mu\text{S}/\text{cm}$ ) on February (19/02/2018). Fig. 8b show clear rises of electrical conductivity in response to high intensity precipitation events. These results reflect that during precipitation events, Lake Titicaca water levels rise and might recharge the aquifer. Moreover, additional information should be acquired during the “dry season” from April to September.

The monitoring well P-2 is also located at subdomain 4, towards the northwest of Pucarani City, 2000 m SE away Lake Titicaca (Puerto Pérez Bay 2). Results of hourly automatic water level records versus date are displayed in Fig. 9. These records were registered from 30/08/2018 to 21/03/2019. The same as for the monitoring point P-1, lithology descriptions show a first thin clay layer of 2 meters. Groundwater levels are deeper in comparison to the levels encountered at monitoring point P-1.

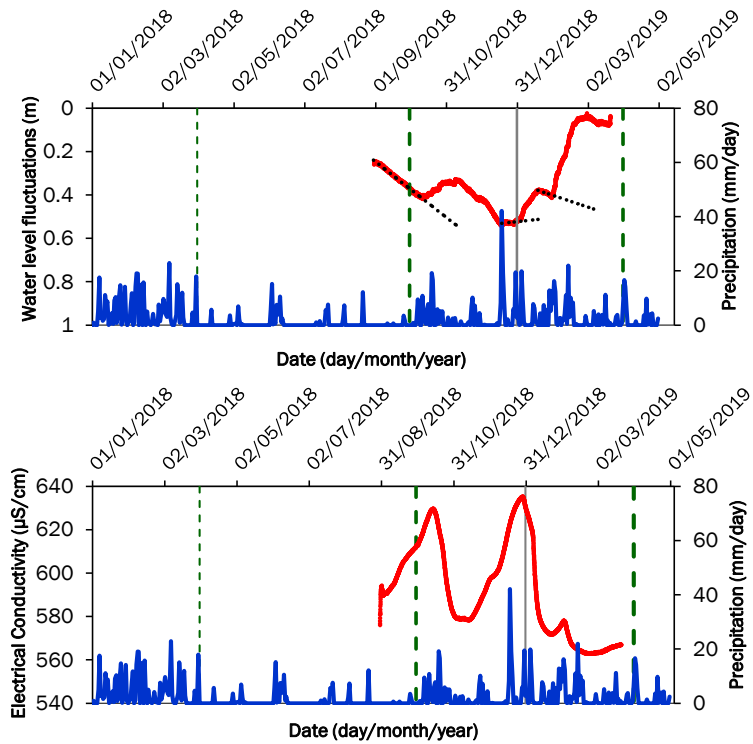


Figure A8. a) Hydrograph of water level fluctuations (red line) at monitoring point P-1, located in subdomain 4 (fluvio-lacustrine deposits) and records of daily average precipitation (blue line) from El Alto station and b) Electrical conductivity measurements recorded at monitoring point P-1. The green dashed lines represent seasonal limits (01/04 to 30/09 – “Dry season”) and (01/10 to 31/03 “Wet season”). Black dotted lines represent the expected position of hypothetical extrapolated recession curves as if there were not any source of recharge.

Indeed, water levels fluctuate from a minimum of 3 m registered on December (14/12/2018) and a maximum of 2.8 m registered on February (25/02/2019). Water level rises of 13 cm were evidenced for the 16-day period of 11/10/2018 to 26/10/2018, 14 cm for the 26-day period of 13/12/2018 to 07/01/2019 and 19 cm for the 30-day period of 28/01/2019 to 26/02/2019. As for P-1, these water levels rise might account for other source of recharge than precipitation, as natural replenishment seems to be restricted by the thin clay layer. The influence of Lake Titicaca could also be proposed in this area, as Fig.9b reflects the same response of water level fluctuations, as for P-1. However, electrical conductivity measurements were only registered for a small period (30/08/2018 to 07/09/2018). These records oscillate around 105  $\mu\text{S}/\text{cm}$ . The low

electrical conductivity, can explain the low recharge due to the distance of location, being 2000 SE away of Lake Titicaca.

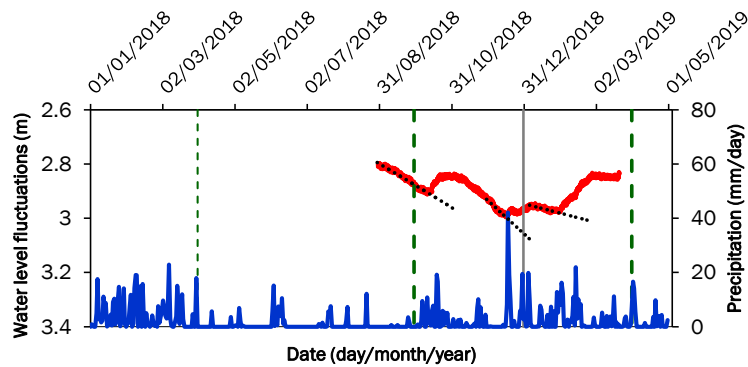
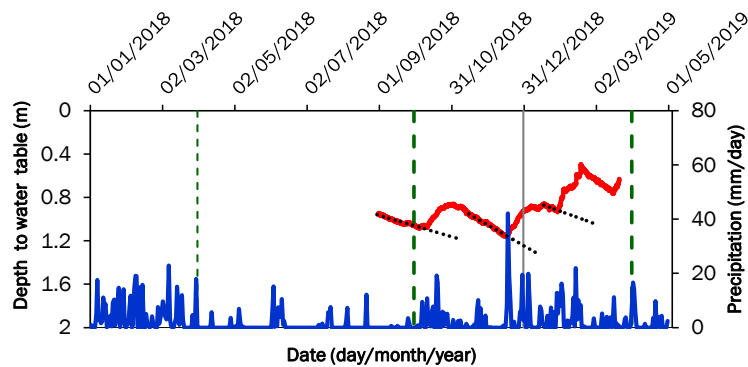


Figure A9. Hydrograph of water level fluctuations (red line) at monitoring point P-2, located in subdomain 4 (fluvio-lacustrine deposits) and records of daily average precipitation (blue line) from El Alto station. The green dashed lines represent seasonal limits (01/04 to 30/09 – “Dry season”) and (01/10 to 31/03 “Wet season”). Black dotted lines represent the expected position of hypothetical extrapolated recession curves as if there were not any source of recharge.

### **Monitoring well located at Subdomain 3 (Alluvial fan deposits)**

The monitoring well P-3 located at the northwest of Pucarani City was drilled (26 m) over subdomain 3. Borehole lithological information show layers consisting of well sorted fine gravel to coarse sand materials with small amount of clay content. In regards to Flores G. et al, (2019) this monitoring point would correspond to the distal part of the major alluvial fan. No aquifer test information was reported in this zone. For the purpose of estimating net recharge, a specific yield of 0.20 was assumed from literature (Healey and Scanlon, 2002) regarding its lithological composition. Results of hourly automatic water level records and daily precipitation registered from 30/08/2018 to 21/03/2019 are displayed in Fig. 10. Groundwater level fluctuations show a delayed response to high-intensity precipitation events. This delay could be attributed to the slow drainage of the thin soil layer that from field observations may comprise significant amount of clay. Water level rises were evidenced for the 27-day period of 11/10/2018 to 06/11/2018, for the 22-day period of 14/12/2018 to 04/01/2019 and for the 20-day period of 28/01/2019 to 16/02/2019. A total net recharge of 29 mm was

calculated for the 27-day period, 41 mm for the 22-day period and 48 mm for the 20-day period. Total precipitations for those periods registered 90 mm, 140 mm and 130 mm, respectively. Results of net recharge suggest that 32% of the total precipitation for the 27-day period, 30% for the 22-day period and 37% for the 20-day period may have reached water table. In addition, electrical conductivity records in this monitoring point, oscillates around 60.6 to 65  $\mu\text{S}/\text{cm}$  during the period of 30/08/2018 to 21/03/2019.



*Figure A10. Hydrograph of water level fluctuations (red line) at monitoring point P-3, located in subdomain 3 (Alluvial fan deposits) and records of daily average precipitation (blue line) from El Alto station. The green dashed lines represent seasonal limits (01/04 to 30/09 – “Dry season”) and (01/10 to 31/03 “Wet season”). Black dotted lines represent hypothetical extrapolated recession curves for WTF (Water table fluctuation) analysis.*

### ***Monitoring well located at Subdomain 6 (Paleo-lacustrine deposits)***

Figure 11 displays results of water level fluctuations in the monitoring point P-5 recorded from 30/08/2018 to 21/03/2019. This monitoring point is located in the subterranean channel (Flores G et al., 2019). Drilling information for this borehole (53 meters depth) registered a first layer of 15 meters of clay and 38 meters of clayey sandy and gravelly sand materials (Layer 5). Even though that the WTF method is not valid for confined aquifers. Water level rises of 0.08 meters were evidenced for the 18-day period of 01/10/2018 to 18/10/2018, 0.03 meters for the 8-day period of 15/11/2018 to 22/11, 0.03 meters for the 9 day-period of 11/12/2018 to 19/12/2018, 0.04 meters for the 5-day period of 24/12/2018 to 28/12/2018, 0.08 meters for the 7 day period of 27/01/2019 to 02/02/2019 and 0.12 meters for the 17 day period of 04/02/2019 to 20/02/2019. These level rises were estimated on the premise of the WTF method. That means that water levels prior to rises were extrapolated to their expected position had

there been no recharge. Water level rises at this point may account for groundwater lateral drainage arriving from the northeast. This evidences the connection between the Piedmont subsystem and Lacustrine plain (Flores G et al. 2019). In addition, electrical conductivity records oscillate around 150.6  $\mu\text{S}/\text{cm}$  (31/08/2018) to 150.1  $\mu\text{S}/\text{cm}$  (19/03/2019).

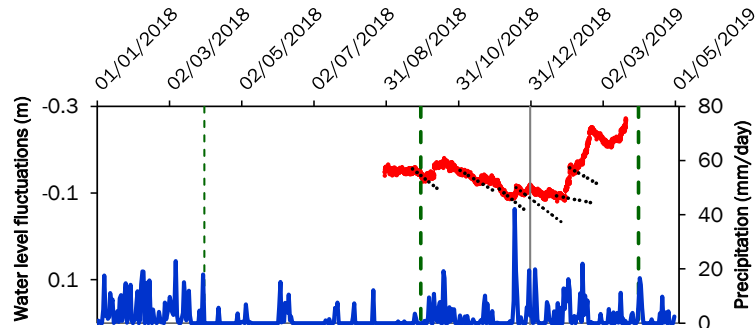


*Figure A11. Hydrograph of water level fluctuations (red line) at monitoring point P-5, located in subdomain 6 (Paleo-lacustrine deposits) and records of daily average precipitation (blue line) from El Alto station. The green dashed lines represent seasonal limits (01/04 to 30/09 – “Dry season”) and (01/10 to 31/03 “Wet season”). Black dotted lines represent the expected position of hypothetical extrapolated recession curves as if there were not any source of recharge.*

### ***Estimation of evaporation from 2013 based on Isotopic Data***

Figure S12 displays the isotopic composition of  $\delta^2\text{H} \text{‰}$  and  $\delta^{18}\text{O} \text{‰}$  from groundwater and surface water at the Purapurani zone reported by MMAyA (2016).

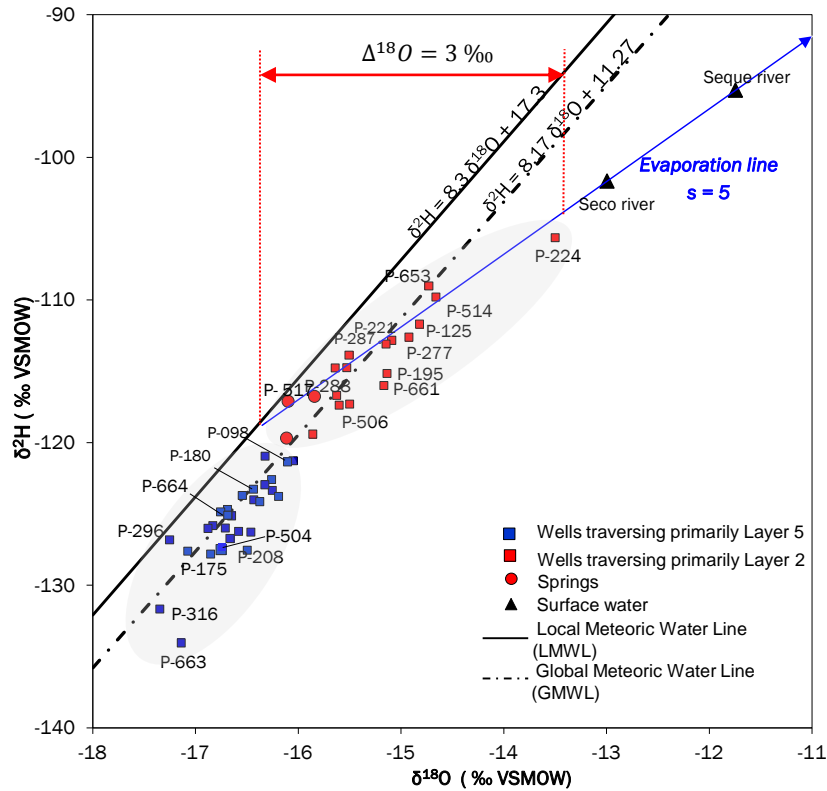


Figure A12. Stable hydrogen and oxygen isotopic composition of surface water and groundwater at the Bolivian Lake Titicaca aquifer system (Purapurani Zone), modified after MMAyA (2016).

According to MMAyA (2016), values lying below the meteoric line of local precipitation should reflect the presence of ancient waters that were originated in a different climatic regime.

Indeed, isotopically lighter values (more negative, blue squares) coincide with the location of groundwater primarily hosted at layer 5 (deposits related to Paleolake invasion). Besides, red squares, represent groundwater mainly hosted at layer 2 (fluvioglacial deposits). However, according to Flores-Avilés et al. (2019) they could also represent a mixing of waters that were pumped from both layers (2 and 5). Moreover, this second type of groundwater (red squares), although represent a mixture of recharge events, they also reflect secondary fractionation by evaporation prior to infiltration. This could be evidenced by the samples following the local “evaporation slope”, showing that groundwater have experienced evaporative enrichment (Fig. S12).

Based on the local evaporation slope ( $s = 5$ ), it is possible to estimate an average of evaporative loss of groundwater. Gonfiantini (1986) presented a mathematical basis showing isotopic enrichment in evaporating water and the effect of humidity (Clark and Fritz et al., 1997). This author proposed the following relationships for describing the kinetic effect in terms of humidity:

$$\Delta\varepsilon^{18}O_{bl-v} = -14.2 (1 - h)\text{‰}$$

$$\Delta\varepsilon^2H_{bl-v} = -12.5 (1 - h)\text{‰}$$

Where  $\Delta\varepsilon^{18}O_{bl-v}$  is the kinetic factor of oxygen 18 from the boundary layer to the vapour reservoir of the open air water-vapour. And  $\Delta\varepsilon^2H_{bl-v}$  is the kinetic factor of deuterium from the boundary layer to the vapour reservoir of the open air water-vapour reservoir (Clark and Fritz et al., 1997).

For a slope of 5, the correspondant humidity factor ( $h$ ) would be closer to 0.75.

Then the kinetic factors will be:

$$\Delta\varepsilon^{18}O_{bl-v} = -3.55 \text{‰}$$

$$\Delta\varepsilon^2H_{bl-v} = -3.13 \text{‰}$$

Besides, the fractionations factors for equilibrium water-vapour exchange ( $\varepsilon_{l-v}$ ) for  $^{18}O$  and  $^2H$  in water-vapour reactions were calculated from Table 1-4 (available at Clark and Fritz, 1997) considering a mean annual temperature of 7.7 °C (from El Alto station for 2013):

$$\varepsilon^{18}O_{l-v} = 10^3 \ln \alpha^{18}O_{w-v} = -10.7\text{‰}$$

$$\varepsilon^2H_{l-v} = 10^3 \ln \alpha^2H_{w-v} = -94.7\text{‰}$$

Then, the overall enrichment for evaporation is given by:

$$\varepsilon_{total} = \varepsilon_{l-v} + \Delta\varepsilon_{bl-v}$$

For  $^{18}\text{O}$ :

$$\varepsilon^{18}\text{O}_{total} = \varepsilon^{18}\text{O}_{l-v} + \Delta\varepsilon^{18}\text{O}_{bl-v}$$

$$\varepsilon^{18}\text{O}_{total} = -14.25 \text{ ‰}$$

For  $^2\text{H}$ :

$$\varepsilon^2\text{H}_{total} = \varepsilon^2\text{H}_{l-v} + \Delta\varepsilon^2\text{H}_{bl-v}$$

$$\varepsilon^2\text{H}_{total} = -97.83 \text{ ‰}$$

The fractional water loss from evaporation can then be modeled according to a Rayleigh distillation. From Fig.S12, the evaporative enrichment for  $\delta^{18}\text{O}$  is up to 3 ‰.

Then:

$$\delta^{18}\text{O}_{gw} - \delta^{18}\text{O}_{prec} = \varepsilon^{18}\text{O}_{total} \cdot \ln f = 3 \text{ ‰}$$

$$\therefore \ln f = \frac{3 \text{ ‰}}{-14.25 \text{ ‰}} = -0.211$$

Yielding a residual water fraction  $f$  of 0.81 and so an average evaporative loss of 19 %